PNNL-11373
UC-510

Pacific Northwest
National Laboratory

Operated by Battelle for the
U.S. Department of Energy

Flammable Gas Data Evaluation Progress Report

P. D. Whitney
P. A. Meyer
N. E. Wilkins
N. E. Miller
F. Gao
A. G. Wood

October 1996

Prepared for the U.S. Department of Energy
under Contract DE-AC06-76RLO 1830

PNNL-11373

DISCLAIMER

PACIFIC NORTHWEST NATIONAL LABORATORY
operated by
BATTELLE
for the
UNITED STATES DEPARTMENT OF ENERGY
under Contract DE-AC06-76RLO 1830

PNNL-11373
UC-510

Flammable Gas Data Evaluation Progress Report

P. D. Whitney
P. A. Meyer
N. E. Wilkins[a]
N. E. Miller
F. Gao
A. G. Wood

October 1996

Prepared for
the U.S. Department of Energy
under Contract DE-AC06-76RLO 1830

Pacific Northwest National Laboratory
Richland, Washington 99352

(a) Westinghouse Hanford Company

Summary

The Hanford Site is home to 177 large, underground nuclear waste storage tanks. Numerous safety and environmental concerns surround these tanks and their contents. One such concern is the propensity for the waste in these tanks to generate, retain, and periodically release flammable gases. This report documents some of the activities of the Flammable Gas Project Data Evaluation Task conducted for Westinghouse Hanford Company during fiscal year 1996.

Described in this report are: 1) the results of examining the in-tank temperature measurements for insights into gas release behavior; 2) the preliminary results of examining the tank waste level measurements for insights into gas release behavior; and 3) an explanation for the observed hysteresis in the level/pressure measurements, a phenomenon observed earlier this year when high-frequency tank waste level measurements came on-line.

Detecting Gas Release Events with Level and Temperature Measurements

Some of the Hanford tank headspaces are currently monitored for flammable gases. However, continuous headspace gas monitoring is relatively recent and does not cover much of the history of the Hanford tanks suspected of generating, retaining and releasing flammable gases. Other tank waste measurements, level and temperature, were examined to obtain a historical view of the gas release behavior of tanks.

Tank waste level and temperature measurements have been made routinely on a weekly or daily basis in many of the tanks; tank waste level measurements often extend back to the early 1980s, and tank waste temperature measurements to the early 1990s. Additionally, in tanks known to release retained gas periodically, level and temperature measurement responses have been observed which can be explained as being caused by the gas release event (GRE).

The response of tank waste temperatures to GREs in the double-shell tanks (DSTs) include an abrupt jump in value or a sudden change in trend. These temperature changes are interpreted as indicative of tank waste movement resulting from the GRE. Not every location in the waste shows a temperature response to GREs.

The responses of tank waste level to GREs include an abrupt level drop or an abrupt level rise.

A methodology was developed to detect these measurement responses in the tank data, and was applied to selected tanks. For temperature, the candidate tanks included all of the single-shell tanks (SST) and a subset of the DSTs. For tank waste level, the candidate tanks included those in which retained gas had been detected previously by means of the level response to atmospheric pressure variations. In both cases, the raw observations were "corrected" for known systematic errors; for the temperature data, the correction was particularly effective in reducing noise.

The temperature data, in conjunction with the methodology used to examine the data, were not very effective at detecting GREs. For the burping DSTs, the methodology detected approximately 15% of the GREs during the time span covered by the temperature data. However, the methodology and data were adequate to discover some apparently gas-related events in Tanks AN–104 and SY–103. Particularly striking was a simultaneous temperature shift and jump in the rate of change of tank waste level, observed once in each of these tanks. A jump in the rate of change in tank waste level is interpretable as an abrupt change in the rate of storage of generated gas in the tank waste.

For the SSTs, numerous temperature anomalies were observed. None of the anomalies were similar to the temperature response to GREs observed in the burping DSTs.

The level data, in conjunction with the methodology used, did a thorough job of detecting level data features that correspond to GREs. In particular, for the double-shell Tank AN–104, almost all of the GREs detected using tank headspace gas monitoring were also detected using the tank

waste level data. The lone exception was a release that occurred during the time the tank level instrumentation was changed from one type of measurement to another. A fair number of potential gas release events were identified for the SSTs.

The feature detection methodologies for both temperature and level data included a human component. In each case, after the initial pass through the data by an algorithm whose purpose was to identify features related to GREs, a human analyst examined the detections and, based on different criteria and additional information for each of the measurement types, further culled the initial feature list. For the tank level data, the decisions to be made were sufficiently complex that the study was designed so that different individuals sometimes evaluated the same tanks. On these tanks common to two or more analysts, a comparison was made of the culling decisions. The decisions made on some of these tanks were different enough that this part of the study was redesigned. It is recommended that the redesigned part of the study be repeated.

Level/Pressure Hysteresis

In some of the Hanford tanks, the tank waste level has been observed to vary with atmospheric pressure changes. Models connecting these changes with the amount of gas in the tank waste, together with information about the pressures at which the gas is held in the waste, have been proposed and used to estimate the amount of gas retained in the tank waste. All these models to explain the waste level fluctuations have been based on the ideal gas law.

A particular implication of all these models is that the level and pressure, over short time windows, vary linearly and inversely with each other. However, when high-frequency level data came on-line for some tanks in late 1995, a clear deviation from this behavior was observed. The observed behavior was that the level tracked the pressure on pressure upswings differently than on downswings.

This report presents a model which, at least qualitatively, explains both of these behaviors in the level/pressure data. The model incorporates features of previous models with tank waste material properties (sludge elasticity and yield). Although a detailed comparison of the model with the data is not yet completed, the results are promising. We describe the model, and show how the results simulated with the model compare with the actual tank data.

The implications of the model include the following:

- Previous models have underestimated the amount of gas retained in the tank waste; the range for the underestimate, which varies by tank, is from about 15% to 55% for the tanks discussed in Section 5.
- There is good potential to improve the accuracy of retained gas volume estimates (based on level and pressure data).
- Information about tank waste material properties can be obtained, for some tanks, from the high-frequency level data.
- The sharp changes in the trend of tank level data which tend to occur at about 9:00am, and which were interpreted as instrumentation anomalies, might instead be a real feature of the tank waste level.

It is recommended that the detailed comparison between the data and this model be aggressively pursued.

Acknowledgments

This report, as is always the case, has benefited greatly from the comments of the peer, program and editorial reviewers: Tom Ferryman, Joe Brothers, Frank Ryan and Andrea Currie, respectively.

Much of the fundamental research behind our understanding of the tank level and temperature measurements, as well as the machinery to handle these data, was supported by the Tank Surveillance group at Westinghouse Hanford Company, which at various times included Richard Raymond, David Barnes, Don Engelman and Tom Rainey.

Acronyms and Abbreviations

CASS	Computer Automated Surveillance System
DLM	dynamic linear model
DST	double-shell tank
ENRAF	Enraf 854 ATG level detector manufactured by Enraf Incorporated
FIC	Tank waste surface level gauge manufactured by the Food Instrument Company
GC	gas chromatograph
GRE	gas release event
ILL	interstitial liquid level
MIT	multifunction instrument trees
MT	manual tape, a tank waste surface level gauge
Neutron ILL	interstitial liquid level measurement based on neutron loggings taken within the tank waste
SACS	Surveillance Analysis Computer System, the database in which the tank waste level data are stored
SHMS	Standard Hydrogen Monitoring System
SST	single-shell tank
TC	thermocouple
TMACS	Tank Monitoring and Control System

Contents

Summary iii

Acknowledgments v

Acronyms and Abbreviations vi

1 Introduction 1

2 Data Sources and Data Used 3
- 2.1 Tank Waste Level Data . . . 3
- 2.2 In-Tank Temperature Data . . . 4
- 2.3 Hanford Meteorological Station Data . . . 4
- 2.4 Gas Composition Monitoring Data . . . 6

3 Temperature Response to Gas Release Events 7
- 3.1 Expected Temperature Response to Gas Release Events . . . 7
- 3.2 Systematic Error Components of Temperature Measurements . . . 10
  - 3.2.1 Features Particular to Manual Temperature Data . . . 10
  - 3.2.2 Temperature Data Features of TMACS Data . . . 12
- 3.3 Methodology . . . 18
- 3.4 Results . . . 18

4 Level Changes in Response to GREs 27
- 4.1 Features of Tank Waste Level Data . . . 29
- 4.2 Tank Waste Level Response to Gas Release Events . . . 31
- 4.3 Methodology . . . 36
  - 4.3.1 Algorithm to Detect Breaks in Tank Level Data . . . 36
  - 4.3.2 Analyst Decisions to Refine Detected Breaks . . . 38
- 4.4 Preliminary Results . . . 42
  - 4.4.1 Methodology Strengths and Weaknesses . . . 42
  - 4.4.2 Results Summaries . . . 43

5 A Sludge Yield Model for Level - Pressure Hysteresis 49
- 5.1 Introduction . . . 49
- 5.2 A Model for Sludge Elasticity . . . 49
  - 5.2.1 Physical Basis of Model . . . 49
  - 5.2.2 Solution for a Gas Bubble in an Elastic Solid . . . 50
  - 5.2.3 Elastic Contribution to dL/dP . . . 52
- 5.3 Hysteresis in Level vs. Pressure . . . 53
  - 5.3.1 Yield Criterion . . . 53
  - 5.3.2 The Hysteresis Parallelogram . . . 54
- 5.4 Application of Model to Tank Data . . . 56
  - 5.4.1 Model Inputs . . . 56
  - 5.4.2 Results . . . 56
- 5.5 Implications . . . 57

6 References 89

Appendix A - Supporting Material for the Temperature Screening A.1

Appendix B - Precisions of tank Waste Level Measurements B.1

Appendix C - Graphic Summaries of Level Change Detection C.1

Figures

1 Vertical temperature profiles in Tank SY–101 before and after a GRE 8
2 SY–103 temperature measurements from Riser 4A, TCs 1-6 9
3 Temperature measurements for Tank A–101 11
4 Temperature measurements from thermocouples 3 and 13 for Tank A–101 12
5 Temperature measurements from thermocouples 3 and 13, with the measurement from thermocouple 1 subtracted, for Tank A–101 13
6 Tank BY–101 thermocouple 2 and 14 temperature measurements 14
7 Tank BY–101 thermocouple 2 and 14 temperature measurements, offset by thermocouple 1 measurements 15
8 Vertical temperature profiles in Tank AN–104 before and after the TMACS cabinet fan repair 16
9 Tank AN–104 TC14 temperatures bracketing the fan repair 17
10 Tank AW–101 waste level with temperature breaks 20
11 Tank waste level data for Tank SY–101 with GREs marked 31
12 SY–103 ENRAF surface level measurements 32
13 GC H_2 measurements for Tank AN–104 34
14 Level measurements for Tank AN–104 with GC-estimated GREs marked on the plot 35
15 Forward and backward extrapolations at a break point 36
16 Graphic representation of algorithm output for Tank S–102 39
17 Tank AN–103 detected breaks and break sizes. 45
18 Tank S–102 detected breaks and break sizes. 46
19 Tank SX–104 detected breaks and break sizes. 47
20 Linear-elastic stress-strain behavior with plastic yield. 50
21 Geometry of an elastic sphere surrounding a bubble. 51
22 The hysteresis parallelogram. 55
23 Tank S–106 model and data comparison 8-15-95 to 1-8-96 59
24 Tank S–106 model and data comparison 10-1-95 to 10-3-95 60
25 Tank S–106 model and data comparison 10-31-95 to 11-9-95 61
26 Tank S–106 model and data comparison 11-23-95 to 11-27-95 62
27 Tank S–106 model and data comparison 12-10-95 to 12-17-95 63
28 Tank S–106 model and data comparison 1-1-96 to 1-7-96 64
29 Tank S–107 model and data comparison 10-18-95 to 1-7-96 65
30 Tank S–107 model and data comparison 11-3-95 to 11-7-95 66
31 Tank S–107 model and data comparison 11-23-95 to 11-28-95 67
32 Tank S–107 model and data comparison 12-9-95 to 12-22-95 68
33 Tank S–107 model and data comparison 12-27-95 to 1-1-96 69
34 Tank S–111 model and data comparison 8-31-95 to 12-6-95 70
35 Tank S–111 model and data comparison 9-30-95 to 10-2-95 71
36 Tank S–111 model and data comparison 10-31-95 to 11-4-95 72
37 Tank S–111 model and data comparison 11-6-95 to 11-10-95 73
38 Tank S–111 model and data comparison 11-25-95 to 11-28-95 74
39 Tank S–111 model and data comparison 11-29-95 to 12-2-95 75
40 Tank U–103 model and data comparison 9-14-95 to 12-2-95 76
41 Tank U–103 model and data comparison 9-15-95 to 9-26-95 77
42 Tank U–103 model and data comparison 10-3-95 to 10-7-95 78

43 Tank U–103 model and data comparison 10-16-95 to 10-21-95 79
44 Tank U–103 model and data comparison 10-31-95 to 11-4-95 80
45 Tank U–103 model and data comparison 11-16-95 to 11-19-95 81
46 Tank U–107 model and data comparison 9-14-95 to 12-2-95 82
47 Tank U–107 model and data comparison 9-15-95 to 9-26-95 83
48 Tank U–107 model and data comparison 10-11-95 to 10-15-95 84
49 Tank U–107 model and data comparison 10-19-95 to 10-22-95 85
50 Tank U–107 model and data comparison 11-10-95 to 11-12-95 86
51 Tank U–107 model and data comparison 11-26-95 to 12-1-95 87
A.1 Tank BX–110 thermocouple 2 temperatures with drawn breaks A.2
A.2 Tank BX–110 thermocouple 3 temperatures with drawn breaks A.3
A.3 Tank C–103 thermocouple 2 temperatures with drawn breaks A.4
A.4 Tank C–103 thermocouple 3 temperatures with drawn breaks A.5
A.5 Tank S–101 thermocouple 2 temperatures with drawn breaks A.6
A.6 Tank SX–101 thermocouple 2 temperatures with drawn breaks A.7
A.7 Tank SX–101 thermocouple 3 temperatures with drawn breaks A.8
A.8 Tank SX–101 thermocouple 4 temperatures with drawn breaks A.9
A.9 Tank SX–101 thermocouple 5 temperatures with drawn breaks A.10
A.10 Tank SY–103 thermocouple 2 temperatures with drawn breaks A.11
A.11 Tank SY–103 thermocouple 5 temperatures with drawn breaks A.12
A.12 Tank SY–103 thermocouple 2 temperatures with drawn breaks A.13
A.13 Tank SY–103 thermocouple 7 temperatures with drawn breaks A.14
A.14 Tank SY–103 thermocouple 4 temperatures with drawn breaks A.15
A.15 Tank SY–103 thermocouple 6 temperatures with drawn breaks A.16
A.16 Tank SY–103 thermocouple 10 temperatures with drawn breaks A.17
A.17 Tank T–111 thermocouple 2 temperatures with drawn breaks A.18
A.18 Tank T–111 thermocouple 5 temperatures with drawn breaks A.19
A.19 Tank T–203 thermocouple 2 temperatures with drawn breaks A.20
A.20 Tank T–203 thermocouple 7 temperatures with drawn breaks A.21
A.21 Tank U–103 thermocouple 2 temperatures with drawn breaks A.22
A.22 Tank U–103 thermocouple 5 temperatures with drawn breaks A.23
C.1 Tank A–101 detected breaks and break sizes. C.2
C.2 Tank A–103 detected breaks and break sizes. C.3
C.3 Tank AN–104 detected breaks and break sizes. C.4
C.4 Tank AN–105 detected breaks and break sizes. C.5
C.5 Tank AW–101 detected breaks and break sizes. C.6
C.6 Tank AW–103 detected breaks and break sizes. C.7
C.7 Tank AW–104 detected breaks and break sizes. C.8
C.8 Tank AX–103 detected breaks and break sizes. C.9
C.9 Tank AY–101 detected breaks and break sizes. C.10
C.10 Tank BX–104 detected breaks and break sizes. C.11
C.11 Tank BX–107 detected breaks and break sizes. C.12
C.12 Tank BX–112 detected breaks and break sizes. C.13
C.13 Tank BY–109 detected breaks and break sizes. C.14
C.14 Tank C–105 detected breaks and break sizes. C.15
C.15 Tank C–107 detected breaks and break sizes. C.16
C.16 Tank S–101 detected breaks and break sizes. C.17

C.17 Tank S–103 detected breaks and break sizes. C.18
C.18 Tank S–105 detected breaks and break sizes. C.19
C.19 Tank S–106 detected breaks and break sizes. C.20
C.20 Tank S–107 detected breaks and break sizes. C.21
C.21 Tank S–109 detected breaks and break sizes. C.22
C.22 Tank S–111 detected breaks and break sizes. C.23
C.23 Tank SX–101 detected breaks and break sizes. C.24
C.24 Tank SX–102 detected breaks and break sizes. C.25
C.25 Tank SX–103 detected breaks and break sizes. C.26
C.26 Tank SX–105 detected breaks and break sizes. C.27
C.27 Tank SX–106 detected breaks and break sizes. C.28
C.28 Tank SY–101 detected breaks and break sizes. C.29
C.29 Tank SY–103 detected breaks and break sizes. C.30
C.30 Tank T–107 detected breaks and break sizes. C.31
C.31 Tank T–111 detected breaks and break sizes. C.32
C.32 Tank TX–107 detected breaks and break sizes. C.33
C.33 Tank TY–102 detected breaks and break sizes. C.34
C.34 Tank TY–103 detected breaks and break sizes. C.35
C.35 Tank U–102 detected breaks and break sizes. C.36
C.36 Tank U–103 detected breaks and break sizes. C.37
C.37 Tank U–105 detected breaks and break sizes. C.38
C.38 Tank U–106 detected breaks and break sizes. C.39
C.39 Tank U–107 detected breaks and break sizes. C.40
C.40 Tank U–108 detected breaks and break sizes. C.41
C.41 Tank U–109 detected breaks and break sizes. C.42

Tables

1 Number of temperature observations for each tank 5
2 Comparison of detected temperature breaks with dates of GREs since 1990. 19
3 Temperature Data Comments 21
4 Tanks and level data analyzed 28
5 Tank AN–104 comments from the SACS database 30
6 Tank AN–104 GRE dates detected by GC H_2 measurement 33
7 Tank AN–104 GREs detected using the tank level data and our methodology. 35
8 Tank S–102 detected features in 1983 and categorization 41
9 Comparison of analyst decisions on common tanks 42
10 Frequencies of detected level jumps 48
11 Hysteresis model inputs 56
12 Comparison of dL/dP from the previous and proposed model 58
B.1 Estimated precision of tank waste level measurments B.1

1 Introduction

The Hanford Site is home to 177 large, underground nuclear waste storage tanks. Numerous safety and environmental concerns surround these tanks and their contents. One such concern is the propensity for the waste in these tanks to generate, retain, and periodically release flammable gases. This report documents some of the activities of the Flammable Gas Project Data Evaluation Task conducted for Westinghouse Hanford Company during fiscal year 1996.

Described in this report are 1) the results of examining the in-tank temperature measurements for insights into gas release behavior; 2) the preliminary results of examining the tank waste level measurements for insights into gas release behavior; and 3) an explanation for the observed hysteresis in the level/pressure measurements, a phenomenon observed earlier this year when high-frequency tank waste level measurements came on-line. Background information on the data and measurements used in this report is presented in Section 2.

Each of these three activities is described in a separate section of this report; these sections may be read in any order. Section 3 presents the methodology and results of the study to detect GREs in temperature data. Section 4 presents the methodology and results of the study to detect GREs in tank waste level data. Section 5 presents a model which combines gas retention and tank waste physical properties to explain observed behaviors in tank waste level measurements. Supporting information is contained in Appendices A, B, and C.

2 Data Sources and Data Used

The data used in this report include tank waste level measurements, in-tank temperatures, atmospheric pressure data and tank headspace gas composition measurements. These measurements are discussed, respectively, in Sections 2.1, 2.2, 2.3 and 2.4.

2.1 Tank Waste Level Data

Tank waste level measurements are taken in the Hanford tanks to monitor for leaks and intrusions. Recently, these measurements have also been used to estimate retained gas volume. Four devices are used widely in these tanks. Three of these measure the level of the waste surface: they are the FIC (made by the Food Instrument Company), manual tape (MT), and ENRAF (not an acronym, but the capitalized name of the manufacturer) devices. The fourth device measures from within a well embedded in the waste, thereby monitoring the liquid level even if the liquid level is below a dry waste crust. This measurement is referred to as `Neutron ILL.` (for neutron(-count-based) interstitial liquid level). Typically, only one of the three surface level instruments is used in a tank for any extended time period. The current deployment of these devices in the Hanford tank farms is described for each tank in Hanlon (1996).

The FIC and ENRAF level measurement devices are the most accurate of the four. The work described in this report was based on these measurements.

All of the waste level measurements used in this report were retrieved from the Surveillance Analysis Computer System (SACS) database (Glasscock 1993). The level data on which this report is based represent a complete dump of the waste level measurements in the SACS database as of July 1, 1996. The initial date for the data in the dump was January 1, 1981. Measurements marked as "Suspect" in the SACS database were not considered (a waste level measurement is marked "Suspect" in SACS when it is judged to be far from the main trend of the data).

The FIC device, a plummet on the end of a steel tape, is lowered into the tank from the ground level. The waste surface is detected by the level at which an electrical circuit is completed.

The FIC plummet is controlled mechanically, and the level measurement can be recorded by a data acquisition system to the nearest tenth of an inch. Some of the FICs are read by the Computer Automated Surveillance System (CASS) data acquisition system (Spurling 1991); the rest are read manually. The manual readout on the FIC, similar to an automobile odometer, can be read to slightly better resolution than that available through CASS.

The 0.1-inch resolution provides a lower bound on the accuracy of the FIC instrument. This accuracy can be expressed as a statistical variance by noting that given an observation of, say, 78.1 inches, the level is believed to be within a 0.1-inch interval containing the value 78.1. With no other information, one may assume that the possible observations are distributed uniformly over a 0.1-inch interval. The variance of such a uniform distribution is $0.1^2/12$ inches^2.[a] This quantity is taken as a lower bound on the variance of the FIC observations.[b]

The FIC is often deployed so that the plummet is suspended just slightly above the waste

[a]The 12 in the denominator for the variance calculation results from the assumption of a uniform distribution

[b]Similarly, a lower bound on the variance of the manual tape, a measurement with a resolution of 0.25 inches, is $0.25^2/12$ inches^2

surface. The plummet is lowered every minute to obtain a reading, which is available through CASS. Typically, one of these measurements per day is recorded in the SACS database. All the FIC measurement devices are being replaced with ENRAFs.

The ENRAF gauge detects the waste surface by the change in buoyancy of a weight on the end of a wire as the weight encounters the liquid or solid waste surface. Daily measurements for this device are recorded in the SACS database. References providing more details on these devices are Brewster et al.[c] and Peters & Park (1993).

Recently, other tanks have been fitted with ENRAF instruments and connected into the tank monitoring and control system (TMACS) for data acquisition; providing the potential for very frequent level observations. In the TMACS system, a measurement (and its time) is recorded when the next measurement differs from the previous recorded measurement by at least a "delta-band" amount. The delta-band is an input quantity. For instance, if the previous level measurement were 154.667, and the delta-band for this particular measurement stream is 0.01, then the next recorded measurement would occur when the measurement differs from 154.667 by at least 0.01.

These data, when available, may be accessed from the same database as SACS. In this report we worked with data for selected tanks that spanned, approximately, the last half of 1995.

2.2 In-Tank Temperature Data

Temperature measurements are made routinely in the underground nuclear waste storage tanks by thermocouples. For many tanks, the thermocouples are arrayed on a vertical probe, accessible from above ground. The probe is installed in the tank and extends into the tank waste. These arrays are called thermocouple trees; see Appendix C of Hanlon (1996) for a brief description of this measurement device. Most tanks have only one thermocouple tree. The thermocouples on a tree are referred to by number: the thermocouple closest to the bottom of the tank is number 1, and successive numbers correspond to successively higher thermocouples. The temperature data analyzed here were obtained from SACS.

Temperature data are taken at varying frequencies, ranging from quarterly to monthly to minute-by-minute, depending on the tank and whether or not the thermocouple tree is connected to a data acquisition system. For most tanks, continuous data are available since 1991. Before then, temperatures were typically recorded only monthly for the single-shell tanks. Regular weekly or daily temperature records began for many of the Hanford tanks between 1991 and late 1995. Table 1 summarizes the availability of in-tank temperature data in SACS.

2.3 Hanford Meteorological Station Data

The Hanford Meteorological Station is the source of atmospheric pressure data used in this study. This weather station is located between the 200 East and 200 West areas on the Hanford Site (Hoitink & Burk 1994). The atmospheric pressure measurements used are single hourly measurements (not hourly averages of finer time resolution measurements). The data, including instrumentation and format of computer files, are described in Andrews & Buck (1987).

[c]Brewster, M., E. Eschbach, and Z. Antoniak. 1995. *Uncertainty Status of Selected Instruments in Tank 241-SY-101.* Letter Report PNLMIT:013095, Pacific Northwest Laboratory, Richland, Washington.

Table 1: Number of temperature observations for each tank before and after January 1, 1990. Tanks with no SACS temperature data (as of July 1 1996) are C–204, SX–115, TX–114, TX–116 and TX-117.

Tank	pre-1990	post-1990
A-101	130	283
A-102	83	19
A-103	114	21
A-104	625	751
A-105	1626	3112
A-106	112	21
AN-101	0	5113
AN-102	0	5141
AN-103	0	5244
AN-104	0	4889
AN-105	0	5246
AN-106	0	5236
AN-107	0	5247
AP-101	7	236
AP-102	20	245
AP-103	17	286
AP-104	17	248
AP-105	23	283
AP-106	24	214
AP-107	24	229
AP-108	24	239
AW-101	24	395
AW-102	24	387
AW-103	24	381
AW-104	24	376
AW-105	24	368
AW-106	24	277
AX-101	88	287
AX-102	72	106
AX-103	58	279
AX-104	87	20
AY-101	0	917
AY-102	0	1002
AZ-101	0	645
AZ-102	0	684
B-101	130	11
B-102	23	11
B-103	23	309
B-104	27	11
B-105	17	11
B-106	22	11
B-107	37	11
B-108	23	11
B-109	25	11

Tank	pre-1990	post-1990
B-110	25	11
B-111	27	8
B-112	24	11
B-201	35	12
B-202	28	147
B-203	26	12
B-204	28	11
BX-101	41	803
BX-102	35	990
BX-103	24	798
BX-104	36	0
BX-105	117	811
BX-106	35	1794
BX-107	23	800
BX-108	24	804
BX-109	0	1597
BX-110	41	999
BX-111	41	971
BX-112	24	807
BY-101	60	1378
BY-102	35	1
BY-103	66	1469
BY-104	140	2633
BY-105	121	2694
BY-106	134	1383
BY-107	53	1487
BY-108	68	1474
BY-109	15	3
BY-110	137	2302
BY-111	44	2507
BY-112	60	2496
C-101	84	815
C-102	5	814
C-103	167	979
C-104	120	843
C-105	288	1059
C-106	107	2039
C-107	126	961
C-108	62	1805
C-109	48	1947
C-110	89	852
C-111	48	1122
C-112	49	1941
C-201	33	840

Tank	pre-1990	post-1990
C-202	32	840
C-203	34	840
C-204	–	–
S-101	14	296
S-102	17	587
S-103	14	296
S-104	0	295
S-105	0	298
S-106	0	297
S-107	14	311
S-108	0	297
S-109	0	296
S-110	14	299
S-111	0	567
S-112	0	622
SX-101	18	622
SX-102	20	611
SX-103	20	623
SX-104	39	621
SX-105	19	633
SX-106	15	645
SX-107	31	912
SX-108	29	916
SX-109	37	1214
SX-110	35	914
SX-111	44	907
SX-112	32	905
SX-113	2	295
SX-114	44	908
SX-115	–	–
SY-101	6	4490
SY-102	0	2654
SY-103	0	3466
T-101	48	996
T-102	22	0
T-103	31	763
T-104	19	762
T-105	14	0
T-106	34	763
T-107	36	1409
T-108	26	759
T-109	29	758
T-110	35	961
T-111	35	817

Tank	pre-1990	post-1990
T-112	17	765
T-201	27	762
T-202	31	762
T-203	28	763
T-204	22	762
TX-101	24	0
TX-102	36	32
TX-103	47	39
TX-104	57	39
TX-105	61	329
TX-106	45	38
TX-107	58	40
TX-108	26	38
TX-109	33	39
TX-110	44	3
TX-111	63	39
TX-112	49	39
TX-113	17	38
TX-114	–	–
TX-115	31	38
TX-116	–	–
TX-117	–	–
TX-118	112	1410
TY-101	40	1520
TY-102	34	202
TY-103	21	1512
TY-104	40	1730
TY-105	46	209
TY-106	45	205
U-101	1	330
U-102	4	355
U-103	4	582
U-104	1	0
U-105	4	580
U-106	5	596
U-107	5	597
U-108	4	578
U-109	4	576
U-110	4	350
U-111	6	451
U-112	1	332
U-201	25	328
U-202	1	332
U-203	19	412
U-204	29	415

2.4 Gas Composition Monitoring Data

Standard Hydrogen Monitoring Systems (SHMS) have been installed near the exhaust headers of Tanks AW–101, SY–103, AN–103, AN–104, and AN–105. Hydrogen in the exhaust gas is detected with two Whittaker cells, which rely on the reaction of the gas with an electrode in an electrolyte. One cell has a range of 0-1%, and the other has a range of 0-10%. These instruments are tested and calibrated quarterly.

Tanks AW–101 and AN–105 are also monitored with Gas Characterization Systems (GCS). These tanks have had GREs that exceeded 6250 ppm H_2 , the current control limit for hydrogen. To learn more about the gases emitted from these tanks, GCSs were installed and began recording data in April 1996. A GCS comprises three instruments, two gas chromatographs, GCs, and a Fourier Transform Infrared Spectrometer (FTIR), which measure hydrogen, nitrous oxide, methane, and ammonia. Tank AN–104 also has a gas chromatograph which monitors the tank head space for hydrogen.

3 Temperature Response to Gas Release Events

The candidate tanks for which temperature data were examined for GRE behavior include all the SSTs, and the DSTs which are known to contain or are suspected of containing significant quantities of gas: SY–101, SY–103, AN–103, AN–104, AN–105, and AW–101. We concentrated on temperature data taken since 1990. Note that large amounts of temperature data are not available for all the SSTs.

This section reports the results of examining the in-tank temperature measurements for signs of gas releases. In the SSTs, no clear signs of gas release were detected in the temperature measurements. The rest of this section describes 1) the patterns in the temperature data that might indicate gas release; 2) the features of the data which affect the detectability of various patterns; 3) the extent to which the pattern is detectable with the available data; 4) the methodology used to examine the available data; and 5) more detailed results of the examination. Appendix A contains selected detailed data summaries showing representative temperature data; we include detailed plots of temperature data from five randomly selected tanks, including tanks for which the data was "well behaved," and tanks for which the data was not easy to interpret.

3.1 Expected Temperature Response to Gas Release Events

Some of the Hanford DSTs show a temperature measurement response to gas release events. This response was initially observed for Tank SY–101; the temperature profile changed subsequent to a GRE. The temperature change was interpreted as tank waste movement related to the gas release event. Figure 1 shows two such temperature profiles which bracket the SY–101 gas release event of April 20, 1992. A comparison of the temperature profiles before and after the gas release clearly shows a response. For other tanks, however, the temperature response to GREs is best detected by other means.

As reported in 1995,[d] Tank SY–103 sometimes shows a temperature response to gas release, but the response is not apparent in the temperature profiles. However, other views of the data clearly show the temperature response to GREs. Figure 2 shows measurements from thermocouples 1 through 6 on the thermocouple tree in riser 4A of Tank SY–103. A gas release event occurred on March 1, 1995. The gas release is marked by a sudden 2°C drop, especially noticeable for thermocouples 3 and 4 in Figure 2, and the temperature stays depressed for at least a week before gradually returning to its former value. Similar jumps in temperature occur in other burping DSTs (see data displays for Tanks AN–104, etc., in Appendix A).

[d]Neerchal, N. and Whitney, P. 1995 Letter Report "Measurement Responses to Gas Release Events in Tank 241-SY-103"

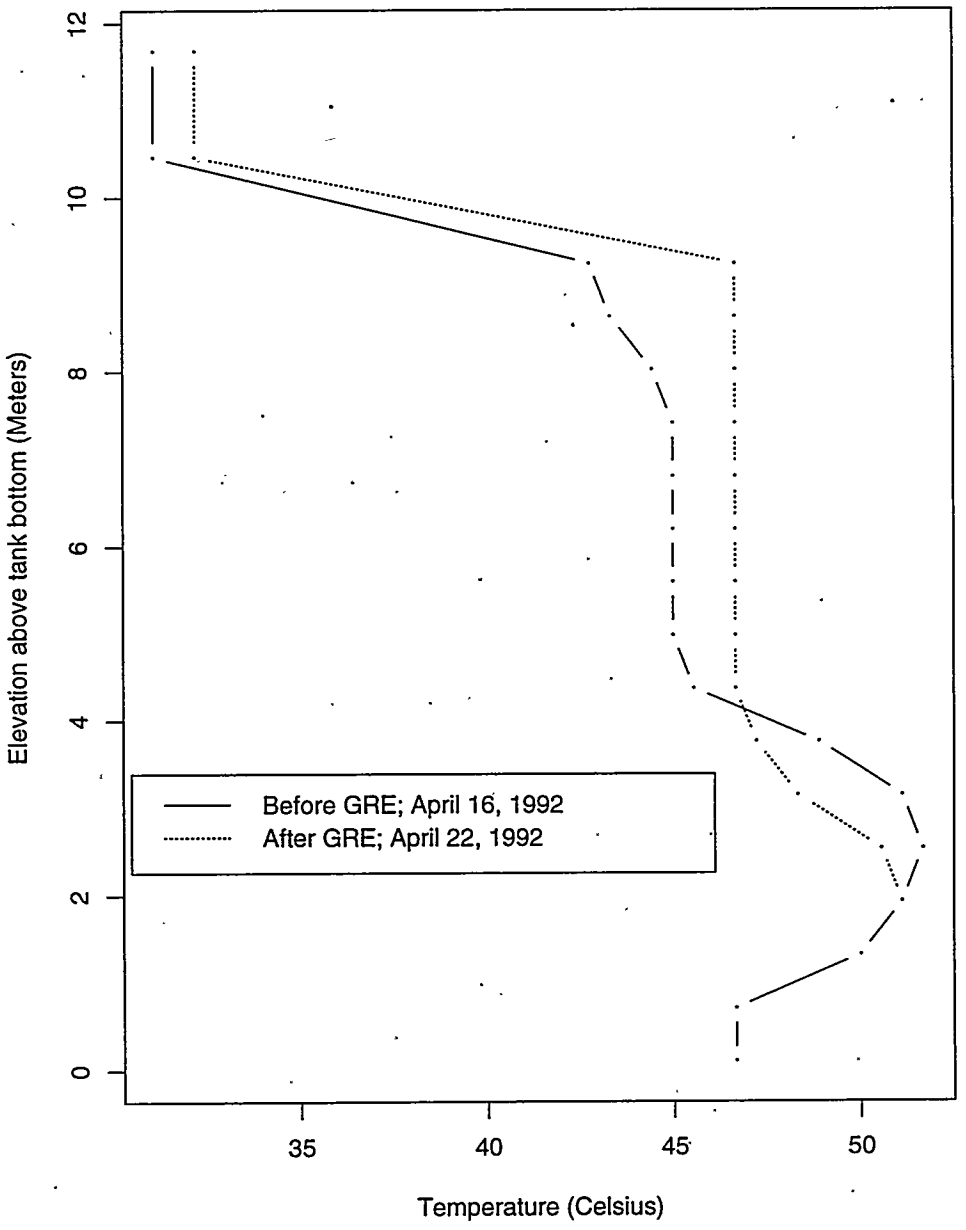

Figure 1: Vertical temperature profiles in Tank SY–101 before and after the GRE of April 20, 1992. The level drop for this gas release event is the second smallest of the 15 level drops presented in Table A.1 of (Stewart et al. 1996).

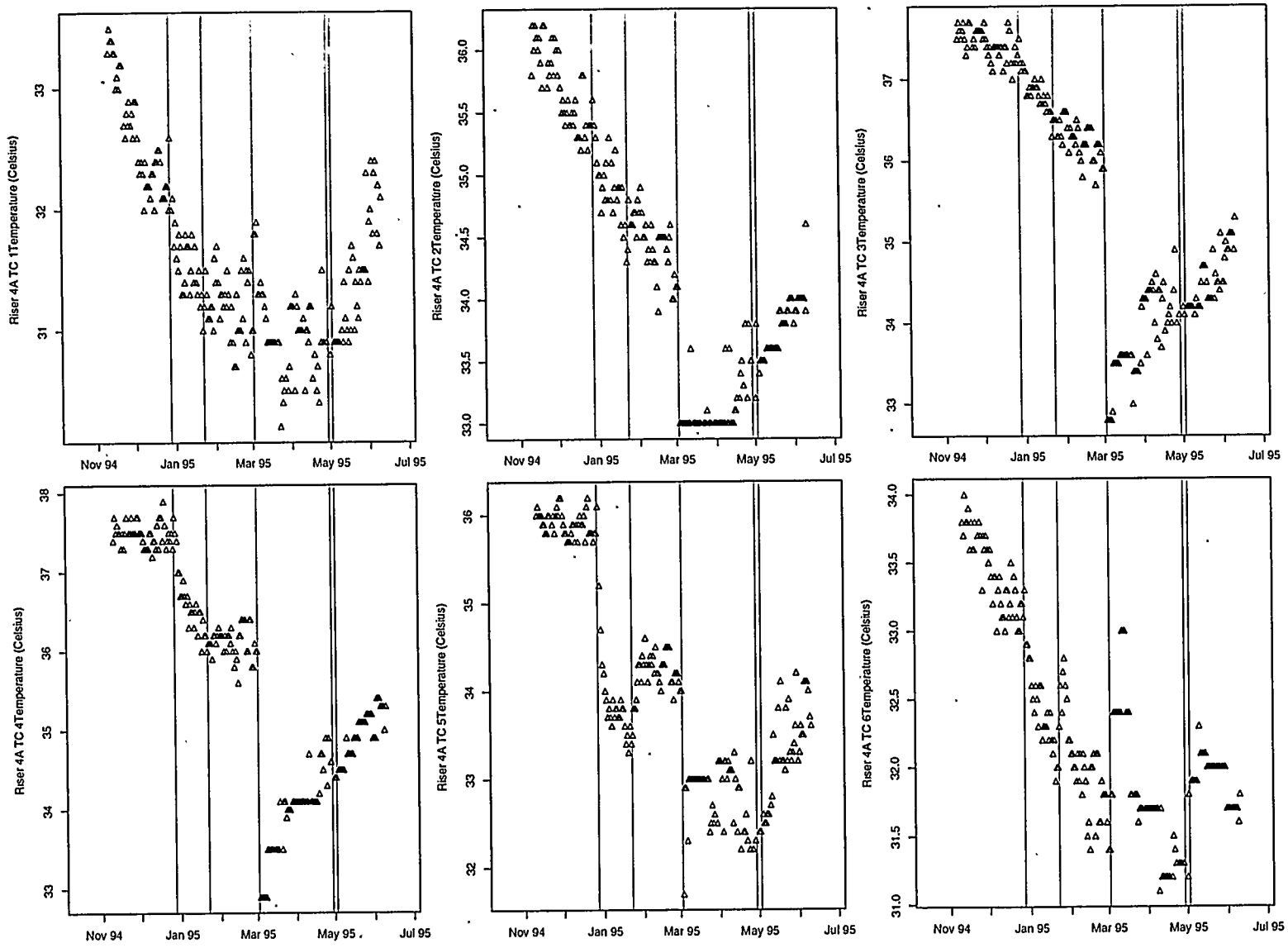

Figure 2: SY–103 temperature measurements from Riser 4A, TCs 1-6. The vertical lines mark times at which a GRE was observed using the SHMS measurements. It is not clear whether the visually apparent 1°C jump in TC 2 temperatures near March 95 is due to the delta-band change or to a temperature shift

3.2 Systematic Error Components of Temperature Measurements

Temperature measurements are obtained from thermocouple trees either by reading a voltage off a portable meter, or through the TMACS data acquisition system. Each of these paths has an effect on the accuracy of the temperature measurements.

3.2.1 Features Particular to Manual Temperature Data

One component of the error in the Hanford temperature measurements is a common, additive offset in the measurements for all the thermocouples in the tree. This additive component appears to be noticeable only for temperature data taken using the hand-held potentiometer. This section describes that error component and presents procedures to view and handle the temperature data in a way which removes this systematic error.

Two tanks are investigated below: Tank A–101 and Tank BY–101. These temperature measurements show a common offset, and various views of the data are presented which strip away this offset. A model to account for the common offset is described. Finally, the model is used to suggest ways of handling the data to eliminate the common offset.

The temperature data for Tank A–101, from 1991 through March 1995, are presented in Figure 3. The measurements from different thermocouples on the tree are distinguished by plot symbols; "a" corresponds to thermocouple 1, "b" to thermocouple 2, etc. Remember that thermocouples are numbered from the bottom of the tank to the top. Within the tank waste (i.e., near the top of the figure), the thermocouple readings are plotted on top of each other and cannot be distinguished separately. In the tank headspace (lower portion of the figure), a few thermocouples can be readily identified, particularly near the surface of the waste (e.g., thermocouple "l" or 12). The temperatures in the headspace show a clear annual cycle. Note that this cycle is not apparent in the thermocouples at the lower or bottom part of the tank (at the top of the plots).

Another feature of the data is the jump in *all* measurements that appears in mid-1992. The time of this event — June 29, 1992 — is marked with a triangle on the time axis of the plot. A change in the variability of the estimates is also evident near October 15, 1991; a triangle also marks this transition on the plot.

Figure 4 focuses on the measurements from thermocouples 3 and 13 within Tank A–101. To a large degree, the measurement fluctuations for these two thermocouples are synchronous. This observation is generally true for the in-tank temperature measurements taken using the hand-held potentiometer at the Hanford tank farms. This effect can be eliminated by subtracting one thermocouple's measured value from the other. Figure 5 presents the measurements from thermocouples 3 and 13 minus the simultaneous measurement made at thermocouple 1. The noise is significantly lessened by taking this view; indeed, it now becomes apparent that some of the thermocouple 3 ("c") measurements in this tank taken in the latter part of 1993 are systematically lower than the others.

The temperature measurements for each thermocouple at a particular point in time appear to be offset by a constant value. This offset appears to be additive, shifting all the measurements on a particular thermocouple tree up or down by some fixed amount. This behavior suggests the

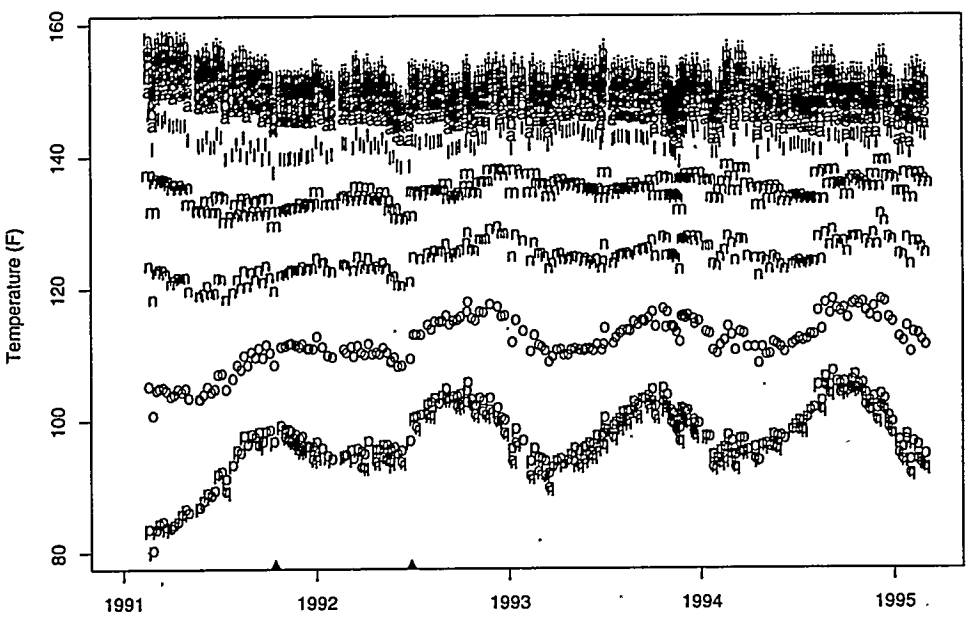

Figure 3: Temperature measurements for Tank A–101

following model:

$$\begin{aligned} T_{1j} &= f_1(t_j) + o_j + \epsilon_{1j} \\ T_{2j} &= f_2(t_j) + o_j + \epsilon_{2j} \\ &\vdots \\ T_{Mj} &= f_M(t_j) + o_j + \epsilon_{Mj}, \end{aligned} \tag{1}$$

where T are the temperature readings at times j, $j = 1, \ldots, N$, and f_i, $i = 1, \ldots, M$ represent the "true" temperature at thermocouple i. The $o_j, j = 1, \ldots, N$ terms represent the offset at the jth point in time, and the ϵ_{ij} terms represent the random error. The observed variability in temperature measurements includes both the o_j and ϵ_{ij} terms.

Subtracting thermocouple 1 measurements from thermocouple 2 measurements yields the following:

$$T_{2j} - T_{1j} = f_1(t_j) - f_2(t_j) + \epsilon_{1j} - \epsilon_{2j} \tag{2}$$

The o_j terms in T_{1j} and T_{2j} cancel out, and the observed variability is in the $\epsilon_{1j} - \epsilon_{2j}$ term. It turns out that the variability in this term is less than that in the o_j term, which is why the jump in TC3 measurements is visible in Figure 5 and is not visible in Figure 4.

Typically, when viewing the temperature data, we used TC1 to compute the offset for the other TCs on that tree. The measurement at TC1 is typically at the bottom of the tank, and so the temperature measurements for this TC are expected to be more constant over time than those higher in the tank, which clearly have a seasonal component. Another alternative for calculating the offset

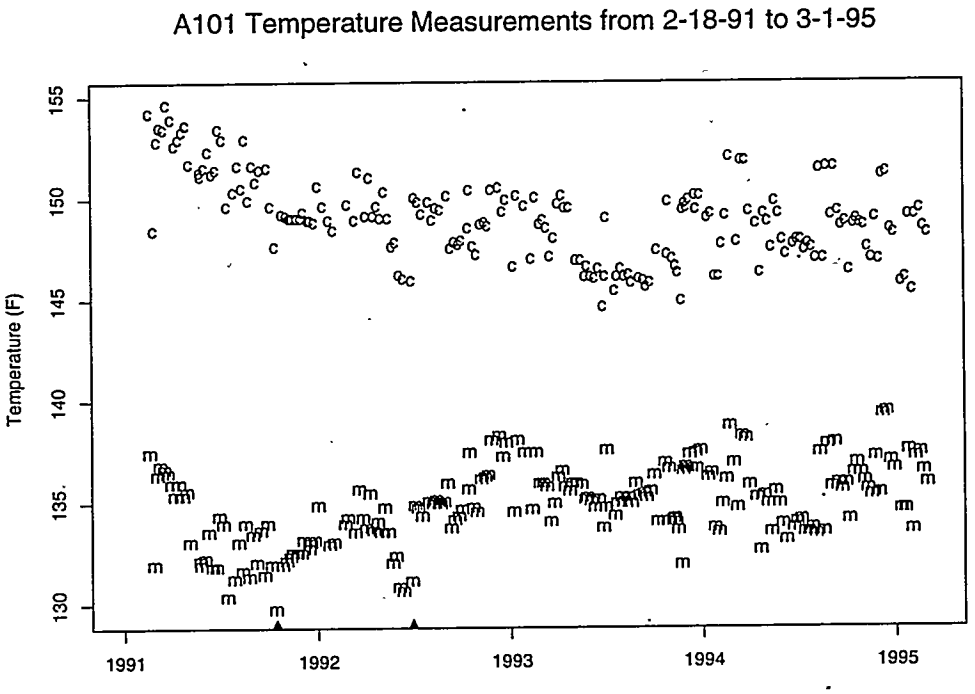

Figure 4: Temperature measurements from thermocouples 3 and 13 for Tank A–101

would be to use a (possibly weighted) average of other thermocouple measurements. A practical difficulty with this strategy is that not every thermocouple on a tree has a good measurement in the database at every sampled time.

The thermocouple tree in Tank BY–101 was connected to the TMACS in March 1993, but manual data (using the hand-held meter) is also available for this tank. Figure 6 shows temperature measurements from thermocouples 2 (in the tank waste) and 14 (in the tank headspace). The plotting characters distinguish between measurements obtained manually and measurements obtained through TMACS. Note that there is an upward jump in the TC2 temperature measurements just before the TMACS measurements came on-line. Also, the variability of the manual measurements is much higher than that of the TMACS measurements, for both TC2 and TC14.

The Tank BY–101 temperatures for TC2 and TC14, offset by TC1, are shown in Figure 7. Except for a few outliers, the variability of the TC1 offset manual and TMACS measurements now appear similar. The general observation is that the offset data view typically provides no advantage for TMACS temperature data.

3.2.2 Temperature Data Features of TMACS Data

The temperature measurements from TMACS also reflect known sources of systematic error. This section discusses a source of this systematic error and its cause. The above-ground electrical cabinet which houses the TMACS circuitry contains a fan to keep the air circulating around the Acromags and keeps their reference junction temperatures in better agreement. The fan for Tank AN–104 broke in late 1995 and was fixed near the end of February. The effect of the failure and repair is

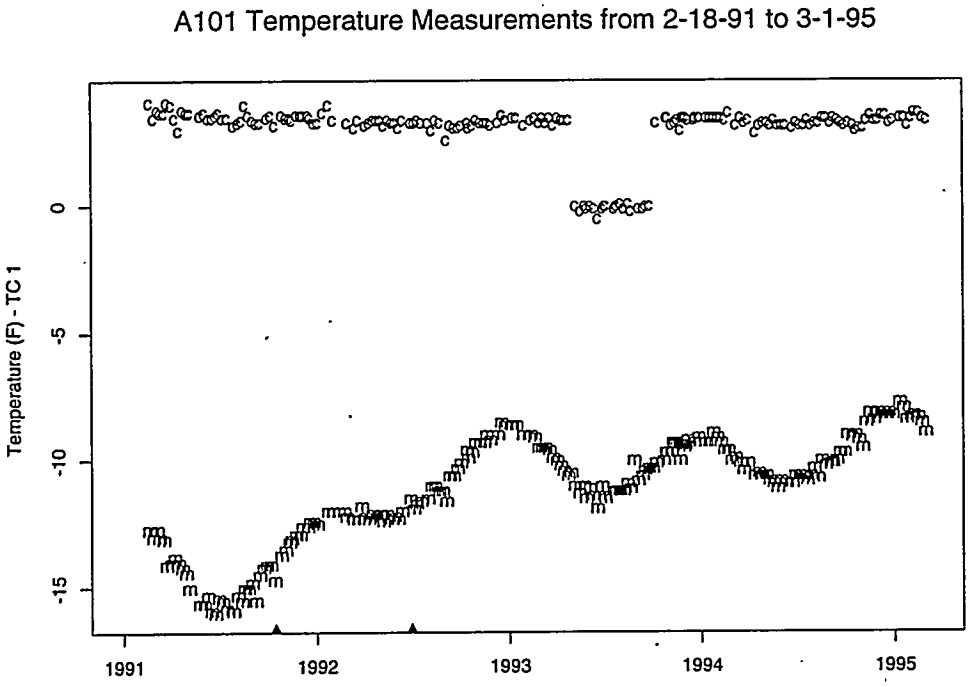

Figure 5: Temperature measurements from thermocouples 3 and 13, with the measurement from thermocouple 1 subtracted, for Tank A–101

exhibited in the vertical temperature profile shown in Figure 8. The plot shows that, prior to the fan repair, temperature increased with elevation in the "convective layer" of the tank; see Stewart et al. (1996) for a discussion of the layering of waste in this tank. The convective layer, in this case the region from about 5 meters to 9 meters above the bottom of the tank, is that portion of the waste which is primarily liquid (rather than semi-solid or sludge) and in which heat is transferred by means of convection currents. If that zone of the waste really is convective, the temperature should be approximately constant. If it is non-convective, the temperature should, at some elevation, begin to get cooler with increasing elevation. Since the temperature behavior corresponds to neither the convective nor the non-convective case, one can only conclude that the temperature measurements are suspect. The repair and return to service of the cabinet fan removed this defect from the temperature measurements. Note that the return to service of the fan also resulted in an abrupt drop of temperature measurements in the higher elevations of the tank; see Figure 9. No correction was made to the data for the period during which the fan was in disrepair, other than to note the problem.

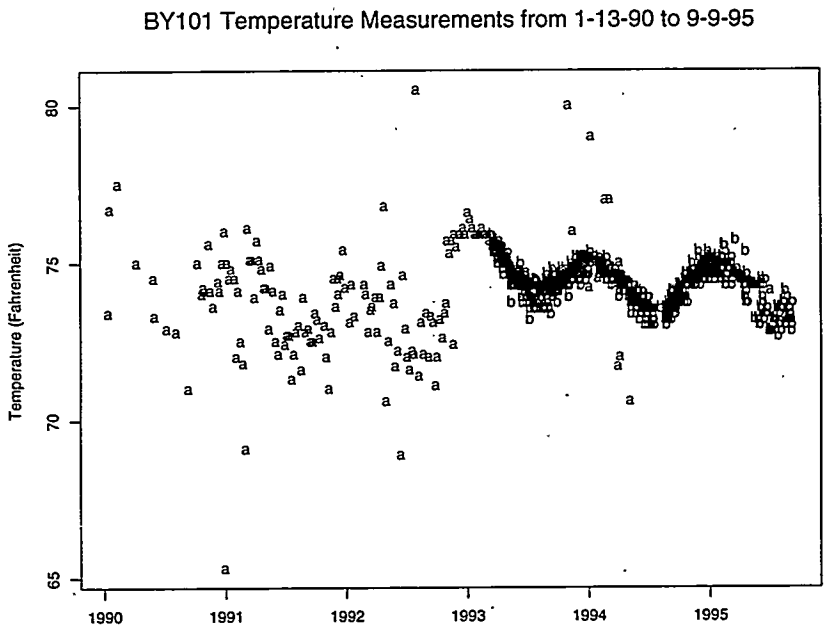

(a) Tank BY-101 thermocouple 2 temperature measurements

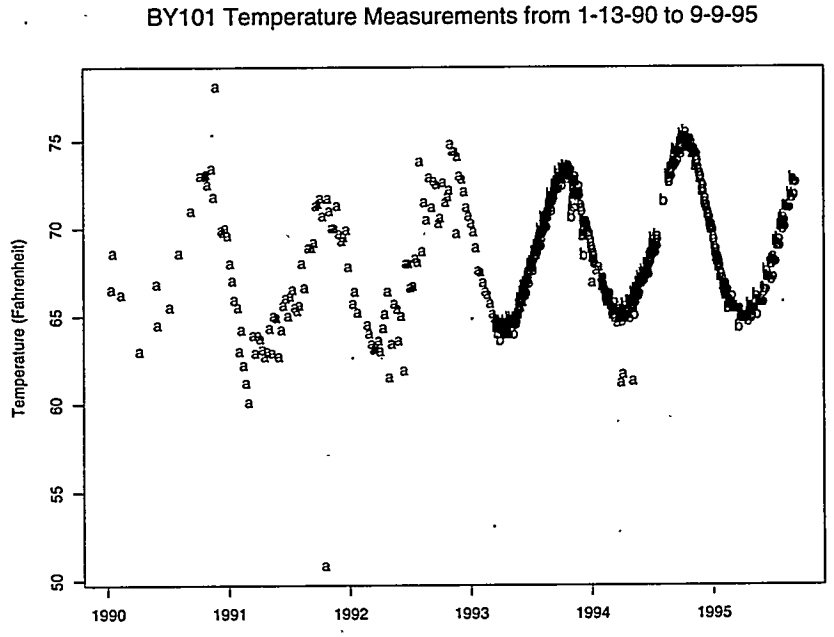

(b) Tank BY-101 thermocouple 14 temperature measurements

Figure 6: Tank BY–101 thermocouple 2 and 14 temperature measurements. Measurements labeled "a" were obtained using the hand-held meter; measurements labeled "b" were obtained through TMACS

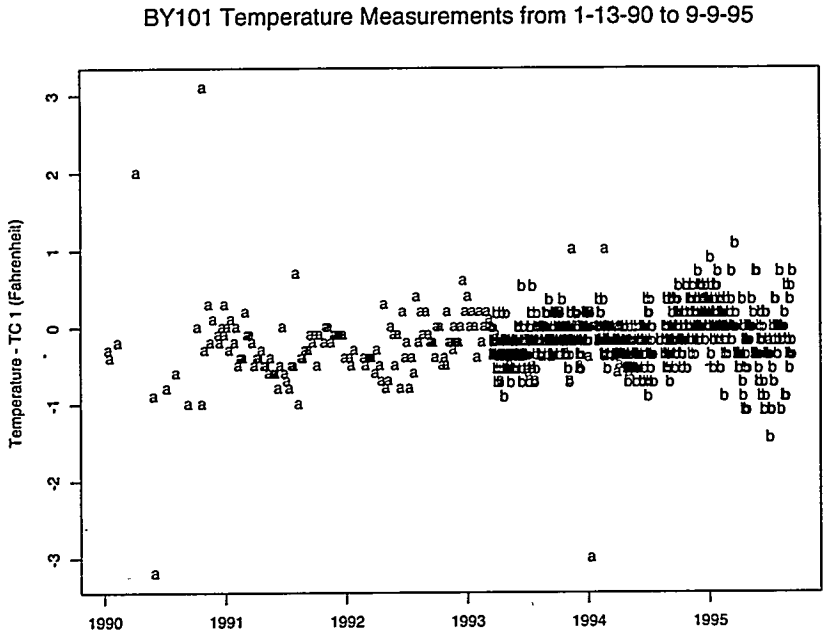

(a) Tank BY–101 thermocouple 2 minus thermocouple 1 temperature measurements

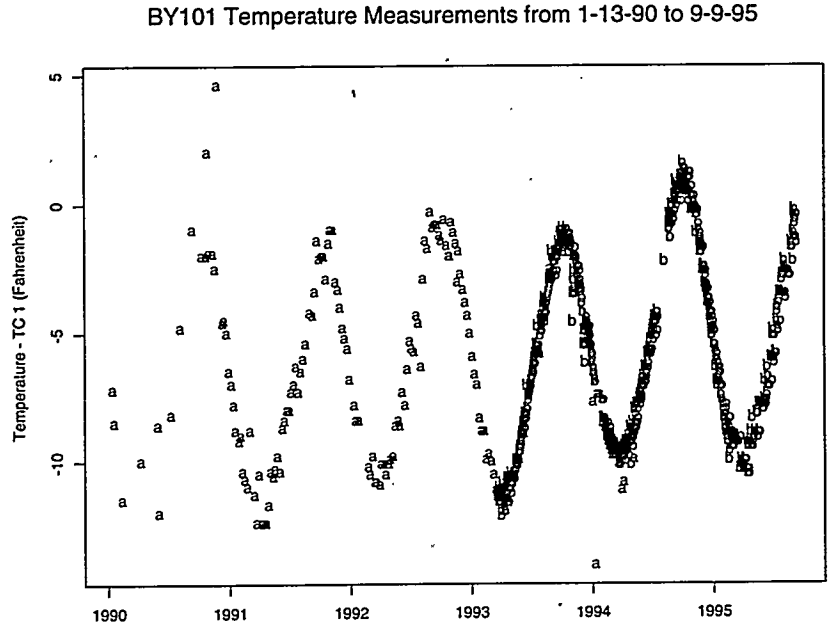

(b) Tank BY–101 thermocouple 14 minus thermocouple 1 temperature measurements

Figure 7: Tank BY–101 thermocouple 2 and 14 temperature measurements, offset by thermocouple 1 measurements. Measurements labeled "a" were obtained using the hand-held meter; measurements labeled "b" were obtained through TMACS

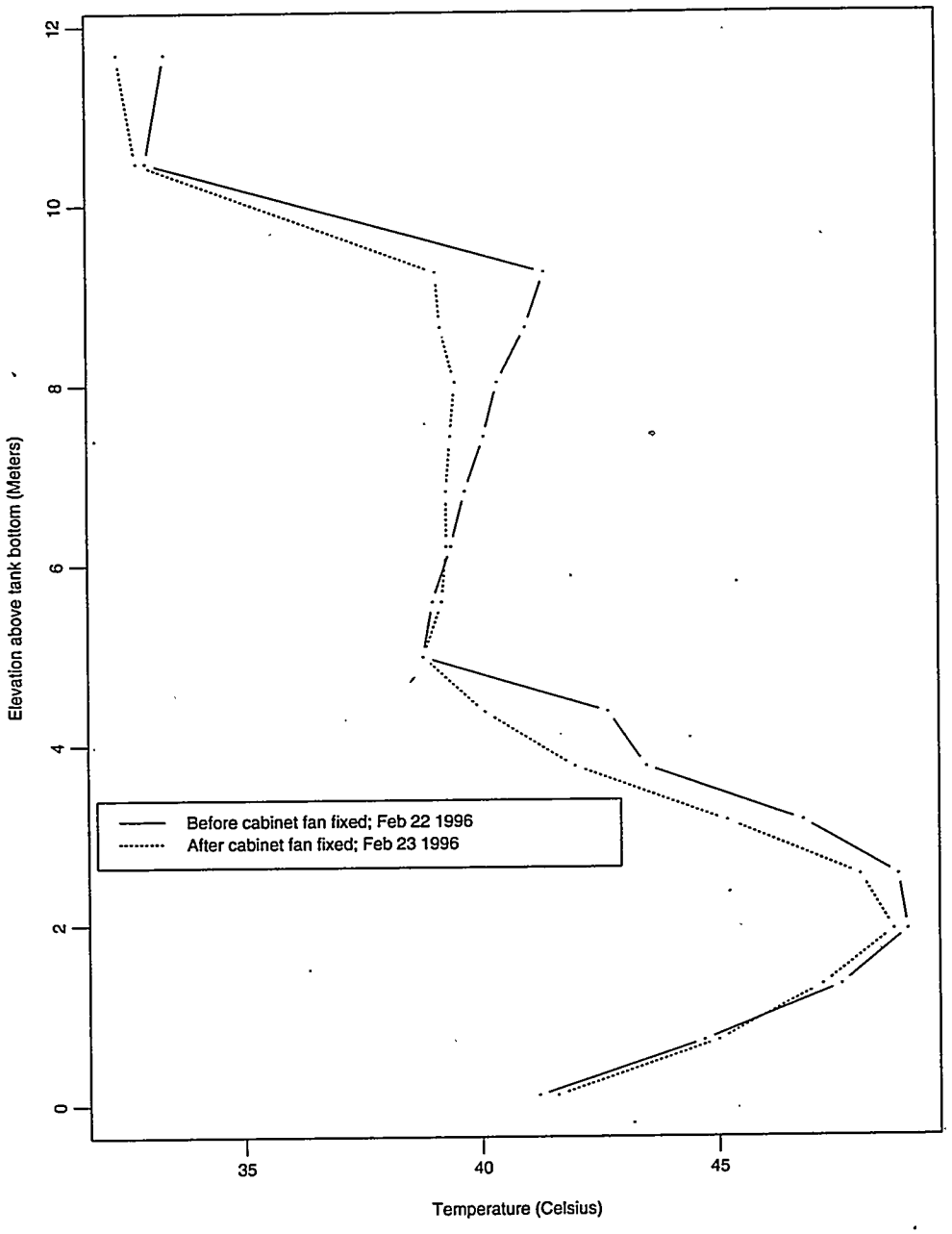

Figure 8: Vertical temperature profiles in Tank AN–104 before and after the TMACS cabinet fan repair.

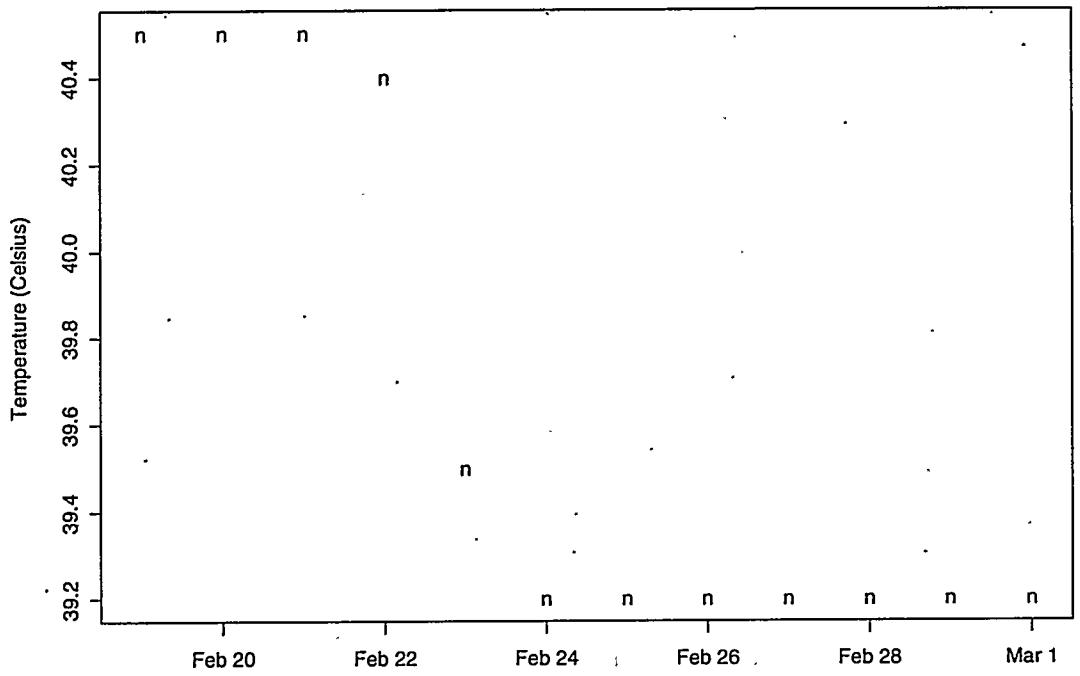

Figure 9: Tank AN–104 TC14 temperatures bracketing the fan repair.

3.3 Methodology

To find temperature changes in other tanks that might signal a gas release, the "offset" temperature was calculated, and this data was examined for jumps of 2°C or larger. From plots of the temperature data and the times of the 2°C jumps, a decision was made as to whether the jumps were "clean breaks" or not. Samples of these plots are in Appendix A.

If any of the following conditions held, the temperature jumps, or other disturbances found in the data, were discounted (that is, the data was not regarded as indicating a possible gas release event).

- The jumps were the result of a single outlying point.

  An isolated measurement more than 2°C away from others would result in two flags; see, for instance, Figure A.1 in Appendix A.

- The jumps were coincident with saltwell pumping of the tank waste.

  Saltwell pumping results in motion of the waste, which results in temperature changes in the part of the tank in which the waste is moving. See Figure A.1 for an example of the effect of saltwell pumping on in-tank temperature measurements.

- The jumps occurred in most of the thermocouple measurements, including those in the tank headspace.

  While a gas release might result in enough motion of the waste that an abrupt temperature change occurs, the effect on the headspace temperature has been observed to be minimal. Hence, events where the temperature measurement jumps at the same time in the headspace and in the waste are interpreted as instrumentation-related, as opposed to GRE-related.

- The jumps occurred when the thermocouple tree measurements were put onto TMACS.

  The jumps, if present, are interpreted as due to the change in instrumentation.

This filter was applied to all TMACS temperature data since 1990, on all SSTs and on selected DSTs, including data from thermocouple trees and Multifunction Instrument Trees (MITs) — with only two exceptions: waste temperature data was not analyzed (1) for any tank that did not have at least 6 months of weekly (or higher frequency) measurements or (2) for any tank with a waste level of less than 50 centimeters. Finally, as noted earlier, some tanks have no temperature data in SACS (see Table 1).

3.4 Results

Some detected temperature changes showed the temperature suddenly decreasing or increasing, then gradually returning to its baseline. This behavior signals some form of tank activity. In double-shell tanks, such temperature patterns sometimes reflect gas releases (confirmed by hydrogen measurement data) or waste transfers. In single-shell tanks, this behavior sometimes indicates saltwell pumping. However, other than the jump in TC3 for Tank A–101 shown in Figure 5, most of the jumps detected in offset temperatures for SSTs were discounted by one of the four criteria discussed in Section 3.3. Additionally, since most tanks have only a single thermocouple tree and

many GREs are local, any GRE on the opposite side of the tank from the thermocouple tree will likely not be observed by temperature changes.

This jump in TC3 temperature for Tank A–101 has no corresponding feature in other TCs on the same tree, suggesting that the jump is instrumentation-related, rather than reflecting a local shift in the tank waste.

Other unexplained features in the SST temperature measurements do not resemble the gas release behavior of the DSTs. For instance, TC4 in Tank SX–101 is very noisy for 3.5 years, and then the noise level decreases significantly; see Figure A.8 in Appendix A. This behavior suggests some sort of repair or change in the system, perhaps related to the introduction of TMACS for this tank's temperature measurements. Also for this tank, in TC3, a number of unusual measurements occurred near the beginning of 1994; see Figure A.7.

To calibrate these results, we compared the detected temperature breaks for some DSTs with the current best estimates of GRE dates. The conclusion is that the temperature data misses many known GREs, and makes a couple of unusual, possibly incorrect, calls. On the other hand, the temperature data also detected some previously undetected (possible) GREs. Table 2 summarizes the comparison. In this table, the counts in the "Number of GREs" column are obtained from (Stewart et al. 1996). Overall, 12 of 86 GREs are detected via the temperature data and the methodology used in this report.

Some of the temperature breaks not matching any of the GRE dates are interesting. The temperature break in Tank AN–105 of October 28, 1994 does not correspond to a jump in tank waste level. But, at that time the rate of increase in the level decreased abruptly, suggesting that on this date some gas-related event occurred in this tank. For Tank AW–101, the temperature break detected on December 6, 1993 occurs during a time span when no FIC or ENRAF level data are available. However, amazingly enough, this date corresponds with a huge drop in the MT waste level measurements (see Figure 10). For Tank SY–103, temperature breaks not matching known GREs occur in November 1995, July 1991 and March 1993. The November 1995 temperature break does not correspond with any features in the tank waste level measurements. The July 1991 temperature break corresponds with a time at which the level data changes from trending downward to trending upward. The March 1993 temperature break corresponds with a small drop in tank waste level. The simultaneous behavior of the temperature and the level measurements supports the hypothesis that two of these three apparent "false calls" are indeed gas release related. Table 3 summarizes the entire analysis, and provides more details on these behaviors.

Table 2: Comparison of detected temperature breaks with dates of GREs since 1990.

Tank	Number of GREs	Number of Temperature Breaks matches GRE date / does not match
AN–103	17	0/0
AN–104	25	5/1
AN–105	12	2/2
AW–101	9	1/1
SY–103	23	4/2

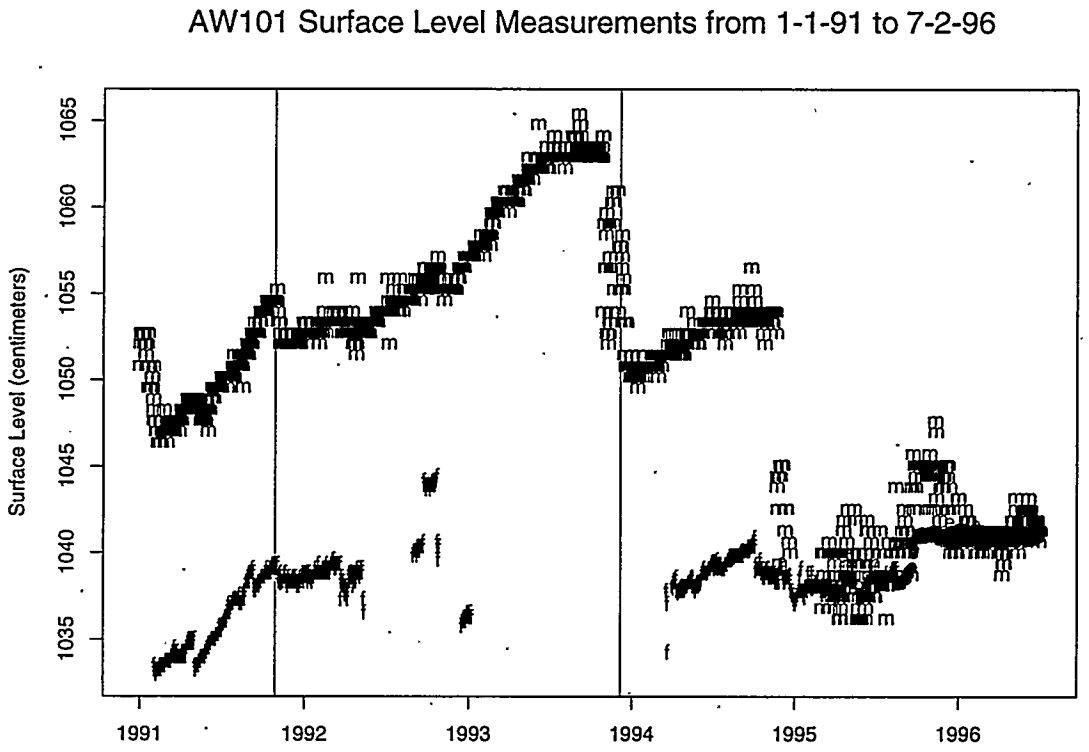

Figure 10: Tank AW–101 waste level with temperature breaks drawn as vertical lines. Interestingly, the manual tape data (drawn as "m"'s) confirms the GREs estimated from the temperature data.

Table 3: Temperature Data Comments

Tank	Comment
A–101	data anomoly; TC 3 jumps down then up about Apr-Dec 1993
A–102	Less than 50cm of tank waste level 19 observations since 1990
A–103	21 observations since 1990
A–104	Less than 50cm of tank waste level
A–105	Less than 50cm of tank waste level
A–106	21 observations since 1990
AN–103	TMACS fan turned on in fall '94; temperature jumps down then back up (Apr 94): gap in data is present, these 3 TC's lower after gap
AN–104	TC 5 contains a break in late 1990. TC 3 and 5 breaks resembling GREs at Jan 6, 1991 (closest level drop occurred Jan 16), also August 30, 1993 (level drop occurred Aug. 28). Also June 1992 GRE detected. For TC5, 6 Algorithm caught May '96 GRE; also see shifts in fall '94 and spring '96, where TMACS cabinet fan was turned off and on
AN–105	No breaks
AW–101	TC 5, 6 Late 91 GRE; early 90 GRE detected as well.
AW–104	No breaks
AX–101	No breaks
AX–102	Less than 50cm of tank waste level
AX–103	No breaks
AX–104	Less than 50cm of tank waste level 20 observations since 1990
AY–101	No breaks
B–101	11 observations since 1990
B–102	Less than 50cm of tank waste level 11 observations since 1990
B–103	Less than 50cm of tank waste level
B–104	11 observations since 1990
B–105	11 observations since 1990
B–106	11 observations since 1990
B–107	11 observations since 1990
B–108	11 observations since 1990
B–109	11 observations since 1990
B–110	11 observations since 1990
B–111	8 observations since 1990
B–112	Less than 50cm of tank waste level 11 observations since 1990
B–201	12 observations since 1990
B–202	TC 3 (offset with TC 1) data anomaly early '96; jump up, then down below baseline, then back to baseline The raw temperature data shows a general disturbance lstr 95 to early 96.
B–203	12 observations since 1990
B–204	11 observations since 1990
BX–101	No breaks
BX–102	No breaks
BX–103	No breaks
BX–104	No post 1990 temperature data in SACS

Table 3: *(continued)*

Tank	Comment
BX–105	No breaks
BX–106	No breaks
BX–107	No breaks
BX–108	Less than 50cm of tank waste level
BX–109	No breaks
BX–110	No breaks
BX–111	No breaks
BX–112	No breaks
BY–101	No breaks
BY–102	1 observations since 1990
BY–103	No breaks
BY–104	No breaks
BY–105	No breaks
BY–106	TC4,5: gradual decrease then gradual increase back to just below the baseline in Aug '95 (saltwell pumped, surface level decrease from 620 to 540 cm)
BY–107	TC1,2; increase in late '91 (looks like instrument calibration change) offset.tc=1. No jump in the measurements in the headspace; however, TC 10 in the headspace transition from not showing seasonalality to showing seasonality at about the same time.
BY–108	Very similar behavior with BY107; jump shown in late 1991.
BY–109	3 observations since 1990
BY–110	TC5: decrease in early '92, then back to baseline; manual tape decreased from 256 to 250 cm during that time; likely due to saltwell pumping.
BY–111	No breaks
BY–112	No breaks
C–101	No breaks
C–102	No breaks
C–103	No breaks
C–104	No breaks
C–105	No breaks
C–106	For a detailed discussion of tank C-106 temperatures, see Eyler (1995).
C–107	No breaks
C–108	Less than 50cm of tank waste level
C–109	Less than 50cm of tank waste level
C–110	No breaks
C–111	Less than 50cm of tank waste level
C–112	No breaks
C–201	Less than 50cm of tank waste level
C–202	Less than 50cm of tank waste level
C–203	Less than 50cm of tank waste level
C–204	Less than 50cm of tank waste level No temperature data in SACS
S–101	TC1 drops 3C in mid 1993.

Table 3: *(continued)*

Tank	Comment
S–102	Jump in late 1995, due to transition to TMACS.
S–103	No breaks
S–104	No breaks.
S–105	Data gap in May 1996, all temperatures down after the gap, slow increase to normal after that em even in the headspace temperatures
S–106	No breaks
S–107	No breaks
S–108	TC5, 6 early 96, temperatures change in response to saltwell pumping.
S–109	No breaks
S–110	No breaks
S–111	No breaks
S–112	No breaks
SX–101	No breaks
SX–102	No breaks
SX–103	No breaks
SX–104	No breaks
SX–105	No breaks
SX–106	No breaks
SX–107	No breaks
SX–108	No breaks
SX–109	No breaks
SX–110	No breaks
SX–111	No breaks
SX–112	No breaks
SX–113	Less than 50cm of tank waste level
SX–114	No breaks
SX–115	Less than 50cm of tank waste level No temperature data in SACS
SY–101	No breaks
SY–103	The thermocouple tree in riser4A shows jumps at various TC's as follows: TC2,4 give 5-9-91 or 4-29-91, 1-13-92, 7-22-91 (using the offset), 3-29-93 and 3-2-95. The 1993 and earlier breaks were called based on weekly data. Two of these dates (1-13-92 and 3-2-95) correspond with a GRE as called in Wilkins (1996). The measurements from the MIT in riser 17 are more noisy; however, breaks are observed at 10-19-95 (TC7) and 2-7-95 (TC9). Neither of these dates correspond with a GRE.
T–101	No breaks
T–102	Less than 50cm of tank waste level No post 1990 temperature data in SACS
T–103	Less than 50cm of tank waste level
T–104	No breaks
T–105	No post 1990 temperature data in SACS
T–106	Less than 50cm of tank waste level
T–107	No breaks
T–108	Less than 50cm of tank waste level

Table 3: *(continued)*

Tank	Comment
T–109	No breaks
T–110	No breaks
T–111	No breaks
T–112	No breaks
T–201	No breaks
T–202	No breaks
T–203	No breaks
T–204	No breaks
TX–101	No post 1990 temperature data in SACS
TX–102	No breaks
TX–103	No breaks
TX–104	No breaks
TX–105	No breaks
TX–106	No breaks
TX–107	Less than 50cm of tank waste level
TX–108	No breaks
TX–109	No breaks
TX–110	3 observations since 1990
TX–111	No breaks
TX–112	No breaks
TX–113	No breaks
TX–114	No temperature data in SACS
TX–115	No breaks
TX–116	No temperature data in SACS
TX–117	No temperature data in SACS
TX–118	No breaks
TY–101	No breaks
TY–102	No breaks
TY–103	No breaks
TY–104	No breaks
TY–105	No breaks
TY–106	Less than 50cm of tank waste level
U–101	Less than 50cm of tank waste level
U–102	No breaks
U–103	No breaks
U–104	No post 1990 temperature data in SACS
U–105	No breaks
U–106	No breaks
U–107	No breaks
U–108	No breaks
U–109	No breaks
U–110	No breaks
U–111	No breaks

Table 3: *(continued)*

Tank	Comment
U–112	Less than 50cm of tank waste level
U–201	No breaks
U–202	No breaks
U–203	No breaks
U–204	Less than 50cm of tank waste level

4 Level Changes in Response to GREs

Tank headspace gas monitoring is relatively recent in the Hanford tanks. For DSTs, gas monitoring extends back a few years (Wilkins 1995). For SSTs, gas monitoring extends back less than a year (Brown 1996). However, the contents of many SSTs have remained unchanged since the late 1970s. Further, the contents of all but one (SY–103) of the burping DSTs have remained unchanged since the mid-1980s (see Table 4). Thus, for a more complete view of the tanks' GRE history, tank waste level changes were identified and catalogued for selected tanks. This section presents the results of detecting abrupt changes in the tank waste level data. Generally, the DSTs AN–104, AN–105, AW–101, SY–101 (historical) and SY–103 show the most level changes. Tank AN–103's estimated frequency of level changes is comparable to some of the SSTs.

A subset of the Hanford tanks was examined. Tanks selected for this study were those for which a level response to atmospheric pressure changes was detected. Only the FIC and ENRAF level data were examined for these tanks. These level measurements are the most accurate available over a long time period. Finally, for the DSTs, the level measurements were examined starting approximately at the time of the last transfer of waste into or out of the tank. Table 4 shows the tanks and time periods analyzed, as well as whether the tanks have FIC or ENRAF data. In addition, the information for SY–101 was collected before the the mixer pump was inserted, primarily to provide a point of reference for the other tanks.

Gas releases have been observed to result in rapid changes in tank waste level; however, numerous factors besides GREs cause abrupt changes in tank waste level. Waste transfers result in rapid level changes. The instrumentation itself can be related to level changes. For instance, tank waste tends to build up on the tip of the FIC device probe. When the waste breaks off (or is flushed off as part of instrument maintenance) a large change in the level measurements can result. The ENRAF calibration procedure also introduces the potential for a change in the level measurement. Thus, knowing when events like these occur is an important part of interpreting the waste level data.

The methodology used to catalogue rapid changes in tank waste level combines an algorithm, to detect changes in the level, and human intervention, to interpret the comments noted in the database and to refine the selections of the algorithm. Details and an example are provided later (section 4.3).

The primary source for the level data in this report are the comments in the SACS database. The comments were used to determine whether a specific level change corresponded to any of the above events or otherwise, if instrument performance was suspect. Note that the SACS comments are not a formal recording of tank activities. There is no requirement to enter comments associated with the various tank activities, nor are there "standard" comments associated with the various activities. Thus, the comments are expected to be incomplete, and different individuals will, potentially, interpret the comments in different ways.

The following section provides background on the FIC and ENRAF level measurements. Section 4.2 describes the behavior of the tank waste level measurements subsequent to known GREs for Tanks SY–101, SY–103, and AN–104. For SY–101, SY–103, and AN–104, the times of GREs are known for fairly extended periods, based on monitoring the H_2 concentration in the tank headspace. Additionally, Section 4.2 describes the performance of the break detection methodology in detecting GREs for Tank AN–104. Section 4.3 describes the methodology used for the break detection. Section 4.4 presents the results. Supporting material is contained in Appendices B and C.

Table 4: Tanks and level data analyzed. The default starting date was 1-1-81. For the DSTs, the analysis started shortly after the last waste transfer into or out of the tank.

Tank	Data start date	Data end date	Number of FIC Measurements	Number of ENRAF Measurements
A–101	1-1-81	7-1-96	71	126
A–103	1-1-81	7-1-96	2101	0
AN–103	2-1-86	7-1-96	2222	335
AN–104	4-1-85	7-1-96	2446	333
AN–105	4-1-85	7-1-96	2407	333
AW–101	7-1-86	7-1-96	1593	322
AW–103	11-1-94	7-1-96	558	34
AW–104	5-1-91	7-1-96	1700	171
AX–103	1-1-81	7-1-96	480	19
AY–101	9-1-96	7-1-96	0	0
BX–104	1-1-81	7-1-96	1871	99
BX–107	1-1-81	7-1-96	1766	27
BX–112	1-1-81	7-1-96	2425	109
BY–101	1-1-81	7-1-96	1	0
BY–102	1-1-81	7-1-96	0	0
BY–103	1-1-81	7-1-96	0	0
BY–105	1-1-81	7-1-96	0	0
BY–109	1-1-81	6-1-91	889	0
C–104	1-1-81	7-1-96	2049	0
C–105	1-1-81	7-1-96	2498	0
C–107	1-1-81	7-1-96	2088	707
S–101	1-1-81	7-1-96	1602	501
S–102	1-1-81	7-1-96	3388	89
S–103	1-1-81	7-1-96	1832	944
S–105	1-1-81	7-1-96	658	20
S–106	1-1-81	7-1-96	2000	907
S–107	1-1-81	7-1-96	2035	913
S–109	1-1-81	7-1-96	786	18
S–111	1-1-81	7-1-96	1970	859
SX–101	1-1-81	7-1-96	209	33
SX–102	1-1-81	7-1-96	264	30
SX–103	1-1-81	7-1-96	1482	30
SX–104	1-1-81	7-1-96	524	420
SX–105	1-1-81	7-1-96	284	30
SX–106	1-1-81	7-1-96	1805	863
SY–101	1-1-81	7-1-93	4221	0
SY–103	5-1-89	7-1-96	1649	743
T–107	1-1-81	7-1-96	1714	1336
T–111	1-1-81	7-1-96	1790	357
TX–102	1-1-81	7-1-96	0	5
TX–107	1-1-81	7-1-96	2006	19
TX–111	1-1-81	7-1-96	0	4
TX–112	1-1-81	7-1-96	0	4
TX–113	1-1-81	7-1-96	0	1
TX–115	1-1-81	7-1-96	0	4
TY–102	1-1-81	7-1-96	2138	420
TY–103	1-1-81	7-1-96	242	184
U–102	1-1-81	7-1-96	223	14
U–103	1-1-81	7-1-96	1932	995
U–105	1-1-81	7-1-96	1335	1000
U–106	1-1-81	7-1-96	1973	992
U–107	1-1-81	7-1-96	3110	995
U–108	1-1-81	7-1-96	218	76
U–109	1-1-81	7-1-96	3062	1004

4.1 Features of Tank Waste Level Data

Waste levels are measured in the Hanford tanks primarily to monitor for leaks and intrusions. An overview of the measuring instruments and a description of their deployment in the Hanford tanks is provided in Hanlon (1996). This section provides additional information about the FIC (made by the Food Instrument Company) and ENRAF (not an acronym, but the capitalized name of the manufacturer) devices. As discussed in Section 2.1, all of the waste level measurements used for this investigation were retrieved from the SACS database.

Two aspects of measurement accuracy need to be kept in mind:

- The absolute accuracy, that is, the level of the surface (at the point the measurement is being taken) relative to the bottom of the tank;
- The accuracy from one measurement to another, that is, how well the instrument measures level changes.

While both aspects of the measurement accuracy are important in evaluating flammable gas hazards, the measurement-to-measurement accuracy is an explicit input to the methodology described in Section 4.3.1.

Table B.1 in Appendix B contains estimated standard deviations for the measurement-to-measurement accuracy for the Hanford tank level measurements; a standard deviation is provided for each tank and instrument. The standard deviation is estimated in a way that corrects some of the known systematic contributions to the measurement-to-measurement error: atmospheric pressure fluctuations and linear trends are both accounted for, using the methodology described in Whitney (1995). The ENRAF tends to be the most accurate of these measurements, followed by the FIC, Manual Tape and Neutron ILL. Appendix B contains additional details on how these standard deviations were estimated.

Another key feature of the tank waste level measurements in SACS is that sometimes maintenance or repair performed on the level measurement device, or other events of note related to the measurement, are recorded in a comment field associated with the measurement. Table 5 is a subset of the comments associated with recent FIC and ENRAF measurements for Tank AN–104. Note that the comments can sometimes appear cryptic (e.g., the comment on 1-5-95); but on the whole, these comments provide valuable supplementary information for interpreting the tank waste level data. These comments are used to determine whether a level break is due to instrumentation, waste transfer or some other cause; see Section 4.2 for more details.

Table 5: Tank AN–104 comments from the SACS database for the ENRAF and FIC level data from 10-1-94 through 7-1-96. Such comments are associated with a specific level measurement. The comments are presented here exactly as they were found in the database. The associated level measurement is described as "Manual" or "Automatic" depending on whether the level measurement was taken in the field and typed into the database or arrived via a data acquisition system.

Date	Instrument	Comment
11-7-94	Auto FIC	drop due to Hg (sic) release
1-5-95	Manual FIC	Taken by Ins. Tech.
2-16-95	Auto FIC	Hydrogen release
4-24-95	Auto FIC	Not bobbing correctly–reads between 385 and 385.6
4-25-95	Auto FIC	30 Gal. to FIC flush port for better continuity
5-24-95	Manual FIC	Swings-rolled up for flush
7-31-95	Auto FIC	FIC removed on swings for ENRAF install–Baseline set at zero on 8/17/95 from B.L. of 385.90
9-10-95	Manual ENRAF	Days reading –365.94 from graves reading recorded wrong??
10-2-95	Manual ENRAF	Hydrogen release
10-3-95	Manual ENRAF	Hydrogen release
10-8-95	Manual ENRAF	Hydrogen release
2-13-96	Manual ENRAF	6 Gal. fush-Calibrated (sic), level difference =.10"
3-26-96	Manual ENRAF	106.7 gals install viscometer
3-27-96	Manual ENRAF	222 Gal. for viscometer work
3-28-96	Manual ENRAF	128.9 gals-water lance
4-1-96	Manual ENRAF	26.6 Gal flush viscometer
4-2-96	Manual ENRAF	105gals-flush voidmeter
4-4-96	Manual ENRAF	363 Gal. flush
5-4-96	Manual ENRAF	Gas release

4.2 Tank Waste Level Response to Gas Release Events

This section presents data showing how tank waste level measurements respond to gas release events. The tanks examined here are SY–101, SY–103 and AN–104, because those are the tanks for which we currently have the best information. All are DSTs and all are known to release gas from the tank waste.

In response to gas release events, Tank SY–101 waste levels drop fairly rapidly. Figure 11 shows the levels and the larger GREs; the dates for the GREs were taken from Stewart et al. (1996). The explanation for the level behavior is that, during the time the level is rising, gas is being generated and trapped in the tank waste. The rapid level drops correspond to the release of retained gas from the tank waste.

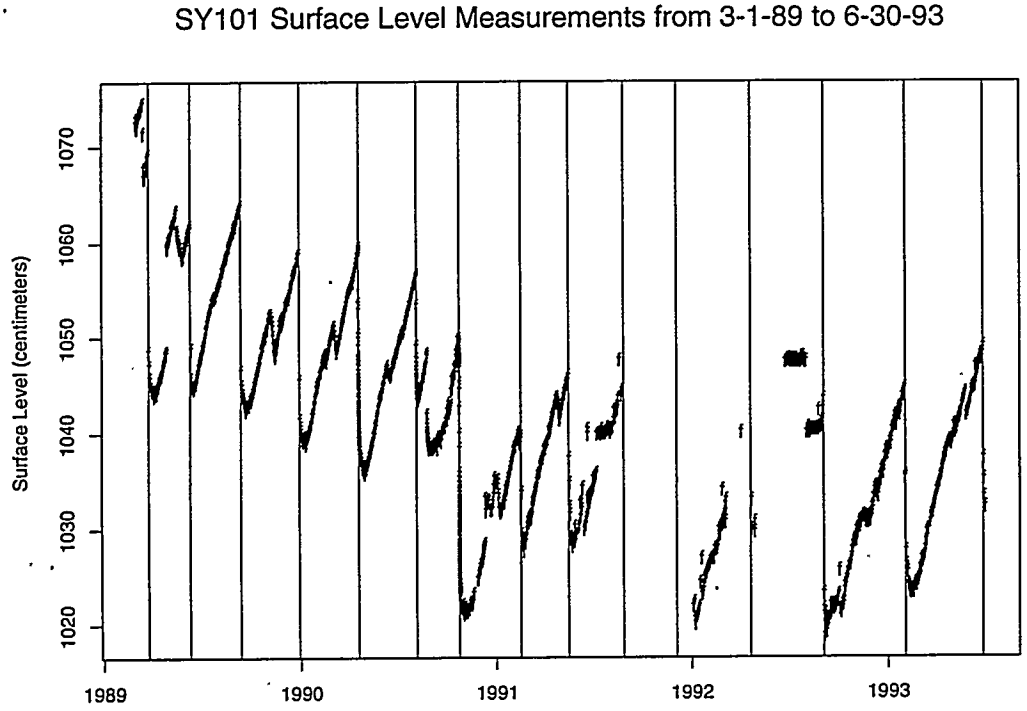

Figure 11: Tank waste level data for Tank SY–101 with GREs marked with vertical lines. All the level measurements are FIC.

The behavior for Tank SY–103 is similar, although not as extreme; see Figure 12. The dates of the GREs were obtained from the H_2 headspace measurements.[e] The rate of level rise is not as large as that of SY–101, and the level drops are not as large. However, there is a good correspondence between the level drops and the gas releases.

The behavior for Tank AN–104 is somewhat different from that of the other two tanks. Dates of GREs were obtained from the H_2 measurements made in the tank headspace using a gas chromatograph (GC); the recorded GC measurements began in October 1994. Figure 13 shows these

[e]Neerchal, N. and Whitney, P. 1995 Letter Report "Measurement Responses to Gas Release Events in Tank 241-SY-103"

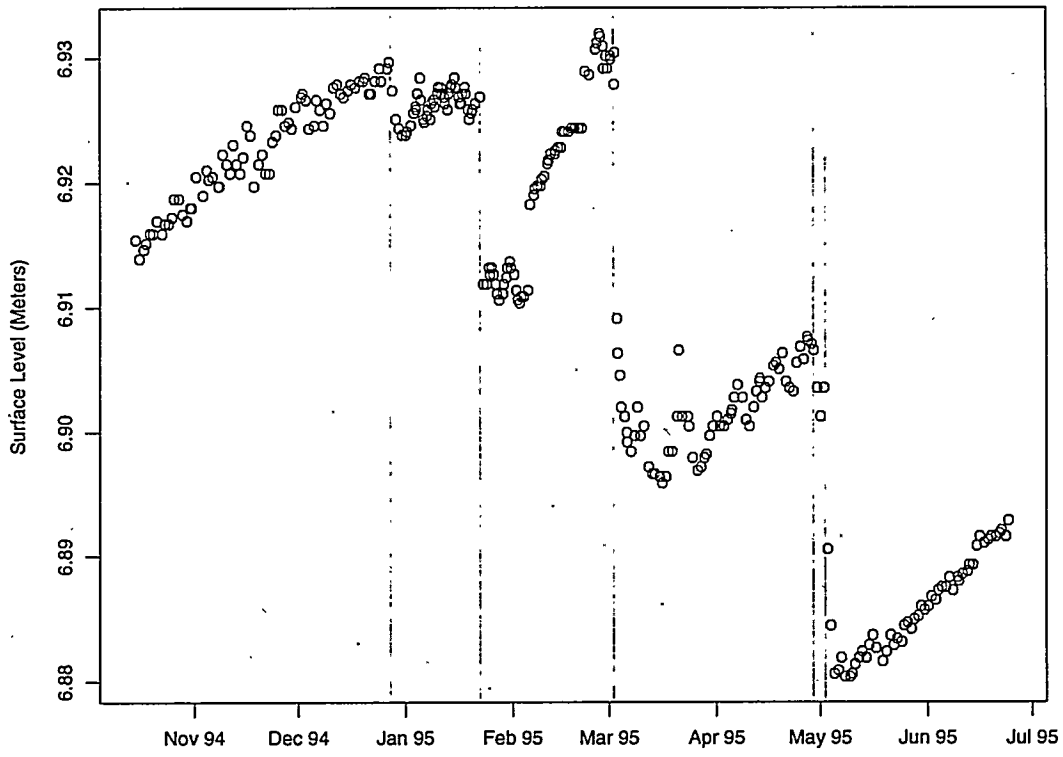

Figure 12: SY–103 ENRAF surface level measurements from 10-15-94 to 6-24-95. The vertical lines mark times of GREs, based on standard hydrogen monitoring system (SHMS) measurements.

measurements. The large spikes are taken as indications of gas release from the tank waste. The band of values (above the baseline) at about 100 ppm are the H_2 measurements made during calibration of the GC. Although not evident from this particular data view, many of the large gas release events are followed by smaller "after-burps." Table 6 lists the dates on which the AN–104 GREs began.

The level data for the same period as the GC measurements is shown in Figure 14. The dates of the GREs are marked on the plot as solid vertical lines. For most of the GREs, the tank waste level drops. The exceptions to this behavior are the GREs that occur on 2-16-95 and on 10-3-95. As can be seen in Table 6, these are typical GREs for this tank. Also, the level drop corresponding to the GRE of 11-6-94 is preceded by an upward jump in tank waste level.

Three level measurement indications of gas releases are shown by these three tanks:

1. a rapid tank waste level drop
2. a rapid level rise
3. a cluster of upward outlying points

There is some overlap among these categories; for example, the rapid level rises corresponding to GREs in Tank AN–104 are followed by a rapid level drop within, at most, a few days.

Table 6: Tank AN–104 GRE dates detected by GC H_2 measurement

Date	Peak H_2 (ppm)	Comment
11-6-94	3000	Subsequent series of smaller GREs. Waste level rose then fell ~4 cm.
2-16-95	2000	Level measurements show a few high outliers.
8-3-95	500	Subsequent series of smaller GREs. Occurs between last FIC and first ENRAF level measurement.
10-3-95	3000	Subsequent series of smaller GREs. Waste level rises.
10-8-95	1700	Subsequent series of smaller GREs Waste level falls back to pre- 10-3 level.
5-4-96	6000	Waste level falls.

The rapid level drop (Item 1 above) is explained readily by a large volume of gas leaving the tank waste. The second and third items are explained by a decrease in the pressure at which the gas is held in the tank waste, which is approximately coincident with part of the gas being released; for example, gas moving upward in the tank waste but still being retained, while another part of the gas is released.

The rest of this section discusses the AN–104 level and GC data in more detail. This discussion provides the technical basis for the labor-intensive phase of looking for GREs in the Hanford tank waste level data. The point of view taken is that we look for anomalies in the level data that might be caused by GREs, and further use the comments in the database to decide whether or not the anomalies are due to instrumentation actions (such as calibration) or instrumentation problems.

Figure 14 has additional markings; the dashed vertical lines anchored at the bottom of the plot with the ▲ indicate when comments appear in the SACS database. Note that the comments for this series of data always are made at or near the time of a gas release. These comments are listed in Table 5. These particular comments point out the GREs.

The letters at the top of the plot indicate times of particular interest in this tank's gas release and level history. At the time indicated by A, the level drops and looks very much like a response to a GRE. However, the GC data for this time do not indicate a large GRE; instead, there is a series of very small releases – 20-40 ppm above baseline – during this time. Such releases are common in the GC data for this tank. Thus, based on the GC data, this level drop is interpreted as a "false alarm." Finally, the comment in the SACS database at this time tersely states "Taken by Ins. Tech."; this comment is not sufficient reason for us to dismiss this level drop as instrumentation-related.

At the time indicated by B, there is an upward clump of level measurements and no gas release. However, in this case, the comments in the SACS database are adequate to correctly dismiss the possibility of a GRE, because the comments document that problems occurred with the FIC.

The time indicated by C marks both the time at which the FIC was replaced with the ENRAF, and a gas release. Because there is often a slight level offset between the last FIC and first ENRAF measurements, the existence of the offset here is expected and would not be interpreted as indicating a GRE. The timing of the instrumentation change and a simultaneous GRE would appear to be an incredible coincidence. The methodology for detecting potential GREs using tank waste level

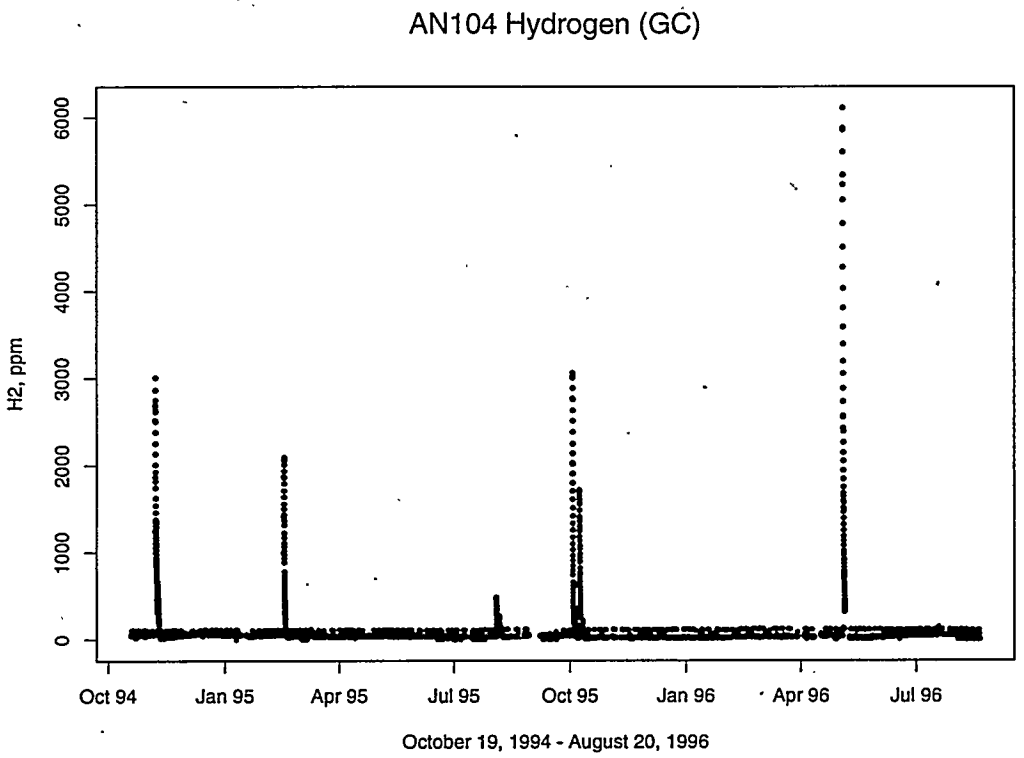

Figure 13: GC H_2 measurements for Tank AN-104. The large spikes are taken as indications of gas release from the tank waste. The band of values (above baseline) at about 100 ppm are the H_2 measurements made during calibration. Note that there are a few gaps in the data; however, the gaps do not coincide with the FIC breaks.

misses this event, because the FIC and ENRAF data are examined separately.

The time indicated by D is noted in the SACS comments as a calibration of the ENRAF, and a level change can result from the ENRAF calibration procedures. Thus, this level drop would not be taken as indicating a GRE.

The time indicated by E corresponds to the times when adjustments were made to the void fraction and related instruments; the SACS comments document the water additions resulting from the flushing of these instruments. Accordingly, this level rise is not taken as indicating a GRE.

Looking ahead to the methodology results, our findings of GREs based solely on the level data (independent of the GC!) for this tank and time span are summarized in Table 7. For AN–104 ENRAF data, the methodology based on the level measurements detects events that correspond precisely with the GC detects. For AN–104 FIC data (in the time span of 10-1-94 through the last FIC measurement), the methodology based on the level measurements *over-detected* gas release events. That is, no GREs were missed; however, three (false) GREs were incorrectly detected. Finally, the release that occurred during the transition time between the FIC and ENRAF measurements was not detected.

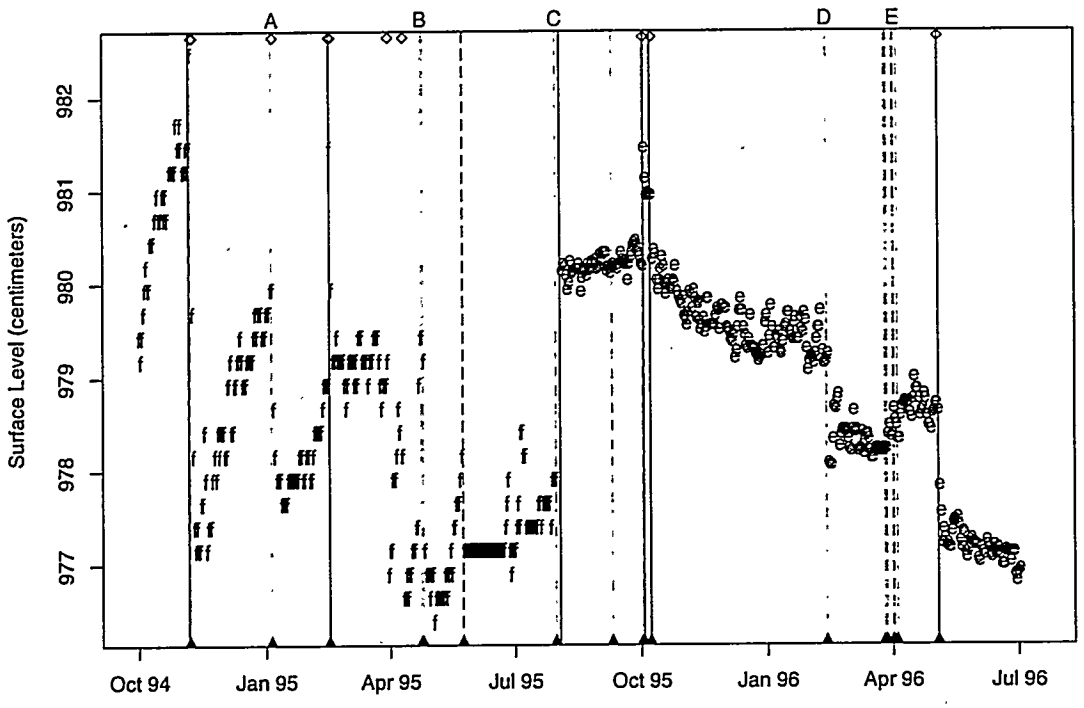

Figure 14: Level measurements for Tank AN–104 with GC-estimated GREs marked on the plot by solid vertical lines. The locations of comments on the level measurements in the SACS database are marked with dashed vertical lines extending upward from triangles. The points on the plot are marked as "e" or "f" according to whether the level measurement was made with an ENRAF or a FIC device. The ◇ symbols along the top of the plot mark the times of gas release events as detected using the tank waste level data.

Table 7: Tank AN–104 GREs detected using the tank level data and our methodology.

Date(s) GRE Detected	Instrument	Comment
11-8-94, 11-9-94	FIC	Correct
1-6-95	FIC	Incorrect; SACS comment not enough to dismiss this level jump
2-16-95, 2-17-95	FIC	Correct
3-31-95	FIC	Incorrect
4-11-95	FIC	Incorrect
10-3-95	ENRAF	Correct
10-9-95	ENRAF	Correct
2-14-96	ENRAF	Correct
5-4-96	ENRAF	Correct

4.3 Methodology

The methodology has two main parts. First, a break detection algorithm was used to process the level data and detect candidate events as possible GREs. Next, the output of the algorithm was considered together with the data itself (i.e., the level measurements and the comments from the SACS database), to refine the selection of features. The algorithm and the subsequent analyst decisions are described below.

4.3.1 Algorithm to Detect Breaks in Tank Level Data

Figure 15 shows the type of break to be detected in the level data. As discussed in Section 4.2, such a pattern (level jumps both up and down) has been observed in some of the Hanford tank waste levels, and they do correspond to GREs. The dashed lines in Figure 15 indicate the extrapolations that would be made from t looking both forward and backward. The backward and forward extrapolations are different, even in the neighborhood of t. Thus, it is expected that comparing forecasts and backcasts in the neighborhood of t will detect these breaks.

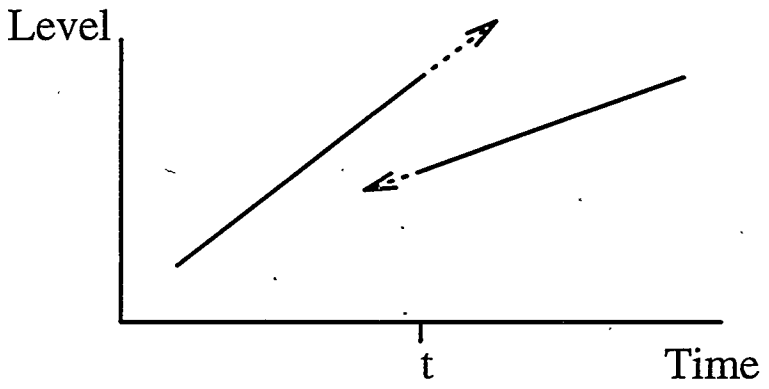

Figure 15: Forward and backward extrapolations at a break point. The solid lines indicate the "true" levels; the dotted lines indicate the forward and backward extrapolations from time t; the extrapolation forward is referred to as a forecast; the extrapolation backward is referred to as a backcast.

The observation just described forms the main part of the feature detection algorithm discussed in this paper. The rest of this Section discusses how the forecasts and backcasts were calculated, precisely how they were compared, and how this comparison was applied recursively to detect features.

The forecasts and backcasts were calculated using a Kalman filter and a model that corrects the observed level for variations induced by fluctuations in atmospheric pressure. This model and the filter are described in Whitney et. al. (1996).[f] Kalman filters are described in numerous references (Brown 1983, West & Harrison 1989). A recent application of a similar Kalman filter model used in an analogous situation is reported by Kitagawa & Matsumoto (1996); in this paper, atmospheric pressure fluctuations were removed from water-table level data, so that the effect of seismic events on the water-table level could be detected.

[f] Whitney, P., Wilkins, N., Miller, N., Meyer, P. and Brewster, M. 1996, "Flammable Gas Data Evaluation Progress Report", Letter Report WTSFG96.1, Pacific Northwest National Laboratory.

The important inputs to the Kalman filter calculations (other than the tank level and atmospheric pressure data) include

- measurement error estimate – The measurement-to-measurement variability is a numerical input.
- a variance describing how smoothly the pressure corrected waste level varies in time – This variance is denoted by σ_w^2.

  This parameter potentially ranges upward from 0. The extreme value of 0 corresponds to an assumption that the true level is linear; larger values correspond to an assumption that the true level varies more. Another interpretation of the parameter is that, for large values of the variance, few data level measurements are being used (averaged together) to estimate the true level. Smaller values of the variance correspond to increasing the size of the time window of level measurements contributing to the estimated level. In other words, $1/\sigma_w^2$ behaves qualitatively like a bandwidth parameter.
- a variance describing how smoothly dL/dP varies in time – The interpretation of this variance is similar to the variance for the level. This parameter was set to 0, which says, strictly, that dL/dP is constant across the data. Given the large uncertainties in dL/dP, and given that we are actually interested in estimating the true level, the choice of 0 is reasonable (it would not be reasonable if these Kalman filter runs were being used to estimate gas volumes).

The key outputs needed from the Kalman filter calculations are (pressure-corrected) estimated levels, along with standard deviations of these estimates. The filter was run on the data in forward and in reverse time, the latter calculations providing the backcasts. In particular, for each time t at which a level observation was made, the forward Kalman filter was used to calculate the pressure-corrected level estimate (along with the standard deviation of the estimate), based on all the level data up through and *including* time t. The Kalman filter was run on the time-reversed level data to calculate the estimate of the pressure-corrected level at time t, using all the level data after and *excluding* time t. These two estimates of the level at time t were then used to calculate a comparison statistic as follows:

$$Z_t = \frac{\text{forward level estimate} - \text{backward level estimate}}{\sqrt{\text{SD of forward level estimate}^2 + \text{SD of backward level estimate}^2}}$$

Z_t denotes the comparison statistic at time t. Theory suggests that Z_t will have a standard normal distribution (approximately). Thus, magnitudes of Z_t on the order of 2 or more will be unusual if there are no feature anomalies. Because we are doing thousands of comparisons for each tank, magnitudes of Z_t larger than 5 were used to indicate a break in the level measurements at time t.

The calculation described above was applied recursively to the level data. An initial pass through the data was made with a large σ_w^2. The data was further refined into segments at the detected breaks, if any were found. Then, the algorithm was applied with a smaller σ_w^2 to the segments. The result was a partitioning of the initial stretch of level measurements into segments that were closer to linear than the original data set. Rules for stopping the recursion were:

- No calculations were done on segments of data containing 10 or fewer level measurements.
- A fixed sequence of σ_w^2 values was available; when the smallest value in that sequence was reached, no further calculations were done.

We refer to this algorithm as the *backward/forward algorithm.*

Experimentation with the procedure suggested that the algorithm behaved better with a sequence of σ_w^2's having smaller steps between the successive sequence members. In particular, the multiple identifications (see Figure 16 on page 39 and the associated discussion in Section 4.3.2) of a single feature decreased as we refined the sequence of σ_w^2 used.

To make the calculation and analyses more manageable, we divided a tank's data into yearly segments (with 15 days overlap at the beginning and end of a year). Also, the FIC and ENRAF data were analyzed separately.

4.3.2 Analyst Decisions to Refine Detected Breaks

The backward/forward algorithm was rich in false calls. These were due to outliers (not cleaned up from the data) and due to the algorithm's tendency to detect multiple dates for a single feature. These points are illustrated in Figure 16.

Figure 16 shows sample output from the algorithm for Tank S–102 FIC data from 1983. This plot and an associated table are the complete and fundamental output of the algorithm, which the analyst then considered to arrive at decisions regarding whether a detected feature was a break or not. Both the upper and lower plot show the level data. The upper plot represents the output and some of the inner workings of the algorithm. The lower plot shows the times of comments made in the SACS database. A sample of the information presented in the output table is shown in Table 8.

The vertical lines on the upper plot show the locations of breaks identified by the algorithm. The numbers shown on each line (at both the top and bottom of the line segment) indicate the level (in the algorithm) at which the break was found. For instance, the first pass through the data found the large break downward in late 1983 (marked with a 1). Next, the data were subdivided into two segments before and after this break. No further breaks were found in the later segment. The very next pass through the earlier segment identified the large upward jump (at the vertical line labeled with the 2). Subsequent iterations found other features in the data.

Figure 16 illustrates the following features of the numerical algorithm as it applies to the tank level data:

1. Large level jumps are found.
2. Sometimes a single data feature results in multiple identifications of breaks; for example, the multiple breaks marked with 7's appearing before the jump upward appear to identify the change in slope that occurred just after July 1983. Similar multiple identifications appear in September 1983.
3. The algorithm detects some slope changes.
4. The algorithm detects outliers (e.g. the sporadic upward measurements occurring just before January 1983).
5. Some detections of the algorithm are difficult to understand (e.g. the 7's before April). Note that this plot does not fully show the data used by the algorithm. Recall that the algorithm uses pressure-corrected tank waste level to detect features.

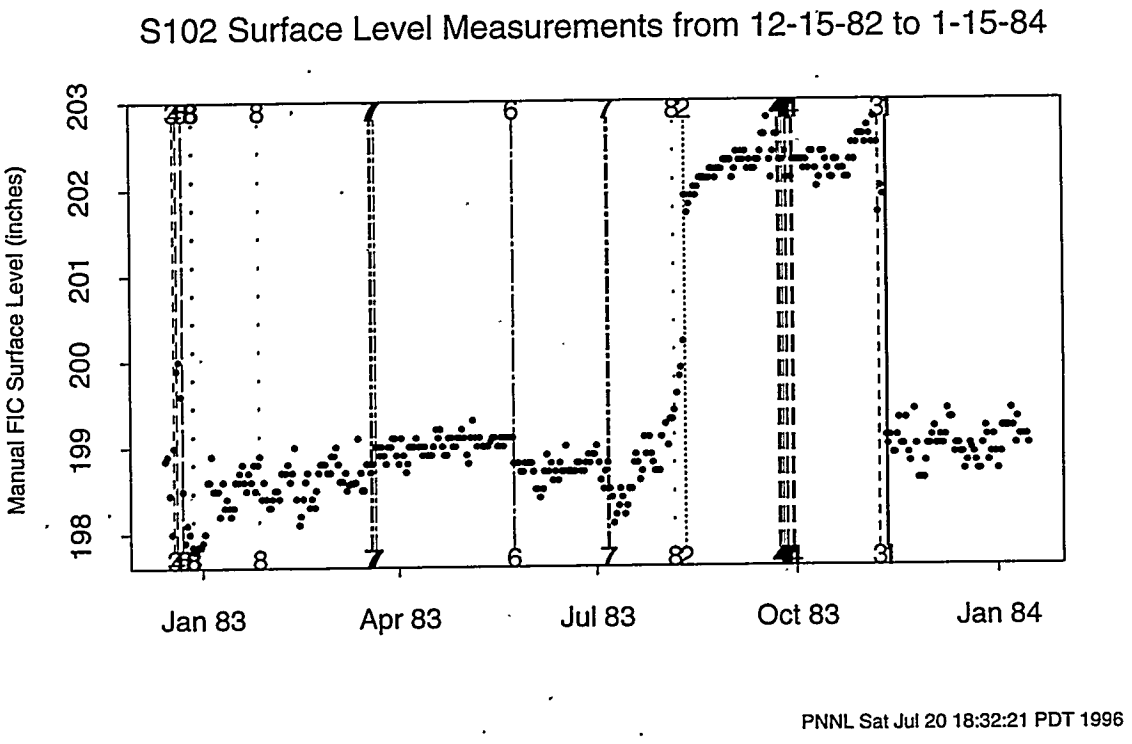

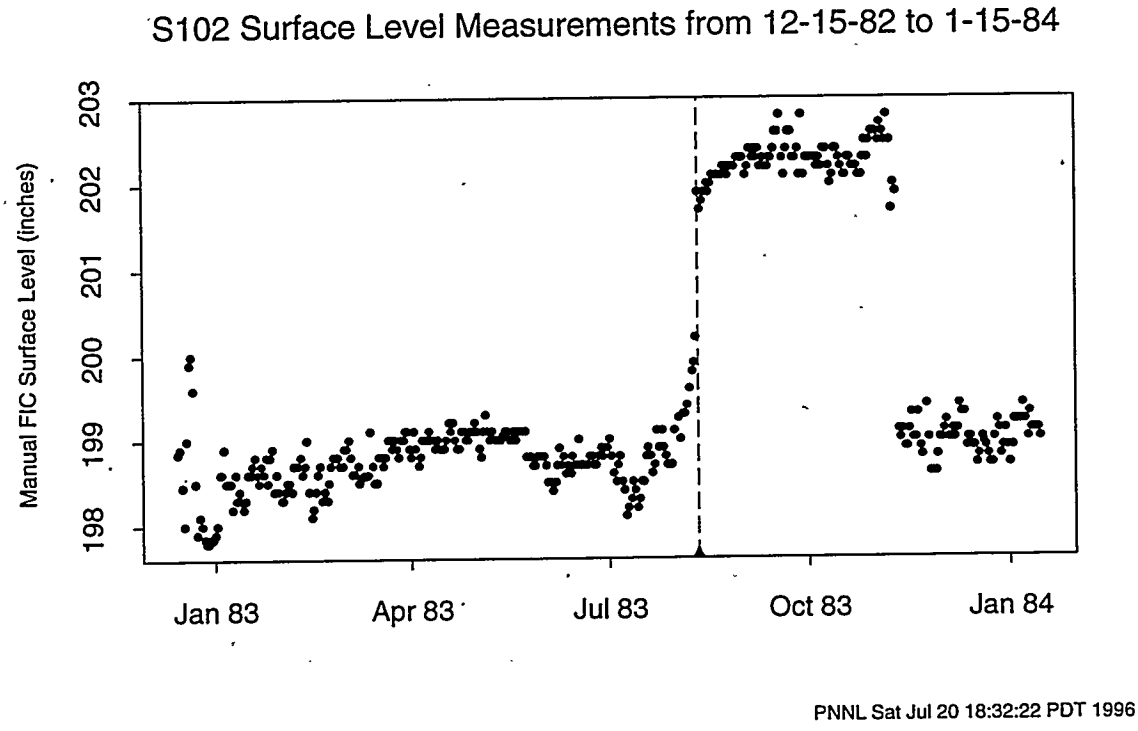

Figure 16: Graphic representation of algorithm output for Tank S–102. Both plots show the same data. The upper plot shows the output of the break detection algorithm. The numbers shown at the bottom and top of each broken line indicate the level in the algorithm at which the break was detected. The lower plot shows dates of comments from the SACS database.

The initial work done by the analyst was to categorize the breaks into one of the five categories listed above. The information portrayed on the lower plot in Figure 16 then came into consideration. The vertical line, anchored by the ▲, shows the date of a comment in the SACS database. This comment corresponds well with the detected upward break. Consequently, if this comment suggested that at that time, maintenance (such as calibration or flushing of the FIC) had been performed, or that the FIC had been behaving poorly (e.g., the tape rolled up, or the FIC wouldn't "bob"), then the upward break would be discounted as a possible gas related level change.

For this particular case, the comment was:

```
Maint. Calibration Check OK Exceeds INC Crit.
```

strongly suggesting that the increase was noted, the instrument was checked, and that the instrument checked out OK. Thus, this rise (and the subsequent fall) were flagged as potential GREs, fitting into a pattern noted in Tank AN–104. The rest of the detected features for Tank S–102 were cataloged as shown in Table 8. The first column shows the date of the detected feature. Additionally, if the entry in the first column starts with an uppercase X, then the feature was considered a break. If the column starts with a lowercase x, then the comments in the SACS data base were ambiguous regarding whether the detected jump was a break or not. Rows that do not begin with an X or an x are features not considered to be level breaks, because they correspond to a slope change, were caused by an outlier, were "echoes" of other features, were just not considered a level jump in light of the level data, or were discounted based on information from the SACS comments. Also calculated and tabulated are the level differences bracketing the time of the detected break.

The activity described above was repeated for all the tanks (with FIC and ENRAF data) in this study, focusing on the breaks upward or downward.

Table 8: Tank S-102 detected features in 1983 and categorization. Upward and downward jumps that could not be discounted as instrumentation-related or as caused by waste transfers are marked with an "X".

	Date	Break Size	Flag	SACS Comments	Analyst Comments
X	1-3-83	0.60	0	-	-
	1-27-83	0.10	2	-	False call
	3-19-83	-0.10	2	-	False call
	3-20-83	0.10	2	-	False call
	3-21-83	0.20	2	-	False call
X	5-24-83	-0.30	1	-	-
	7-6-83	0.10	2	-	False call
X	7-7-83	-0.30	1	-	-
X	8-6-83	0.10	2	-	Kept as a precursor to the large upward jump that follows
X	8-11-83	1.70	5	Maint. Calibration Check OK Exceeds INC Crit.	The comment strongly supports that these are good measurements.
	9-23-83	0.00	2	-	False call
	9-24-83	-0.30	2	-	False call
	9-25-83	0.00	2	-	False call
	9-26-83	0.10	2	-	False call
	9-27-83	-0.30	2	-	False call
	9-29-83	-0.70	2	-	False call
	9-30-83	0.20	2	-	False call
X	11-8-83	-0.80	1	-	-
X	11-11-83	-2.80	1	-	-
	11-12-83	-0.10	2	-	False call

4.4 Preliminary Results

The results of applying the methodology to the (selected) tanks are analyzed here. Section 4.4.1 discusses and quantifies the strengths and weaknesses of the methodology, and offers a proposal on how these weaknesses can be corrected. Section 4.4.2 presents some summarized results from application of the methodology.

4.4.1 Methodology Strengths and Weaknesses

A partial validation of the methodology was presented earlier in Section 4.2, comparing the detected level breaks with the GREs for Tank AN–104. By this overall performance measure, the methodology performed well, detecting all of the GREs possible, but with some false detects for the FIC level measurements.

The analysis methodology has two primary weaknesses. The first is the *human factor*, the judgment applied by the analysts in interpreting the output of the algorithm in light of the observed tank levels and the SACS comments. The second is the strongly suspected lack of *availability* of the waste transfer and instrumentation information in the SACS comments. Recall that recording such information in the SACS database is not a required procedure. Some events as fundamental as saltwell pumping are not recorded in SACS (e.g., the pumping of SX–104 in 1988 is not commented on). Thus, we strongly suspect that we have over-counted the number of breaks in the level data.

Human intervention was applied in two ways: 1) to clean up after the algorithm (deleting the feature echoes, categorizing a feature as an outlier or slope change, and so on) and 2) to make judgments based on the comments in the SACS database about whether a particular feature was the result of instrument maintenance or waste transfer activities. These operations were performed simultaneously. To gauge the effect of the human factor, two separate analysts independently (but with the same instructions) evaluated some of the same tanks. Table 9 compares the results of the evaluations. The table shows two categories into which a detected feature could be classified, along with how each analyst classified the feature. For Tanks C–104, S–102 and T–111, the results compare poorly.

Table 9: Comparison of analyst decisions on common tanks. For two analysts, the table shows the number of detected jumps up and down, which were not identified by the analyst as false calls.

Tank and Instrument	Analyst A		Analyst B	
	# up	# down	# up	# down
AW–101 FIC	4	29	10	29
AW–101 ENRAF	1	1	2	3
A–101 FIC	0	1	0	1
A–101 ENRAF	0	1	0	1
C–104 FIC	14	20	25	30
S–102 FIC	3	12	12	29
T–111 FIC	1	3	8	4
T–111 ENRAF	1	0	1	0

To remedy this weakness of the methodology, we propose to separate the two human intervention

activities – the post-algorithm cleanup and judgment making – and to automate the latter.

To automate the judgment making, each comment will be categorized into one of three groups: the comment leads one to conclude that a level change or other anomaly was instrumentation or waste transfer related; the comment would *not* lead one to conclude that a level change or other anomaly was instrumentation or waste transfer related; or the comment was ambiguous regarding the classification.

In addition, a "time extent" for the applicability of the comment will be assigned. For instance, comments regarding flushing the FIC apply specifically to the date of the FIC flush, and some comments in the database describe saltwell pumping over a period of several months. These two properties of a comment — its category and its time extent — can be applied automatically to the output of a feature detection algorithm. This proposal should improve the repeatability of the analyst performance, because separating the two tasks will result in simpler decisions to be made. Additionally, isolating and automating the decision based on the comments potentially allows incorporation of a variety of information sources, to augment the SACS comments. These activities are recommended in Fiscal Year 1997; the primary benefit would be better estimates of the historical frequencies of level change events.

4.4.2 Results Summaries

The key information from the analyses described in Section 4.3 is the dates and sizes of the breaks detected. Two summaries from the break detection analyses are presented here. First, for each tank analyzed, the detected breaks are plotted against time. Additional information carried on each plot is the date of saltwell pumping (if applicable for that tank), the date the FIC was replaced with the ENRAF, and the dates on which level measurements were taken. The purpose of this summary is to present waste level jump information for each tank. The second summary is a table of estimated level-break frequencies for each tank. Its purpose is to compare waste level jump information across tanks.

Figures 17, 18, and 19 show the displays for Tanks AN–103, S–102 and SX–104. The rest of the displays are collected in Appendix C. For each detected level jump, a line segment running from zero to the size of the level jump is drawn at the date of the detected level jump. A horizontal line is drawn through zero for visual reference. Note that the vertical lines indicating breaks are drawn in two widths. The thin vertical lines indicate that the SACS comments (or other supporting information) suggested that the break was caused by instrumentation properties or by waste transfer activities; however, the evidence was not considered firm. The thicker vertical lines indicate that there was no evidence suggesting that the break was related to instrumentation or waste transfer.

The graphics underneath the date axis at the bottom of these plots indicate the dates at which tank waste level measurements are recorded in the SACS database. A small vertical line is drawn at the time of each level observation. For instance, for Tank AN–103 (Figure 17), tank waste level data have been available almost continuously over the time span shown in the plot. The level data were recorded weekly up through mid-1989. Subsequently, the data have been recorded daily, with a few gaps, the largest in 1995. The ▲'s at the top and bottom of the plot show when the level measurement instrument was changed from FIC to ENRAF.

The summary plot for Tank AN–103, Figure 17, shows that the frequency of downward breaks is small, on the order of 1 or 2 per year. The cluster of upward jumps during mid-1991 is in part due

to some outliers. The large upward jump in 1990 corresponds to both a level rise and an upward outlier. The magnitudes of the downward level changes are small, almost always an inch or less.

A striking feature of the level jumps shown for Tank S–102 in Figure 18 is that the frequency of detected jumps appears to decrease over time. Also, the magnitudes of some of the level drops during the early 1980s rival those of some of the DSTs. The recent level jump behavior of this tank is, however, very quiet. The plot shows a frequency of less than one detected level change per year during the 1990s for Tank S–102.

For Tank SX–104, almost all the detected level jumps occur before the saltwell pumping of the tank. In all of these plots, the ♦'s at the top and bottom of the plots indicate a time near which the tank was saltwell-pumped. Indeed, the larger jumps shown near this time for Tank SX–104 are very likely pumping-related. Even discounting those level jumps, this tank shows a high frequency and large magnitude of level jumps from 1981 through 1988 (Tank A-103 shows similar behavior; see Figure C.2 in Appendix C).

Table 10 shows the estimated frequencies of level jumps. For each tank and instrument (FIC and ENRAF), the number in the column "Duration" shows the total time in years for which weekly (or higher frequency) level data is recorded in SACS. The column labeled "Number of Breaks" shows the number of detected level jumps (corresponding with the number of thick and thin lines on the plots). The next column, labeled "freq (per yr)" is the frequency of detected level jumps, and is equal to the "Number of Breaks" divided by the "Duration (yr)" columns. This information is summarized separately for the FIC and ENRAF devices, and then combined across both instruments in the last block of three columns in this table.

Generally, the SSTs in this study are seen to have fewer level jumps than the DSTs. However, the frequencies for Tank AN–103 (a DST) are comparable to, and smaller than, the frequencies for some of the SSTs. Indeed, the long term level measurement history for Tank AN–103 bears a striking resemblance to the level histories of some of the SSTs; after a rapid initial rise, the rate of increase decreases somewhat. The similarity between the gas release behavior of AN–103 and the hypothesized behavior of releases from SSTs was noted in Stewart et al. (1996).

Finally, the level jump counts presented in this paper are consistently higher than the GRE counts reported for the same tanks (Wilkins 1996, Stewart et al. 1996). Two reasons for this are:

- In this study, large jumps on successive days were counted separately
- In this study, jumps up were counted as well as jumps down.

The previously noted under-reporting of events in the SACS comments will likely affect all of these estimates identically.

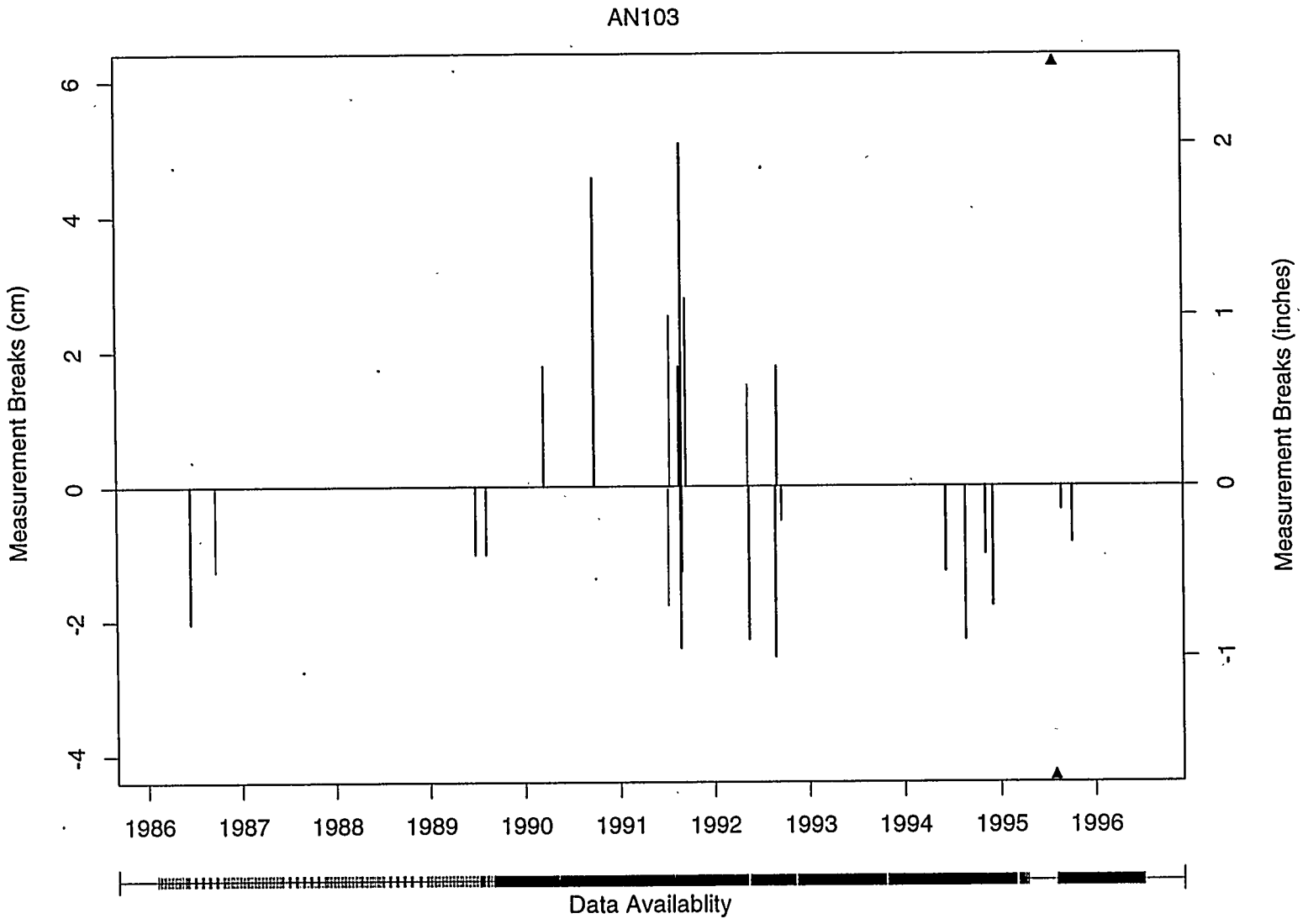

Figure 17: Tank AN–103 detected breaks and break sizes.

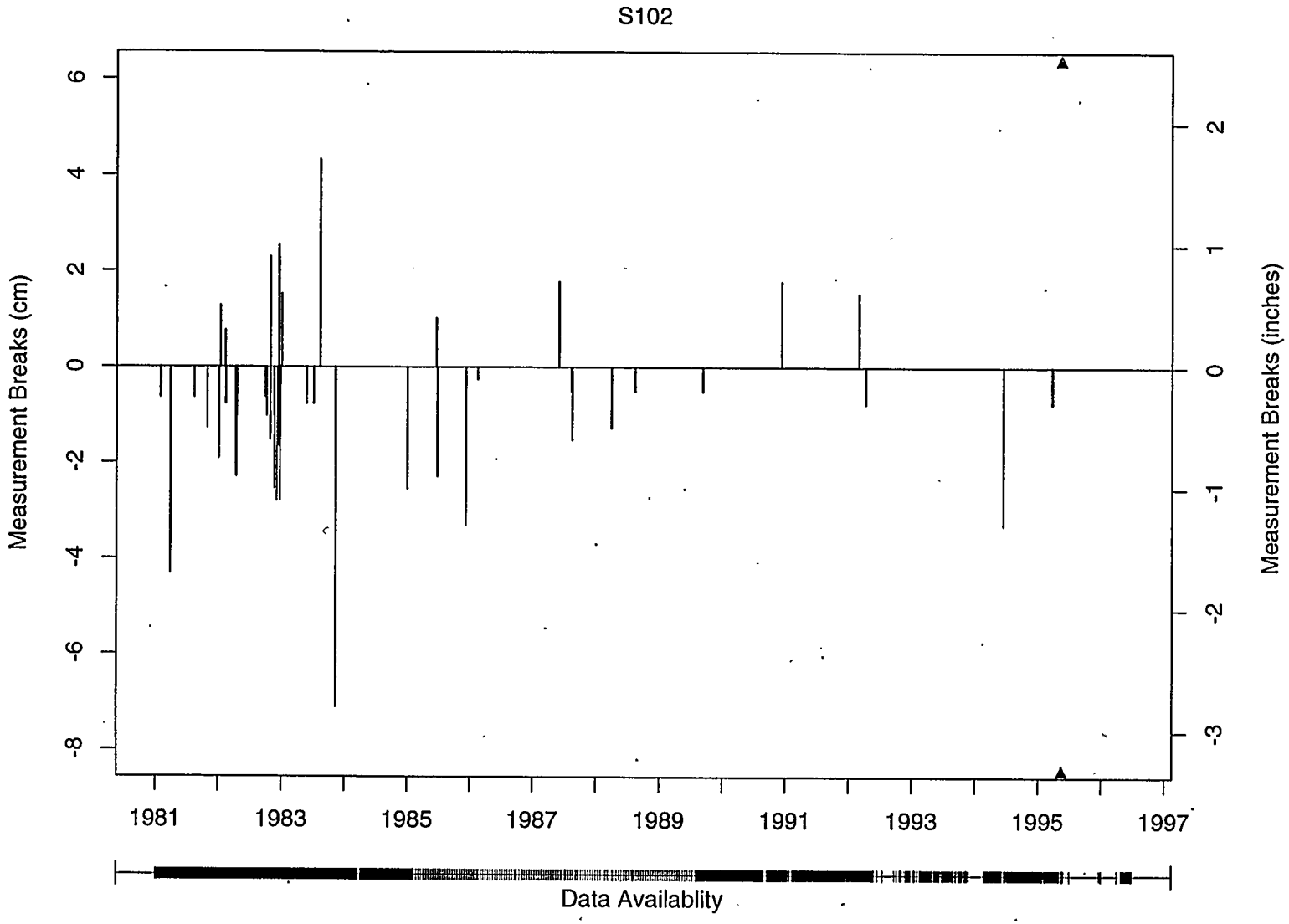

Figure 18: Tank S-102 detected breaks and break sizes.

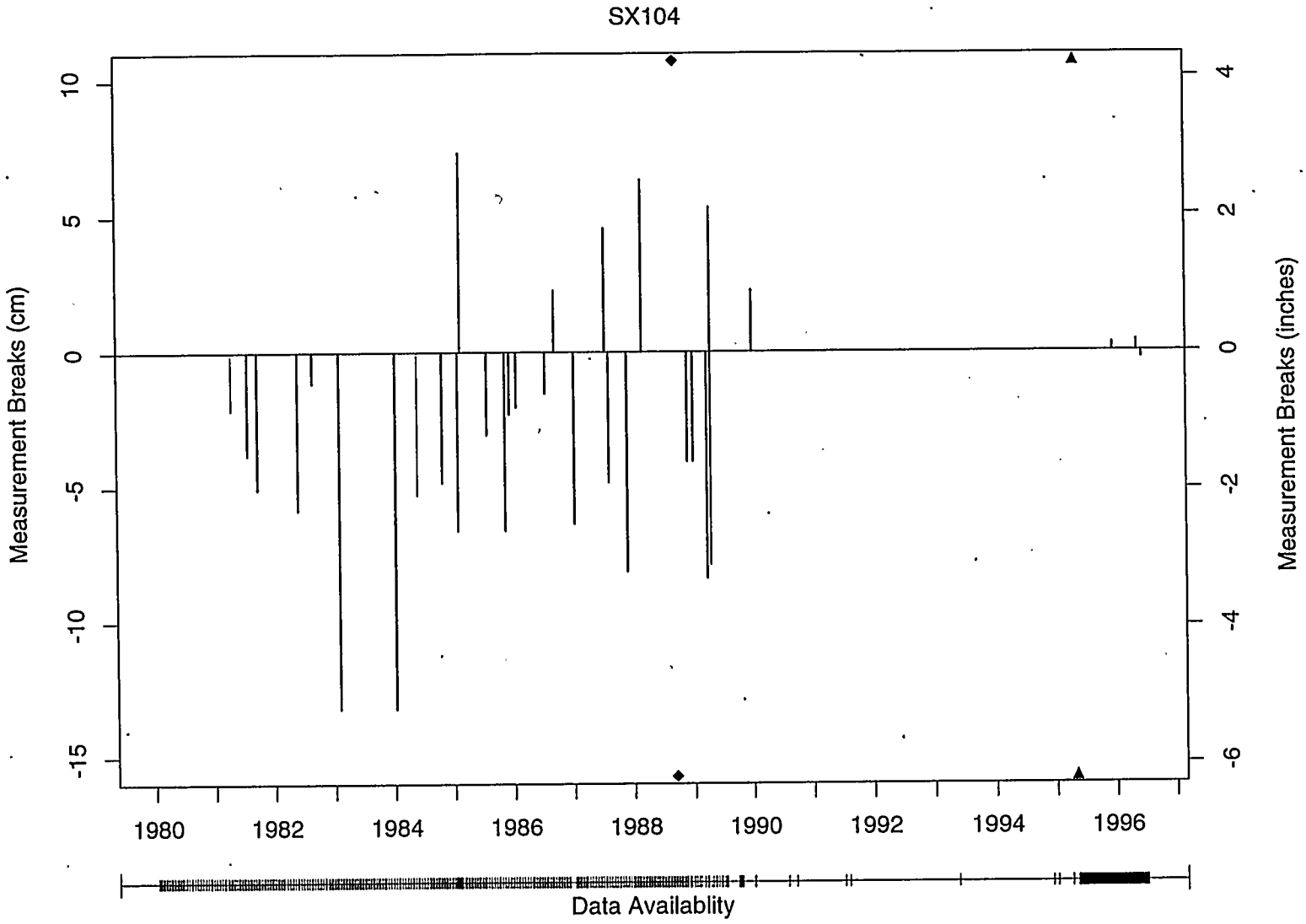

Figure 19: Tank SX–104 detected breaks and break sizes.

Table 10: Frequencies of detected level jumps.

Tank	FIC			ENRAF			Total		
	Duration (yr)	# Breaks	freq (per yr)	Duration (yr)	# Breaks	freq (per yr)	Duration (yr)	# Breaks	freq (per yr)
A–101	1.3	5	3.7	0.4	4	10.6	1.7	9	5.2
A–103	9.7	16	1.6	0.0	0		9.7	16	1.6
AN–103	9.2	18	2.0	0.9	2	2.2	10.1	20	2.0
AN–104	10.3	52	5.0	0.9	4	4.4	11.2	56	5.0
AN–105	10.1	61	6.0	0.9	5	5.5	11.1	66	6.0
AW–101	6.4	44	6.9	0.9	5	5.8	7.3	49	6.7
AW–103	1.5	0	0.0	0.1	0	0.0	1.6	0	0.0
AW–104	4.7	0	0.0	0.5	0	0.0	5.2	0	0.0
AX–103	8.5	10	1.2	0.1	0	0.0	8.5	10	1.2
BX–104	12.9	2	0.2	0.3	0	0.0	13.2	2	0.2
BX–107	13.2	2	0.2	0.1	0	0.0	13.2	2	0.2
BX–112	14.4	0	0.0	0.3	0	0.0	14.7	0	0.0
BY–109	9.8	7	0.7	0.0	0		9.8	7	0.7
C–104	13.2	76	5.8	0.0	0		13.2	76	5.8
C–105	14.6	13	0.9	0.0	0		14.6	13	0.9
C–107	13.3	8	0.6	1.2	1	0.8	14.5	9	0.6
S–101	5.1	5	1.0	1.4	0	0.0	6.5	5	0.8
S–102	13.7	56	4.1	0.2	0	0.0	14.0	56	4.0
S–103	13.0	14	1.1	2.1	5	2.4	15.1	19	1.3
S–105	8.6	36	4.2	0.0	0	0.0	8.6	36	4.2
S–106	13.2	5	0.4	2.0	1	0.5	15.2	6	0.4
S–107	13.3	12	0.9	2.1	4	1.9	15.3	16	1.0
S–109	9.5	4	0.4	0.0	0	0.0	9.5	4	0.4
S–111	12.8	0	0.0	1.9	0	0.0	14.7	0	0.0
SX–101	3.7	3	0.8	0.1	0	0.0	3.8	3	0.8
SX–102	4.0	9	2.2	0.1	0	0.0	4.1	9	2.2
SX–103	11.9	15	1.3	0.1	0	0.0	12.0	15	1.3
SX–104	8.3	26	3.1	1.2	3	2.6	9.5	29	3.1
SX–105	4.9	9	1.8	0.1	0	0.0	5.0	9	1.8
SX–106	11.5	42	3.6	1.9	7	3.7	13.4	49	3.7
SY–101	11.8	324	27.6	0.0	0		11.8	324	27.6
SY–103	4.8	29	6.1	2.0	7	3.6	6.7	36	5.3
T–107	12.4	5	0.4	2.0	3	1.5	14.4	8	0.6
T–111	13.0	13	1.0	1.0	1	1.0	13.9	14	1.0
TX–107	6.3	2	0.3	0.1	0	0.0	6.4	2	0.3
TY–102	8.9	12	1.4	0.8	2	2.7	9.6	14	1.5
TY–103	3.7	1	0.3	0.5	5	9.6	4.2	6	1.4
U–102	3.8	1	0.3	0.0	0	0.0	3.8	1	0.3
U–103	13.2	2	0.2	1.9	3	1.5	15.2	5	0.3
U–105	11.5	24	2.1	1.9	1	0.5	13.5	25	1.9
U–106	13.4	3	0.2	1.9	7	3.7	15.3	10	0.7
U–107	12.9	8	0.6	1.9	0	0.0	14.8	8	0.5
U–108	3.9	1	0.3	0.2	0	0.0	4.1	1	0.2
U–109	13.2	5	0.4	1.9	5	2.6	15.1	10	0.7

5 A Sludge Yield Model for Level - Pressure Hysteresis

5.1 Introduction

Hysteresis loops have been observed in the correlations between ENRAF level and barometric pressure for several single shell tanks[5]. These hysteresis loops are inconsistent with the simple dL/dP model based on the ideal gas laws. Possible causes for this level - pressure hysteresis include sticking ENRAF gauges or some sort of rate-dependent physical phenomena such as viscous compression or expansion. This section presents another possible explanation, based on sludge elasticity and yield. The sludge yield model described here assumes that expansion and compression of gas bubbles within the waste is hindered by the material strength of the surrounding sludge. Further, if the magnitude of the pressure changes is large enough, then the sludge material surrounding the bubbles may yield, allowing the bubbles to expand or compress freely.

The proposed model does not address any of the limitations associated with present dL/dP models such as mean pressure, location of gas, effect of temperature, etc. Rather, it presents some new physics in order to explain observed trends which present models cannot explain.

A model for sludge elasticity and yield is presented in Section 5.2. The physical basis for the model is described, and the solution to the problem of a spherical bubble in an elastic medium is derived from classical elasticity theory. The elastic contribution to dL/dP is then determined. In Section 5.3, the results of Section 5.2 are used to develop a model which predicts the level-pressure hysteresis observed in ENRAF data for certain single-shell tanks. The conditions under which yielding occurs are discussed and the logic and equations for the model are described. In Section 5.4, the model is applied to several single-shell tanks. Finally, Section 5.5 presents some important implications of the model.

5.2 A Model for Sludge Elasticity

To develop a model for sludge elasticity, gas bubbles within the sludge are treated as spherical cavities within an elastic solid. Classical linear elasticity theory is applied to the problem in order to develop the elastic contribution to dL/dP.

5.2.1 Physical Basis of Model

We assume that gas is present in waste sludge in the form of small, spherical bubbles. The sludge is assumed to exhibit the simplest of solid mechanical properties, a linear elasticity with elastic modulus E (units of kPa) and Poisson's ratio ν (dimensionless). When the pressure far from a bubble is increased or decreased, stresses are transmitted within the elastic sludge and act to deform the bubble. If the surrounding pressure field is hydrostatic, then the deformations are radial. If pressure changes are large enough, circumferential stresses at the bubble walls can become large enough to break or fail the solid sludge material. This is assumed to happen when induced stresses exceed the yield strength of the sludge, τ (kPa). Once yielding has occurred, it is likely that plastic flow takes place. This is a rate-dependent phenomenon which is, in general, complex. An ideal

[5]Whitney, P., Wilkins, N., Miller, N., Meyer, P. and Brewster, M. 1996, "Flammable Gas Data Evaluation Progress Report", Letter Report WTSFG96.1, Pacific Northwest National Laboratory.

model for the linear-elastic, finite yield strength sludge is shown in Figure 20. The stress σ increases linearly with strain ϵ for $\sigma < \tau$, and is constant in the plastic region for $\sigma > \tau$. Here the strain is defined as the radial deformation normalized by the bubble radius. It is assumed that the strain at the yield point is very small, so that ϵ_τ is on the order of a few percent or less.

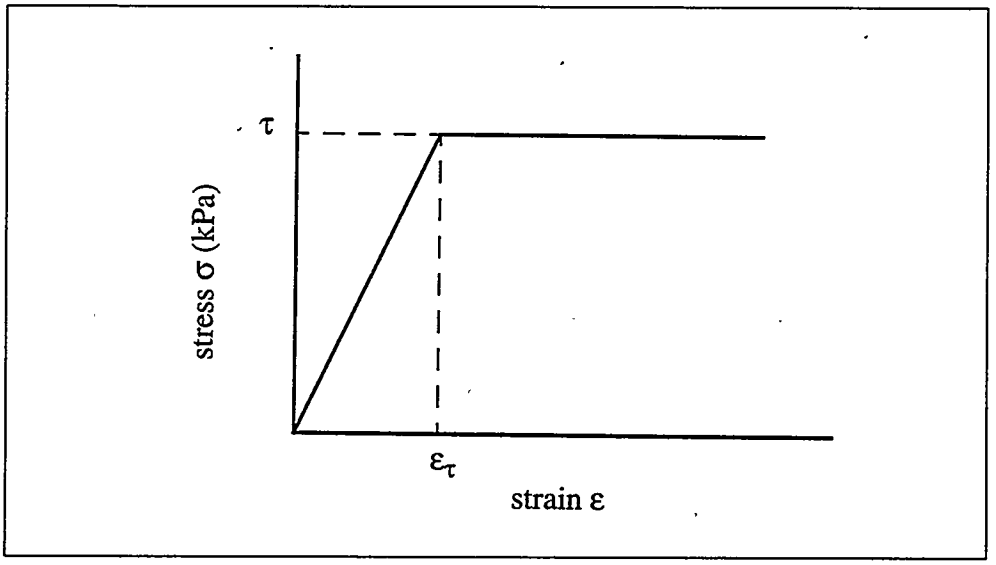

Figure 20: Linear-elastic stress-strain behavior with plastic yield.

5.2.2 Solution for a Gas Bubble in an Elastic Solid

In this section, the solution for the stresses and strains at the boundary of a gas-filled bubble is derived. This solution is used to determine how the volume of the bubble changes in response to a change in the external pressure. This solution is then used to determine how level changes are related to pressure changes for an elastic medium with many gas bubbles.

For a sphere with a hole at the center, the problem has been solved by classical linear elasticity theory. The geometry is shown in Figure 5.2. The solution can be approximated for a cavity in an infinite solid so long as the outer radius b is large compared to the bubble radius a. The solution presented follows the approach of Timoshenko & Goodier (1982).

The equilibrium condition and the stress-strain relations for the spherical geometry are

$$\frac{d\sigma_r}{dr} + \frac{2}{r}(\sigma_r - \sigma_t) = 0 \tag{3}$$

$$\epsilon_r = \frac{1}{E}(\sigma_r - 2\nu\sigma_t) \tag{4}$$

$$\epsilon_t = \frac{1}{E}(\sigma_t - \nu(\sigma_r + \sigma_t)) \tag{5}$$

Here, r is the radial distance to the point under consideration, E is Young's modulus, ν is Poisson's ratio, σ_r and σ_t are the radial and tangential stresses at that point, and ϵ_r and ϵ_t are the radial and tangential strains. The strains can be expressed in terms of the radial displacements u according to

$$\epsilon_r = du/dr \tag{6}$$

$$\epsilon_t = u/r \tag{7}$$

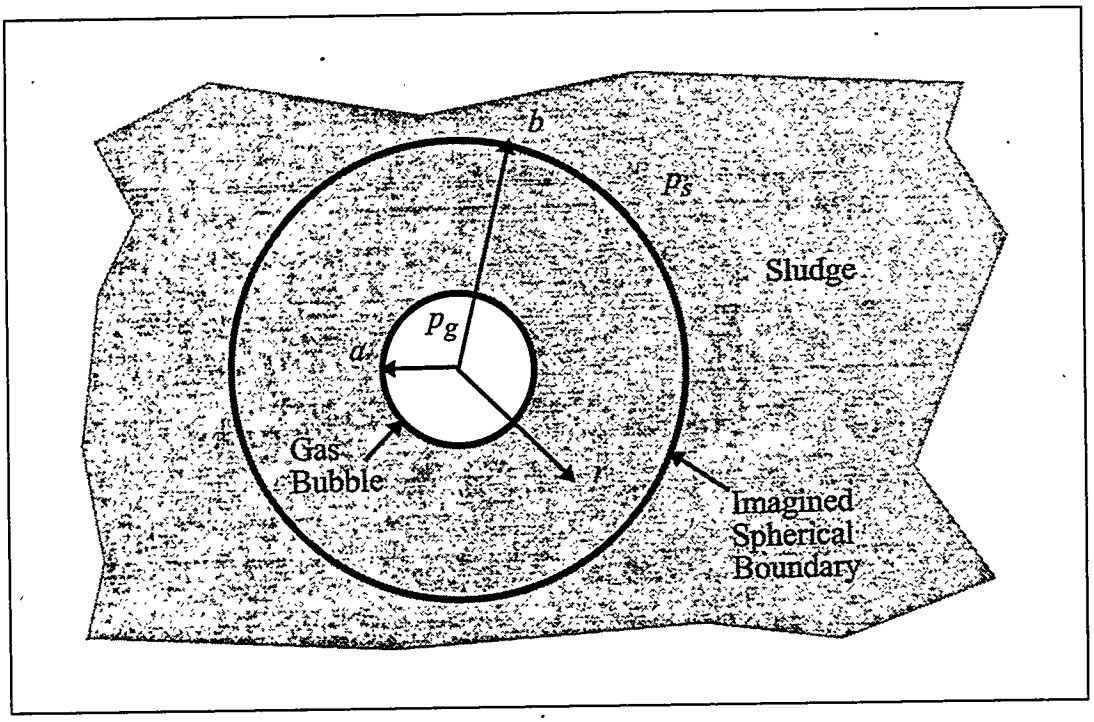

Figure 21: Geometry of an elastic sphere surrounding a bubble.

The displacement u is the dimensional elongation (i.e., change in radius) of a point within the solid due to the applied pressure field. If Equations 5.2 and 5.3 are solved for the stresses in terms of the strains, and together with Equations 5.4 and 5.5 are substituted into Equation 5.1, then the following differential equation for the displacement is obtained:

$$\frac{d^2u}{dr^2} + \frac{2}{r}\frac{du}{dr} - \frac{2u}{r^2} = 0 \tag{8}$$

Equation 5.6 has the solution

$$u = C_1 r + C_2/r^2 \tag{9}$$

so that the strains given by Equations 5.4 and 5.5 are $\epsilon_r = C_1 - 2C_2/r^3$ and $\epsilon_t = C_1 + C_2/r^3$. Substituting this result for the strains into Equations 5.2 and 5.3 and solving for the stresses yields

$$\sigma_r = E\left[\frac{C_1}{1-2\nu} - \frac{2C_2}{1+\nu}\left(\frac{1}{r^3}\right)\right] \tag{10}$$

$$\sigma_t = E\left[\frac{C_1}{1-2\nu} + \frac{C_2}{1+\nu}\left(\frac{1}{r^3}\right)\right] \tag{11}$$

The boundary conditions are $\sigma_r = -p_g$ at $r = a$ and $\sigma_t = -p_s$ at $\sigma_r = -p_g$, where p_s is the sludge pressure and p_g is the gas pressure inside the bubble. Solving Equations 5.8 and 5.9 with these boundary conditions and taking the limit of $b/a \gg 1$ gives

$$C_1 = -\frac{(1-2\nu)}{E}p_s \tag{12}$$

$$C_2 = -\frac{(1+\nu)}{2E}a^3(p_s - p_g) \tag{13}$$

Finally, we find the solution for the radial displacement by substituting Equations 5.10 and 5.11 into Equation 5.7 to obtain

$$u = -\frac{1}{E}\left[(1-2\nu)p_s r + \frac{(1+\nu)}{2}a^3(p_s - p_g)\frac{1}{r^2}\right] \tag{14}$$

If we evaluate Equation 5.12 at the bubble radius $r = a$, the displacement is

$$u = -\frac{a}{E}\left[(1-2\nu)p_s + (1+\nu)(p_s - p_g)/2\right] \tag{15}$$

We wish to measure the displacement u relative to an initial equilibrium condition. In this way, we can look at changes in the displacement which occur due to pressure changes which deviate from an equilibrium value. If the mean sludge pressure is $\bar{p}_s$ and we assume that the initial bubble pressure is equal to this mean, then the initial displacement is $a(1-2\nu)\bar{p}_s/E$. The displacement relative to this initial displacement is

$$\Delta u = -\frac{a}{E}\left[(1-2\nu)(p_s - \bar{p}_s) + (1+\nu)(p_s - p_g)/2\right] \tag{16}$$

5.2.3 Elastic Contribution to dL/dP

If the gas inside the bubble is assumed to undergo isothermal changes, then the gas pressure is always related to the initial pressure according to

$$p_g V = \text{const} = \bar{p}_s \frac{4}{3}\pi a^3 \tag{17}$$

The volume of the gas bubble can be related to the displacement according to

$$V = \frac{4}{3}\pi a^3 + 4\pi a^2 \Delta u \tag{18}$$

For small displacements, the gas pressure can now be expressed in terms of the displacements by combining Equations 5.15 and 5.16 to obtain

$$p_g = \bar{p}_s(1 + 3\Delta u/a)^{-1} \approx \bar{p}_s(1 - 3\Delta u/a) \tag{19}$$

Substituting this result into Equation 5.14 results in

$$\Delta u = -\frac{3a(1-\nu)\Delta p/2}{E + 3(1+\nu)\bar{p}_s/2} \tag{20}$$

where $\Delta p = p_s - \bar{p}_s$ is the change in sludge pressure. Since the change in bubble volume is $4\pi a^2 \Delta u$, then the change in waste level associated with this volume change is $4\pi a^2 \Delta u/A$ where A is the waste surface area. The total change in level due to all the gas bubbles is

$$\Delta L = 3\bar{\alpha} L_0 \Delta u/a \tag{21}$$

where $\bar{\alpha}$ is the mean void fraction of retained gas. Therefore, from Equations 5.18 and 5.19 we have

$$\frac{\Delta L}{\Delta p} = -\frac{(9/2)\bar{\alpha} L_0(1-\nu)}{E + (3/2)(1+\nu)\bar{p}_s} \tag{22}$$

Equation 5.20 gives the pressure-level response for an elastic sludge containing gas-filled bubbles. If $E = 0$ and $\nu = 1/2$ then we have an incompressible liquid and Equation 5.20 becomes

$$\frac{\Delta L}{\Delta p} = -\frac{\bar{\alpha} L_0}{\bar{p}_s} \tag{23}$$

which is the familiar gas-only level-pressure response equation. If the elastic modulus is large compared to the sludge pressure, then Equation 5.20 limits to

$$\frac{\Delta L}{\Delta p} = -\frac{(9/2)(1-\nu)\bar{\alpha} L_0}{E} \tag{24}$$

which has the same form as Equation 5.21 with an effective pressure of $2E/9(1-\nu)$.

5.3 Hysteresis in Level vs. Pressure

In this section, the results of the last section are used to develop a model which predicts the level-pressure hysteresis observed in ENRAF data for certain single-shell tanks. First, the conditions for yielding are discussed and then the logic and equations for the model are described.

5.3.1 Yield Criterion

The simple model for the linear-elastic, finite yield strength sludge is depicted in Figure 5.1. According to the model, the sludge material responds elastically to increasing stress until the applied stress equals the yield stress τ, and then the material fails. For the bubbles in the sludge, it is assumed that yield occurs when the tangential stresses at the bubble walls exceed the yield stress. An expression for tangential stress can be derived in the same manner as the radial displacement was derived, by evaluating Equation 5.9 at the boundary conditions

$$\sigma_t = -\frac{1}{2}(p_s - p_g) = -\frac{\Delta p}{2}\left[1 - \frac{9/2(1-\nu)\bar{p}_s}{E + 3(1+\nu)\bar{p}_s}\right] \tag{25}$$

If the elastic modulus is large compared to the mean sludge pressure, then Equation 5.23 limits to

$$\sigma_t = -\frac{\Delta p}{2} \tag{26}$$

Hence the condition for yield is

$$|\Delta p| > 2\tau \tag{27}$$

If a pressure change is less than twice the yield stress for a given tank sludge(as observed in Equations 5.24 and 5.25), then the level response will be given by Equation 5.22. If the pressure change exceeds twice the yield strength, then the level response will be given by Equation 5.21. It is important to note that the pressure change must be measured relative to the appropriate reference state. We assume that every time the pressure has an inflection (i.e., goes from increasing to decreasing, or vice versa) the material around the bubble is "re-set" to the initial elastic state. Therefore, the pressure change Δp is always measured relative to the last pressure inflection point. This will become evident in the next section.

5.3.2 The Hysteresis Parallelogram

This section outlines the logic and equations applied in the numerical model to compute level changes from pressure data. Figure 5.3 shows a hysteresis parallelogram in the $\Delta L - \Delta p$ plane. This parallelogram represents the model logic. The four sides and the four corners of the parallelogram are labeled. The parallelogram is traversed in the clockwise direction. Corners A and C represent pressure inflection points, given by the maxima and minima of the actual pressure data as the pressure fluctuates. Corners B and D represent sludge yield points, and these points are computed by the model.

The actual pressure is given by

$$p(t) = p_0 + \Delta p(t) \tag{28}$$

where p_0 is the mean ambient pressure. Similarly, the actual tank level is given by

$$L(t) = L_0 + gt + \Delta L(t) \tag{29}$$

Here L_0 is the initial tank level (at time $t = 0$) and g is the average rate of increase of the level due to gas generation. Sides S2 and S4 represent regions where pressure changes (relative to a minimum or maximum) are small so that the sludge elastic response dominates. Hence the slope of S2 and S4 is given by Equation 5.20. Sides S1 and S3 are yielded regions, with slope given by Equation 5.21.

The numerical model begins by assuming that the sludge has yielded and the pressure is falling, which corresponds to side S1 on the parallelogram. The level can be computed by solving Equation 5.21 to obtain the equation for side S1

$$\Delta L_1 = -\gamma(\Delta p + \tau) \tag{30}$$

where $\gamma = L_0\bar{\alpha}/\bar{p}_s$. As long as the pressure continues to fall, Equation 5.28 gives the corresponding level change. If the pressure begins to rise, then a pressure minimum has occurred and the level is now given by S2. The equation for S2 is found by solving Equation 5.20 to obtain

$$\Delta L_2 = -\gamma(\Delta p_{min} + \tau) - \frac{\gamma k}{1+\delta}(\Delta p - \Delta p_{min}), \qquad |\Delta p - \Delta p_{min}| < 2\tau. \tag{31}$$

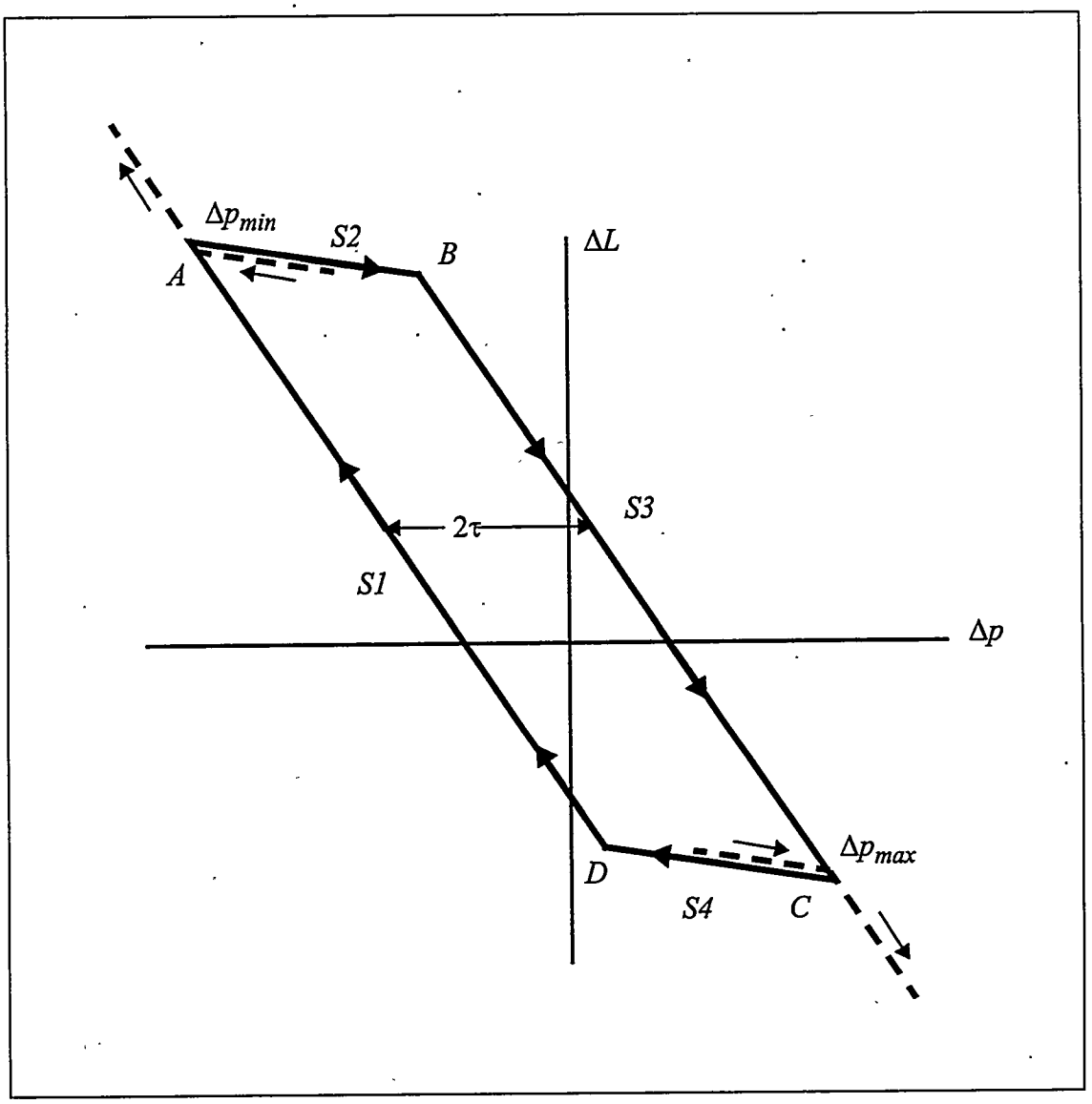

Figure 22: The hysteresis parallelogram.

where $k = 3(1-\nu)/(1+\nu)$ and $\delta = 2E/3\bar{p}_s(1+\nu)$. As the pressure continues to rise, $|\Delta p - \Delta p_{min}| \geq 2\tau$ and yielding occurs. Thereafter, the level is given by S3, which is

$$\Delta L_3 = -\gamma(\Delta p - \tau) \tag{32}$$

After the pressure reaches a maximum, then the level is given by S4 according to

$$\Delta L_4 = -\gamma(\Delta p_{max} - \tau) - \frac{\gamma k}{1+\delta}(\Delta p - \Delta p_{max}), \qquad |\Delta p - \Delta p_{max}| < 2\tau. \tag{33}$$

If $|\Delta p - \Delta p_{max}| \geq 2\tau$, then the sludge yields and the level is given by S1. Finally, we note that if the pressure begins to fall while on S2, then we continue on S2 (but moving counter-clockwise) until the pressure falls below Δp_{min}. If this happens, then we are back on S1 as the pressure continues to fall. Similarly, if the pressure begins to rise while on S4, then we continue back on S4

(counter-clockwise) until the pressure increases above Δp_{max}. Once this happens, we are on S3. These two situations are illustrated by the dashed lines in Figure 5.4.

The equations presented above, along with the logic determining their use, was coded in Fortran. The resulting program reads a pressure-time data file and computes the waste level based on the prescribed inputs shown in Table 11.

5.4 Application of Model to Tank Data

The hysteresis model was applied to the following single-shell tanks: C–103, C–106, C–107, S–103, S–106, S–107, S–111, SX–106, T–102, T–107, U–103, U–105, U–106, U–107, U–109. The data was evaluated for a period approximately equal to the last quarter of 1995. The tanks showing the largest hysteresis were S–106, S–107, S–111, U–103 and U–107. Results for these tanks are presented here to demonstrate the performance of the hysteresis model.

5.4.1 Model Inputs

The model requires several inputs which are either estimated or obtained from data. These inputs are shown in Table 5.1. The average ambient pressure, p_0, was obtained by computing the mean of the pressure data. The initial level, L_0, and the level increase rate, g, were obtained by performing a linear regression on the ENRAF level data for the selected time interval. This interval varied from about 15 days to 4 months, depending on the continuity of the ENRAF data. The mean void fraction is related to the in-situ volume of retained gas according to $\bar{\alpha} = L_0 \bar{V}_g / A$. It was estimated by examining ENRAF data to find average slopes for the sides of hysteresis loops (S1 and S3) and then applying Equation 5.21. The elastic modulus E was obtained in a similar fashion by estimating slopes of the tops and bottoms of hysteresis loops (S2 and S4) and then applying Equation 5.22. Poisson's ration, ν, was assumed to have a value of 0.4 for all cases. The average sludge pressure $\bar{p}_s$ was estimated by assuming that all the gas is located at $L_0/2$ and that the specific gravity of the sludge is 1.5. Finally, the yield stress, τ, was estimated by finding the average spacing between the sides of hysteresis loops.

Table 11: Hysteresis model inputs

Tank	L_0 (cm)	α (%)	$\bar{p}_s$ (kPa)	g (cm/day)	τ (Pa)	E (MPa)
S106	456.0	20.0	131.0	0.0127	550	13
S107	369.8	5.1	126.0	0.00774	500	1.6
S111	517.4	14.0	137.0	0.00423	400	8.1
U103	424.7	12.4	131.0	-0.00129	400	$\geq$20
U107	366.0	7.3	127.0	0.0	200	$>$ 20
$p_0 = 99$ kPa and $\nu = 0.4$ for all cases shown.						

5.4.2 Results

Model results are shown in Figures 5.4 through 5.32. Each plot set shows pressure versus time, ENRAF level versus time, and ENRAF level versus pressure. Also shown are modeled level versus time, modeled level versus ENRAF level, and modeled level versus pressure. Figure 5.4 shows results

for Tank S–106 for a 150-day period beginning Aug 15, 1995. The level-pressure plots show strong agreement. The plot of modeled level versus ENRAF level shows that reasonable accuracy has been achieved. This plot would be a straight line of slope 1 if the model predicts level perfectly. Figures 5.5 through 5.9 show some individual hysteresis loops for Tank S–106. There is qualitative and semi-quantitative agreement among the level-pressure hysteresis loops shown. Figures 5.10 through 5.14 show results for Tank S–107. Excellent agreement is seen in the full range plots shown in Figure 5.10. The model clearly captures the apparent scatter in the data. The modeled hysteresis loops shown in Figures 5.11 through 5.14 show reasonable agreement. Results for Tank S–111 are shown in Figures 5.15 through 5.20. Again, excellent prediction of overall level-pressure data is obtained. The individual hysteresis loops shown in Figures 5.16 through 5.20 reveal remarkable similarity. Results for Tank U–103 are shown in Figures 5.21 through 5.26. The overall level-pressure behavior is captured fairly well. The individual hysteresis loops shown in Figures 5.22 through 5.26 show excellent agreement. Finally, results for Tank U–107 are shown in Figures 5.27 through 5.32. While this tank demonstrated only minor hysteresis, the model is still seen to capture some of the observed trends.

It is important to note that the model input parameters have not been optimized (other than by some limited trial and error) to produce the most accurate simulation of the waste level. The fact that reasonable agreement is seen implies that the basic physics (or at least the essential pattern of parallelogram hysteresis loops) has been captured. Improved results would be obtained by optimizing the input parameters to minimize model error.

5.5 Implications

The sludge-yield model for dL/dP predicts levels which are in good qualitative and somewhat quantitative agreement with ENRAF levels for tanks with prominent level-pressure hysteresis. The model brings to bear several important implications:

- Predictions of retained gas volume that are based on the gas-only dL/dP model may be under-estimated for tanks with significant hysteresis. This is true because the mean slope of a hysteresis loop is less than that of the steeper side.
- The proposed model provides a means of reducing error in the retained gas volume estimates; because the high frequency data (as opposed to the daily data) may be used, and because another systematic component in the level measurement error has been identified.
- Tanks with particularly high sludge strengths may conceal retained gas. If the sludge yield stress is large compared with the magnitude of atmospheric pressure changes then the sludge may never yield and allow the level to respond according to the model. Thus, the retained gas may not be detected.
- Sludge material properties may be inferred from level-pressure data. If the proposed model is accurate, yield stress and elastic modulus may be derived from the ENRAF level and barometric pressure data.

The remainder of this section further discusses the potential underestimate of the retained gas volume.

A simpler model, in which the waste material properties do not enter into consideration, has recently been used to estimate the amount of gas trapped in the tank waste (Hodgson et al. 1995). Equation (5.21) provides the fundamental relation used to relate the waste level fluctuations with the retained gas volume in this simple model. In light of the new model described in this section, the retained gas volume estimates obtained using Equation (5.21) will be underestimates. To assess the underestimate, we tabulated dL/dP estimates, obtained via the current methodology, and compared them with the dL/dP estimates based on the proposed model and parameter estimates. Table 12 contains details of this comparison.

The current methodology uses the simpler model and the daily waste level measurements from SACS. The estimates in the table representing the current methodology are based on the daily ENRAF measurements. Recall that the current methodology summarizes dL/dP with a distribution, and that the upper quartile (the 0.75 percentile of the distribution) has been used to obtain gas volume estimates. Table 12 contains both the median estimate of dL/dP and the upper quartile estimate. While the parameter estimates for the new model presented in this section were not obtained via a formal methodology, they do seem to summarize the behavior of the data.

Table 12 shows the current methodology estimates of dL/dP range from approximately 15 to 55% underestimates, relative to the proposed model and the model parameter estimates. The underestimate in dL/dP translates directly to the same percentage underestimate of retained gas volume. Also, even the "conservative" upper quartile estimates are consistently low: ranging from 6 to 47% underestimates.

Upcoming work to resolve and illuminate these issues includes:

- more detailed comparison of the new model and tank waste level data
- experiments with waste simulants to explore the relationships among material properties of the tank waste, retained gas volume and dL/dP.

It is expected that both of these activities will lead to substantial changes and improvements in our understanding of the relationship between retained gas volume and observed waste level fluctuations.

Table 12: Comparison of dL/dP from the current model and the new model which includes waste material properties. The current model consistently underestimates the dL/dP relative to the new model.

Tank	Current dL/dP Estimate (cm/kPa)		Model dL/dP	Percent underestimate	
	Median	0.75 percentile	(cm/kPa)	Median	0.75 percentile
S-106	-0.34	-0.44	-0.69	51%	36%
S-107	-0.07	-0.08	-0.15	56%	47%
S-111	-0.32	-0.40	-0.52	39%	23%
U-103	-0.21	-0.26	-0.40	47%	34%
U-107	-0.18	-0.20	-0.21	15%	6%

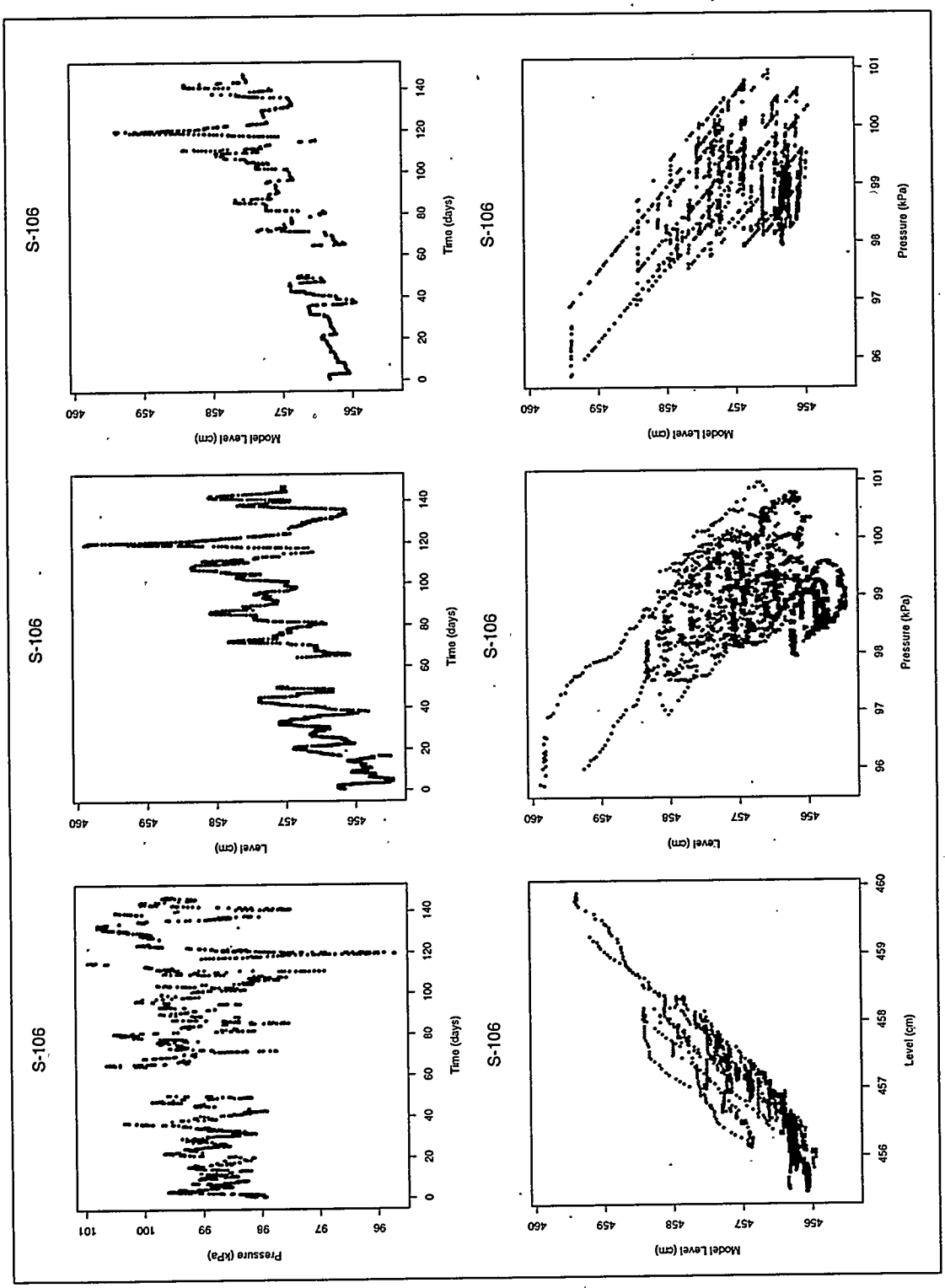

Figure 23: Tank S-106 model and data comparison 8-15-95 to 1-8-96

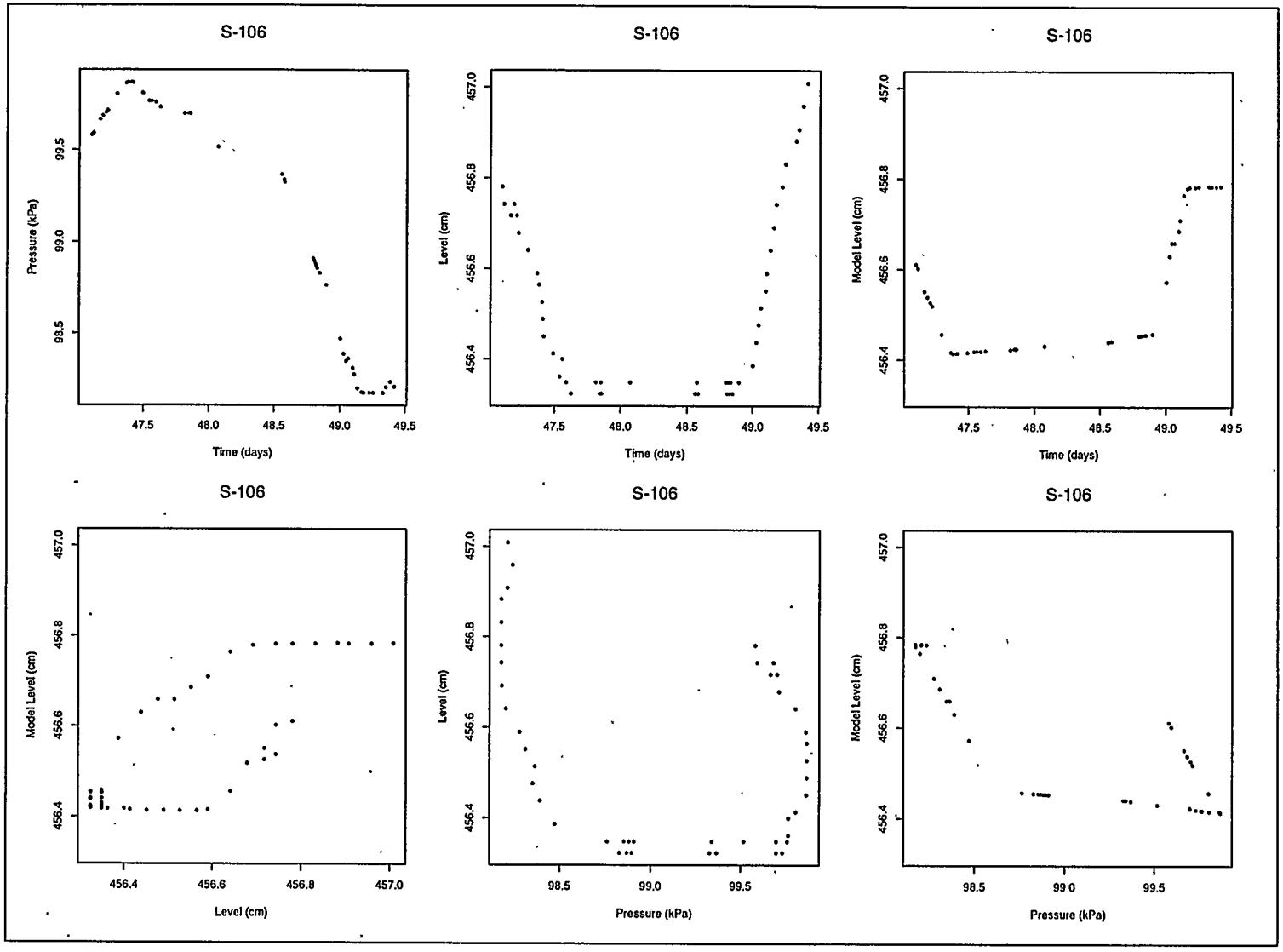

Figure 24: Tank S–106 model and data comparison 10-1-95 to 10-3-95

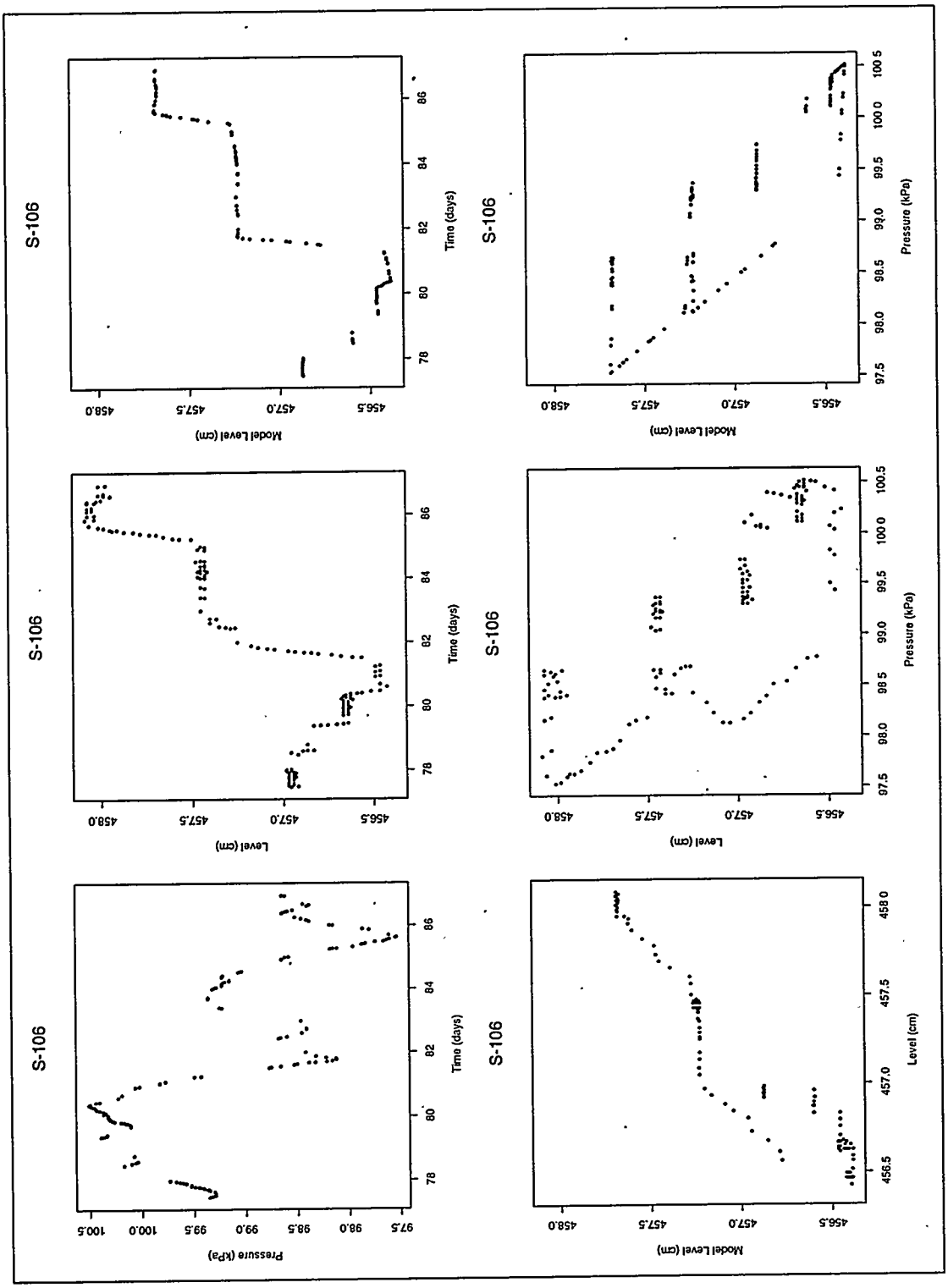

Figure 25: Tank S-106 model and data comparison 10-31-95 to 11-9-95

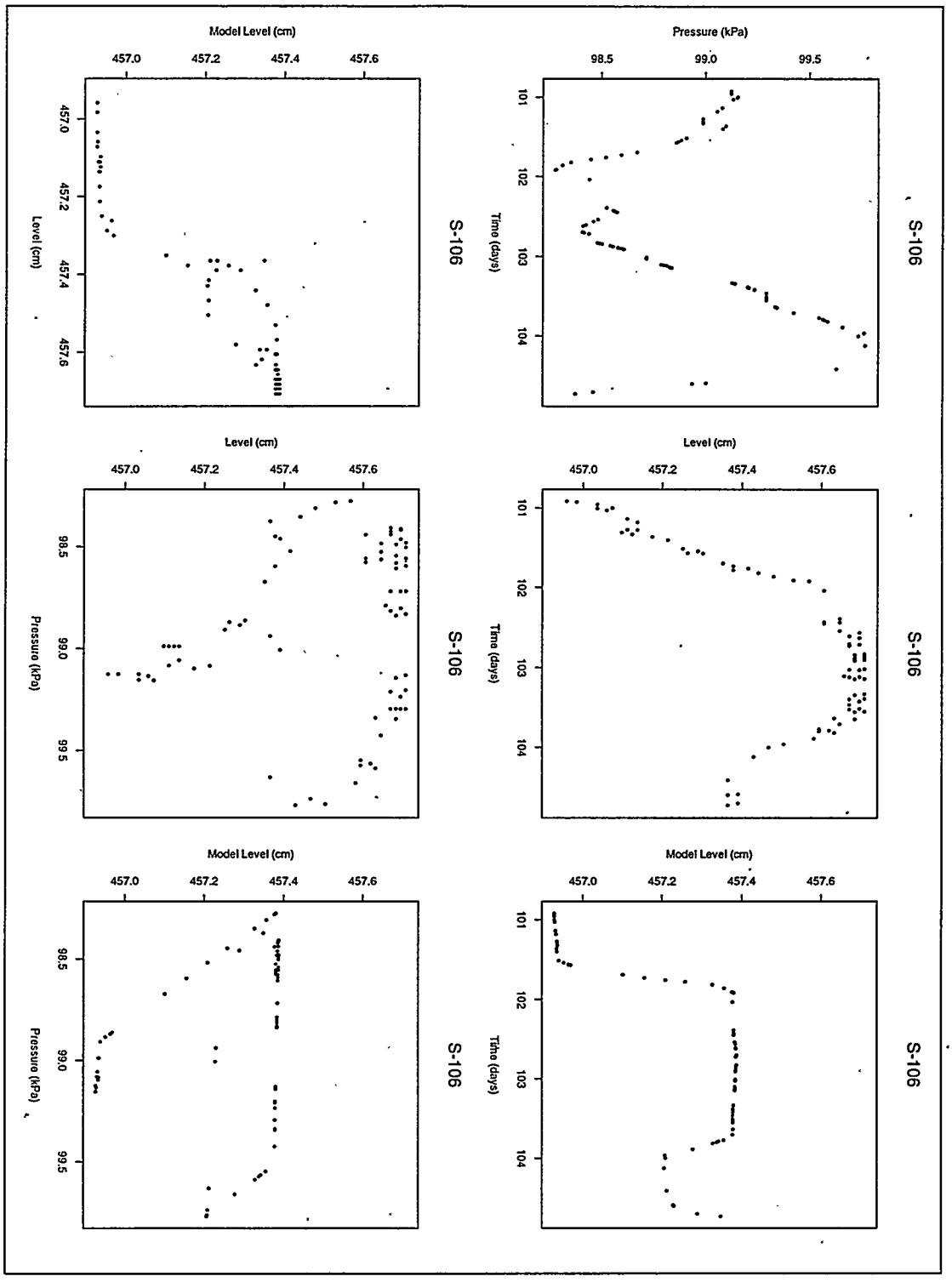

Figure 26: Tank S-106 model and data comparison 11-23-95 to 11-27-95

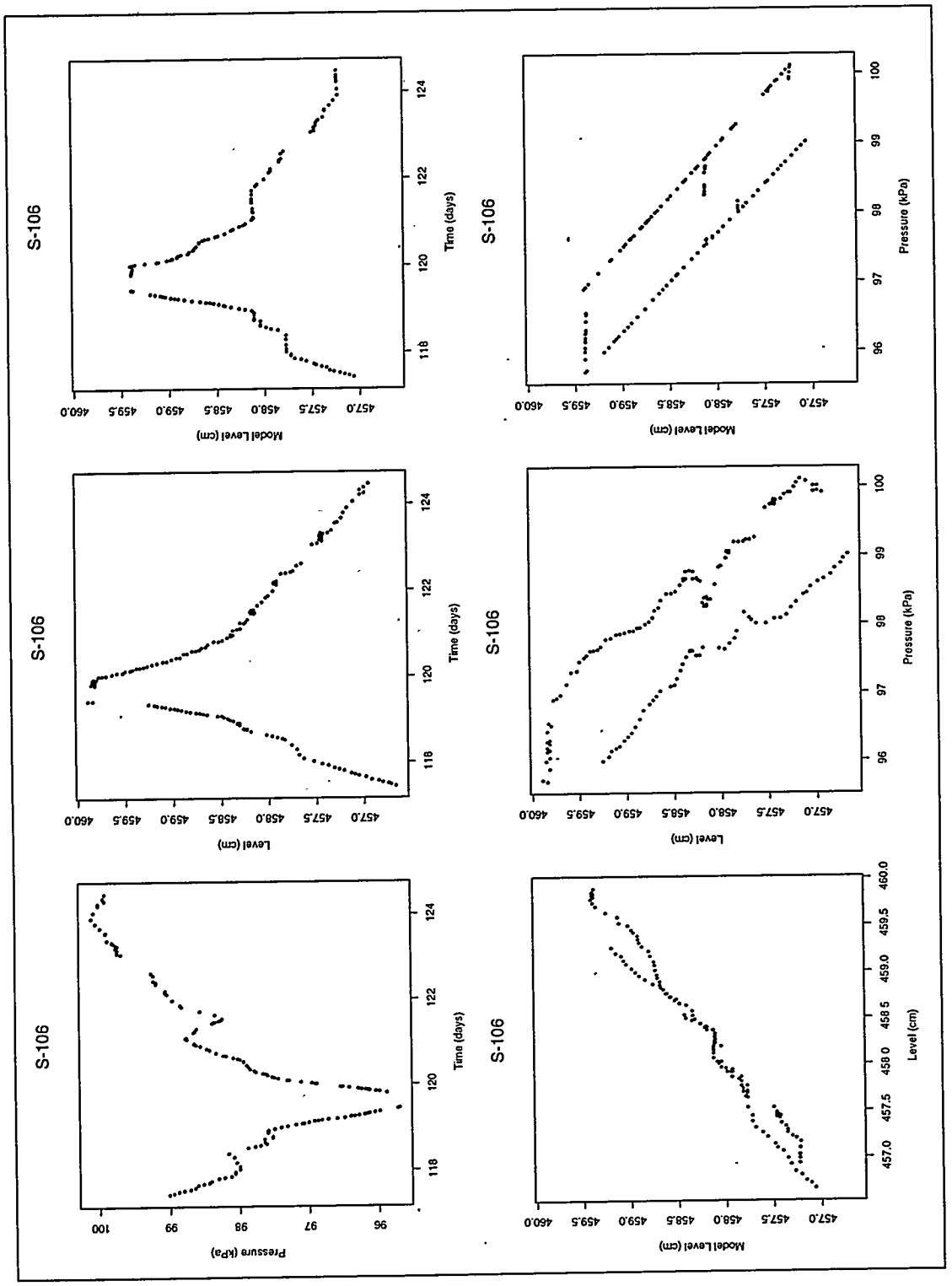

Figure 27: Tank S-106 model and data comparison 12-10-95 to 12-17-95

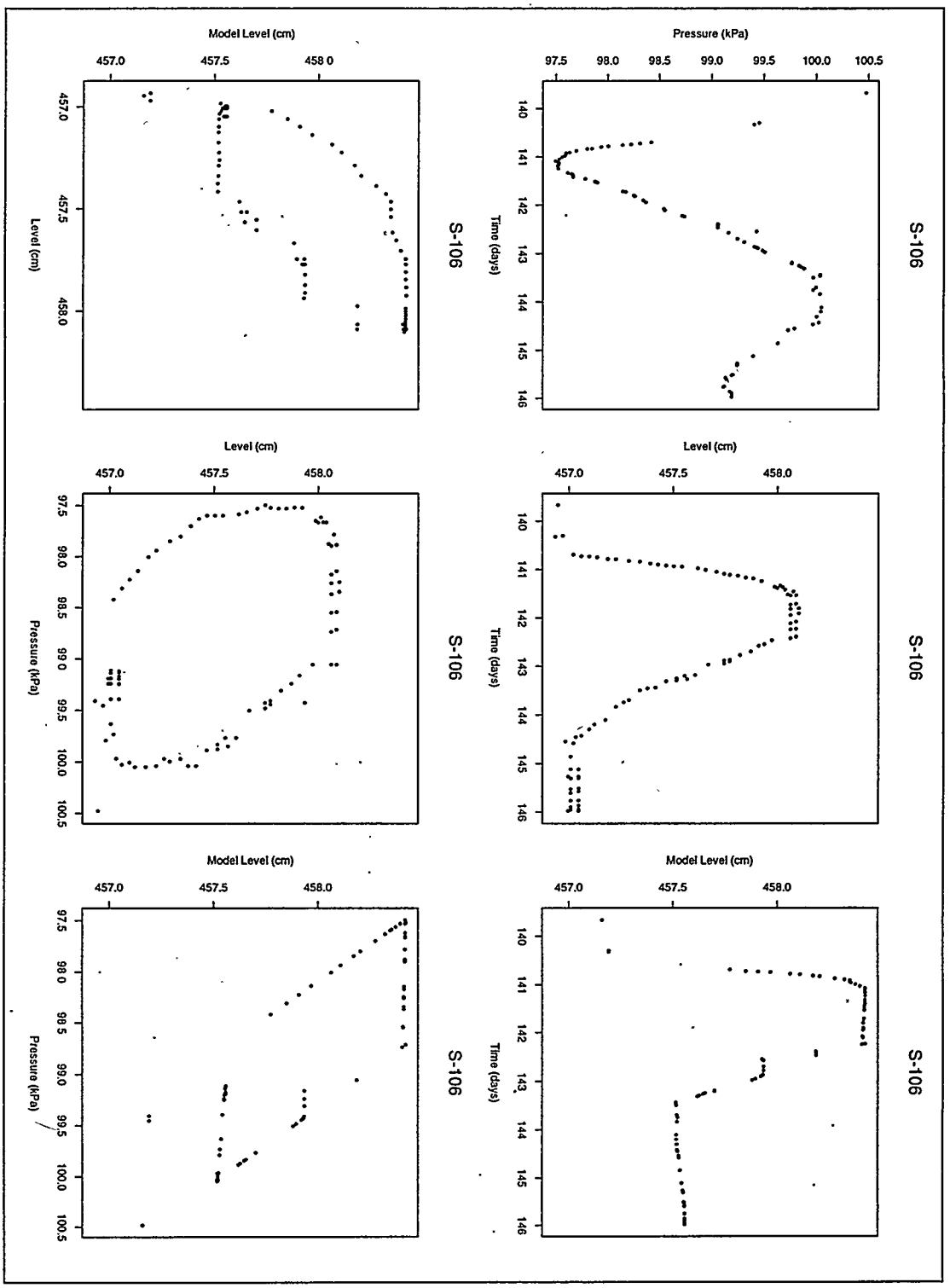

Figure 28: Tank S-106 model and data comparison 1-1-96 to 1-7-96

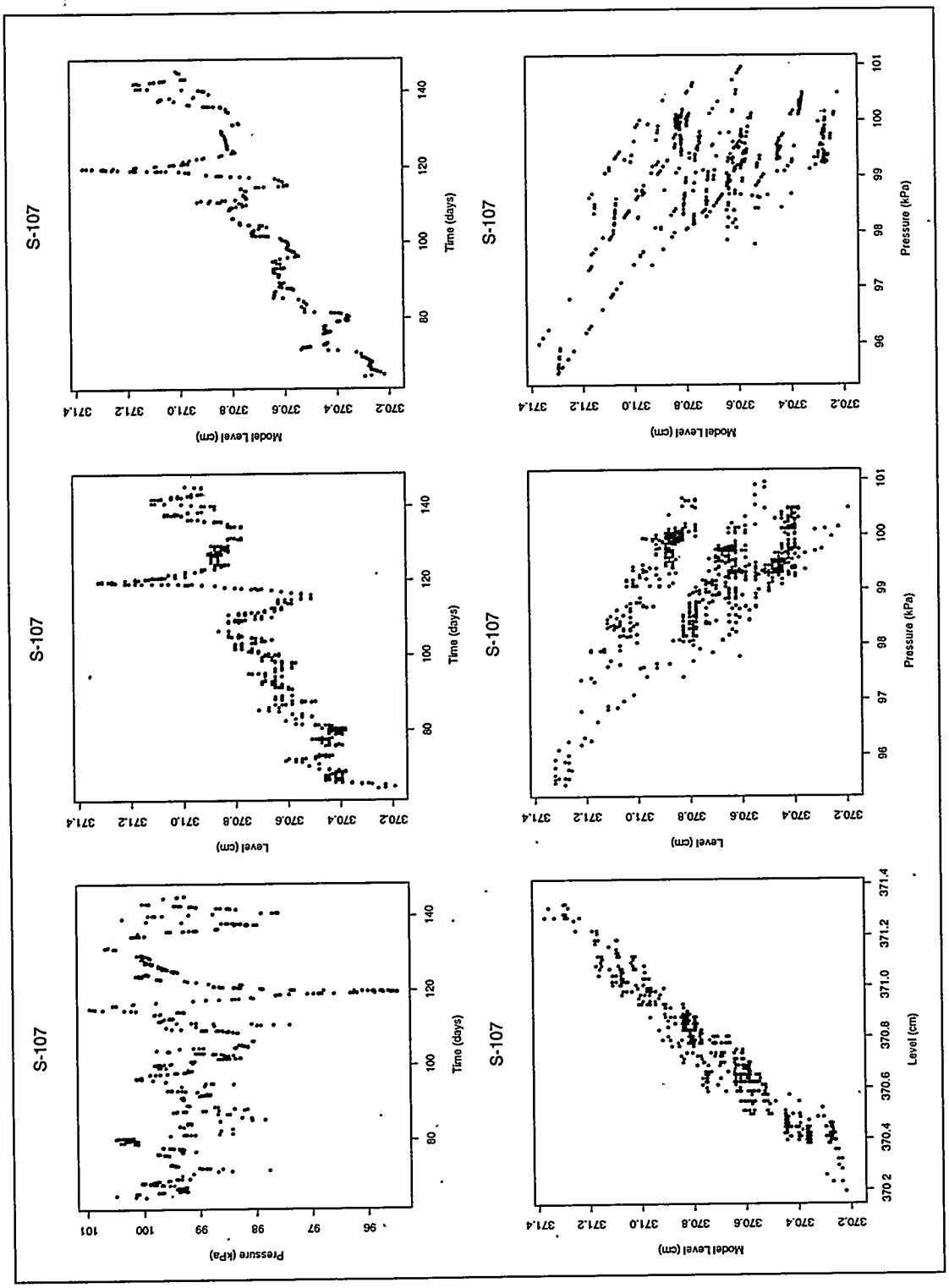

Figure 29: Tank S-107 model and data comparison 10-18-95 to 1-7-96

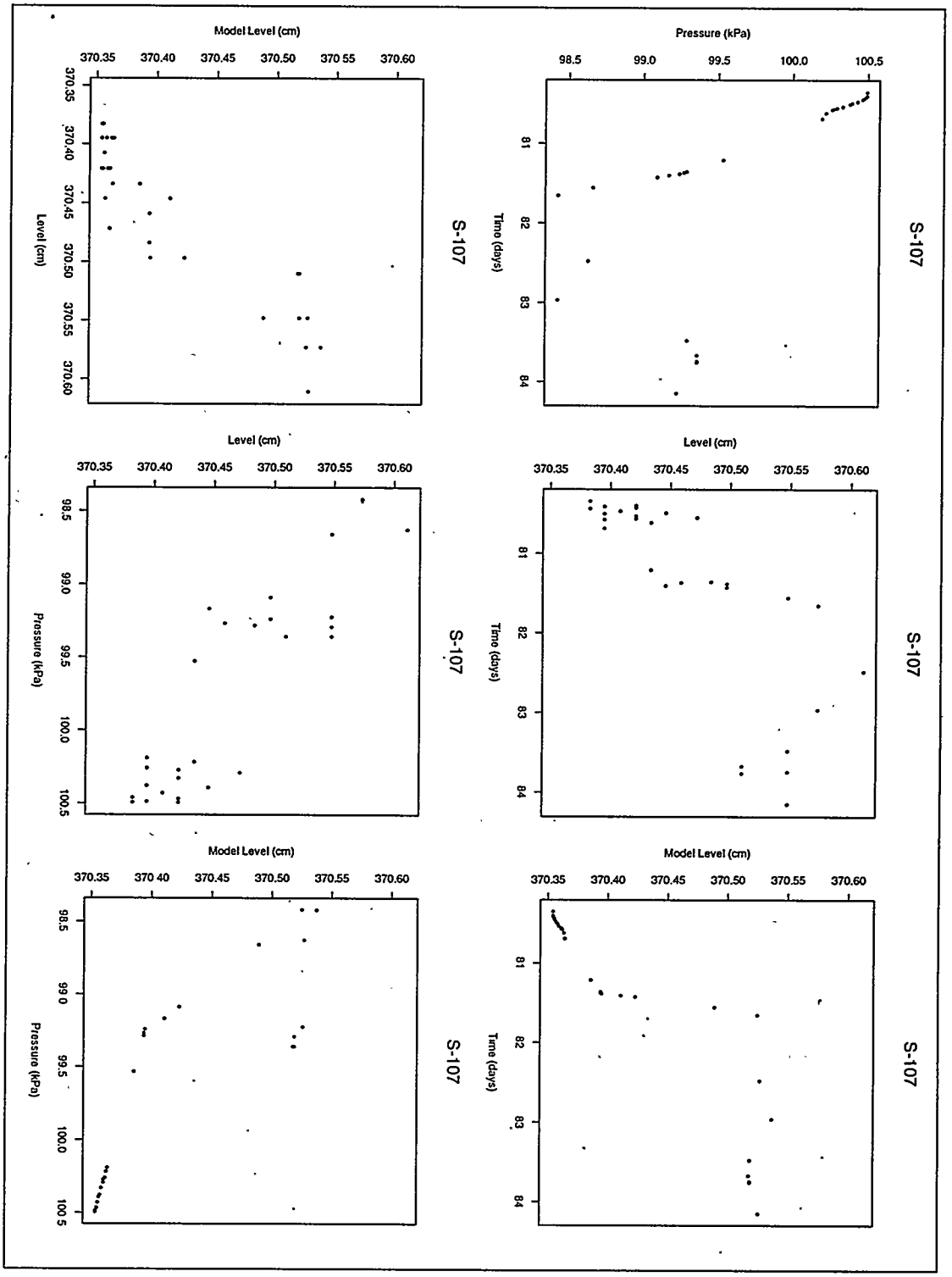

Figure 30: Tank S-107 model and data comparison 11-3-95 to 11-7-95

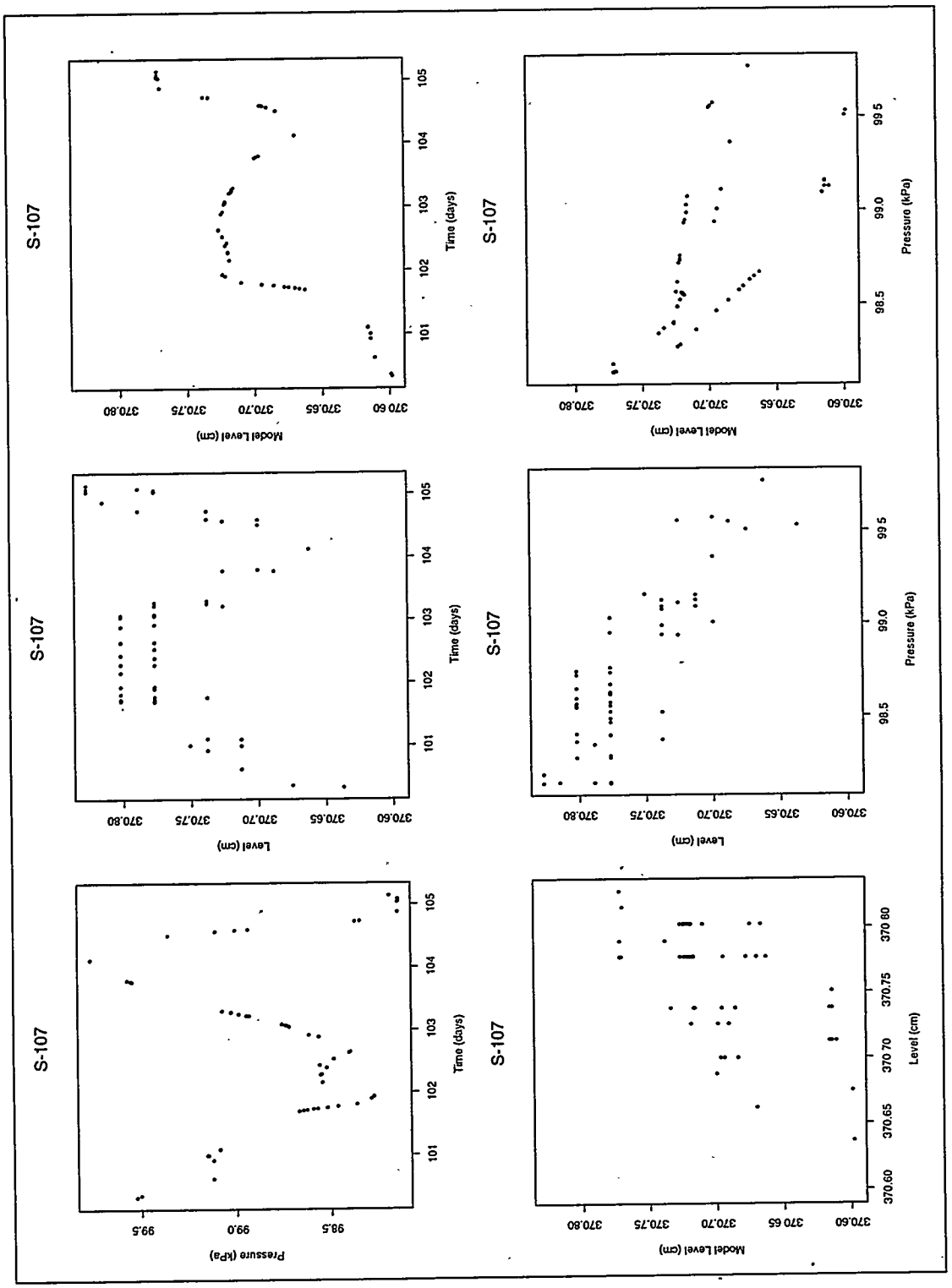

Figure 31: Tank S–107 model and data comparison 11-23-95 to 11-28-95

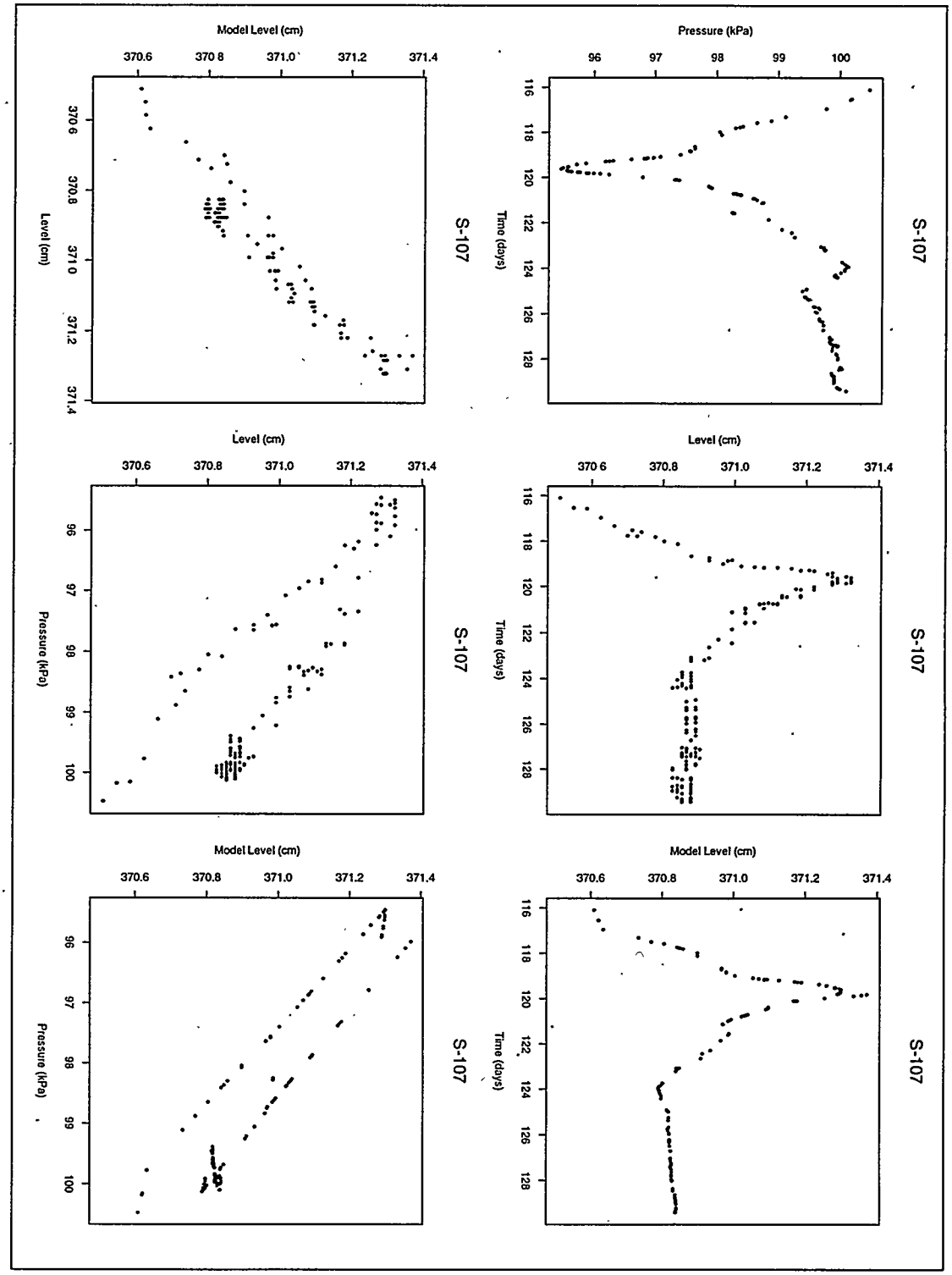

Figure 32: Tank S-107 model and data comparison 12-9-95 to 12-22-95

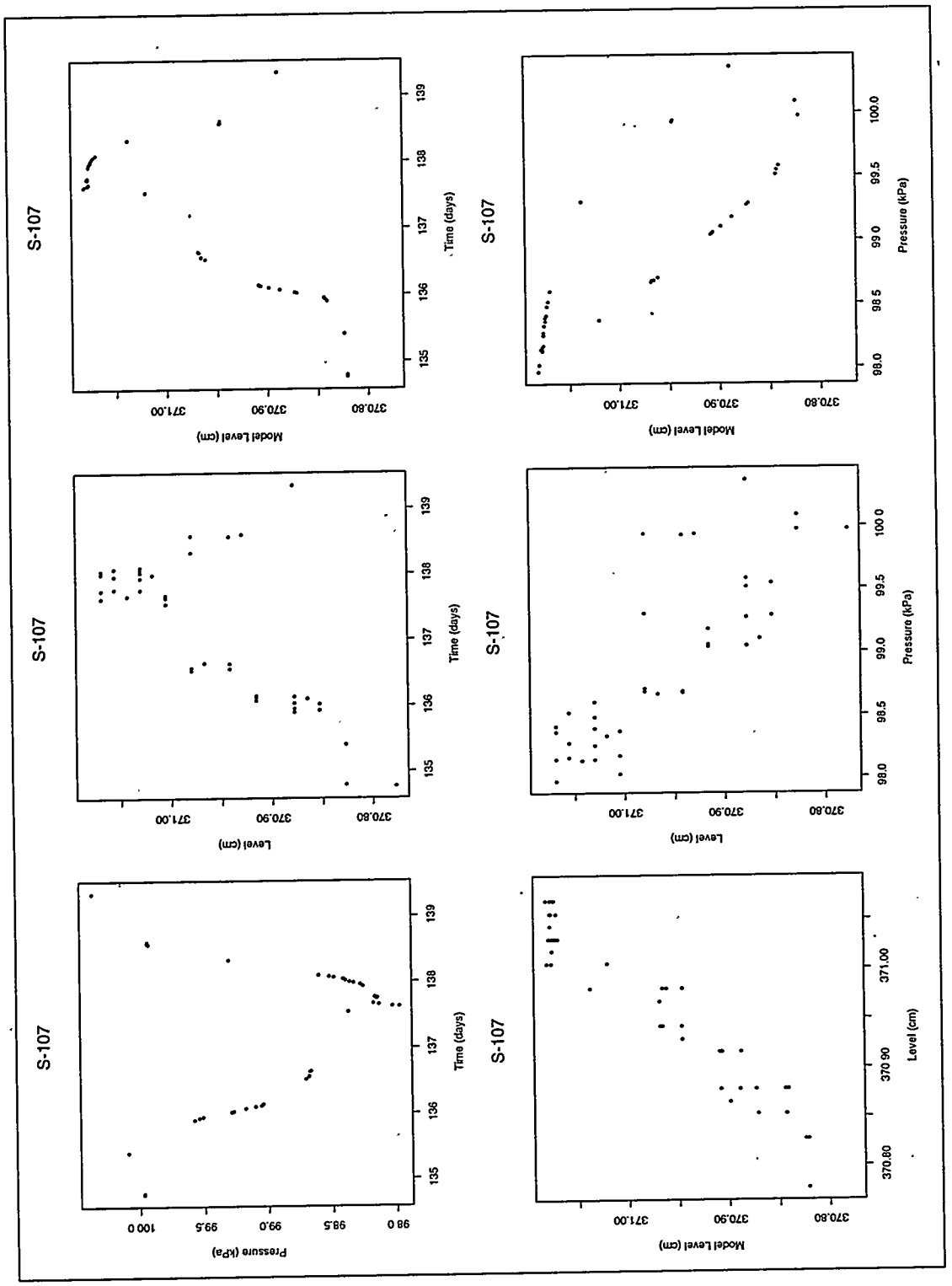

Figure 33: Tank S-107 model and data comparison 12-27-95 to 1-1-96

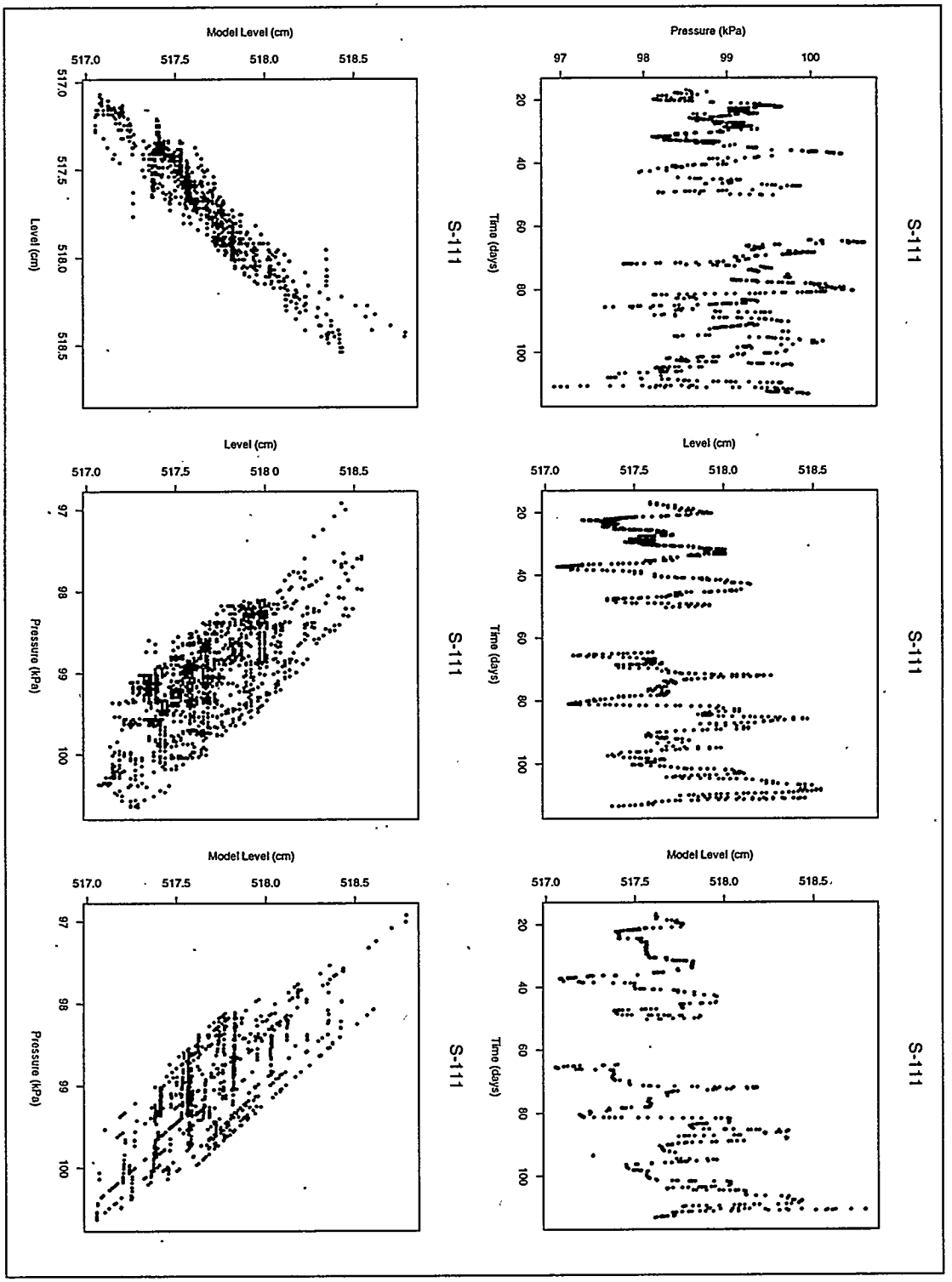

Figure 34: Tank S-111 model and data comparison 8-31-95 to 12-6-95

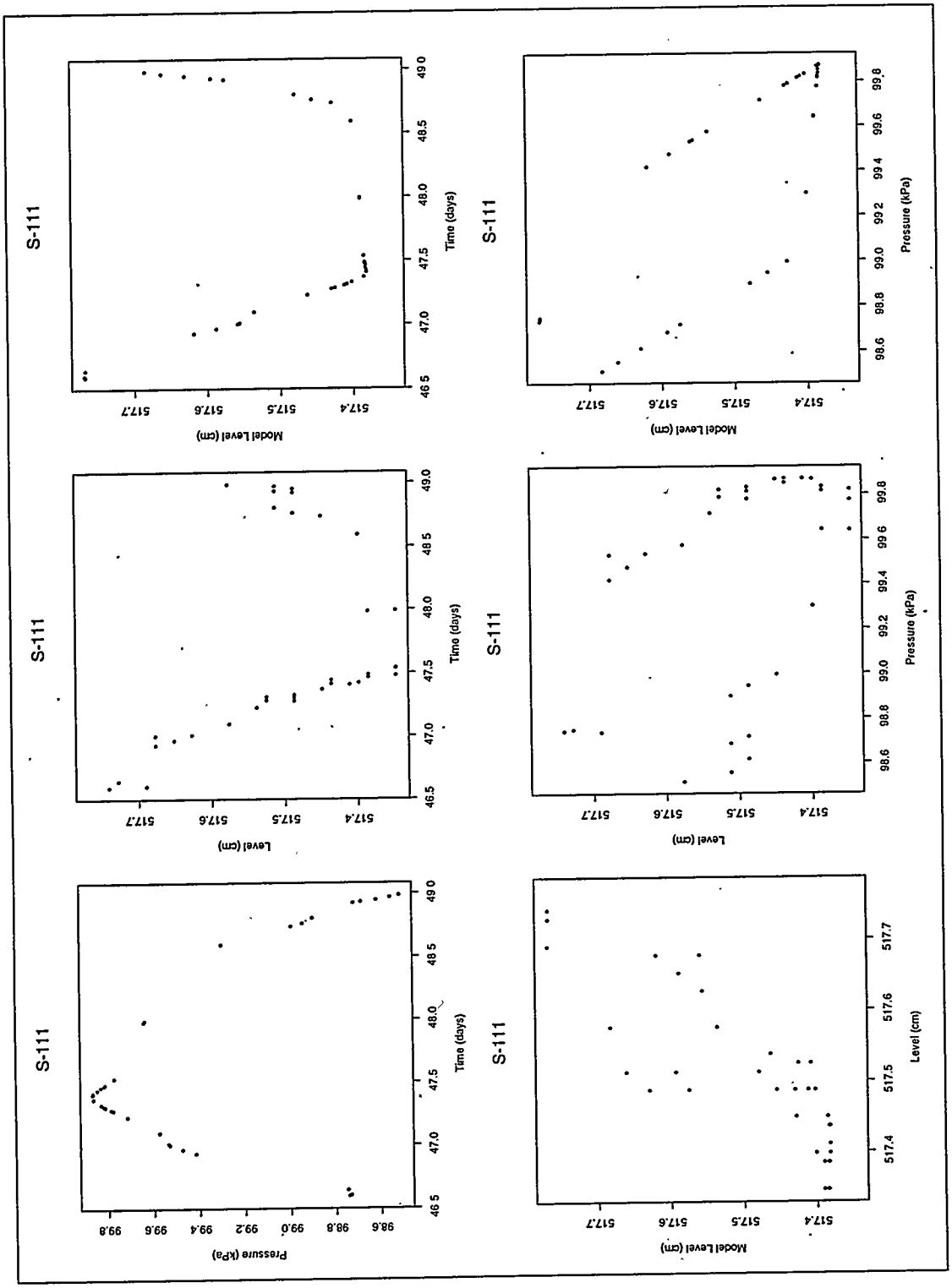

Figure 35: Tank S-111 model and data comparison 9-30-95 to 10-2-95

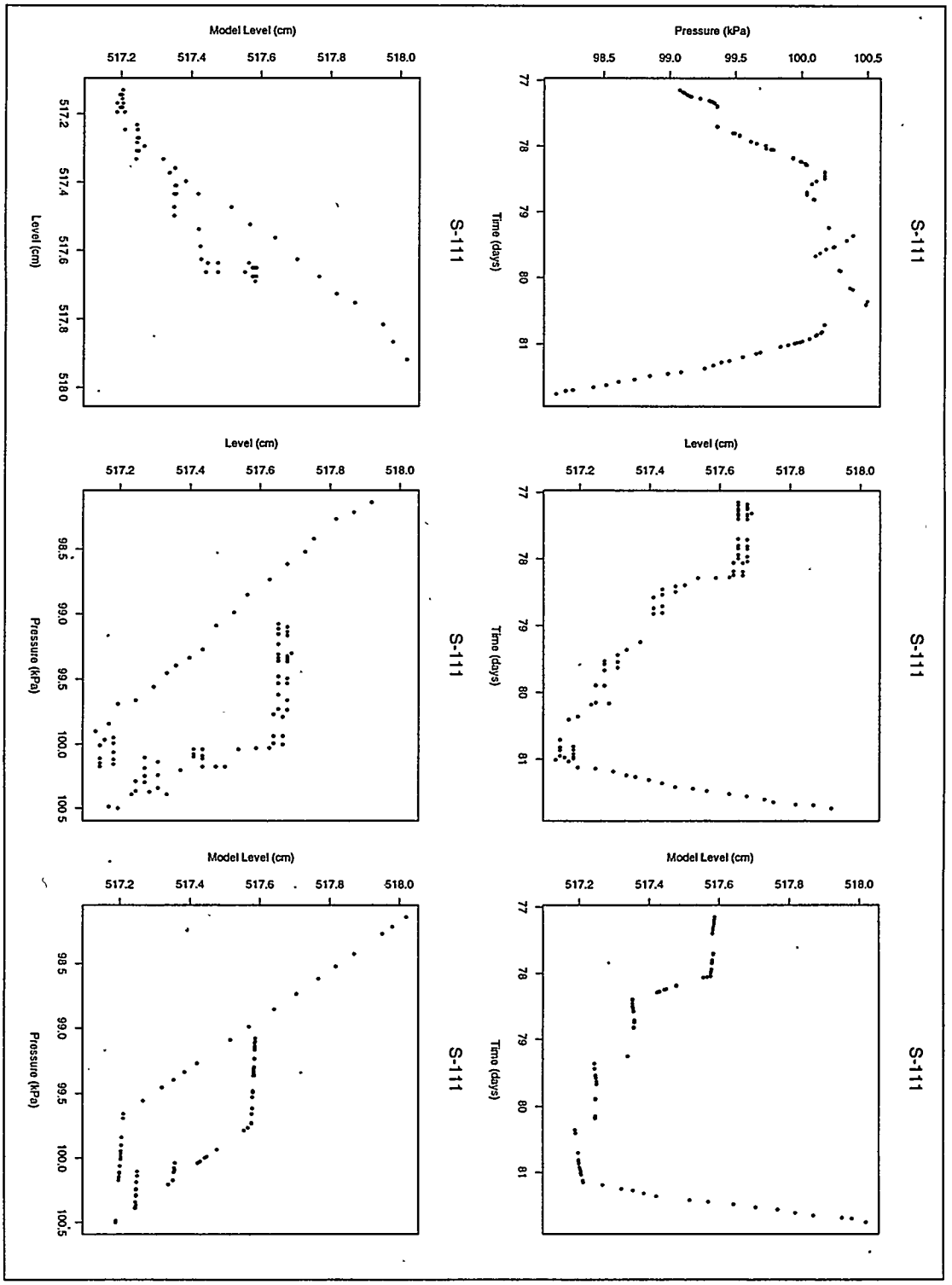

Figure 36: Tank S–111 model and data comparison 10-31-95 to 11-4-95

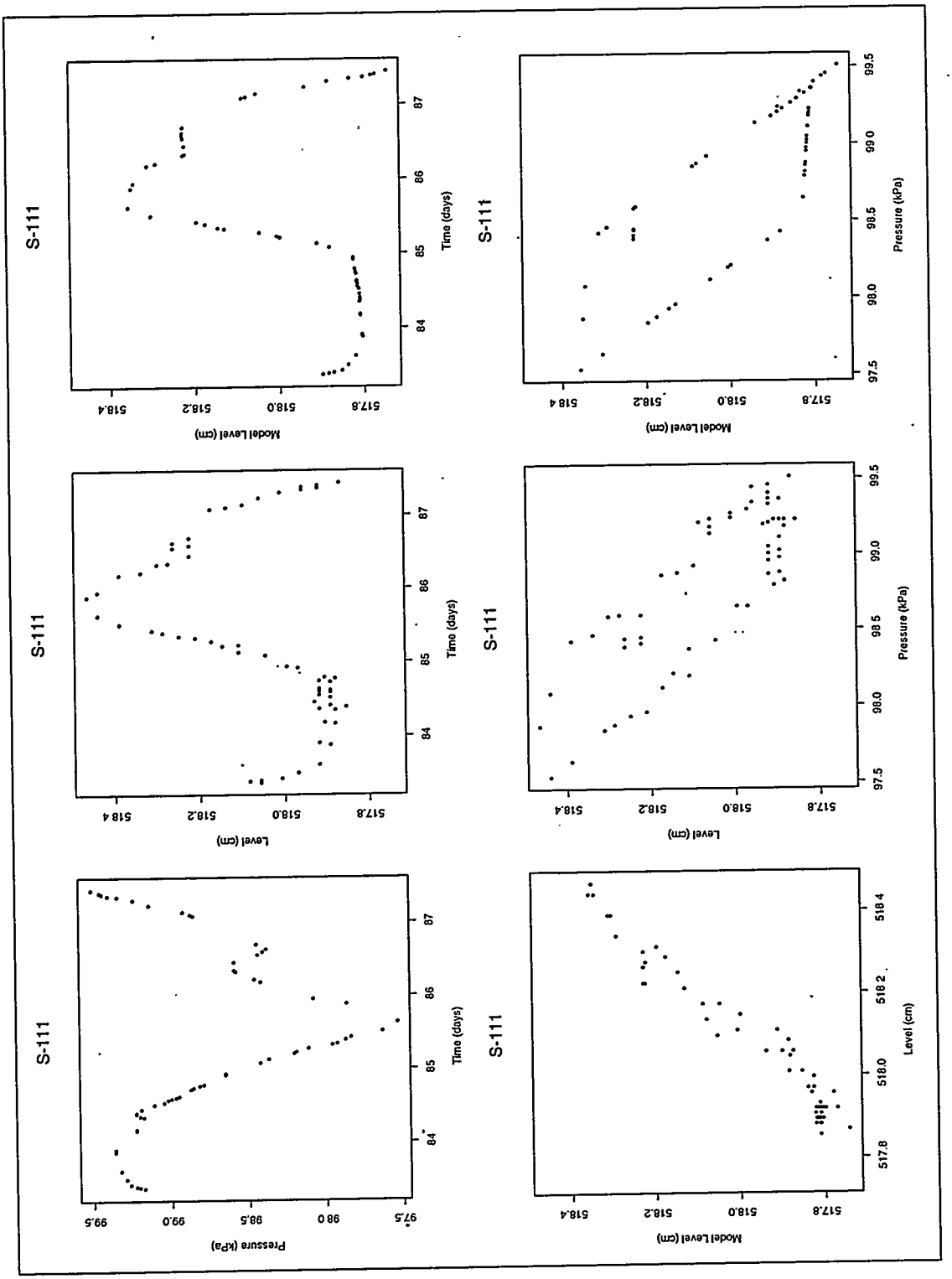

Figure 37: Tank S-111 model and data comparison 11-6-95 to 11-10-95

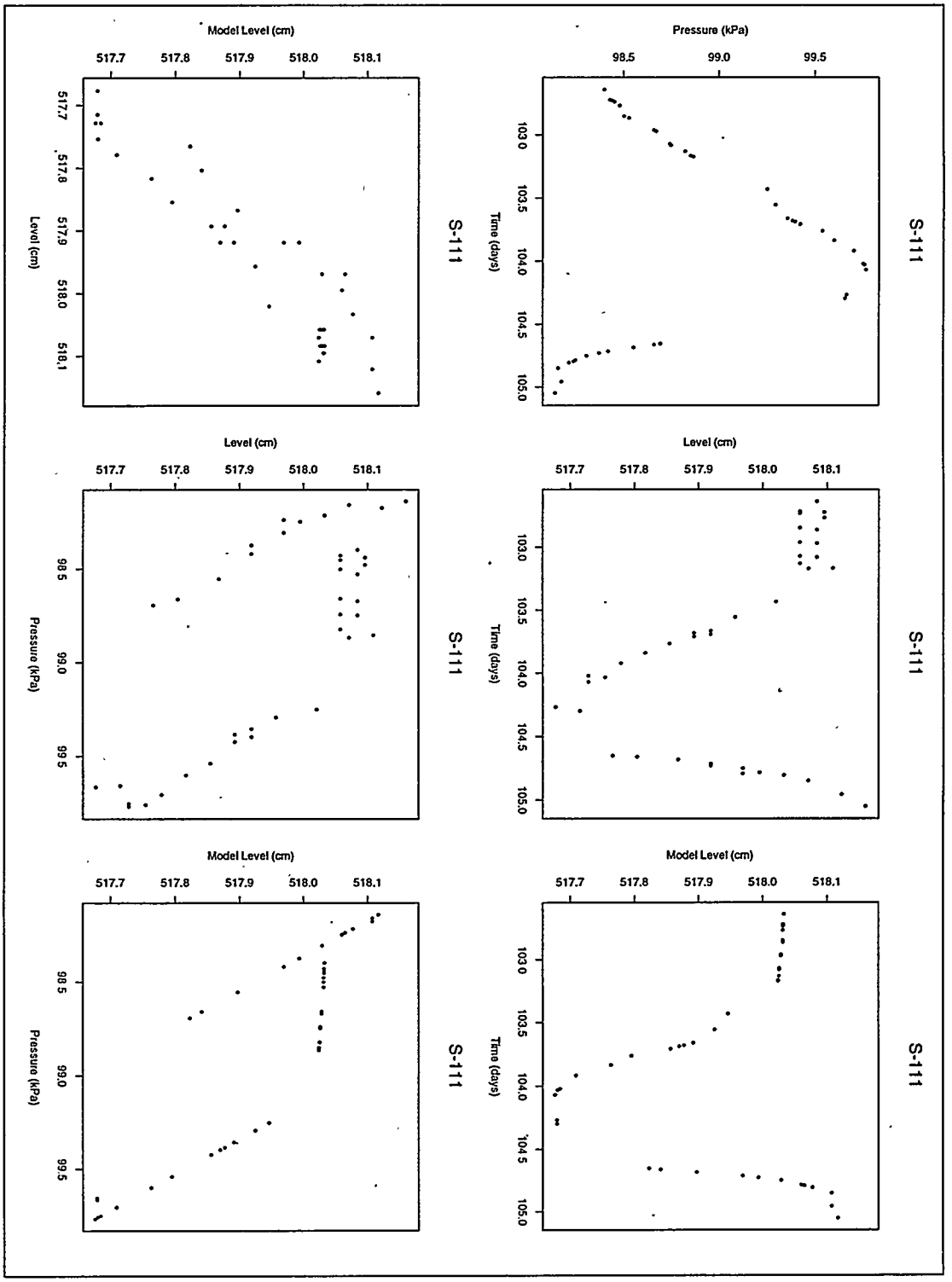

Figure 38: Tank S-111 model and data comparison 11-25-95 to 11-28-95

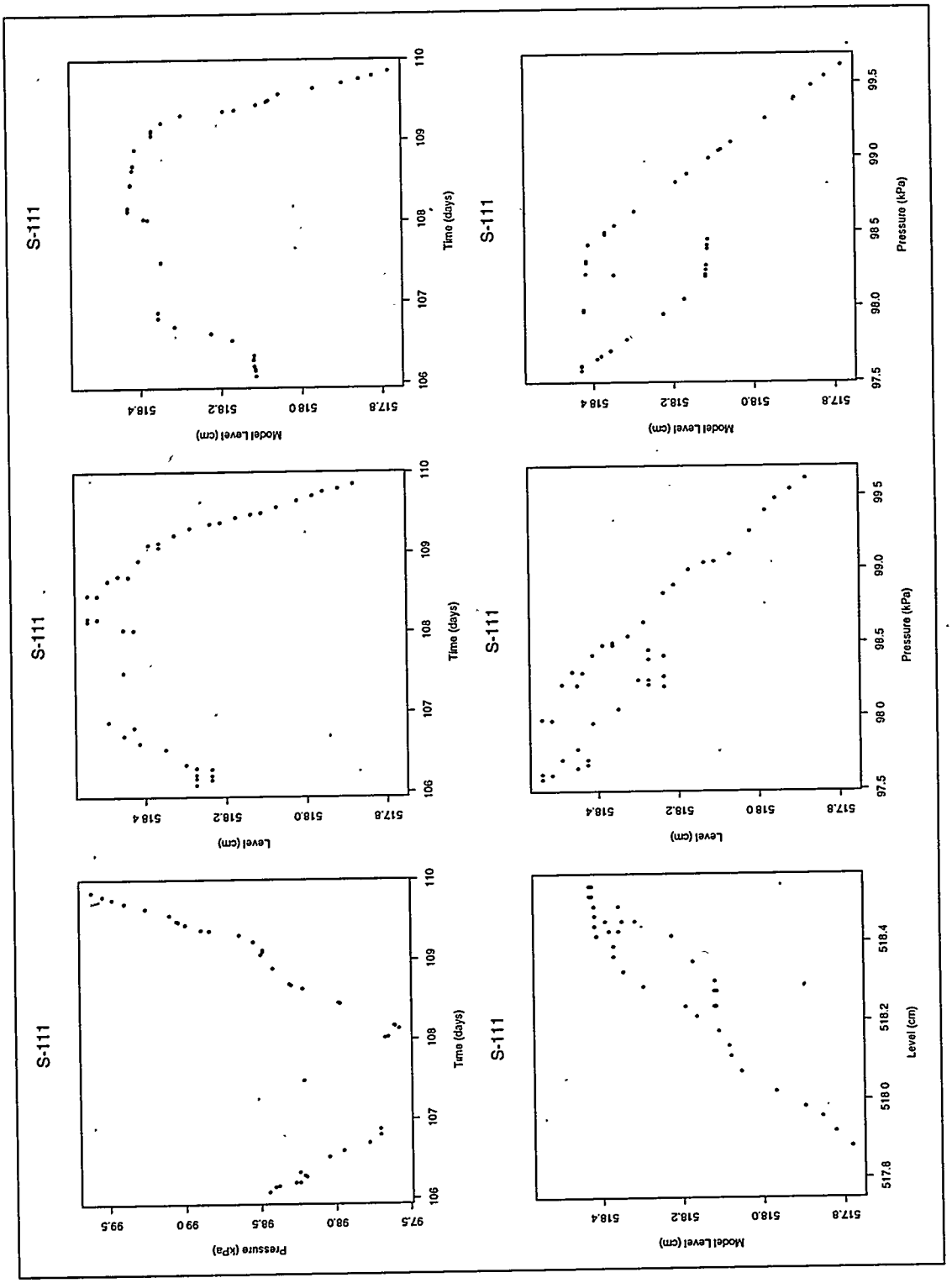

Figure 39: Tank S–111 model and data comparison 11-20-95 to 12-2-95

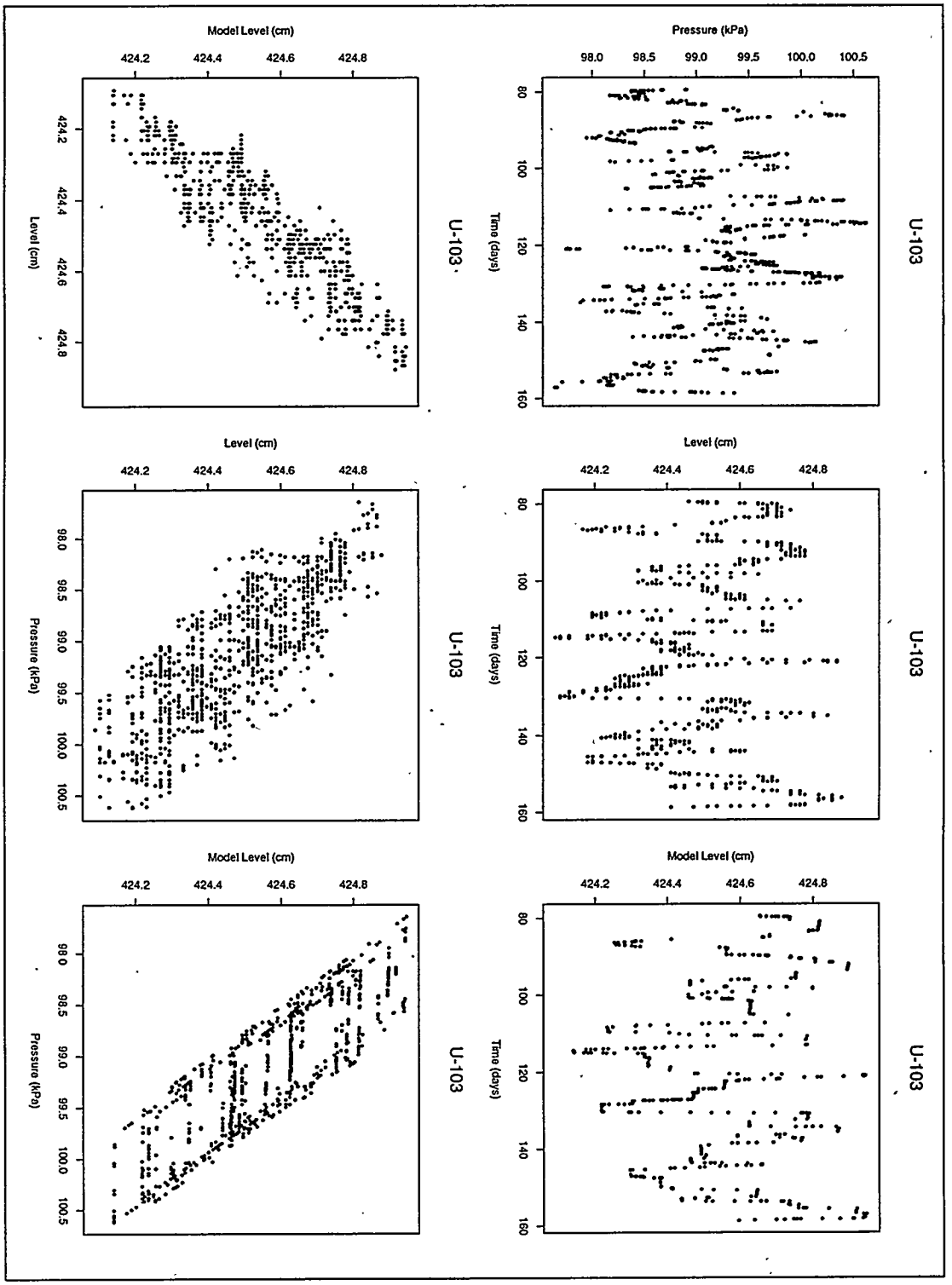

Figure 40: Tank U-103 model and data comparison 9-14-95 to 12-2-95

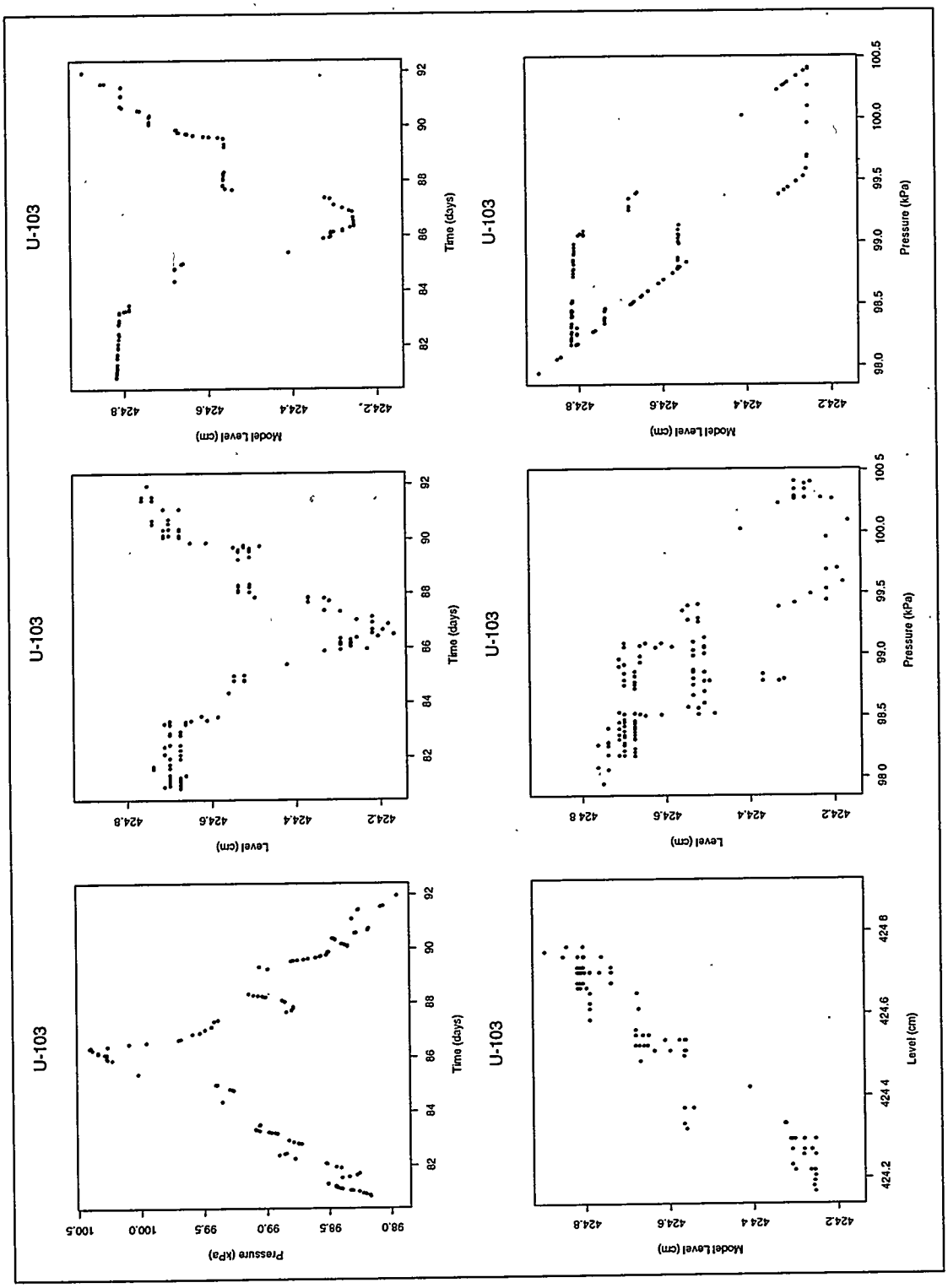

Figure 41: Tank U-103 model and data comparison 9-15-95 to 9-26-95

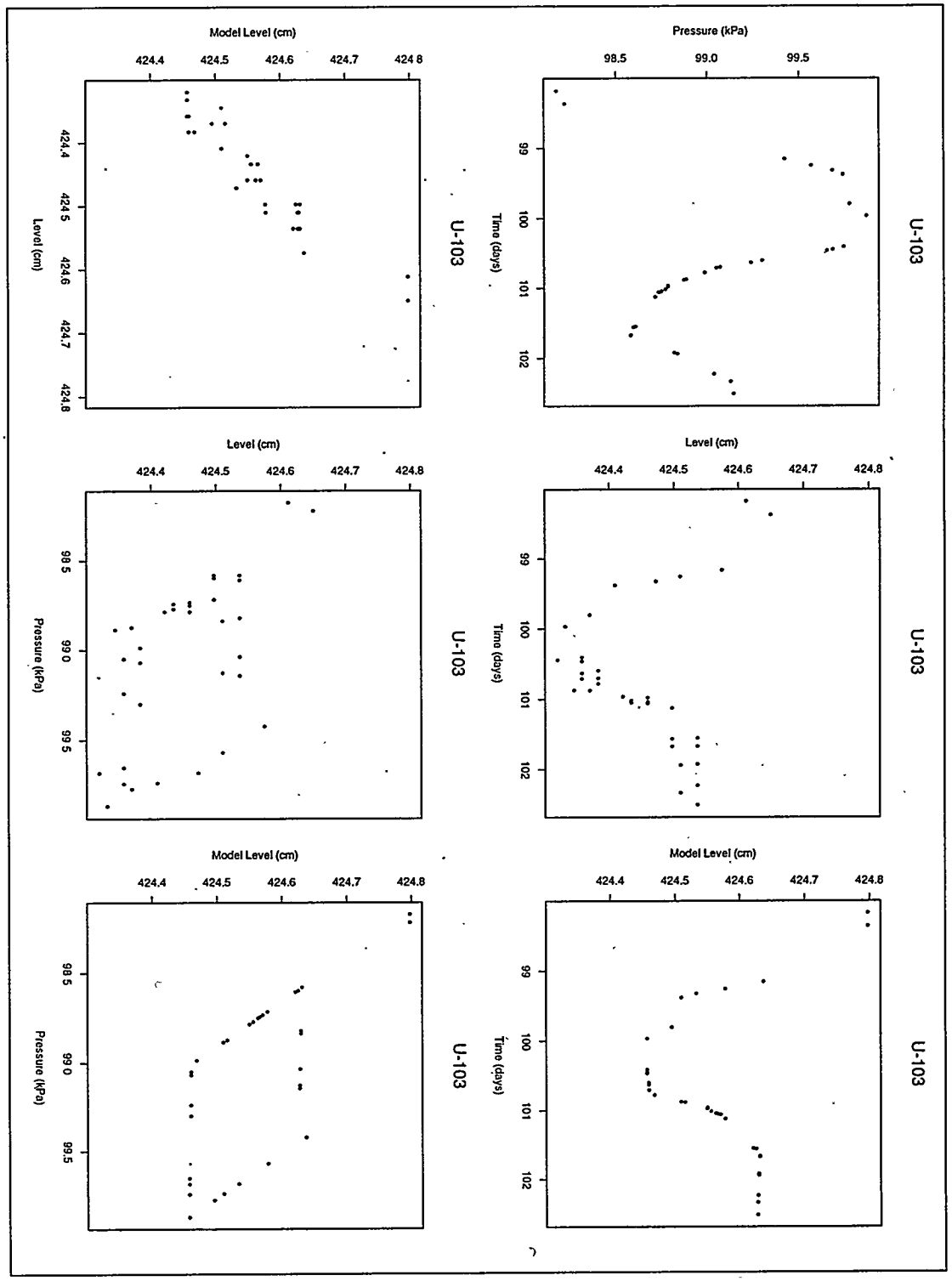

Figure 42: Tank U-103 model and data comparison 10-3-95 to 10-7-95

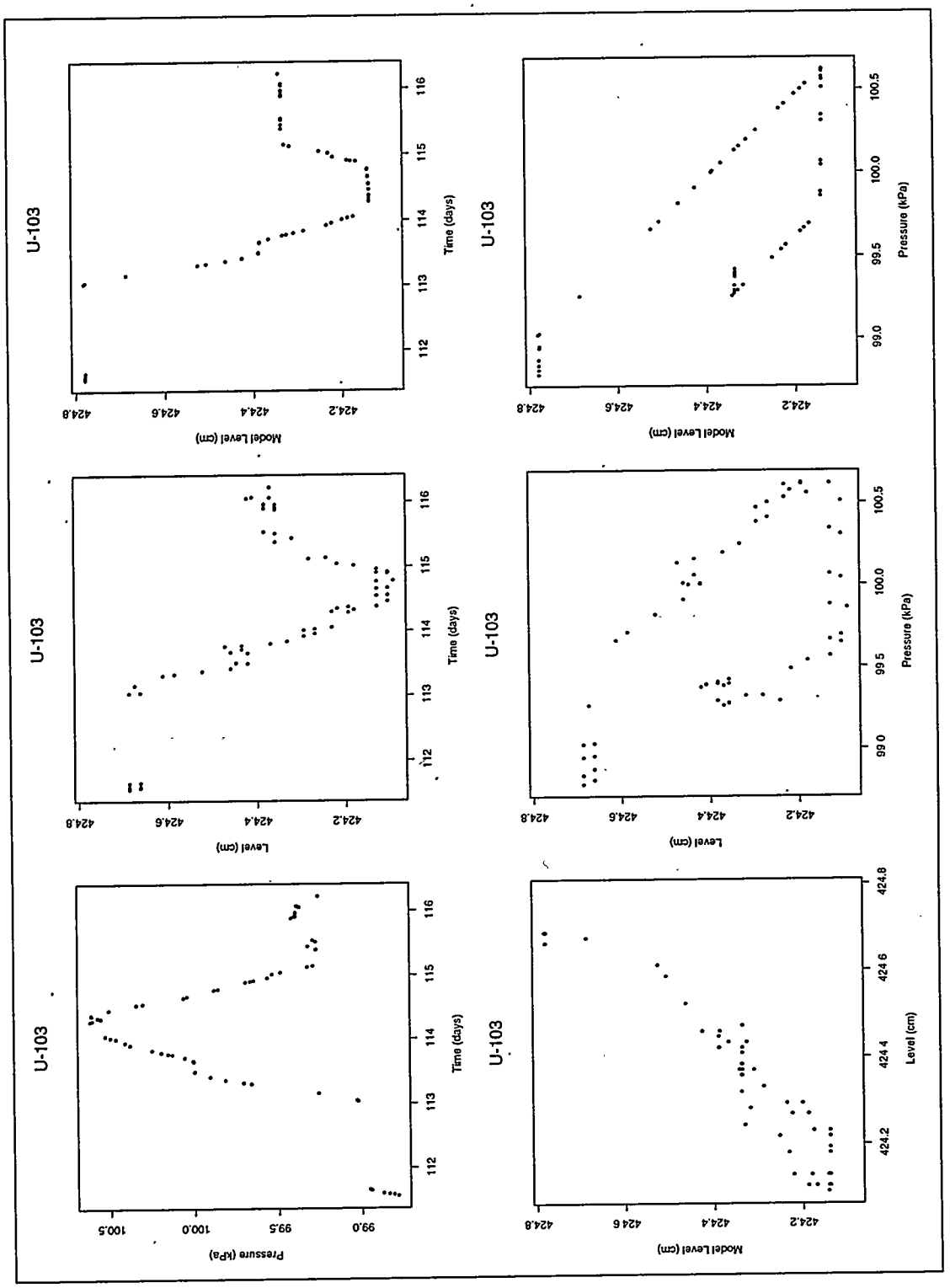

Figure 43: Tank U–103 model and data comparison 10-16-95 to 10-21-95

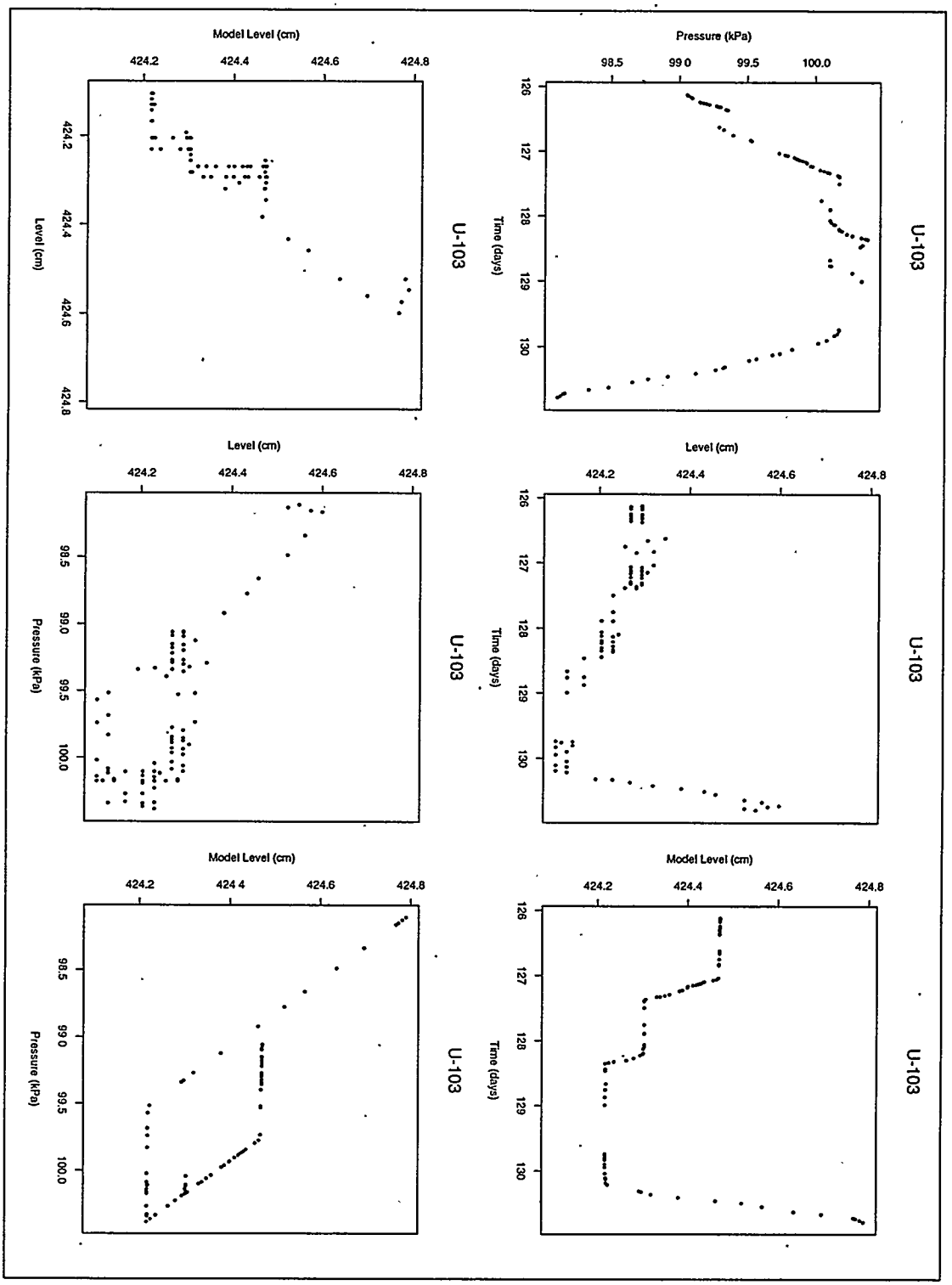

Figure 44: Tank U–103 model and data comparison 10-31-95 to 11-4-95

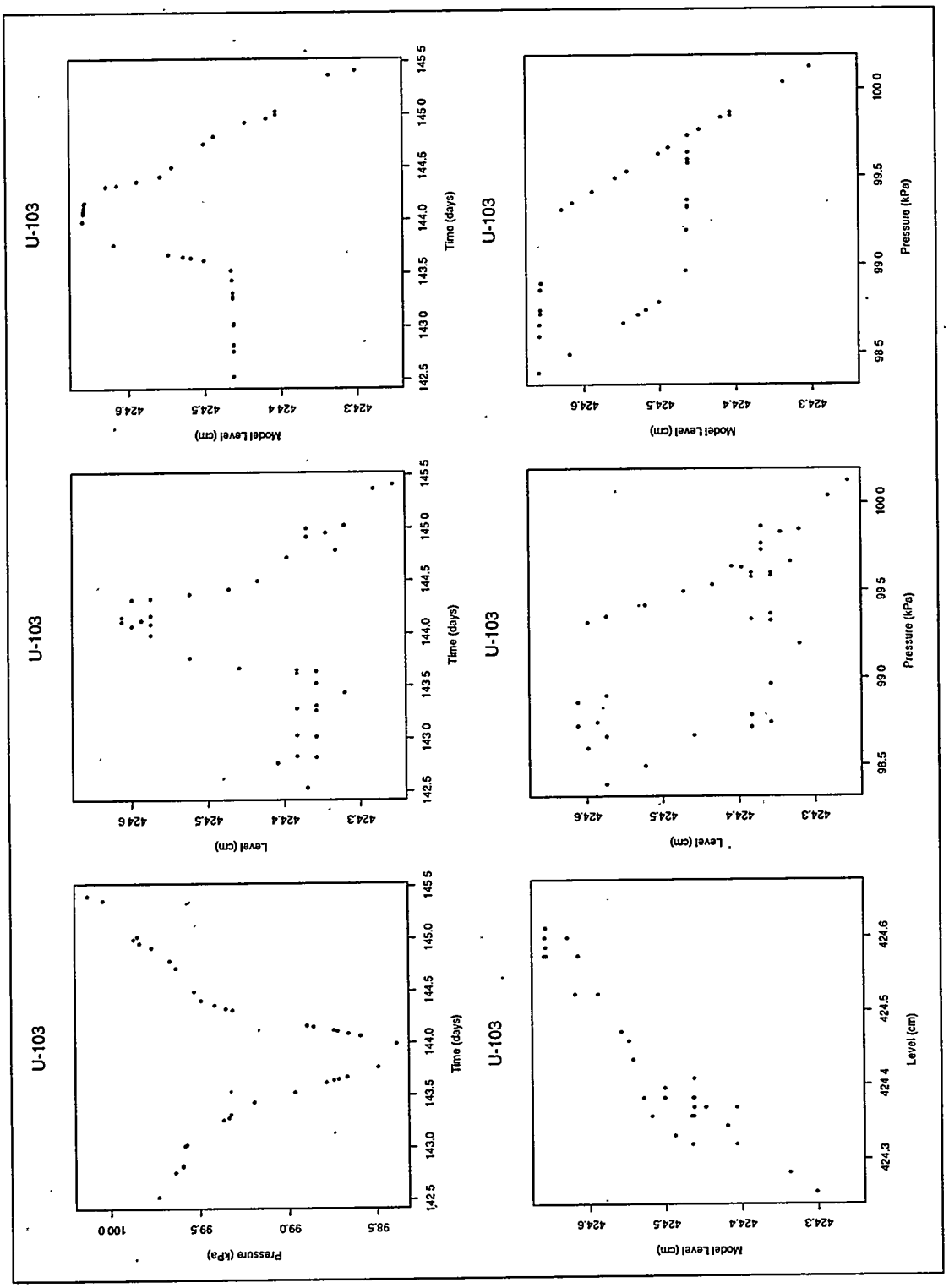

Figure 45: Tank U-103 model and data comparison 11-16-95 to 11-19-95

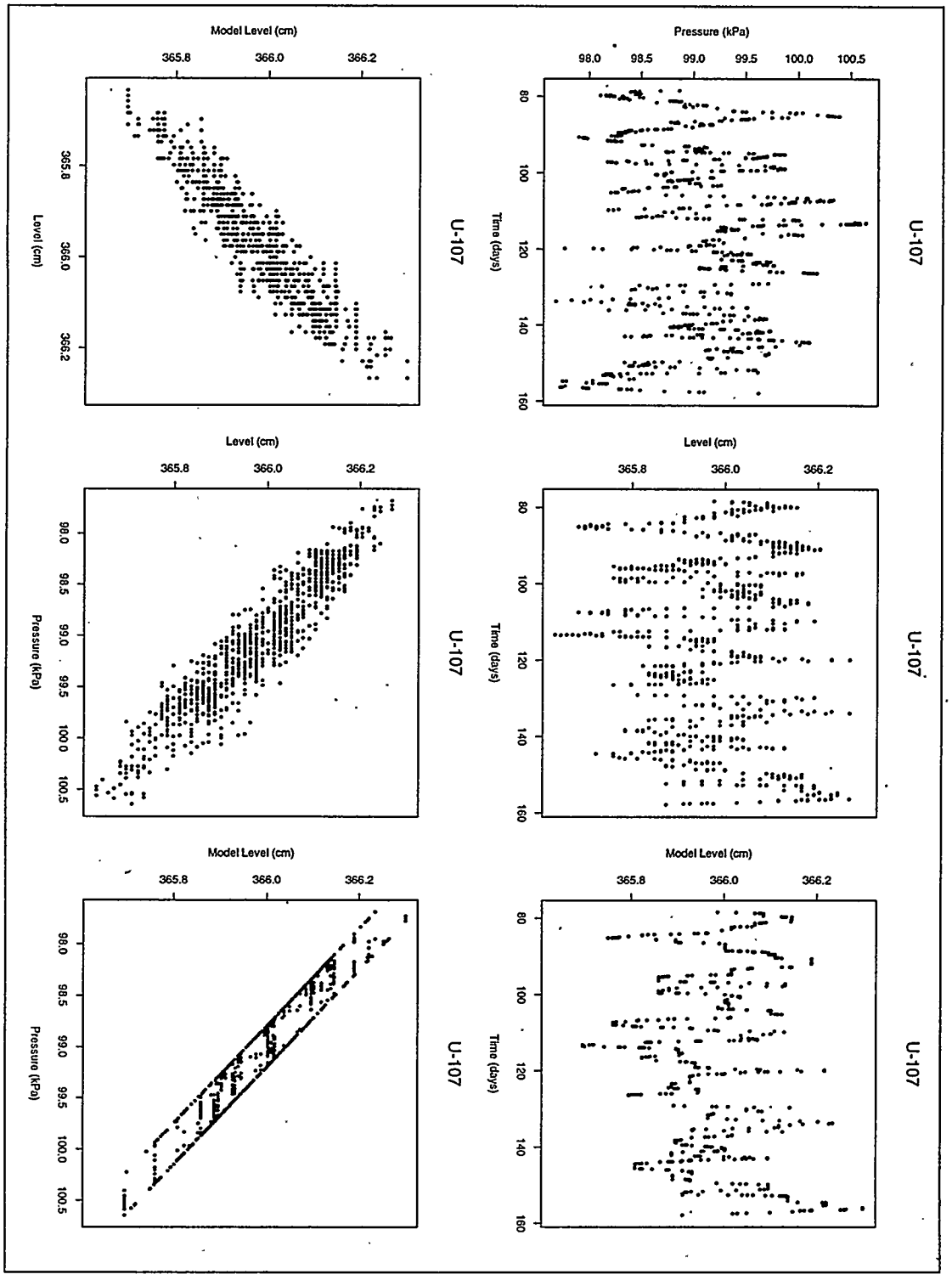

Figure 46: Tank U-107 model and data comparison 9-14-95 to 12-2-95

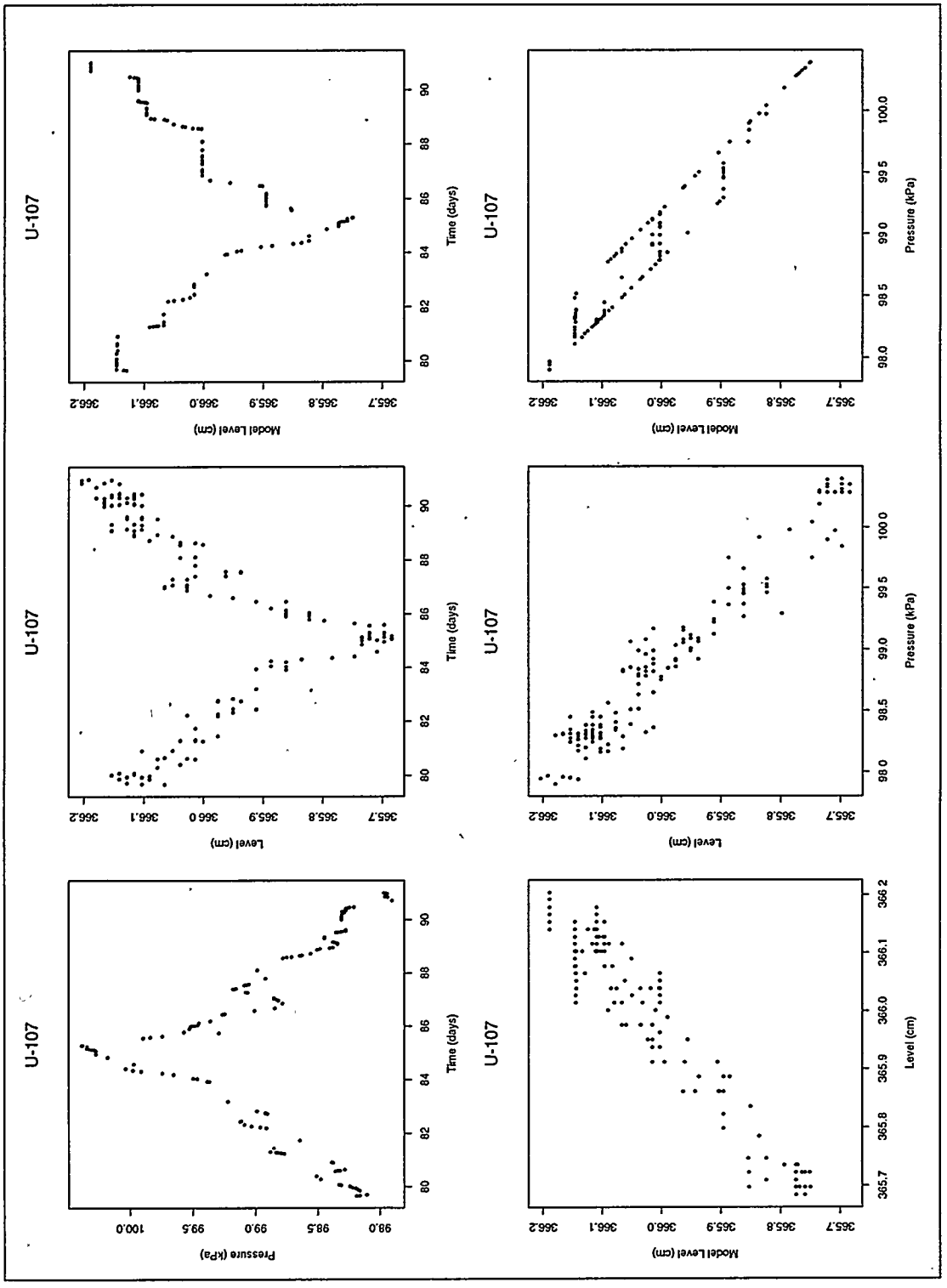

Figure 47: Tank U-107 model and data comparison 9-15-95 to 9-26-95

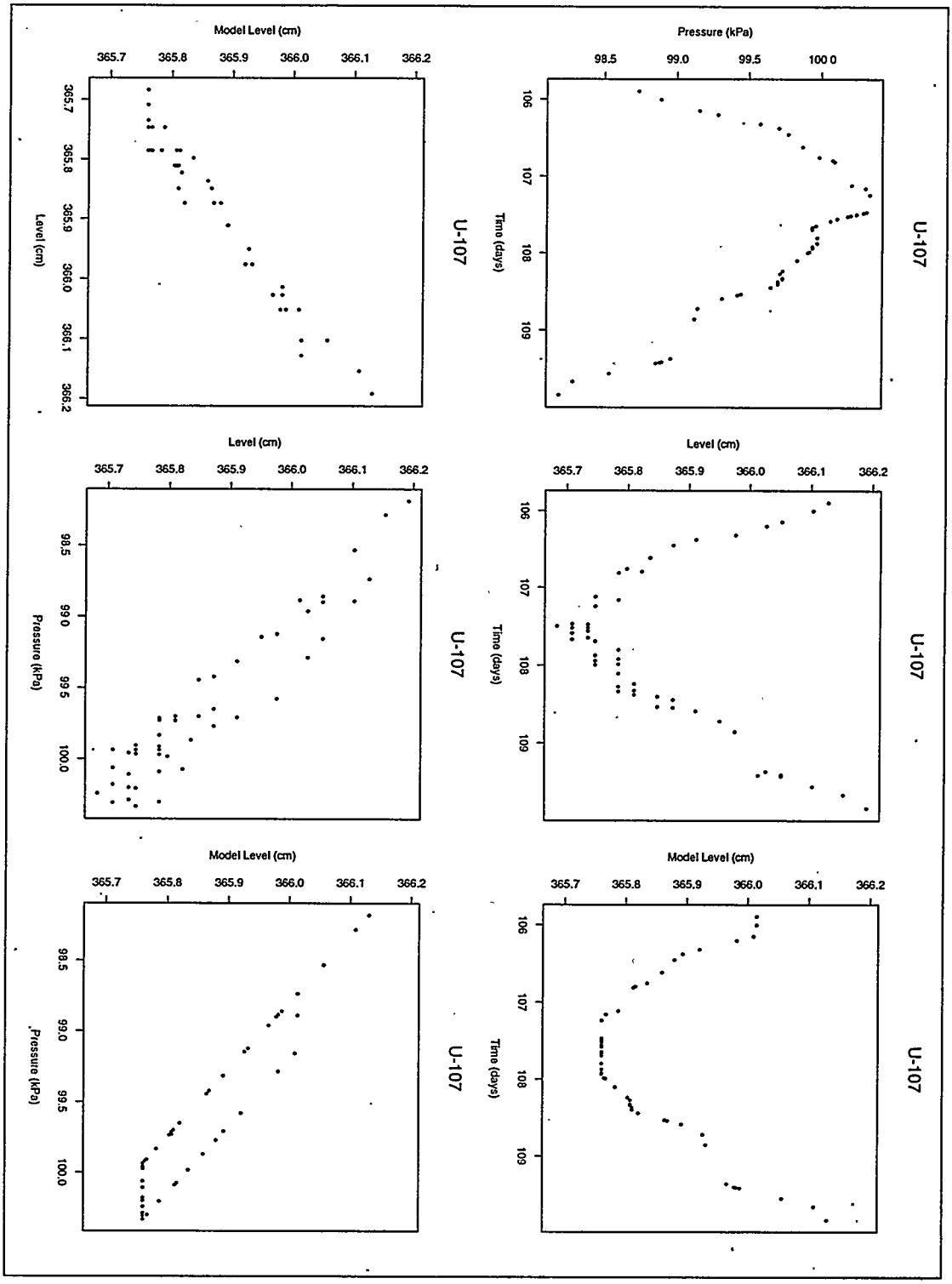

Figure 48: Tank U-107 model and data comparison 10-11-95 to 10-15-95

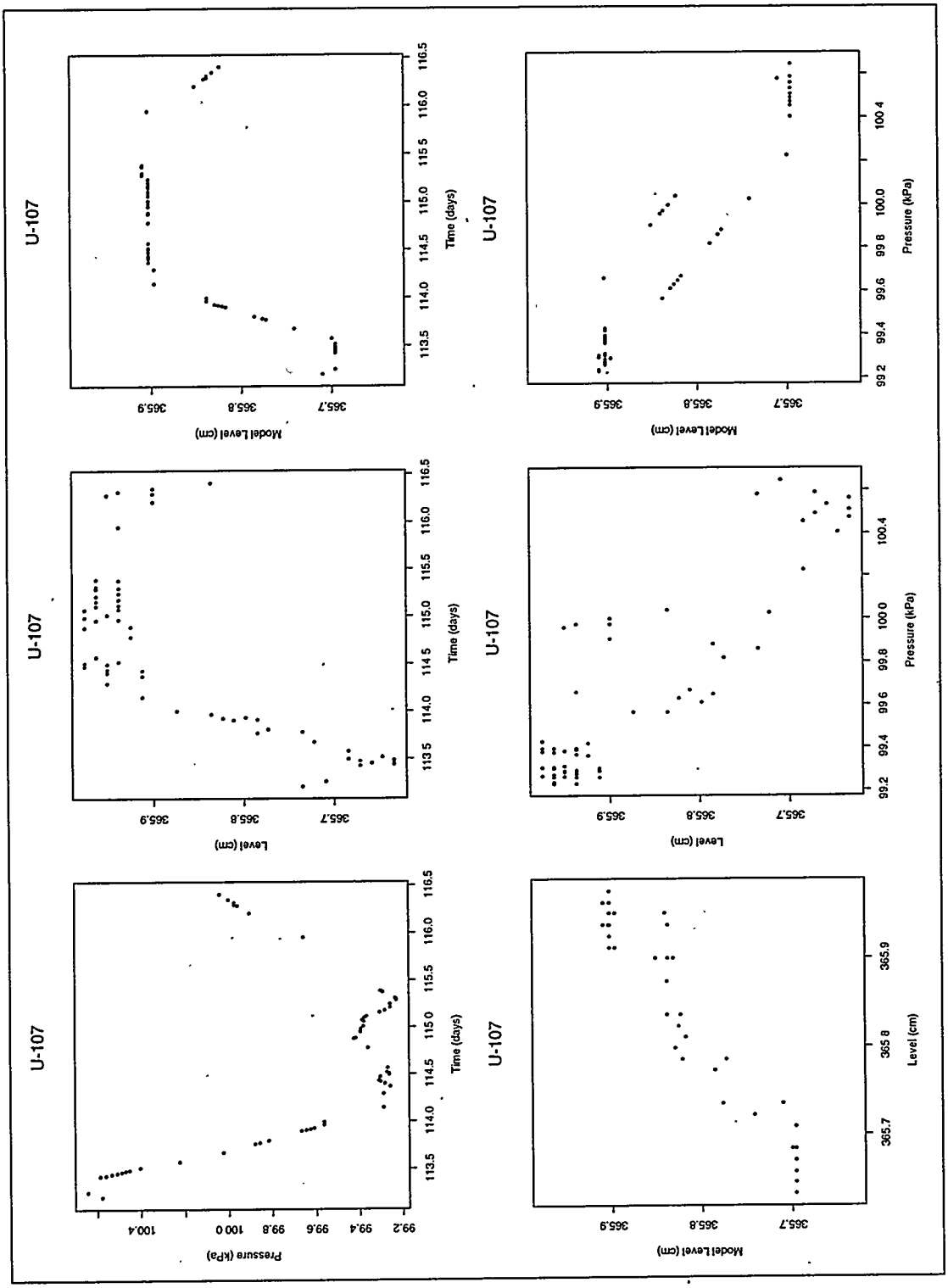

Figure 49: Tank U–107 model and data comparison 10-19-95 to 10-22-95

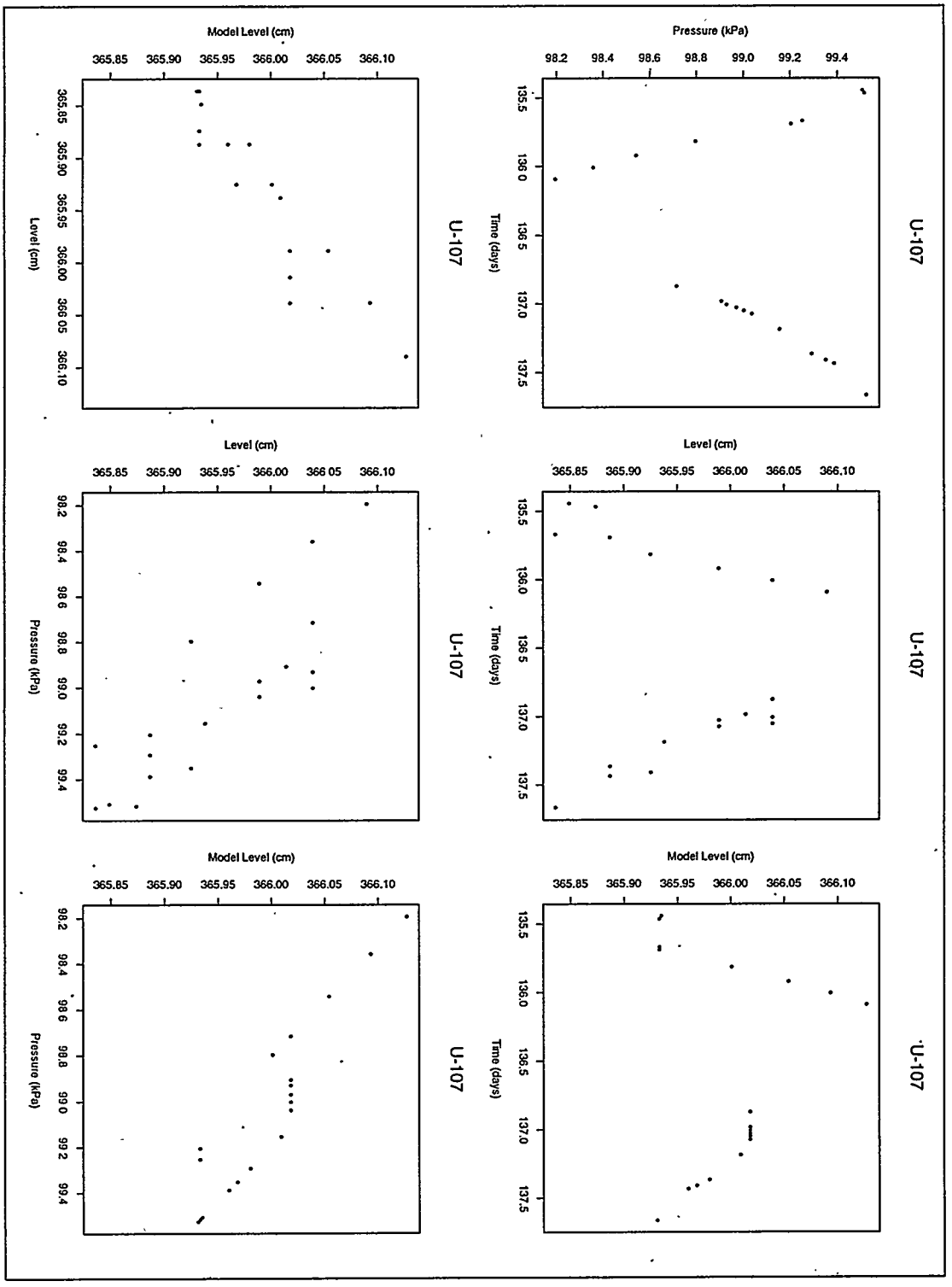

Figure 50: Tank U-107 model and data comparison 11-10-95 to 11-12-95

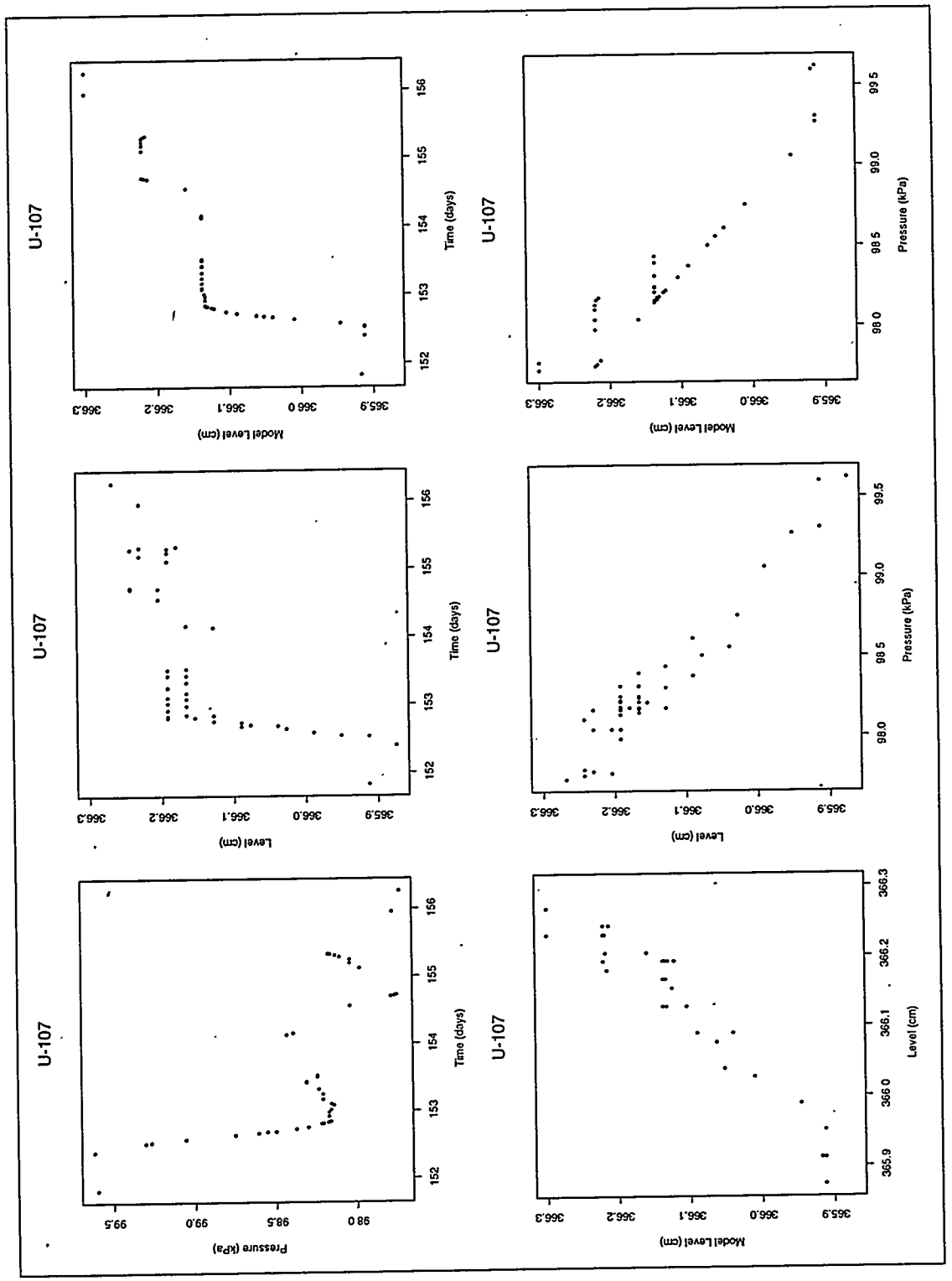

Figure 51: Tank U-107 model and data comparison 11-26-95 to 12-1-95

References

Andrews, G. & Buck, J. (1987), Hanford Meteorological Station Computer Codes, Volume 6 - The SFC Computer Code, Technical Report PNL-6279 Vol. 6, Pacific Northwest Laboratory, Richland, Washington.

Brown, R. G. (1983), *Introduction to Random Signal Analysis and Kalman Filtering*, John Wiley & Sons, New York.

Brown, R. G. (1996), Compilation of Hydrogen Data for 22 Single Shell Flammable Gas Watch List Tanks, Technical Report WHC-SD-WM-ER-576, Westinghouse Hanford Company, Richland, Washington.

Eyler, L. (1995), Assessment of Tank 241–C–106 Temperature Response Indications, Technical Report PNL-10514, Pacific Northwest Laboratory, Richland, Washington.

Glasscock, J. (1993), Surveillance Analysis Computer System Temperature Database Software Requirements Specification, Technical Report WHC-SD-WM-CSRS-007, Rev. 1a, Westinghouse Hanford Company, Richland, Washington.

Hanlon, B. (1996), Waste Tank Summary for Month Ending October 31, 1995, Technical Report WHC-EP-0182-91, Westinghouse Hanford Company, Richland, Washington.

Hodgson, K., Anantamula, R., Barker, S., K.D.Fowler, Hopkins, J., Lechelt, J. & Reynolds, D. (1995), Evaluation of Hanford Tanks for Trapped Gas, Technical Report WHC-SD-WM-ER-526, Rev. 0, Westinghouse Hanford Company, Richland, Washington.

Hoitink, D. & Burk, K. (1994), Climatological Data Summary 1993 with Historical Data, Technical Report PNL-9809, Pacific Northwest Laboratory, Richland, Washington.

Kitagawa, G. & Matsumoto, N. (1996), 'Detection of Coseismic Changes of Underground Water Level', *Journal of the American Statistical Association* **91**(434), 521–528.

Peters, T. & Park, W. (1993), Evaluation of Methods to Measure Surface Level in Waste Storage Tanks: Second Test Sequence, Technical Report PNL-8839, Pacific Northwest Laboratory, Richland, Washington.

Spurling, D. (1991), Software Requirements Specification: CASS Central Facility, Technical Report WHC-SD-SFR-003 Rev 0, Westinghouse Hanford Company, Richland, Washington.

Stewart, C., Alzheimer, J., Brewster, M., Chen, G., Mendoza, R., Reid, H., Shepard, C. & Terrones, G. (1996), In Situ Rheology and Gas Volume in Hanford Double-Shell Waste Tanks – DRAFT, Technical Report PNNL-11296, Pacific Northwest National Laboratory, Richland, Washington.

Timoshenko, S. & Goodier, J. (1982), *Theory of Elasticity*, third edn, McGraw Hill Book Company, New York.

West, M. & Harrison, J. (1989), *Bayesian Forecasting and Dynamic Models*, Springer-Verlag, New York.

Whitney, P. (1995), Screening the Hanford Tanks for Trapped Gas, Technical Report PNL-10821, Pacific Northwest Laboratory, Richland, Washington.

Wilkins, N. (1995), Results of Gas Monitoring of Double Shell Flammable Gas Watch List Tanks, Technical Report WHC-SD-WM-TI-682 Rev. 0A, Westinghouse Hanford Company, Richland, Washington.

Wilkins, N. (1996), Results of Gas Monitoring of Double-Shell Flammable Gas Watch List Tanks, Technical Report WHC-SD-WM-TI-682 Rev. 1, Westinghouse Hanford Company, Richland, Washington.

Appendix A

Supporting Material for the Temperature Screening

A Supporting Material for the Temperature Screening

This appendix contains samples of the data displays generated in the temperature data screening. Displays from four randomly selected tanks are presented: U–103, BX-110, C–103 and T–203. Also, displays from two well behaved (T-111 and SY–103) and two poorly behaved (SX–101 and S–101) tanks are shown.

In all of these plots, the temperature minus an offset from TC1 is calculated and displayed. The vertical lines show the 2°C breaks between successive measurements; the lines are drawn at the measurement immediately preceding the break. Above each plot are the tank name, the thermocouple number, the elevation of the thermocouple as reported in SACS, and a number generated by us from the database that identifies the riser. Note that the same riser can have more than one of these identifiers; however, measurements tagged with the same riser number are from the same thermocouple tree. Finally, temperature measurements are plotted with the characters m and t according to whether they were obtained manually or acquired through TMACS.

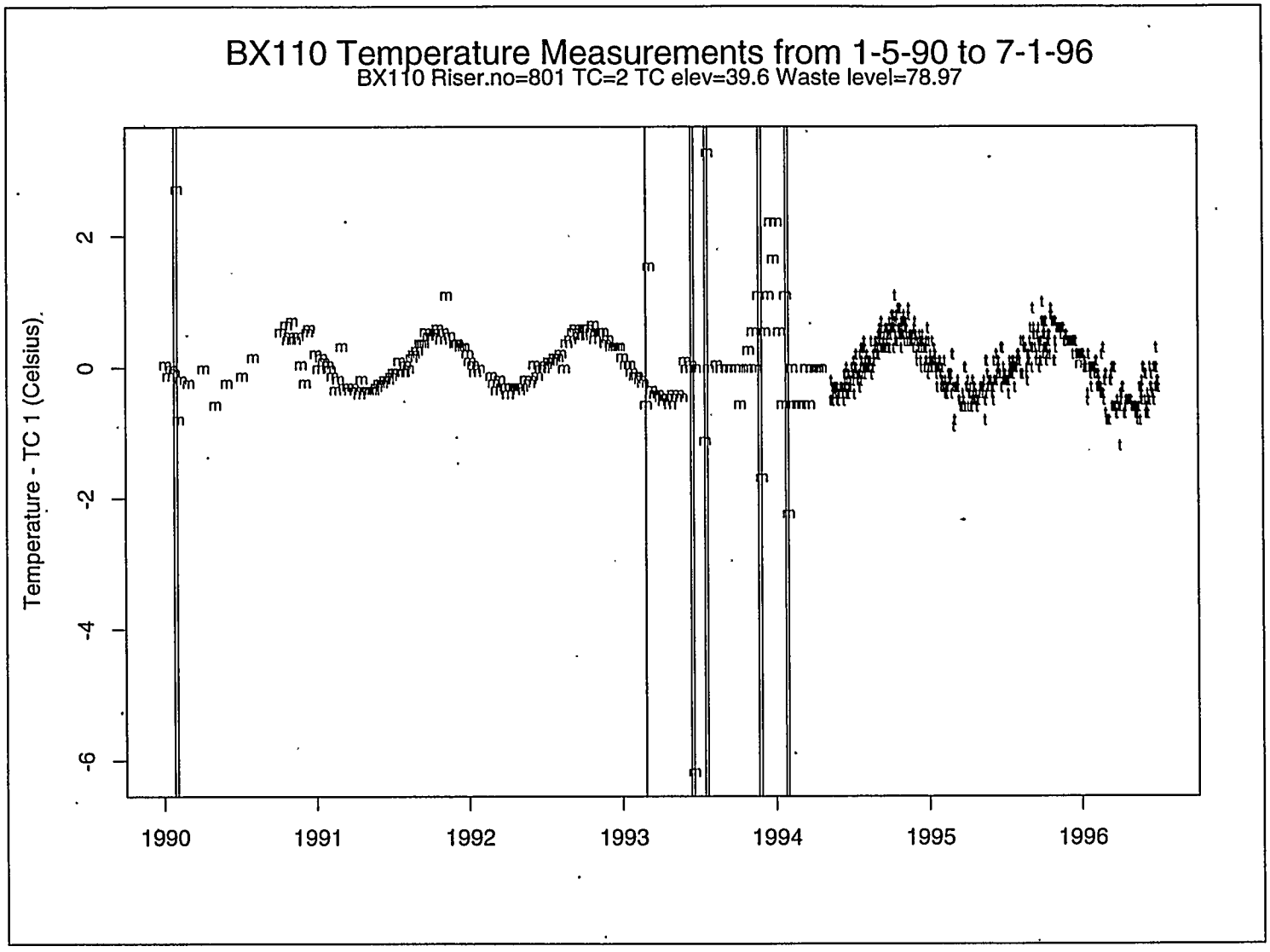

Figure A.1: Tank BX–110 thermocouple 2 temperatures with drawn breaks. The outlier is the cause of the two temperature breaks in early 1990 and the breaks in early 1993. The noisy region of the data seen from 1993 to early 1994 corresponds to time of the saltwell pumping of this tank.

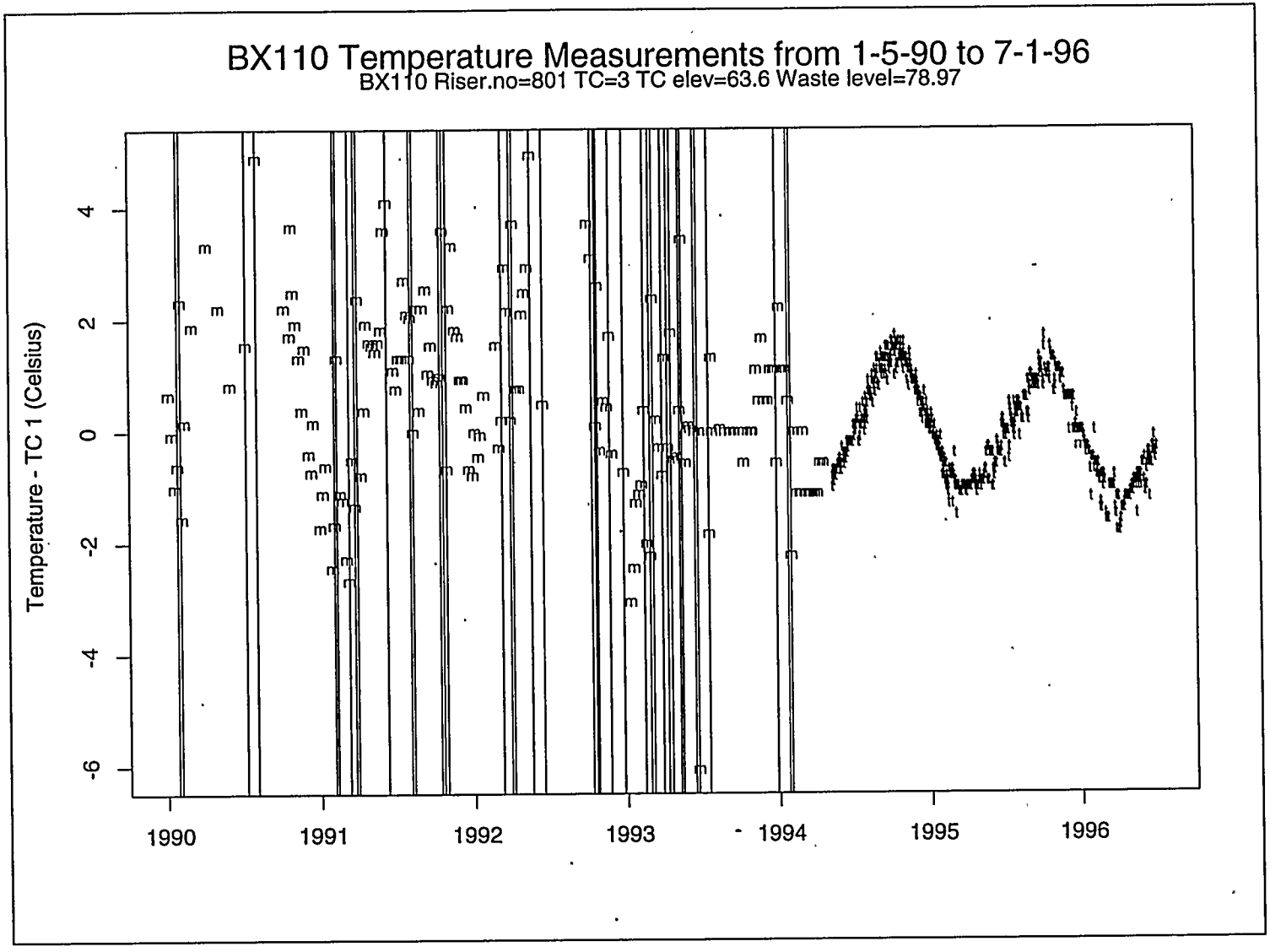

Figure A.2: Tank BX–110 thermocouple 3 temperatures with drawn breaks. The temperature measurements up through early 1994 are very noisy. The introduction of TMACS (where the "t"'s start) corresponds fairly well with the decrease of the noise in this TC's measurements.

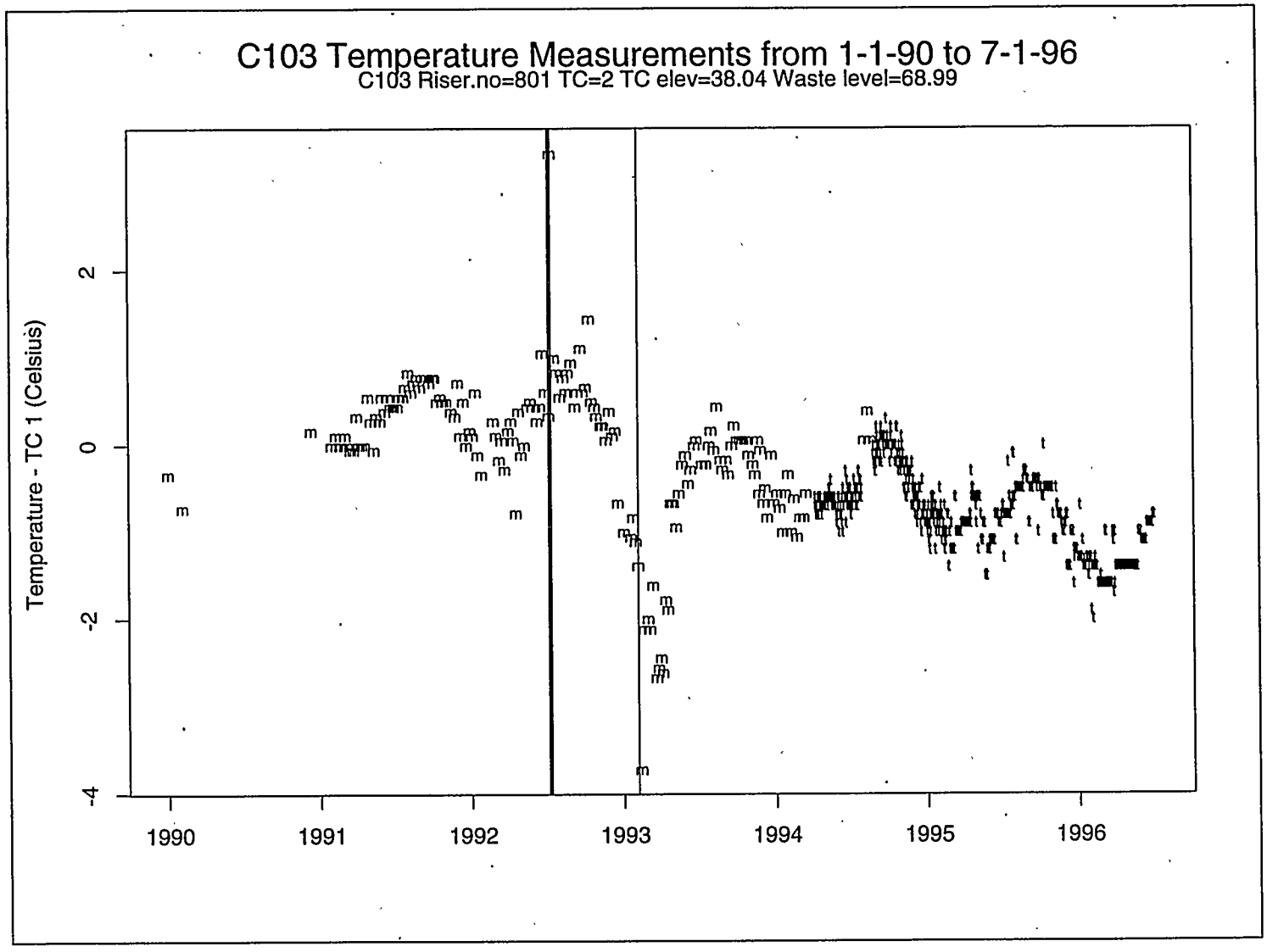

Figure A.3: Tank C–103 thermocouple 2 temperatures with drawn breaks. The downward excursion in early 1993 corresponds with the time the FIC level measurements go from decreasing to level.

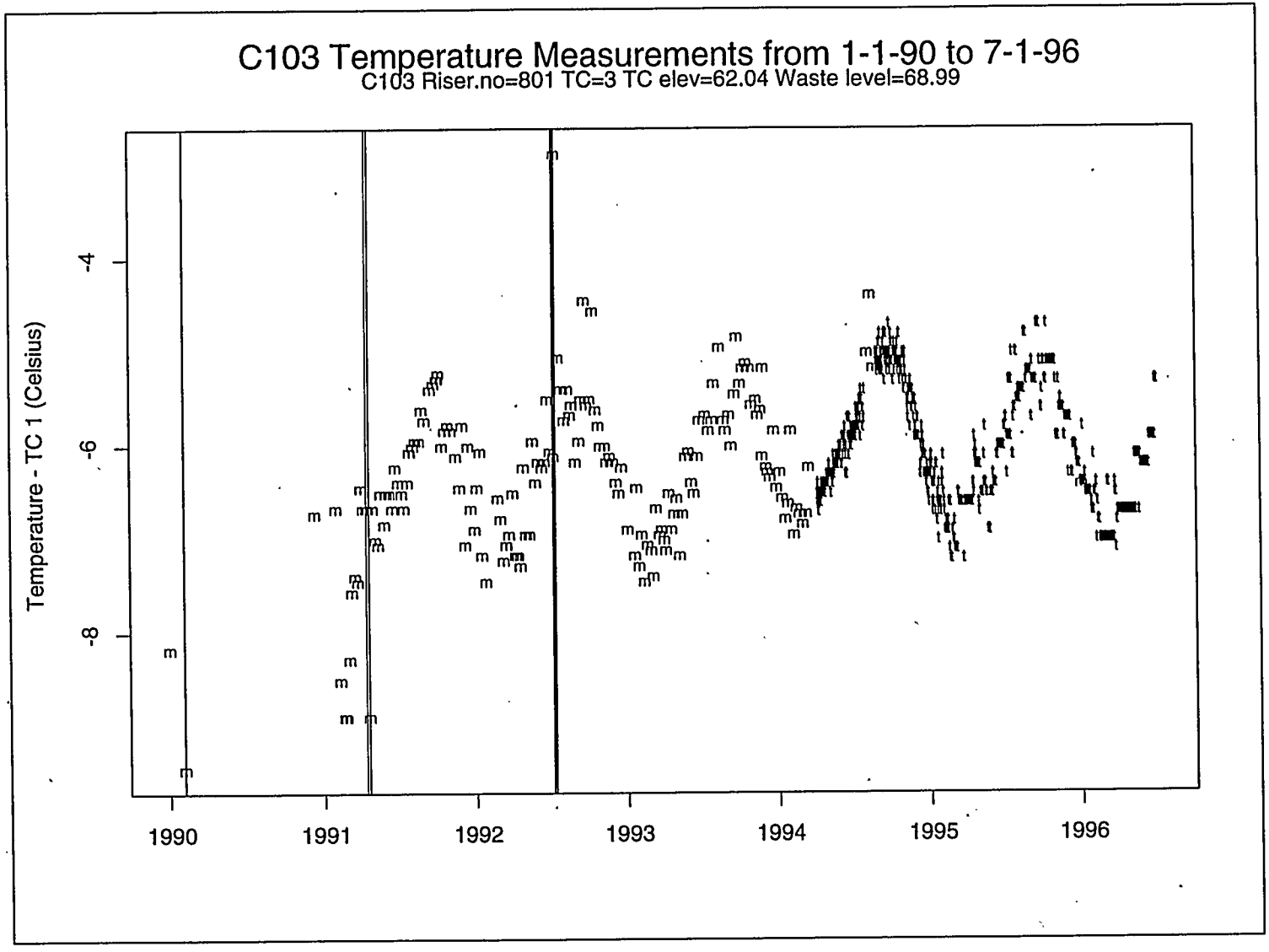

Figure A.4: Tank C–103 thermocouple 3 temperatures with drawn breaks. The noisy region of the measurements in early 1991 was not counted as a temperature break.

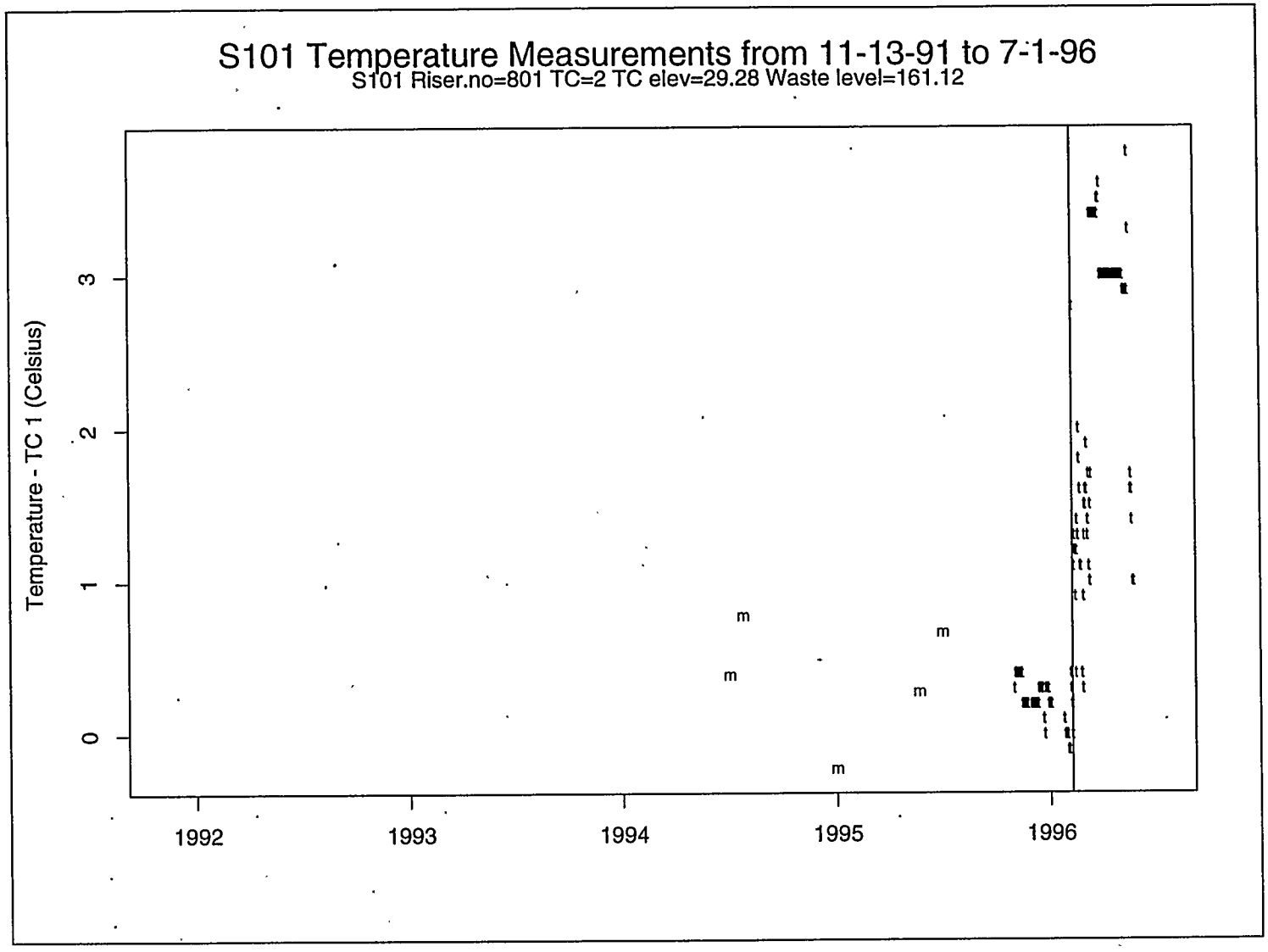

Figure A.5: Tank S–101 thermocouple 2 temperatures with drawn breaks. The upward jump in early 1996 actually reflects a drop in TC1 measurements from ~47°C to ~44°C. The other TC's measurements are fairly well-behaved. The vertical line correspond to an outlying value.

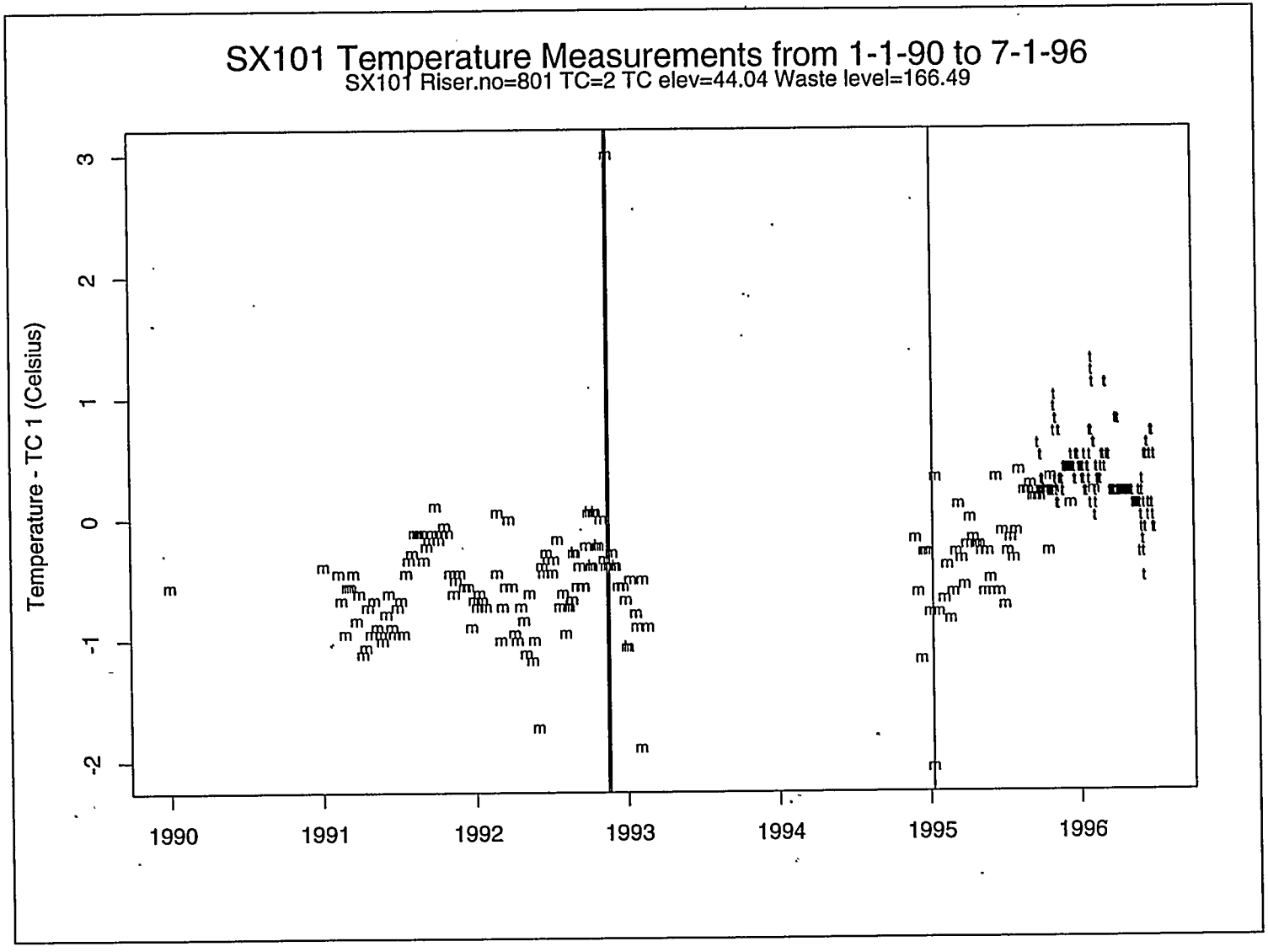

Figure A.6: Tank SX–101 thermocouple 2 temperatures with drawn breaks. The drawn lines are due to outlying points.

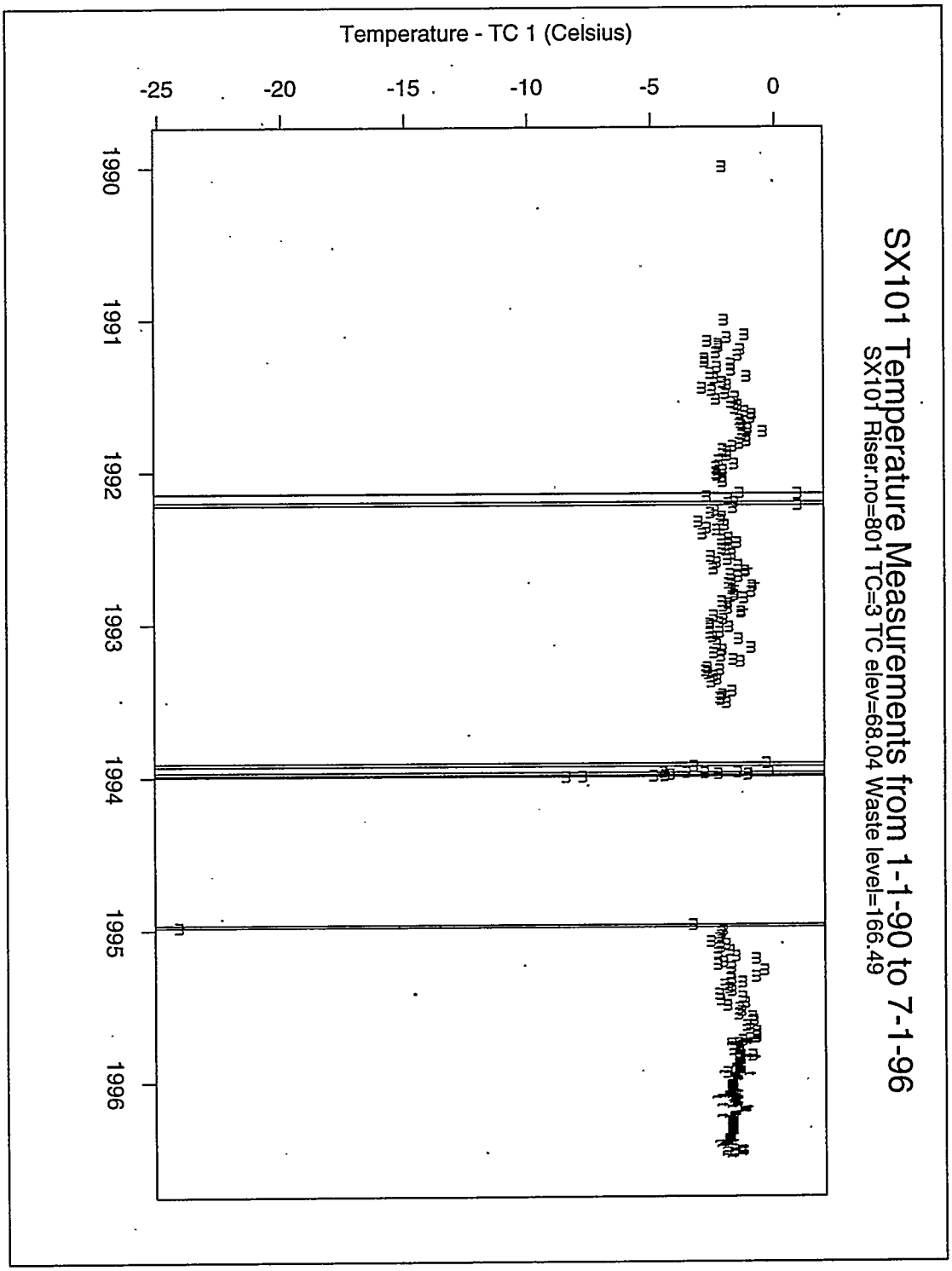

Figure A.7: Tank SX-101 thermocouple 3 temperatures with drawn breaks.

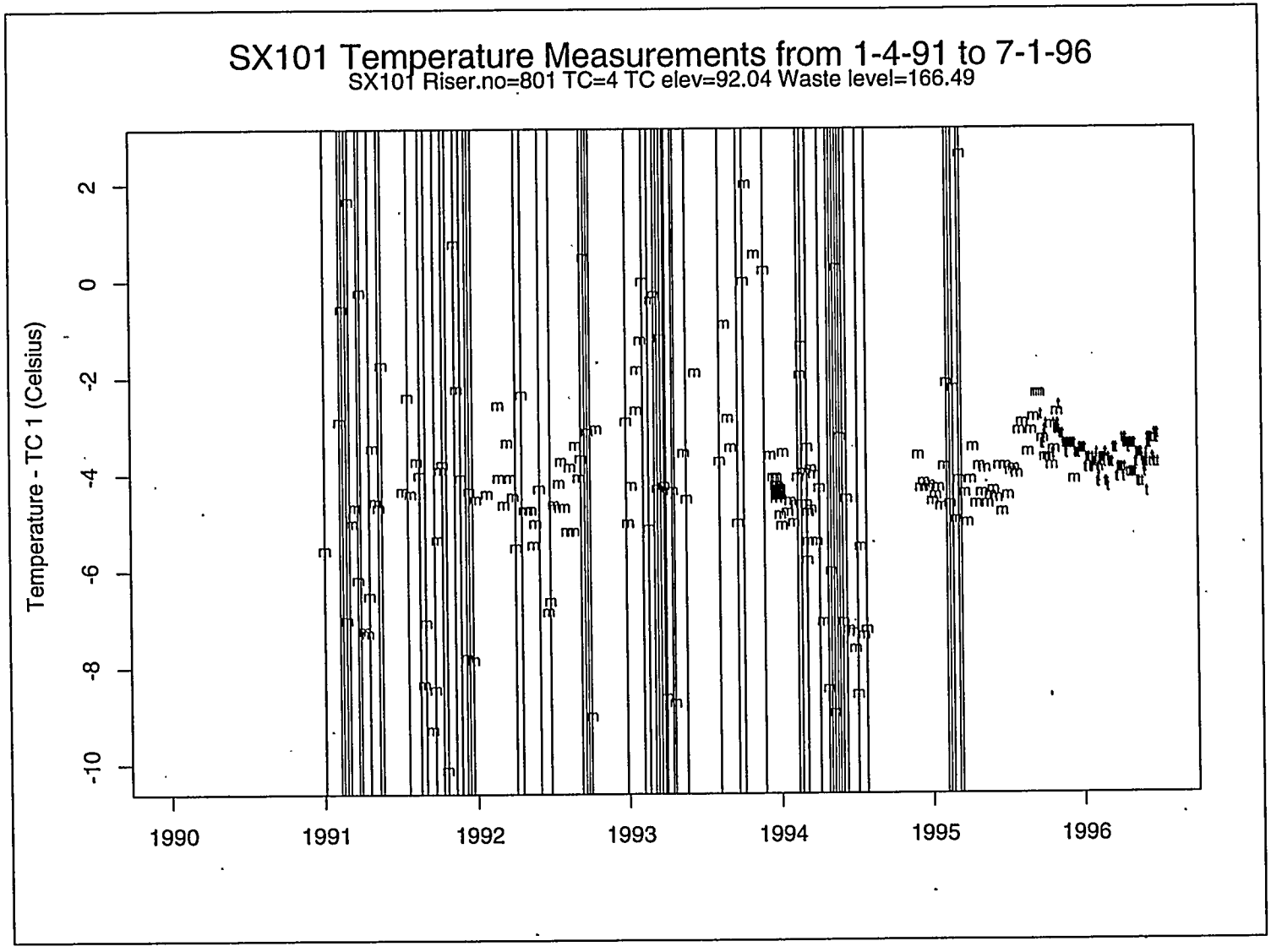

Figure A.8: Tank SX–101 thermocouple 4 temperatures with drawn breaks. The persistent, large, noise level shown through mid-1994 ends after the data gap in late 1994.

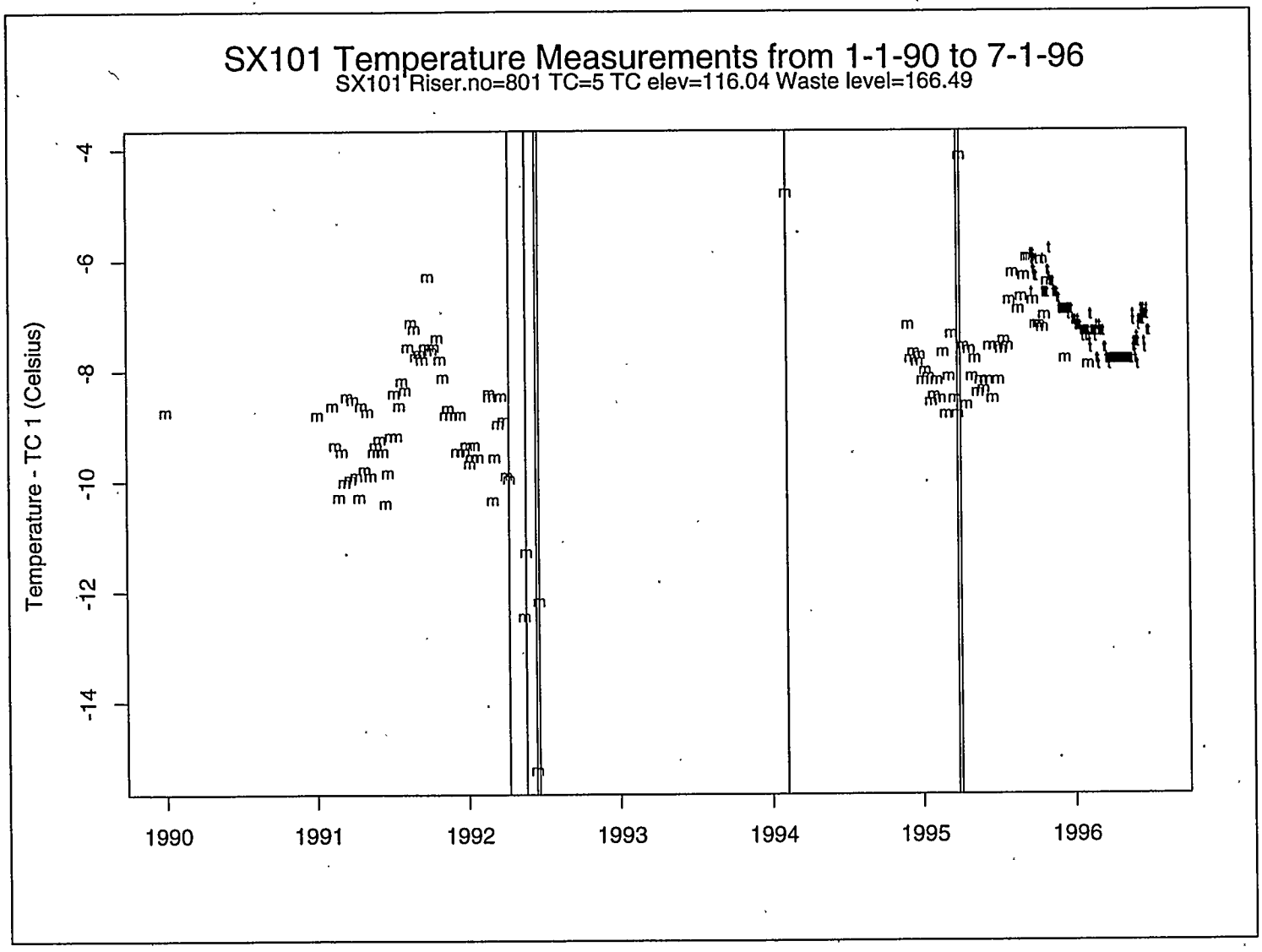

Figure A.9: Tank SX–101 thermocouple 5 temperatures with drawn breaks.

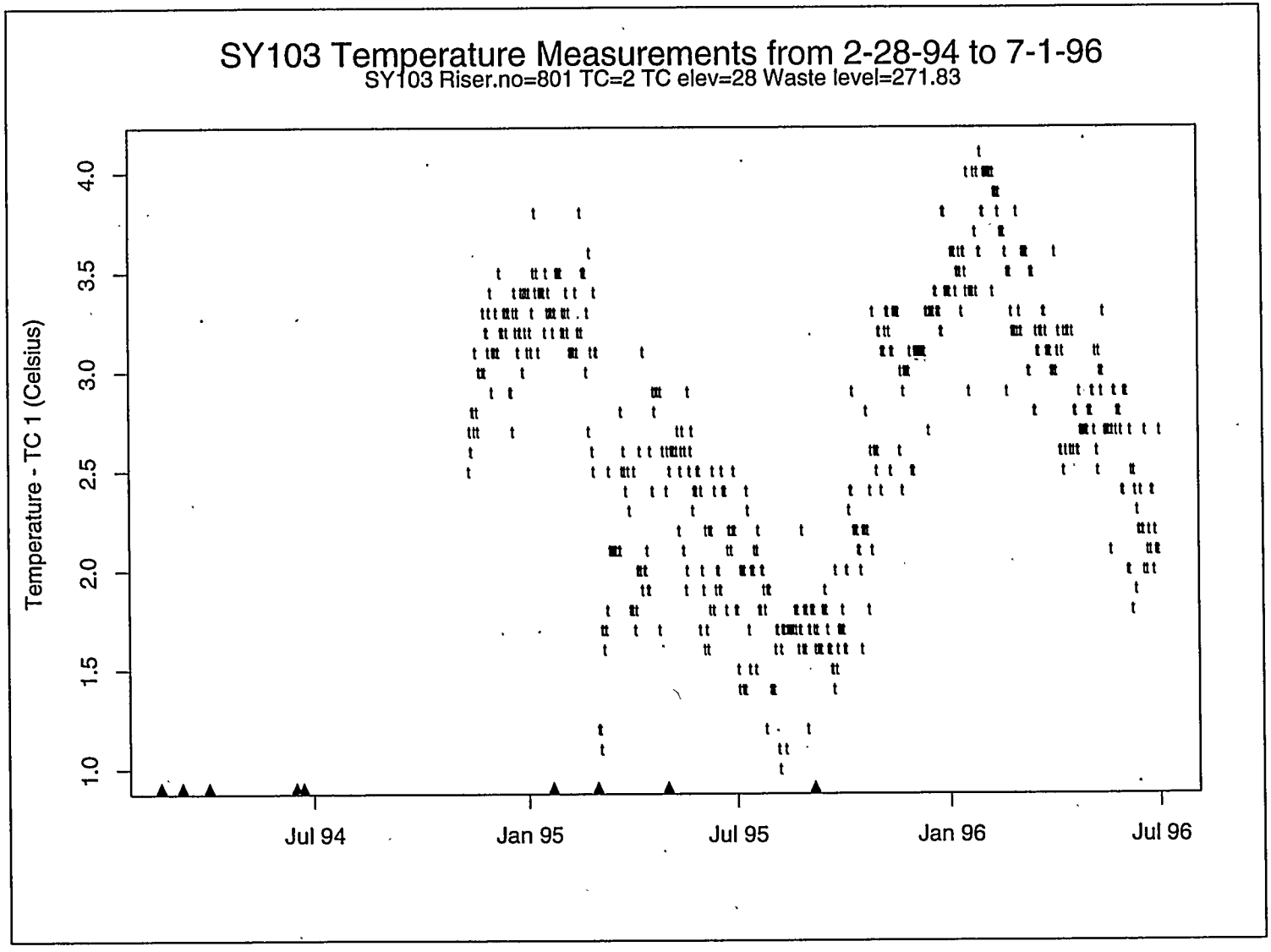

Figure A.10: Tank SY–103 thermocouple 2 temperatures with drawn breaks. No breaks were detected in these measurements from riser 4A. The ▲'s along the bottom of the chart mark the dates of known GREs.

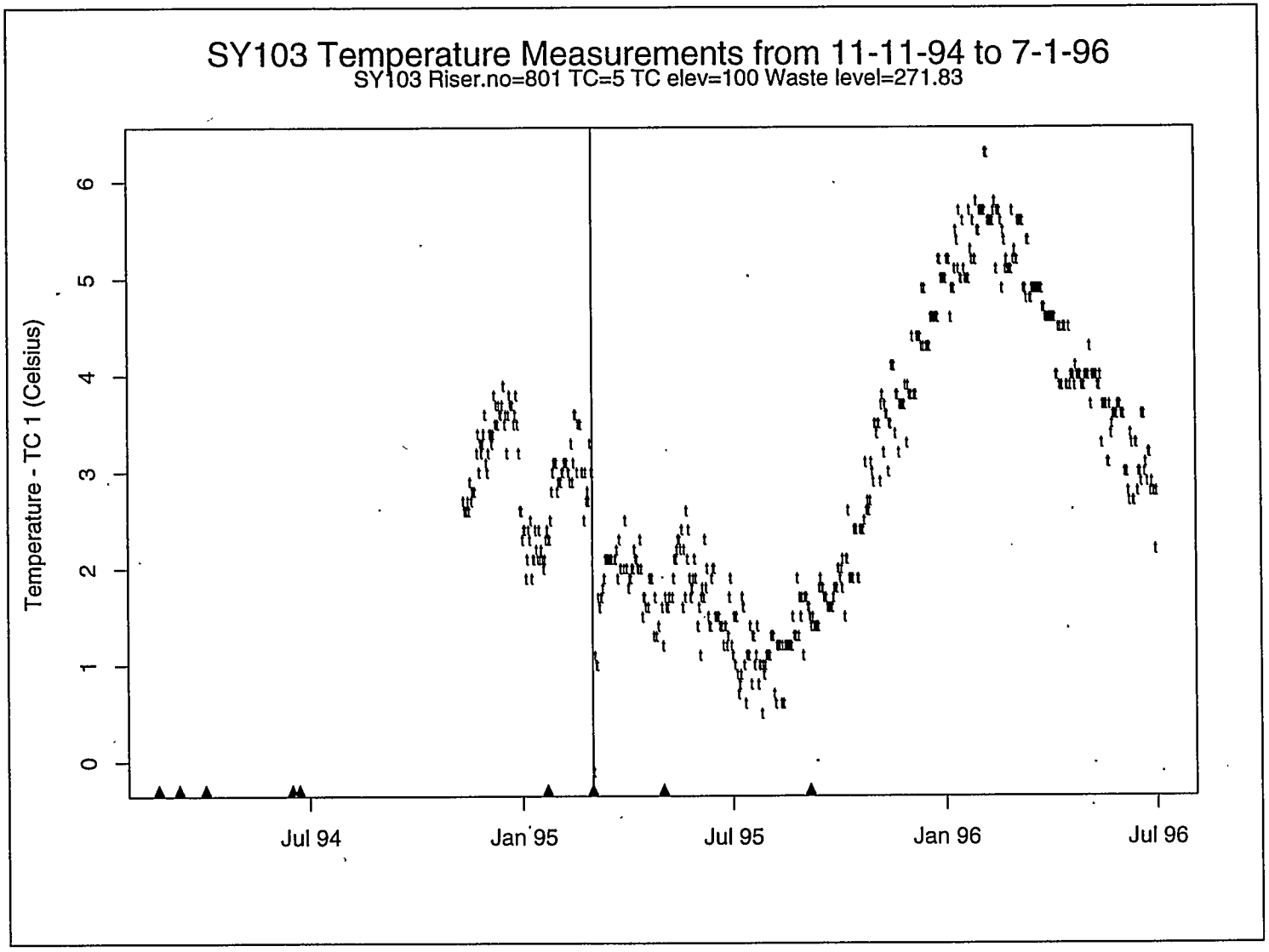

Figure A.11: Tank SY–103 thermocouple 5 temperatures with drawn breaks. These measurements are from riser 4A. The vertical line corresponds to the GRE of March 2, 1995. The feature near January 1995, not detected with the algorithm, corresponds to a small GRE on 12-27-1994.

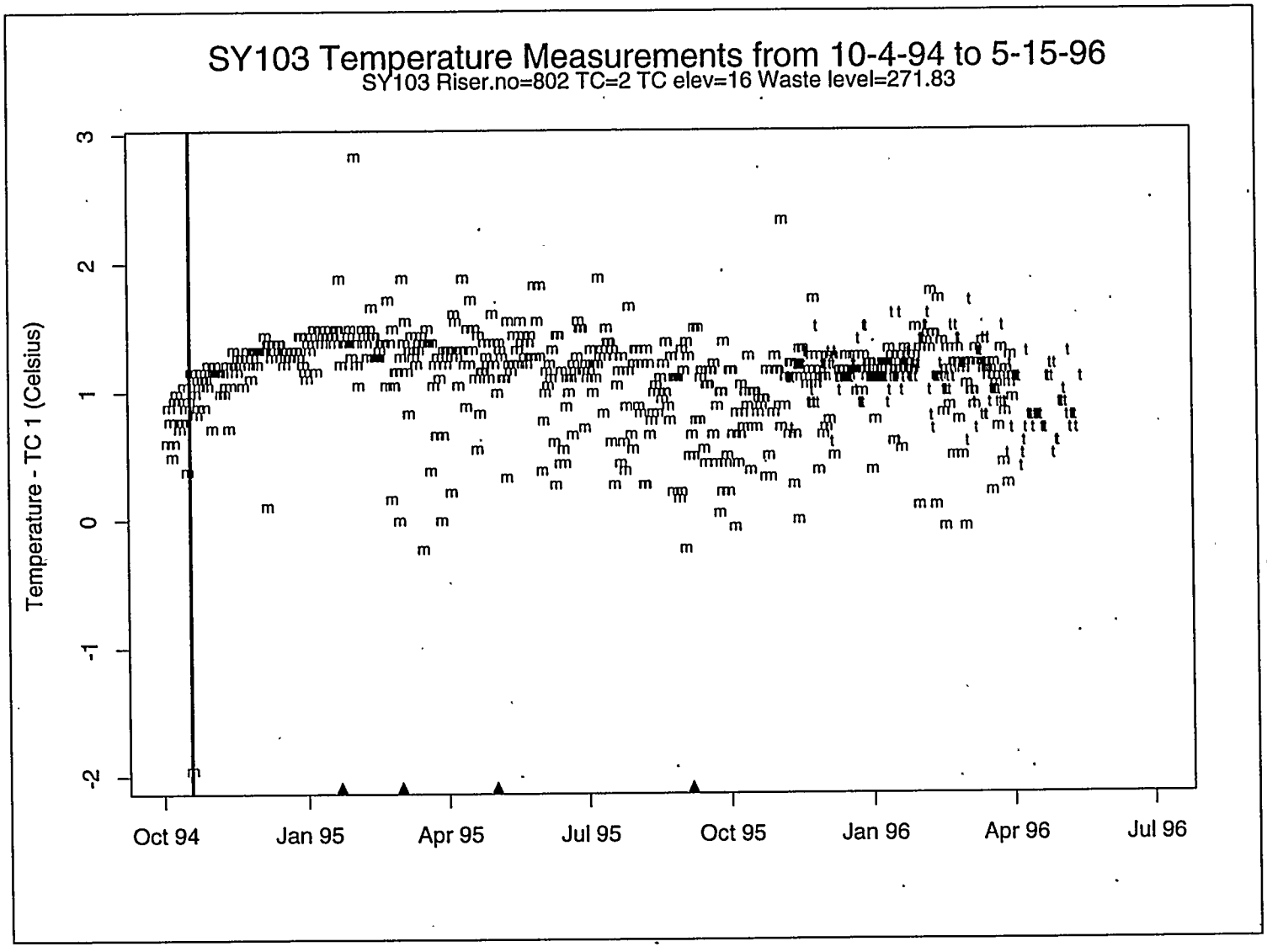

Figure A.12: Tank SY–103 thermocouple 2 temperatures with drawn breaks. These measurements are from riser 17B. The noise level of the measurements changes in early 1995.

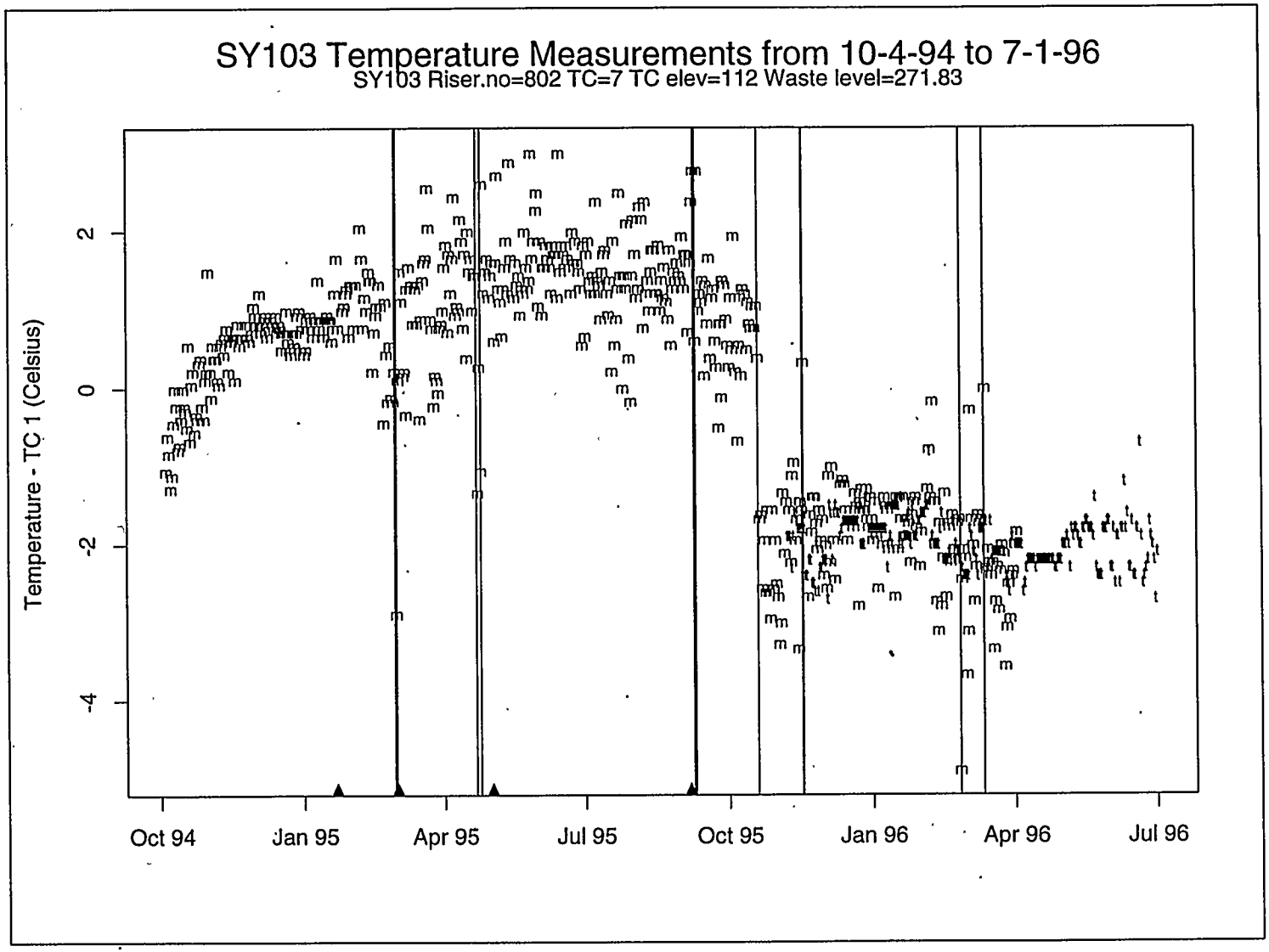

Figure A.13: Tank SY–103 thermocouple 7 temperatures with drawn breaks. These measurements are from riser 17B. The clear drop in (offset) temperature following October 1995 does not correspond to a GRE.

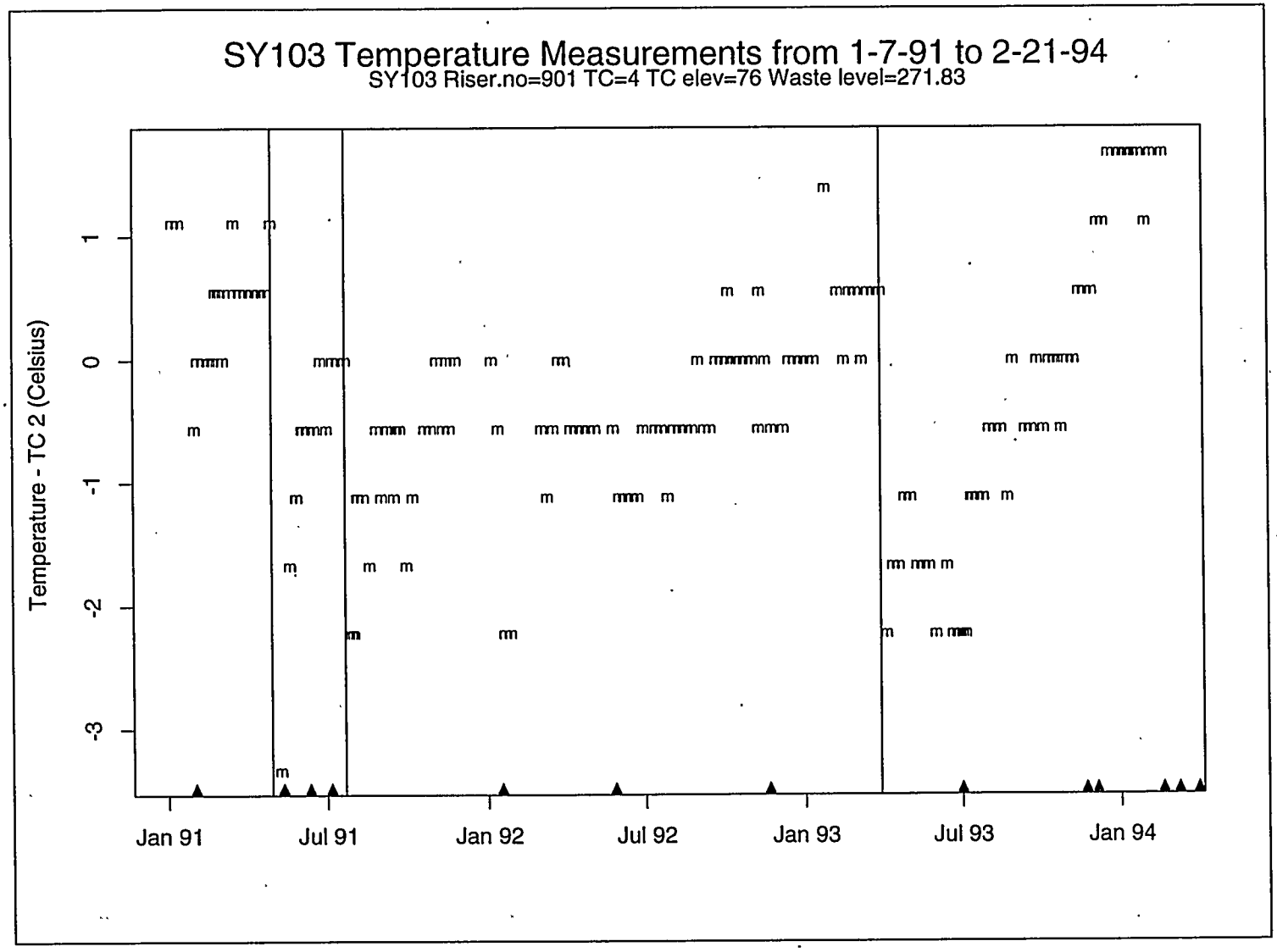

Figure A.14: Tank SY–103 thermocouple 4 temperatures with drawn breaks. Of the three temperature breaks indicated (starting at 4-29-91, 7-22-91 and 3-29-93): one corresponds to a known GRE (the 4-29-91 break actually brackets 4-29-91 and 5-9-91; the temperature data was taken weekly in 1991). The next break, 7-22-91, corresponds to a time at which the level data changes from trending downward to trending upward (probably not a GRE but an "anti"-GRE), and the third, 3-29-93 corresponds to a small level drop.

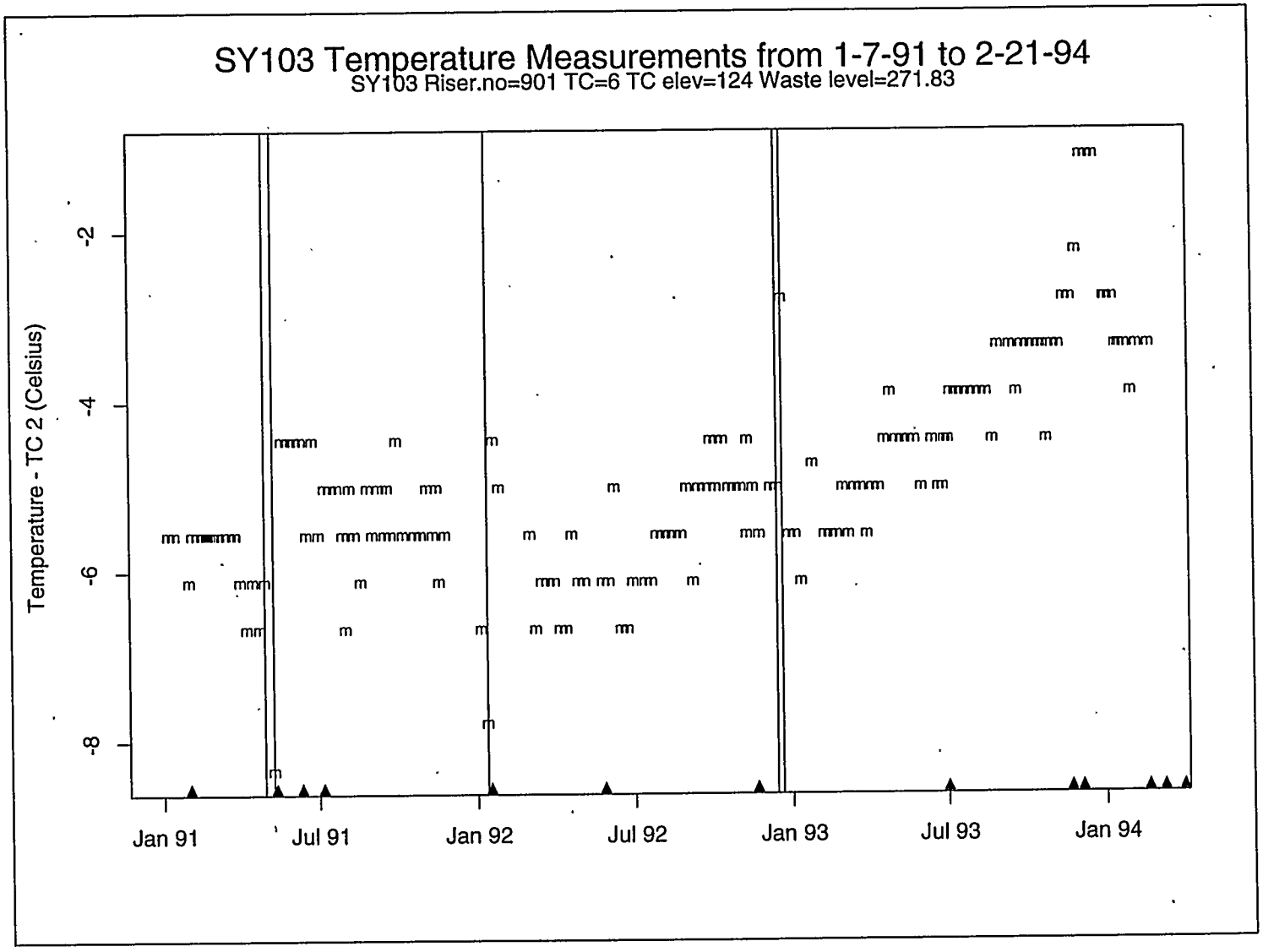

Figure A.15: Tank SY–103 thermocouple 6 temperatures with drawn breaks. Five temperature breaks are detected, two correspond to GREs and the other 3 correspond only to outliers which have triggered the detection algorithm.

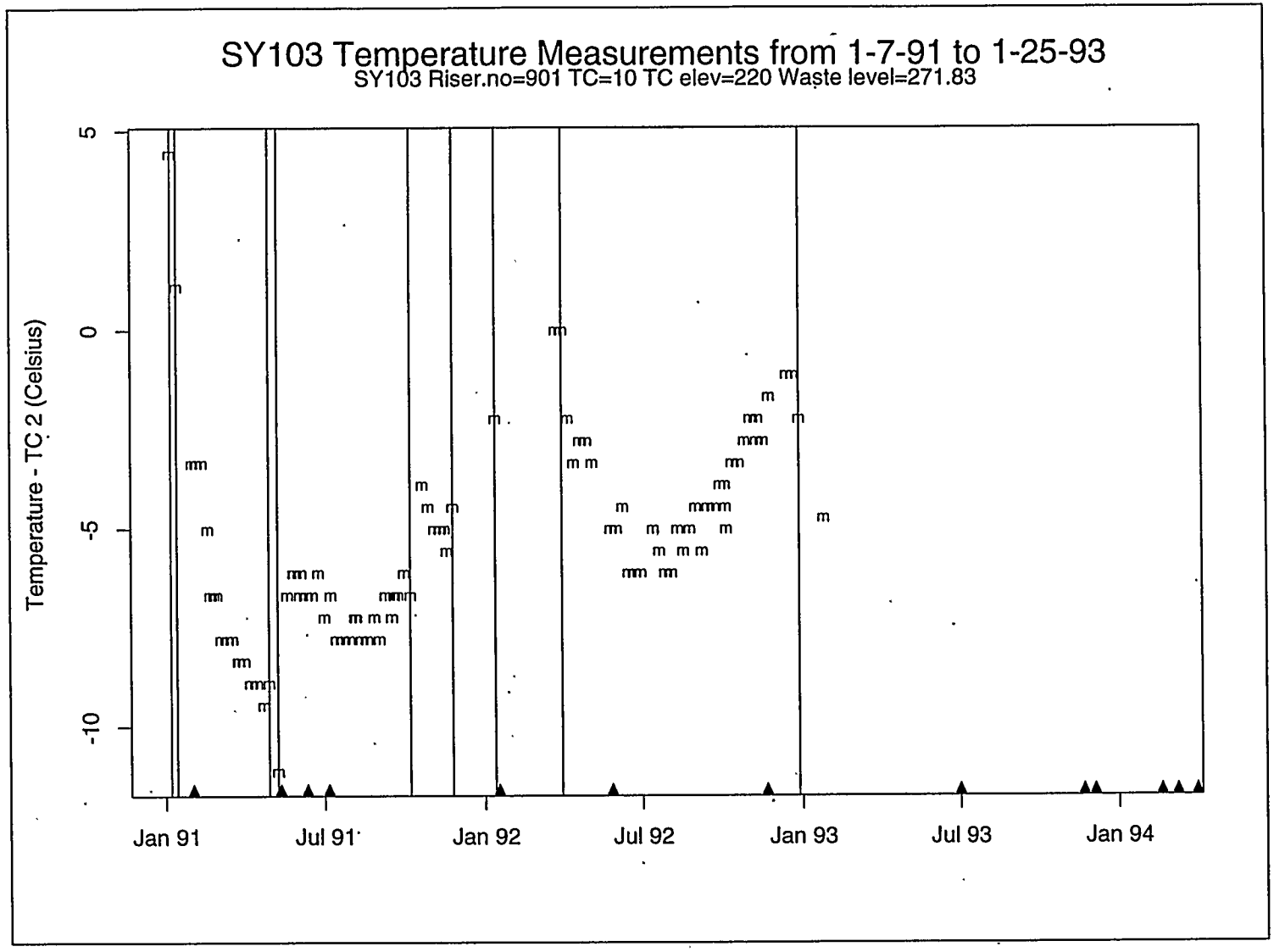

Figure A.16: Tank SY–103 thermocouple 10 temperatures with drawn breaks. Only two of these lines are drawn at temperature breaks; the others are discounted as being caused by outliers (the first vertical lines in 1991) or by an excessively long time period between successive measurements (both lines in 1992), or by an inadequate amount of data bracketing the vertical line (late 1992).

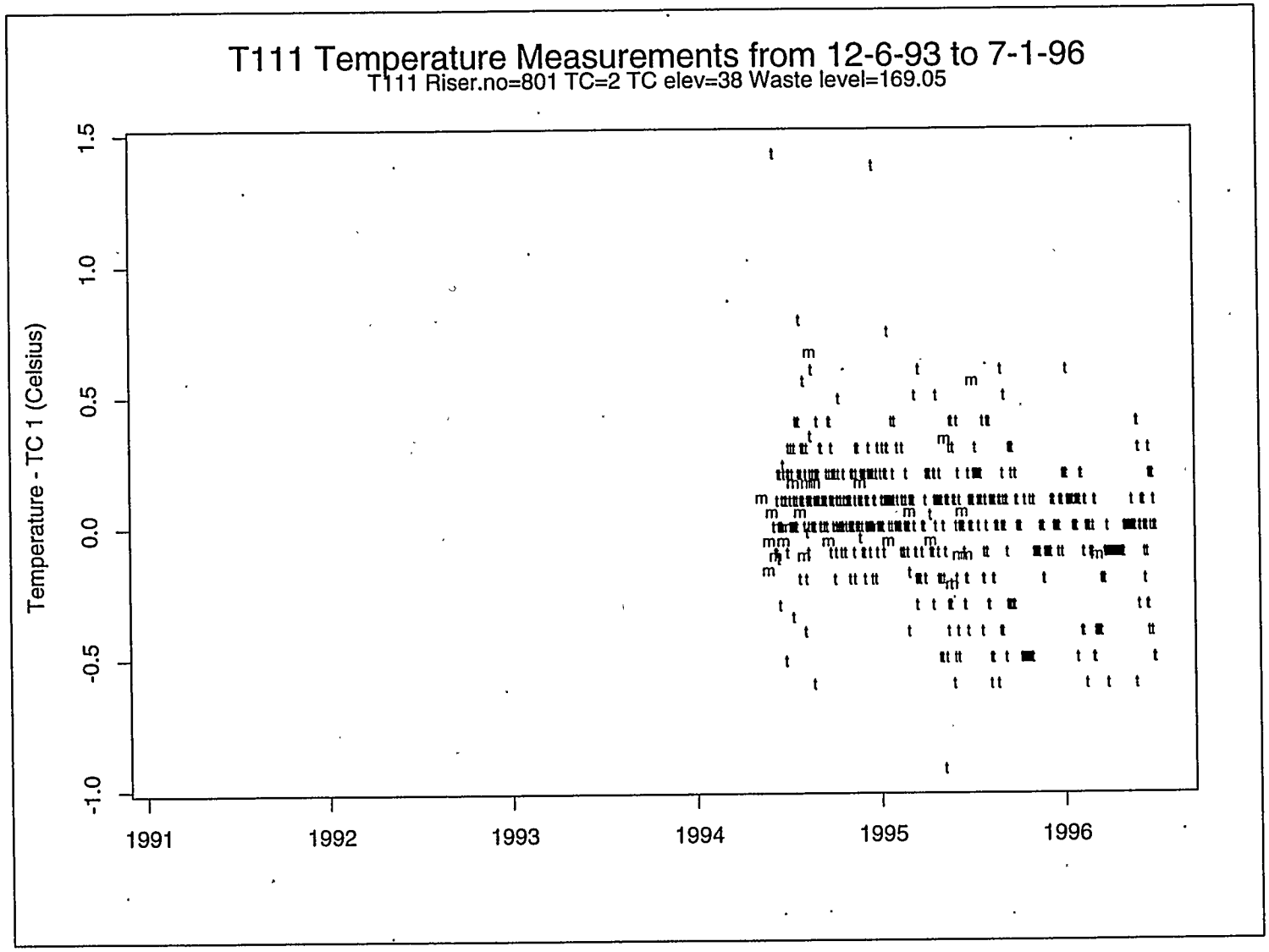

Figure A.17: Tank T-111 thermocouple 2 temperatures with drawn breaks.

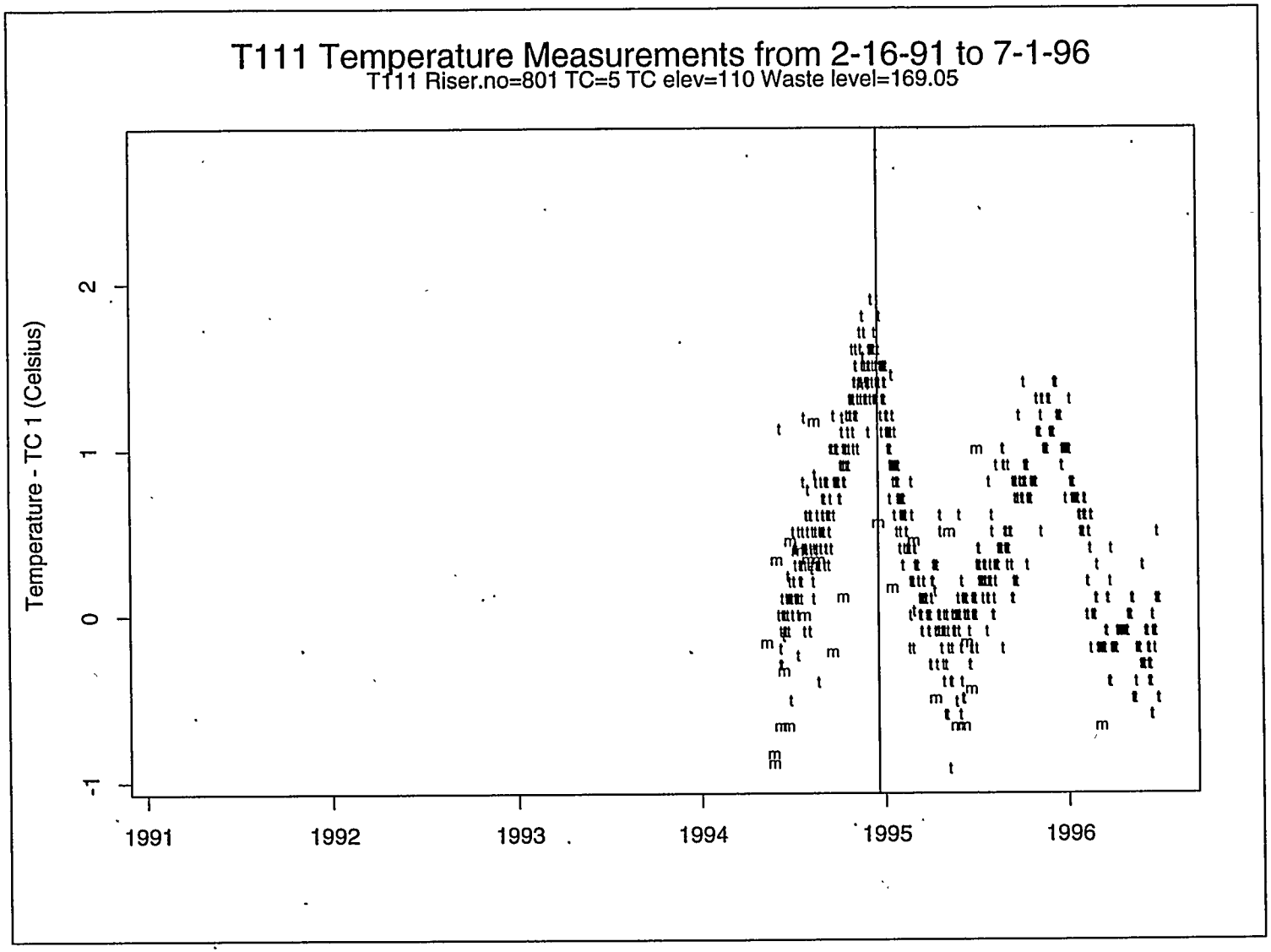

Figure A.18: Tank T–111 thermocouple 5 temperatures with drawn breaks. Note that the outlier is manual data, deviating from TMACS data.

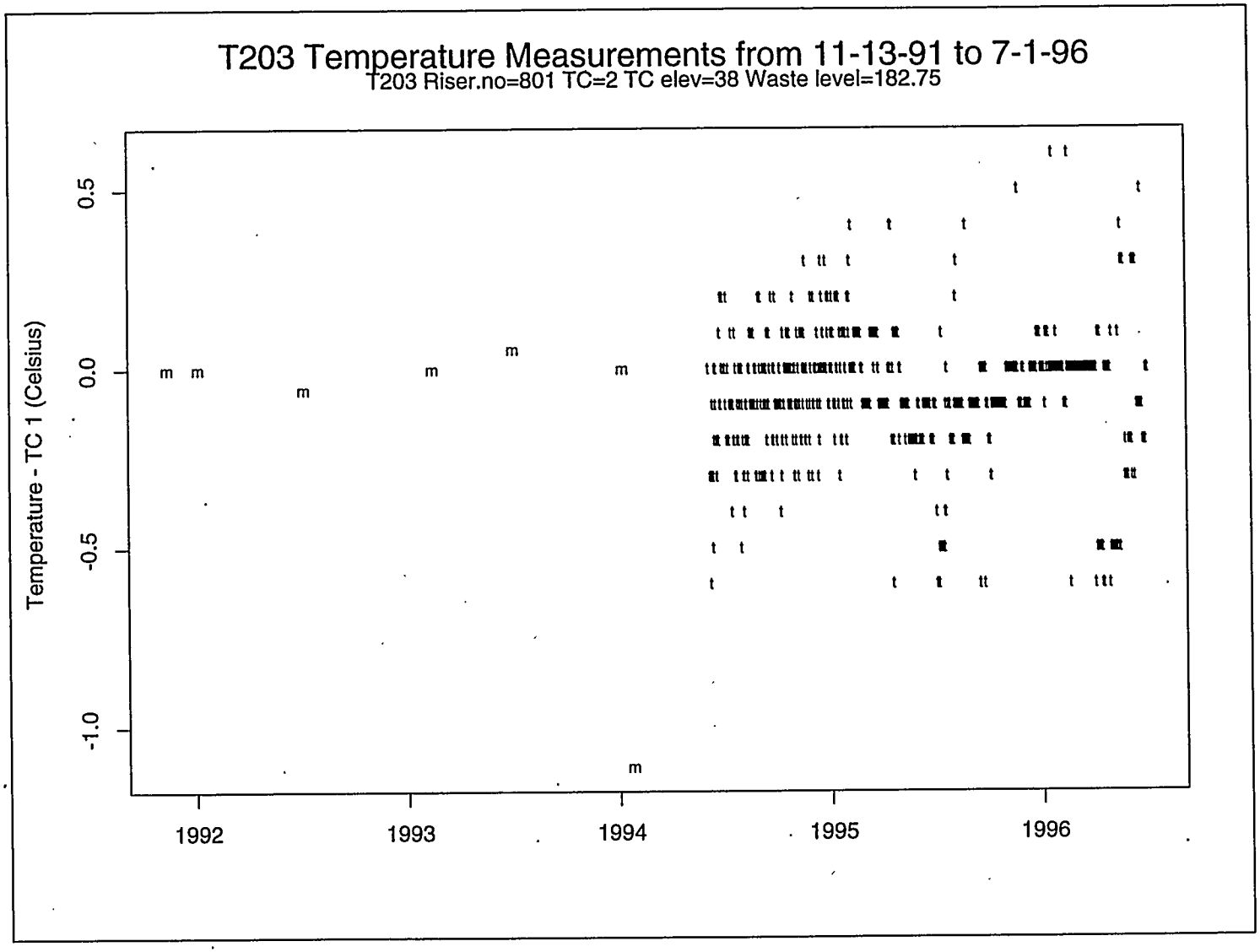

Figure A.19: Tank T–203 thermocouple 2 temperatures with drawn breaks. A small scale on the veritcal axis emphasizes the scatter in the data.

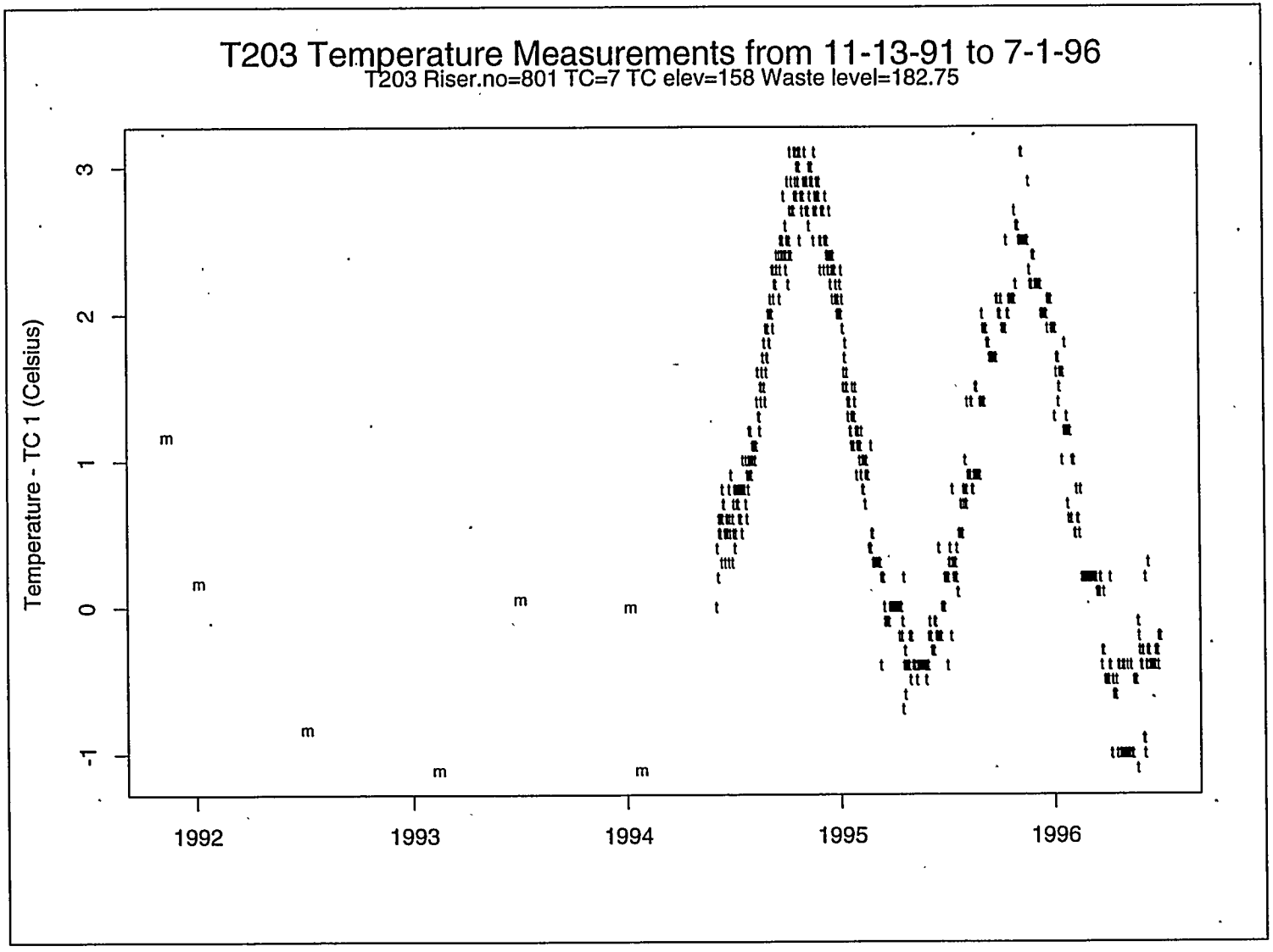

Figure A.20: Tank T–203 thermocouple 7 temperatures with drawn breaks.

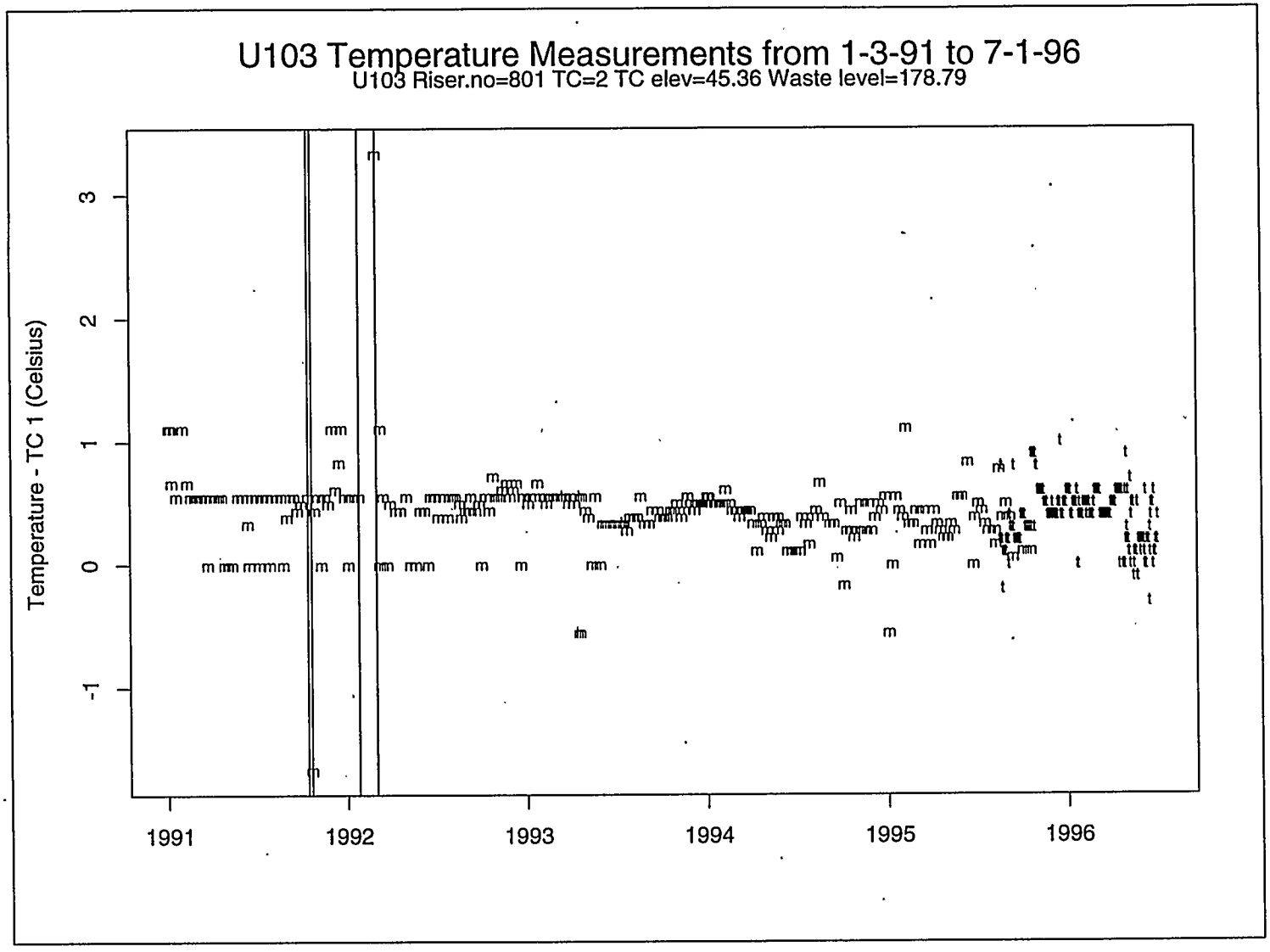

Figure A.21: Tank U–103 thermocouple 2 temperatures with drawn breaks. The horizontal "shelves" of temperature measurements in 1991 and 1992 are the result of the measurements being recorded to the nearest degree Fahrenheit.

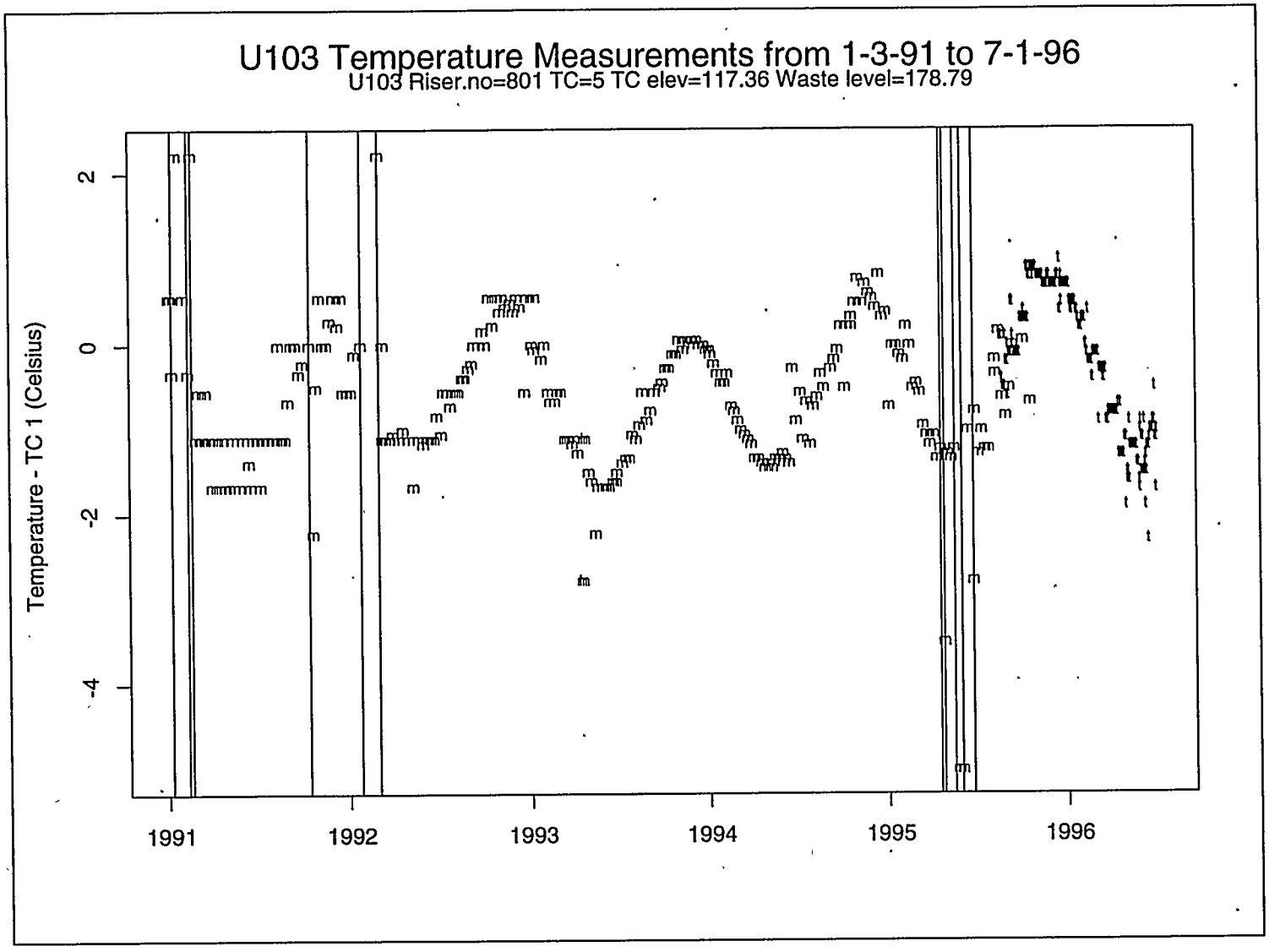

Figure A.22: Tank U–103 thermocouple 5 temperatures with drawn breaks. Both vertical lines in 1992 are caused by the single high outlying point in that year.

Appendix B

Precisions of Tank Waste Level Measurements

B Precisions of Tank Waste Level Measurements

A generic model for the observed tank waste level measurements is:

$$\text{Observed level} = \text{"True Level"} + \text{Systematic Effects} + \text{Noise}$$

The "True Level" is to be estimated by correcting for the "Systematic Effects". So, the "observed" scatter in the level overestimates the measurement precision, as it captures the combined variability of the "Systematic Effects" and "Noise" terms.

We can correct for (at least some of) the systematic effects using the model described in (Whitney 1995). The data was processed as described in that paper, producing lots of individual regressions which were used to estimate model parameters for the above. One of the parameters is the standard deviation of the Noise term. The medians of these standard deviations are summarized in Table B.1.

Table B.1: Estimated precisions of tank waste level measurements (in centimeters)

Tank	ENRAF SD	FIC SD	NEUTRON ILL SD	MT SD
A–101	0.14	0.36	0.81	0.50
A–102	–	0.12	–	–
A–103	–	0.20	1.42	0.30
A–104	–	–	–	0.34
A–105	–	–	–	0.20
A–106	0.06	0.12	–	–
AN–101	–	0.12	–	–
AN–102	–	0.11	–	–
AN–103	0.21	0.27	–	–
AN–104	0.08	0.24	–	–
AN–105	0.10	0.20	–	–
AN–106	–	0.09	–	–
AN–107	–	0.09	–	–
AP–101	–	0.07	–	0.28
AP–102	–	0.14	–	0.30
AP–103	–	0.08	–	0.30
AP–104	–	0.07	–	0.28
AP–105	–	0.08	–	0.26
AP–106	–	0.11	–	0.34
AP–107	–	0.10	–	0.34
AP–108	–	0.12	–	0.28
AW–101	0.12	0.19	–	0.40
AW–102	0.33	1.56	–	0.83
AW–103	0.02	0.11	–	0.25
AW–104	0.07	0.12	–	0.32
AW–105	0.01	0.08	–	0.33
AW–106	0.04	0.15	–	0.28
AX–101	0.03	0.50	1.07	–
AX–102	–	–	–	0.34

Table B:1: *(continued)*

Tank	ENRAF SD	FIC SD	NEUTRON ILL SD	MT SD
AX–103	0.23	0.16	–	–
AX–104	–	–	–	0.18
AY–101	0.08	0.28	–	0.35
AY–102	–	1.15	–	2.90
AZ–101	0.65	4.23	–	0.59
AZ–102	–	0.52	–	0.39
B–101	–	0.10	–	–
B–102	0.03	0.07	–	0.22
B–103	–	0.09	–	–
B–104	–	–	1.07	0.21
B–105	–	–	1.27	0.19
B–106	–	0.07	–	–
B–107	–	–	–	0.21
B–108	–	0.11	–	–
B–109	–	–	–	0.21
B–110	–	–	1.98	0.29
B–111	–	0.07	0.84	–
B–112	0.02	0.07	–	0.23
B–201	–	–	–	0.20
B–202	–	–	–	0.19
B–203	–	–	–	0.20
B–204	–	–	–	0.19
BX–101	0.01	–	–	0.30
BX–102	–	–	–	0.18
BX–103	0.01	0.07	–	–
BX–104	0.04	0.10	–	0.32
BX–105	0.02	0.15	–	0.34
BX–106	0.05	0.07	–	0.31
BX–107	0.05	0.09	–	–
BX–108	0.01	–	–	0.27
BX–109	0.05	0.07	–	–
BX–110	0.02	–	–	0.25
BX–111	0.06	–	2.31	0.29
BX–112	0.02	0.07	–	0.47
BY–101	–	–	2.01	0.31
BY–102	–	–	1.47	0.34
BY–103	–	–	1.42	0.32
BY–104	–	–	1.85	0.26
BY–105	–	–	1.27	0.31
BY–106	–	–	1.24	0.31
BY–107	–	–	1.35	0.21
BY–108	–	–	–	0.21
BY–109	–	0.20	1.55	–
BY–110	–	–	1.55	0.26

Table B.1: *(continued)*

Tank	ENRAF SD	FIC SD	NEUTRON ILL SD	MT SD
BY–111	–	–	1.93	0.21
BY–112	–	–	1.30	0.22
C–101	–	–	–	0.21
C–102	–	0.12	–	–
C–103	0.08	0.07	–	–
C–104	–	0.18	–	0.19
C–105	–	0.15	–	0.35
C–106	0.27	0.36	–	–
C–107	0.08	0.09	–	–
C–108	–	–	–	0.26
C–109	–	–	–	0.18
C–110	–	–	–	0.22
C–111	–	–	–	0.18
C–112	0.21	–	–	0.26
C–201	–	–	–	0.24
C–202	–	–	–	0.18
C–203	–	–	–	0.22
C–204	–	–	–	0.22
S–101	0.05	0.14	0.69	0.45
S–102	0.10	0.27	1.42	0.48
S–103	0.13	0.20	0.84	0.31
S–104	–	–	1.30	0.19
S–105	0.06	0.07	0.97	0.80
S–106	0.32	0.30	1.14	0.41
S–107	0.07	0.12	–	0.30
S–108	0.03	0.10	1.85	0.25
S–109	0.08	0.18	2.36	0.40
S–110	0.24	0.13	0.97	0.18
S–111	0.25	0.18	0.76	0.32
S–112	0.01	0.11	1.98	0.36
SX–101	0.01	0.16	1.09	0.22
SX–102	0.12	0.31	0.74	0.36
SX–103	0.08	0.28	0.86	0.23
SX–104	0.06	0.59	–	0.31
SX–105	0.15	0.56	1.09	0.18
SX–106	0.14	0.23	1.09	0.20
SX–107	–	–	–	0.18
SX–108	–	–	–	0.18
SX–109	–	–	–	0.18
SX–110	–	–	–	0.18
SX–111	–	–	–	0.18
SX–112	–	–	–	0.18
SX–113	–	–	–	0.18
SX–114	–	–	–	0.18

Table B.1: *(continued)*

Tank	ENRAF SD	FIC SD	NEUTRON ILL SD	MT SD
SX–115	–	–	–	0.18
SY–101	0.26	0.43	–	0.54
SY–102	0.07	2.72	–	0.30
SY–103	0.18	0.37	–	0.62
T–101	0.03	0.07	–	0.42
T–102	0.03	0.07	–	–
T–103	0.01	0.12	–	–
T–104	–	–	0.66	0.28
T–105	–	0.09	–	0.18
T–106	–	0.07	–	–
T–107	0.04	0.11	–	–
T–108	0.07	–	–	0.20
T–109	0.02	0.19	–	–
T–110	0.19	0.10	0.66	–
T–111	0.06	0.09	1.65	–
T–112	0.09	0.08	–	–
T–201	–	–	–	0.21
T–202	–	–	–	0.18
T–203	–	–	–	0.23
T–204	–	–	–	0.20
TX–101	0.02	0.12	–	–
TX–102	–	–	1.19	0.40
TX–103	0.07	0.17	–	–
TX–104	–	0.27	–	–
TX–105	–	–	–	0.34
TX–106	–	–	1.14	0.21
TX–107	0.06	0.15	–	–
TX–108	0.03	0.11	2.16	–
TX–109	0.01	0.20	0.79	–
TX–110	–	–	1.24	0.27
TX–111	–	–	1.22	0.24
TX–112	–	–	1.42	0.29
TX–113	–	–	0.89	0.36
TX–114	–	–	1.22	0.24
TX–115	–	–	1.45	0.29
TX–116	–	–	–	0.34
TX–117	–	–	1.47	0.29
TX–118	–	0.22	1.52	–
TY–101	0.07	0.11	–	–
TY–102	0.04	0.15	–	–
TY–103	0.12	0.11	1.24	–
TY–104	0.07	0.07	–	–
TY–105	0.02	–	–	0.26
TY–106	0.02	–	–	0.28

Table B.1: *(continued)*

Tank	ENRAF SD	FIC SD	NEUTRON ILL SD	MT SD
U–101	–	–	–	0.19
U–102	0.07	0.12	1.27	–
U–103	0.15	0.13	0.64	–
U–104	–	–	–	0.23
U–105	0.13	0.22	0.66	0.24
U–106	0.07	0.10	1.04	–
U–107	0.08	0.12	0.43	–
U–108	0.08	0.15	0.66	–
U–109	0.15	0.12	0.69	–
U–110	0.01	0.14	–	–
U–111	0.13	0.44	0.64	–
U–112	–	–	–	0.18
U–201	–	–	–	0.21
U–202	–	–	–	0.18
U–203	–	–	–	0.21
U–204	–	–	–	0.18

Appendix C

Graphic Summaries of Level Change Detection

C Graphic Summaries of Level Change Detection

This appendix contains plots showing the detected level breaks. For each detected level jump, a line segment running from zero to the size of the level jump is drawn at the date of the detected level jump. A horizontal line is drawn through zero for visual reference. Note that the vertical lines indicating breaks are drawn in two widths. The thin vertical lines indicate that the SACS comments (or other supporting information) suggested that the break was caused by instrumentation properties or by waste transfer activities; however, the evidence was not considered firm. The thicker vertical lines indicate that there was no evidence suggesting that the break was related to instrumentation or waste transfer.

The graphics underneath the date axis at the bottom of these plots indicate the dates at which tank waste level measurements are recorded in the SACS database. A small vertical line is drawn at the time of each level observation. The ▲'s at the top and bottom of the plot show when the level measurement instrument was changed from FIC to ENRAF. The ♦'s at the top and bottom of the plots indicate a time near which the tank was saltwell-pumped.

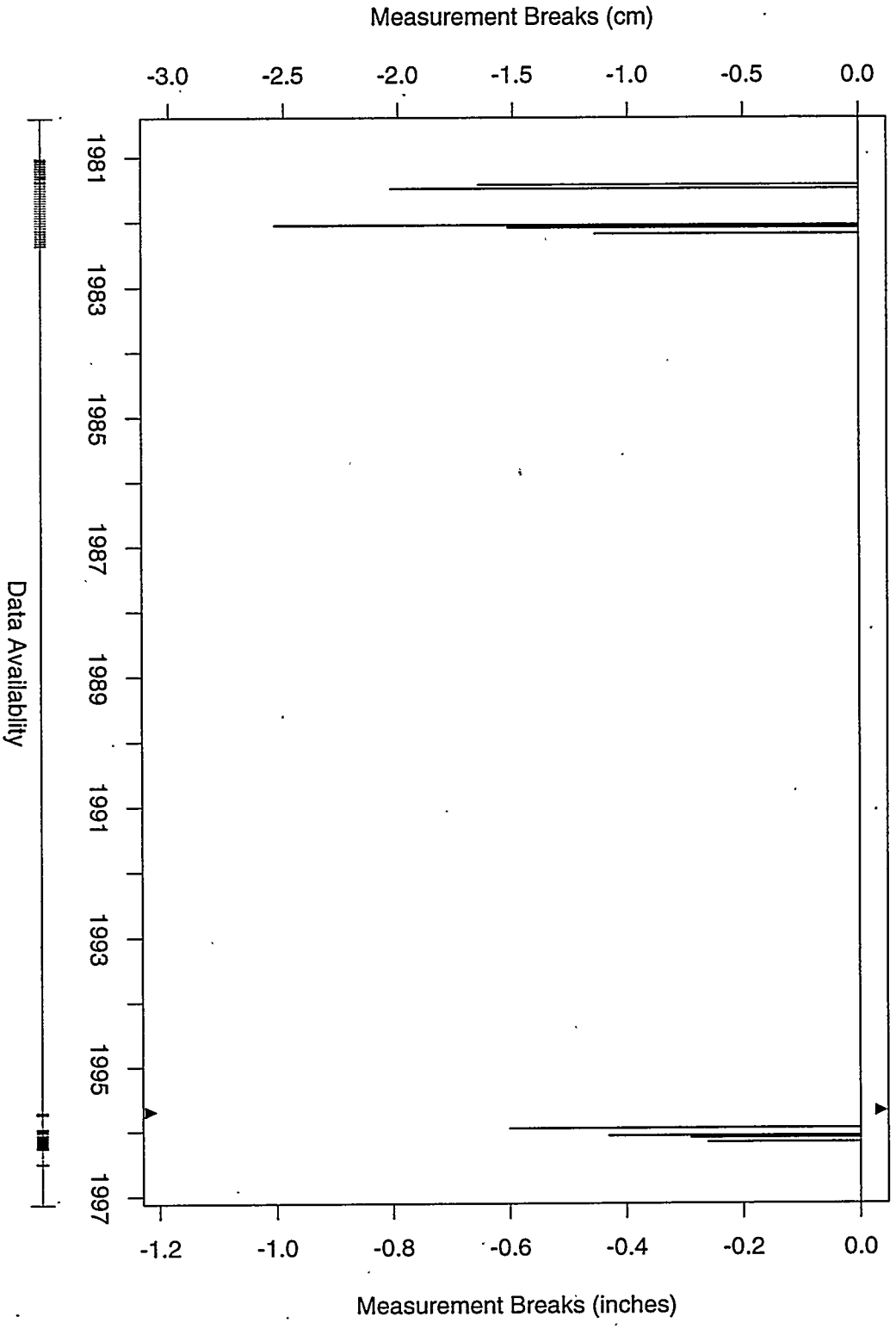

Figure C.1: Tank A-101 detected breaks and break sizes.

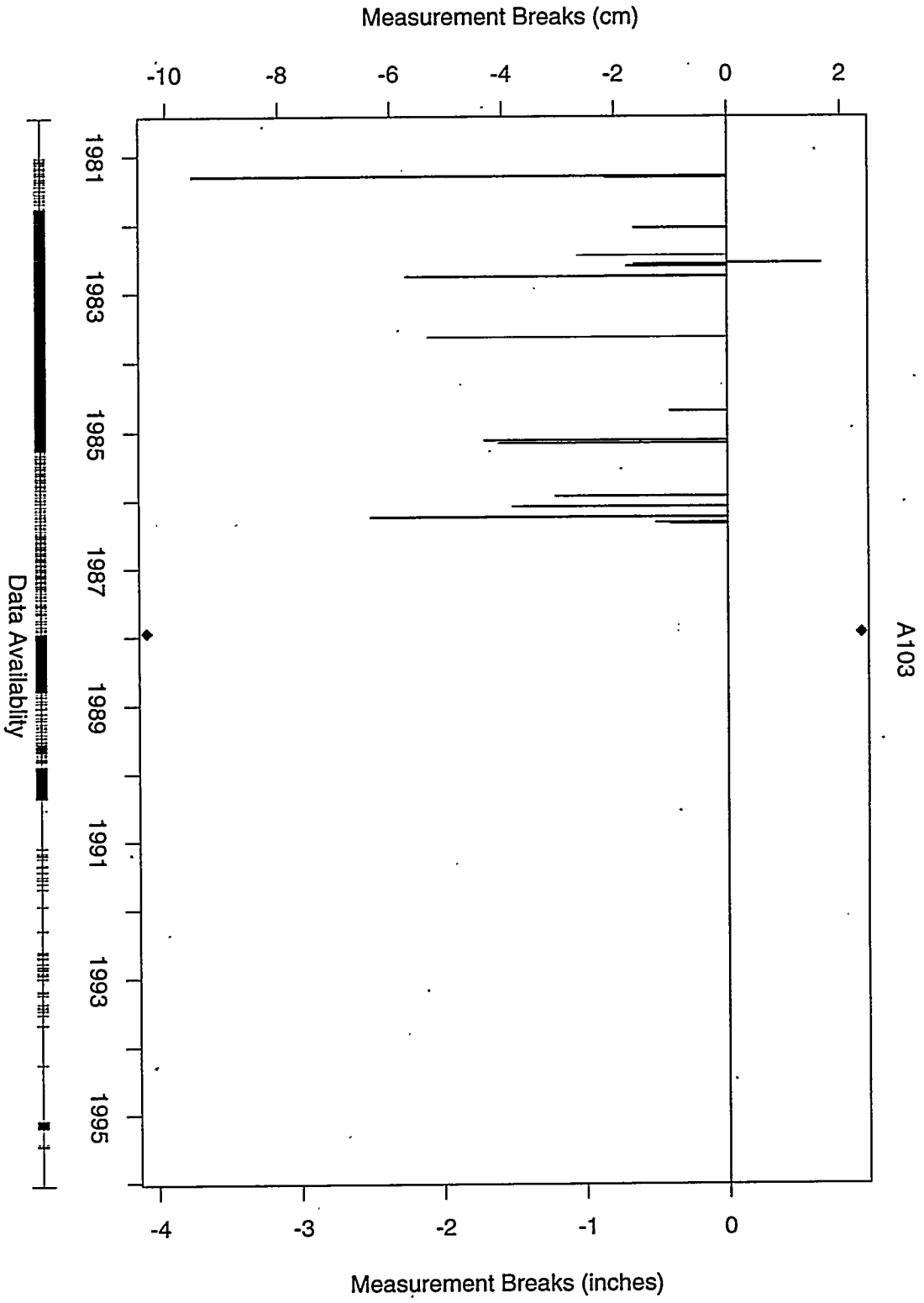

Figure C.2: Tank A-103 detected breaks and break sizes.

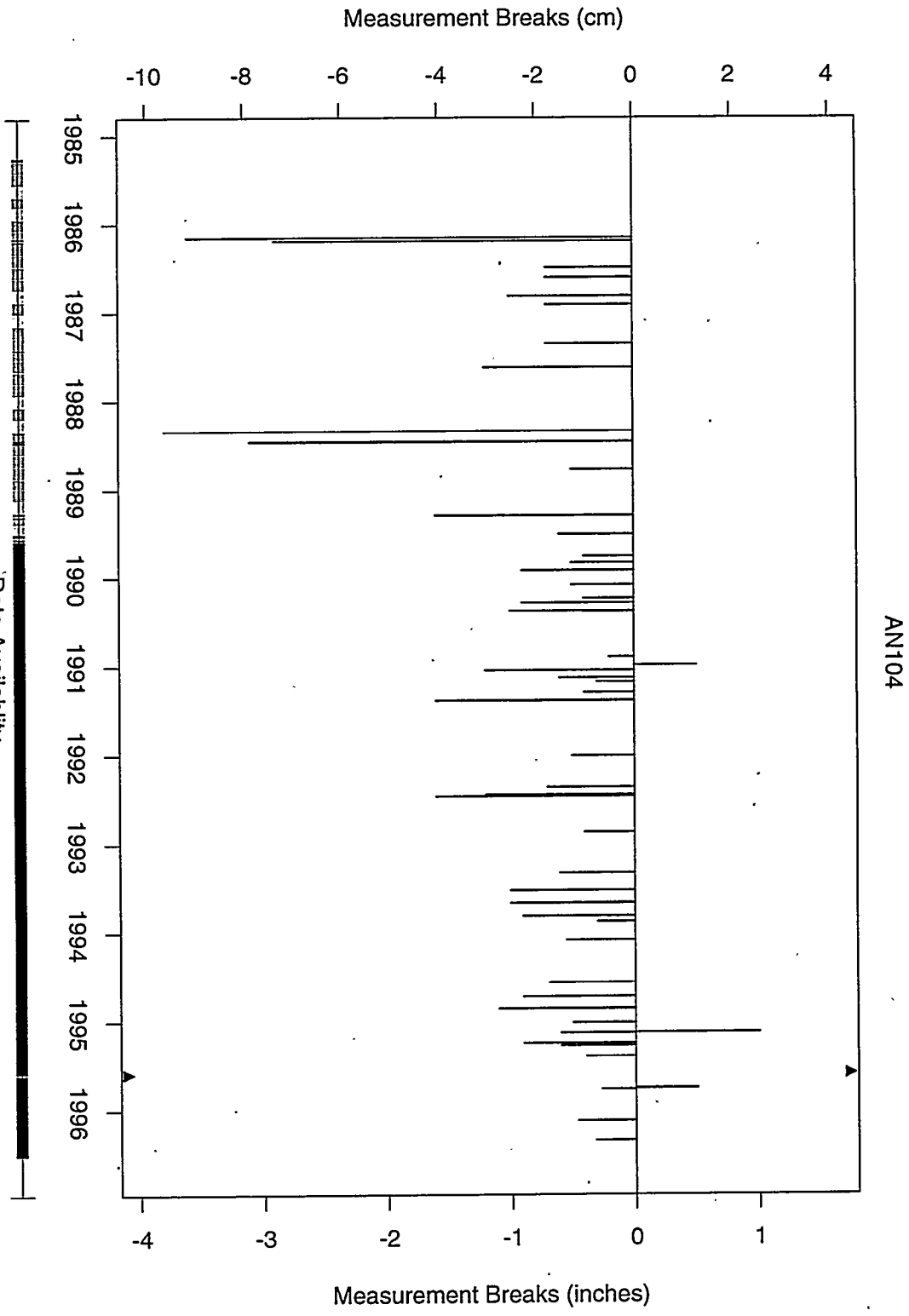

Figure C.3: Tank AN-104 detected breaks and break sizes.

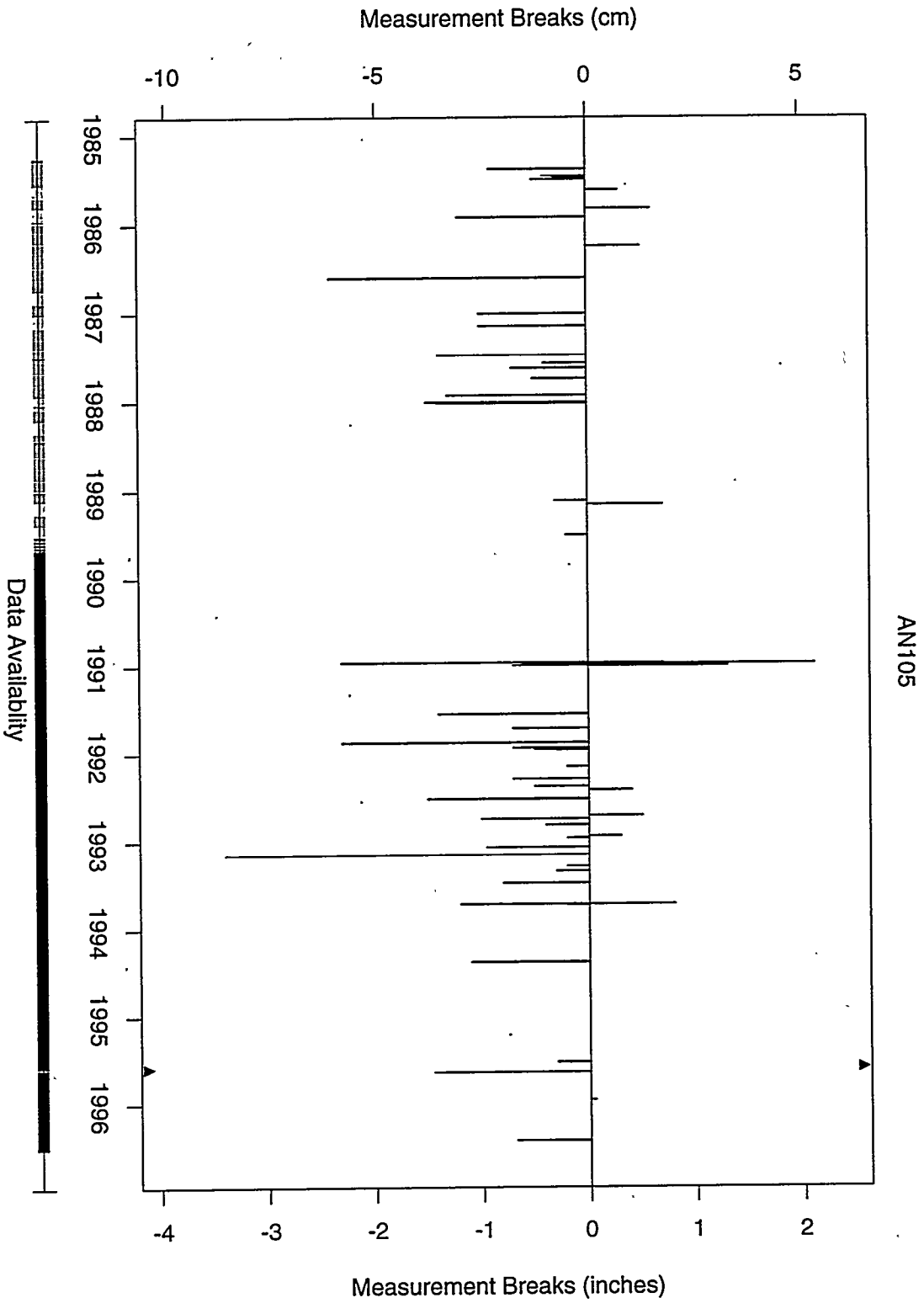

Figure C.4: Tank AN–105 detected breaks and break sizes.

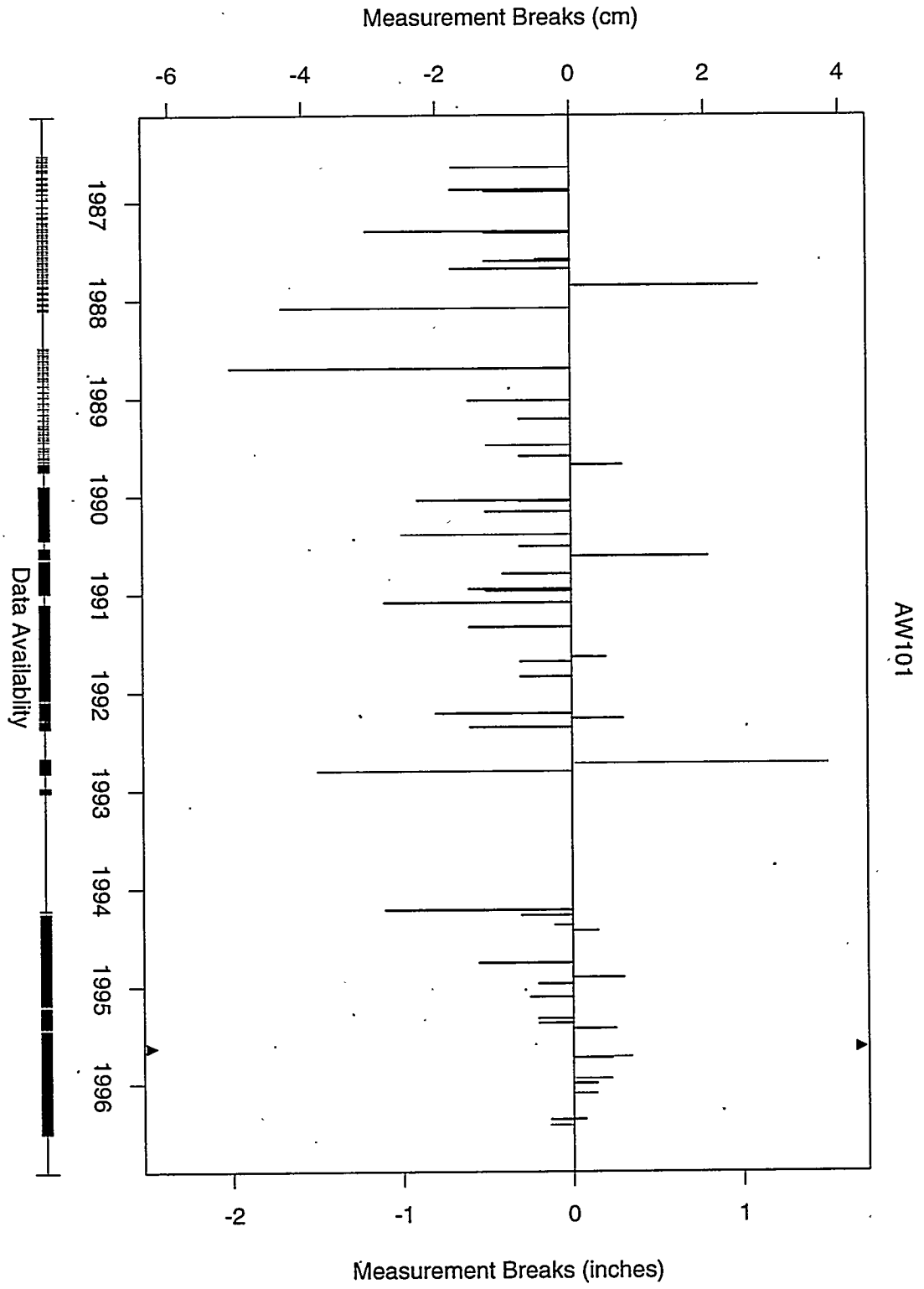

Figure C.5: Tank AW-101 detected breaks and break sizes.

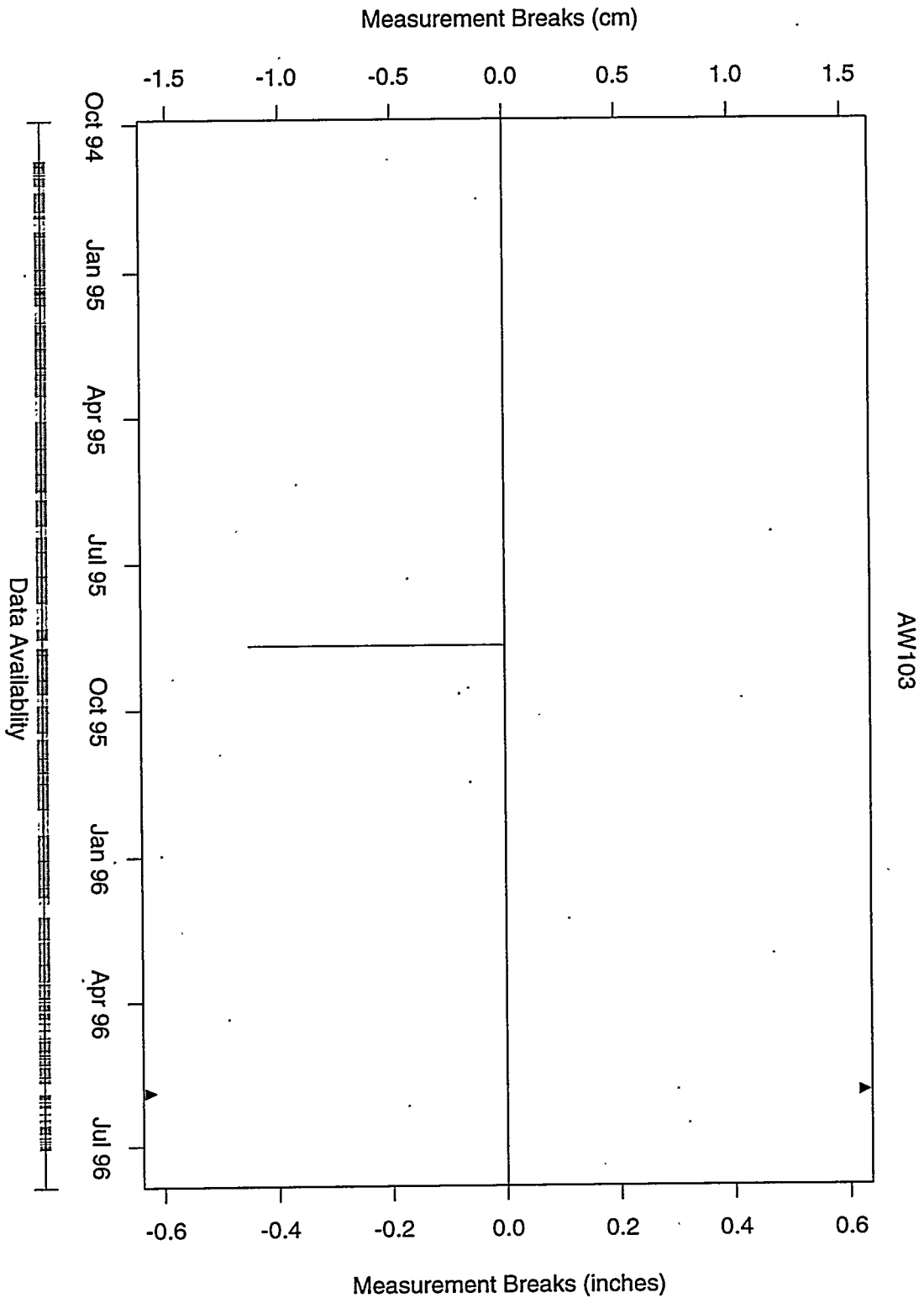

Figure C.6: Tank AW-103 detected breaks and break sizes.

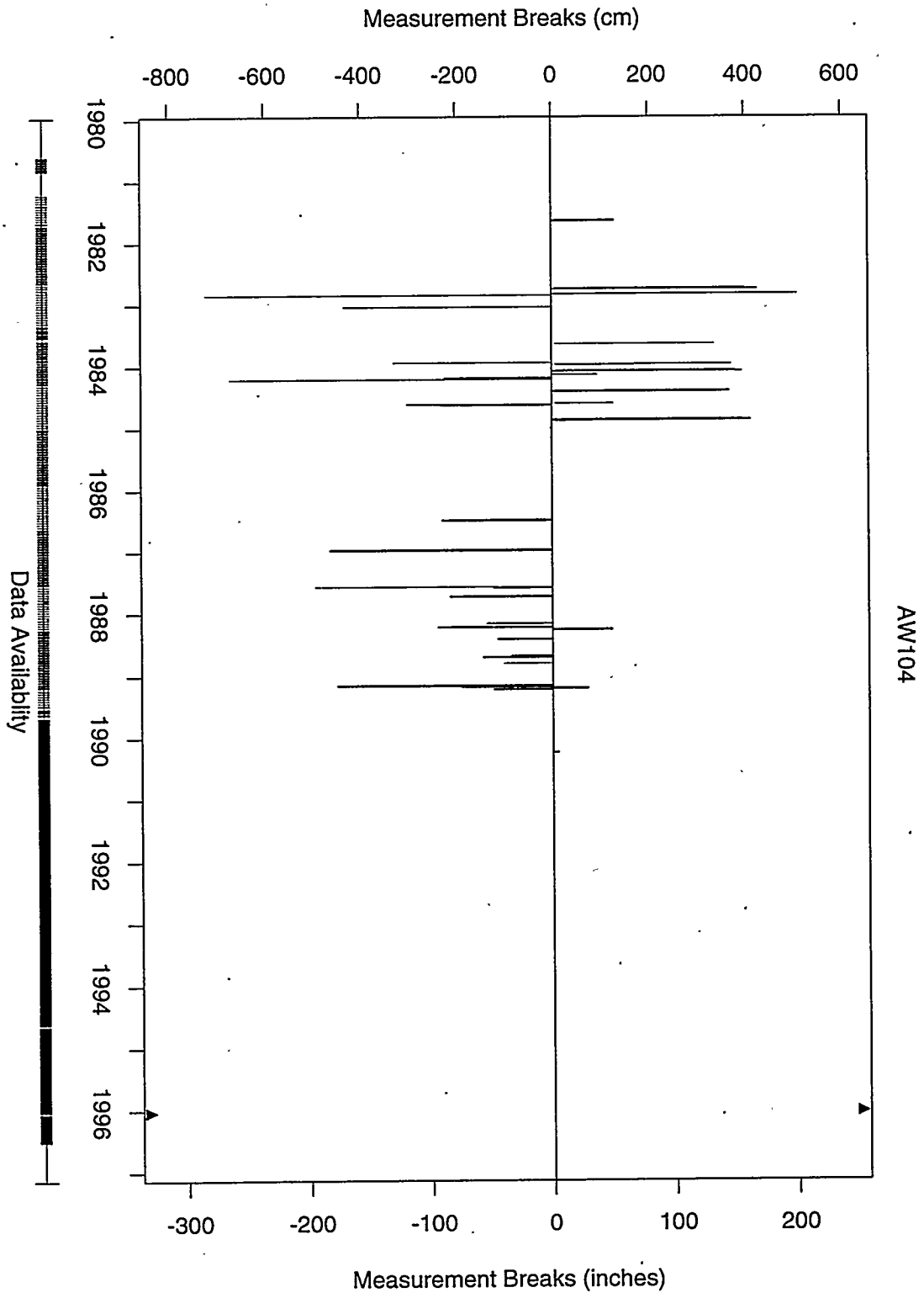

Figure C.7: Tank AW-104 detected breaks and break sizes.

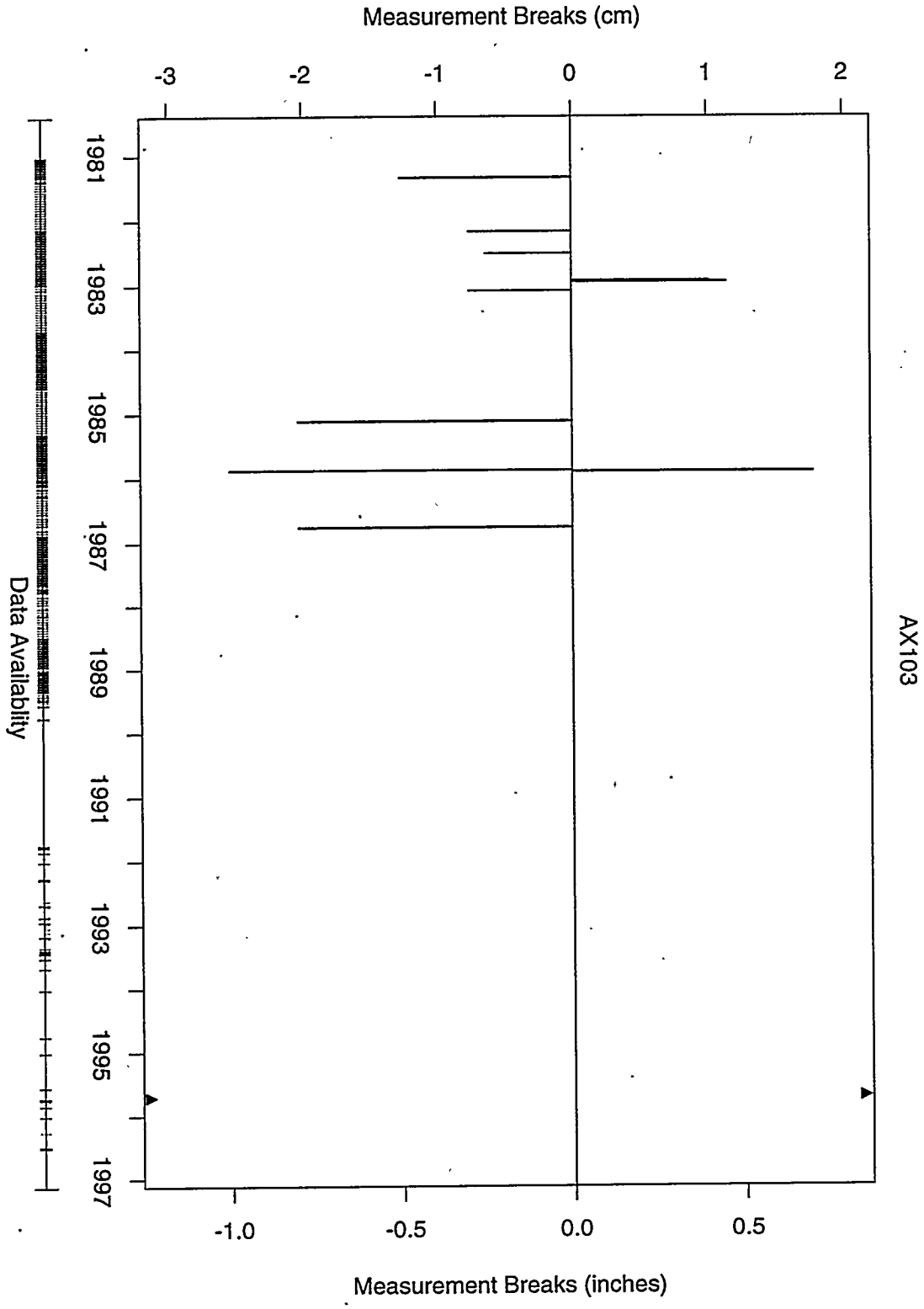

Figure C.8: Tank AX-103 detected breaks and break sizes.

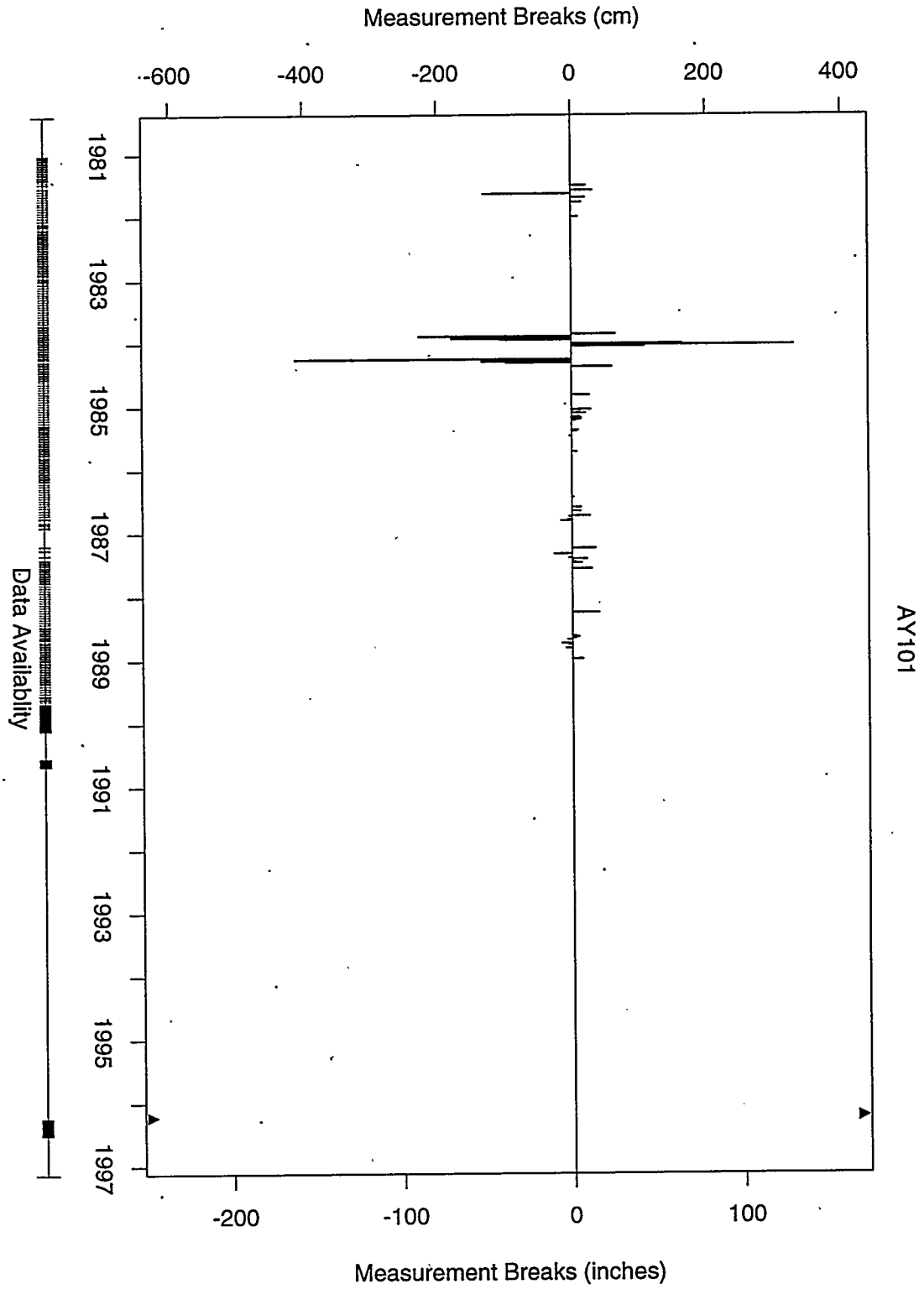

Figure C.9: Tank AY-101 detected breaks and break sizes.

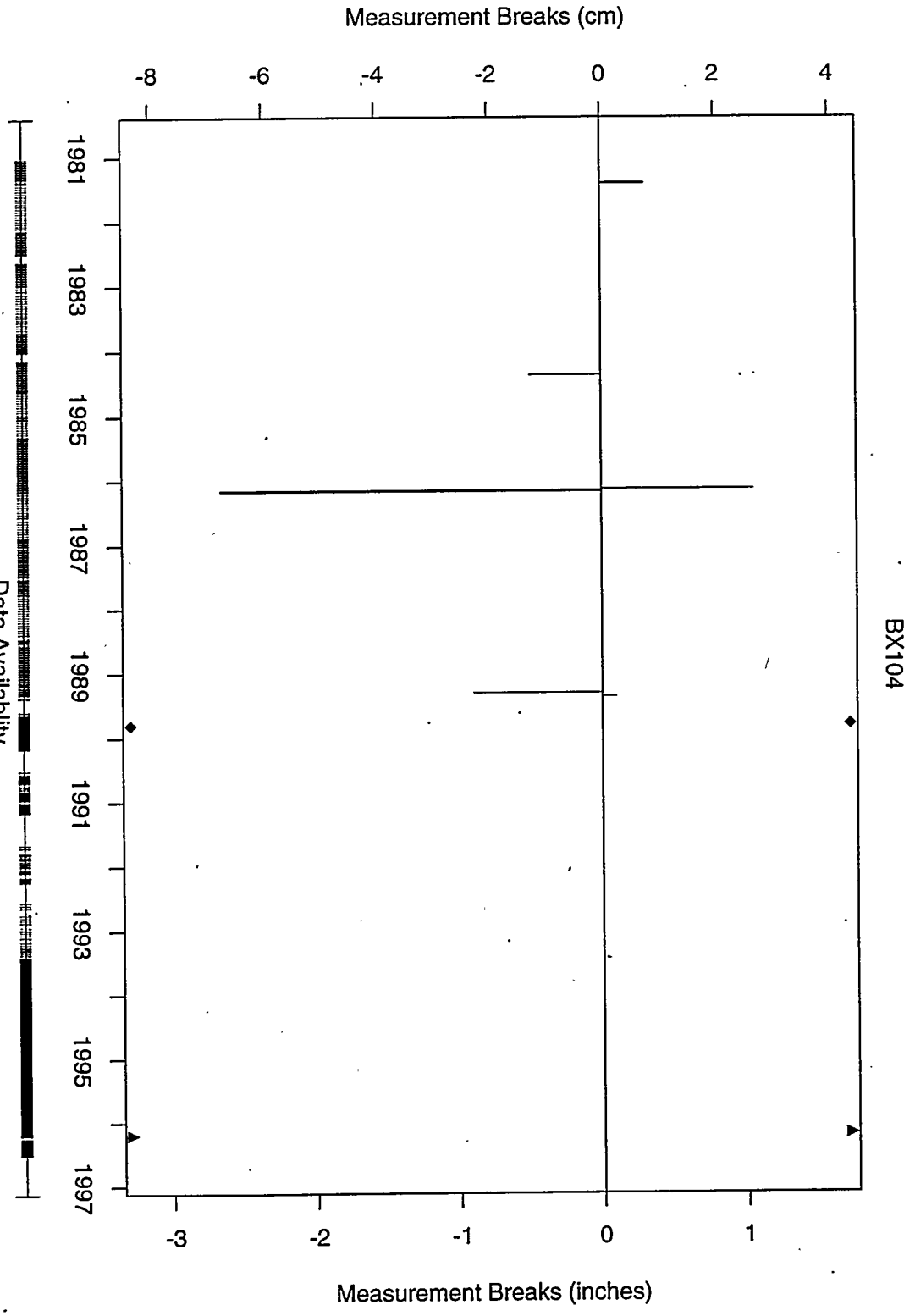

Figure C.10: Tank BX-104 detected breaks and break sizes.

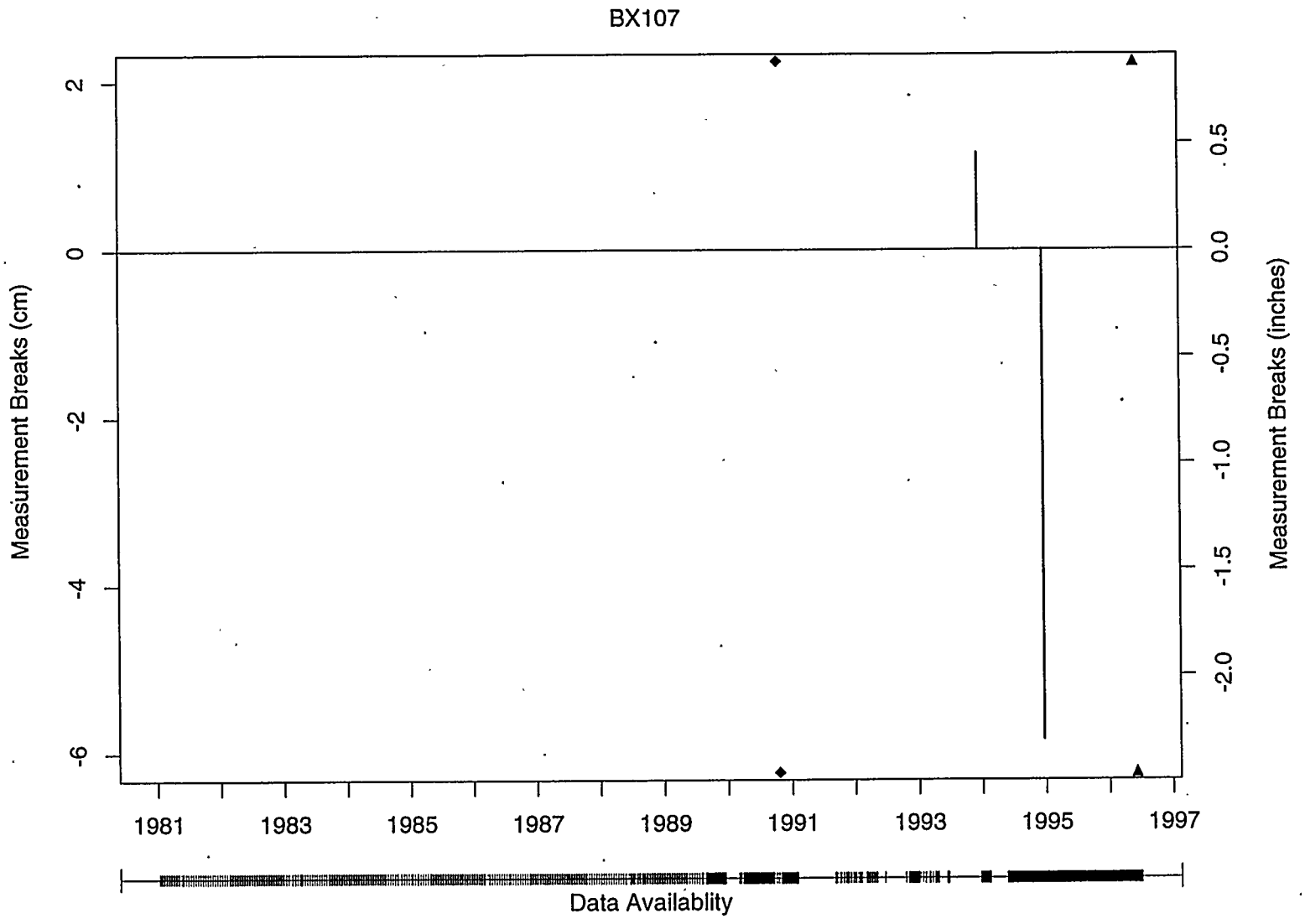

Figure C.11: Tank BX-107 detected breaks and break sizes.

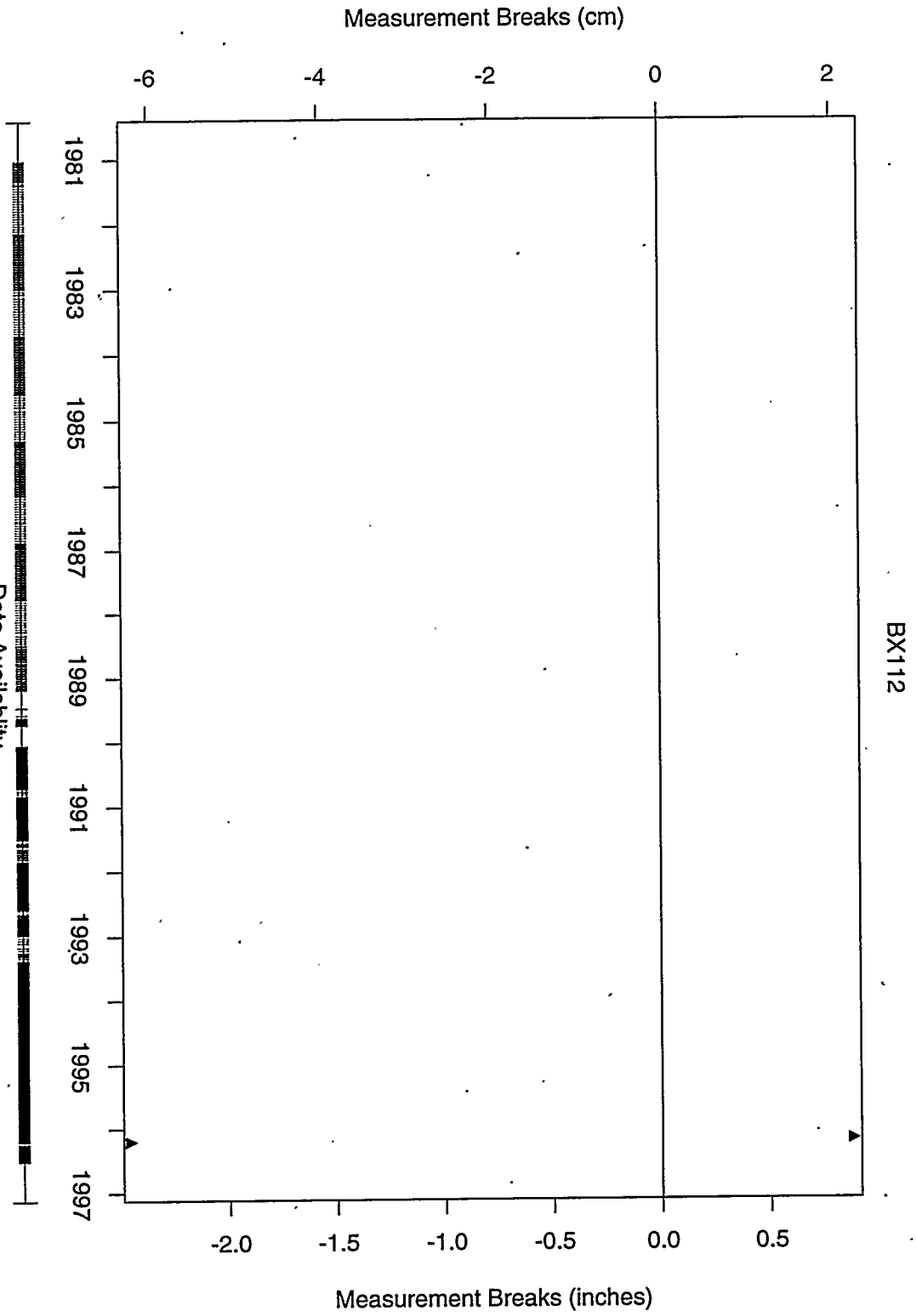

Figure C.12: Tank BX-112 detected breaks and break sizes.

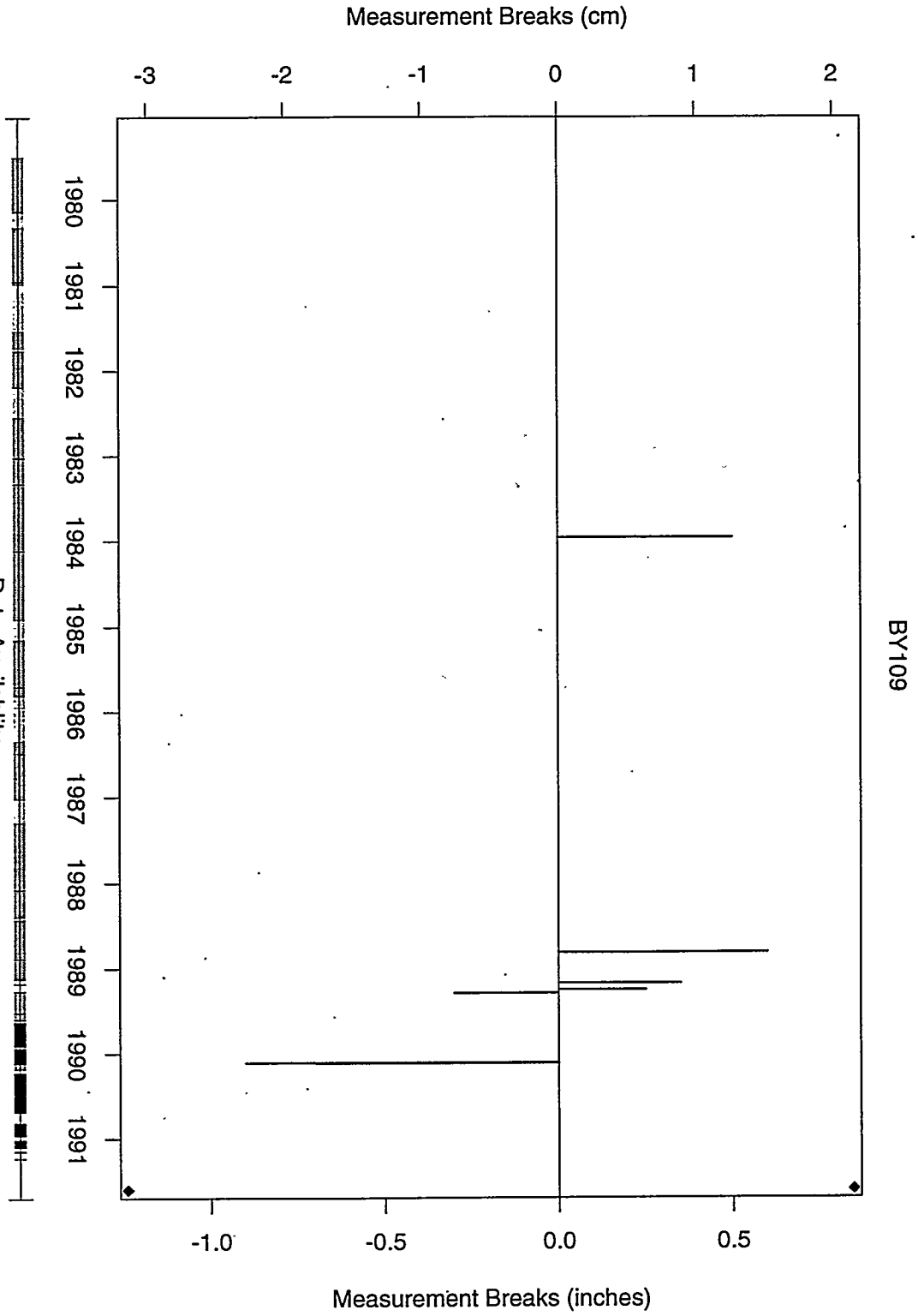

Figure C.13: Tank BY-109 detected breaks and break sizes.

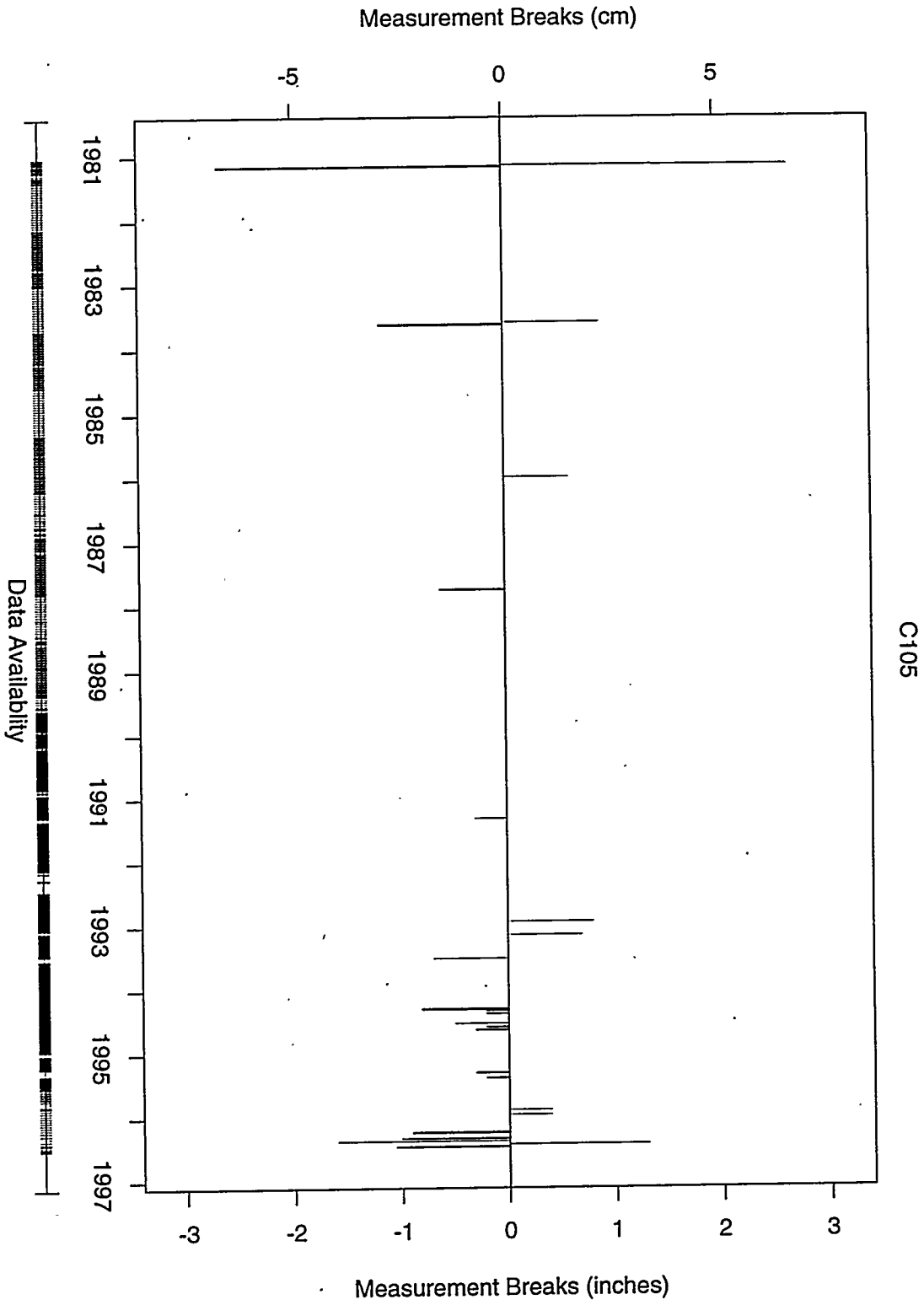

Figure C.14: Tank C–105 detected breaks and break sizes.

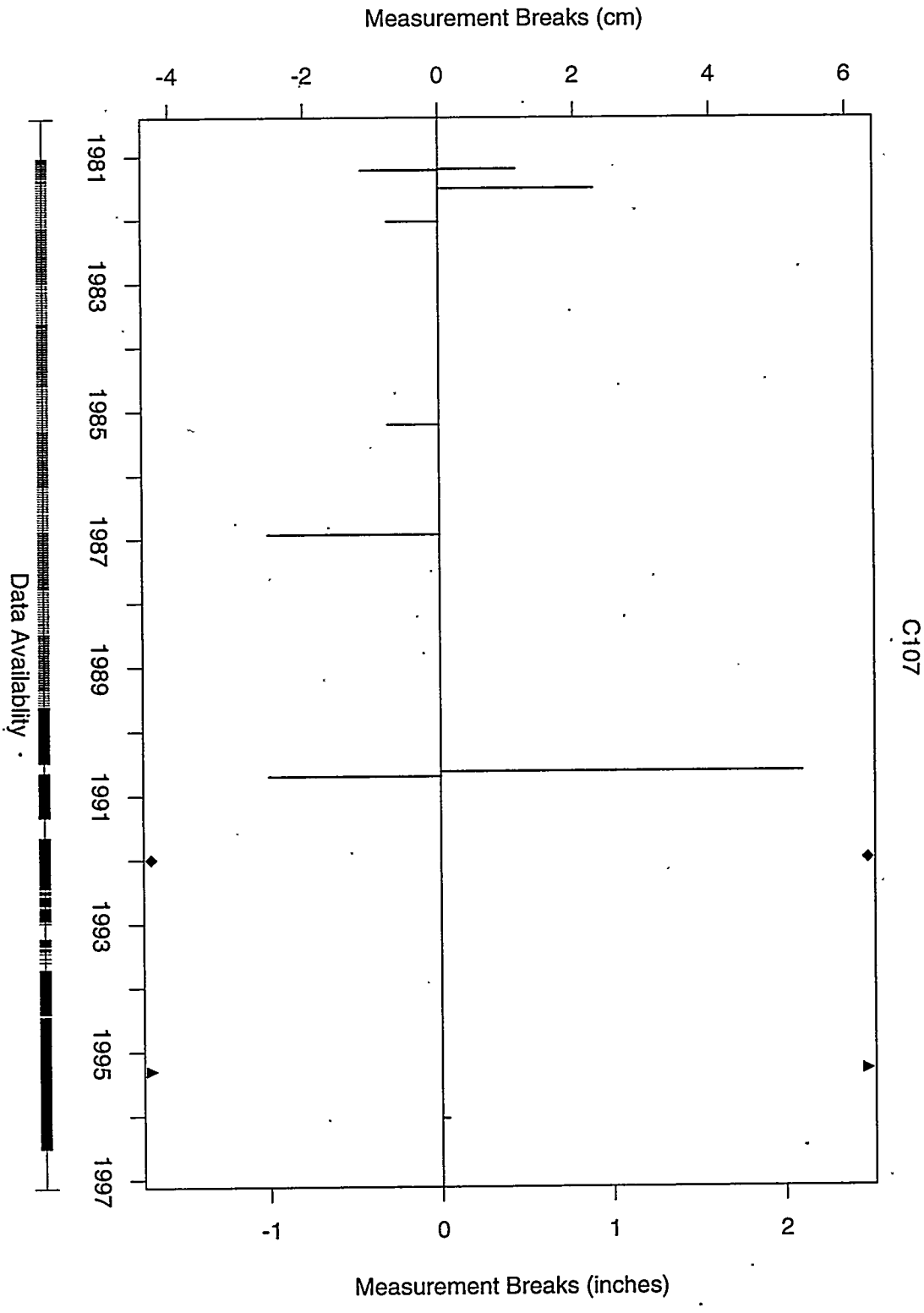

Figure C.15: Tank C-107 detected breaks and break sizes.

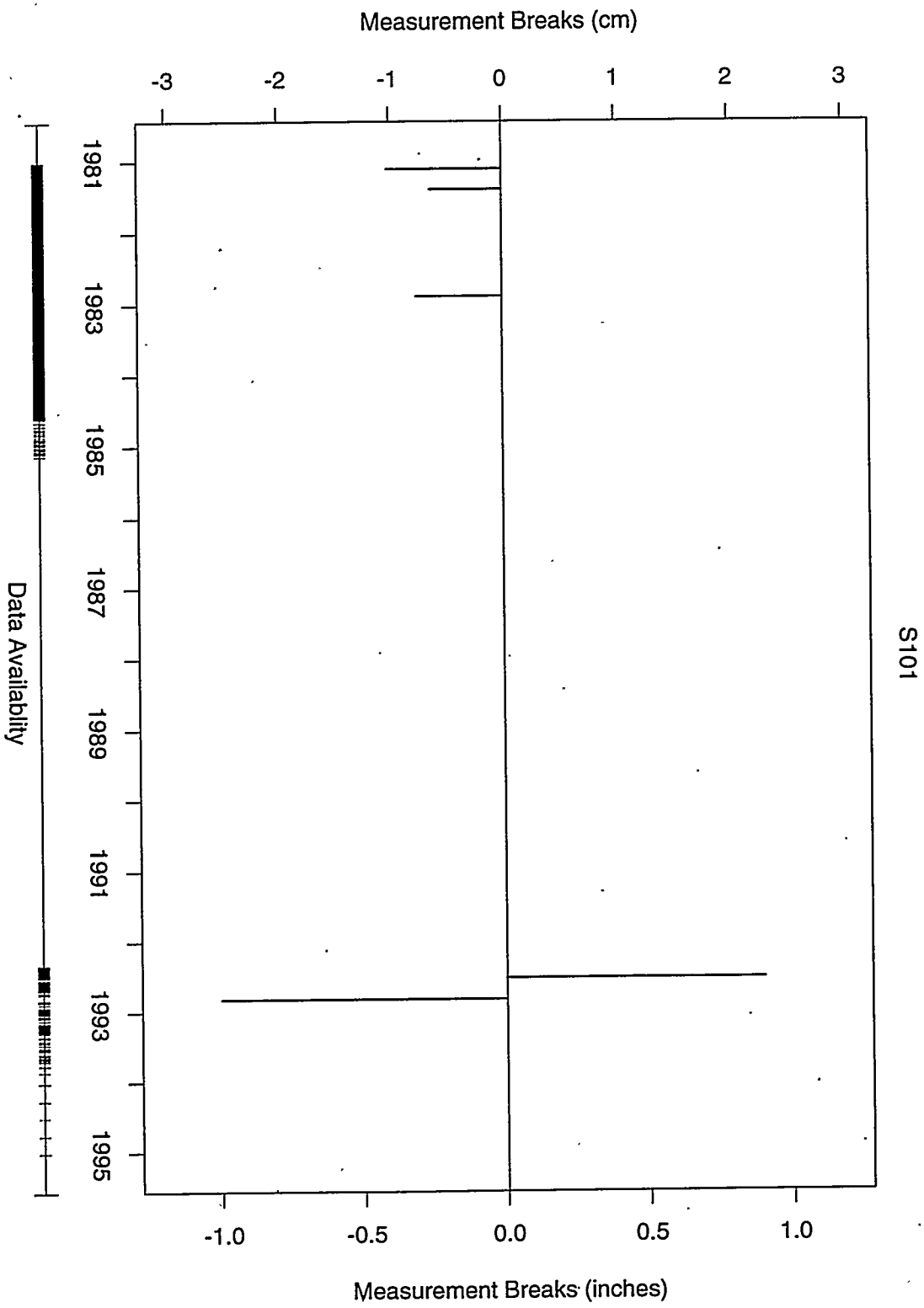

Figure C.16: Tank S-101 detected breaks and break sizes.

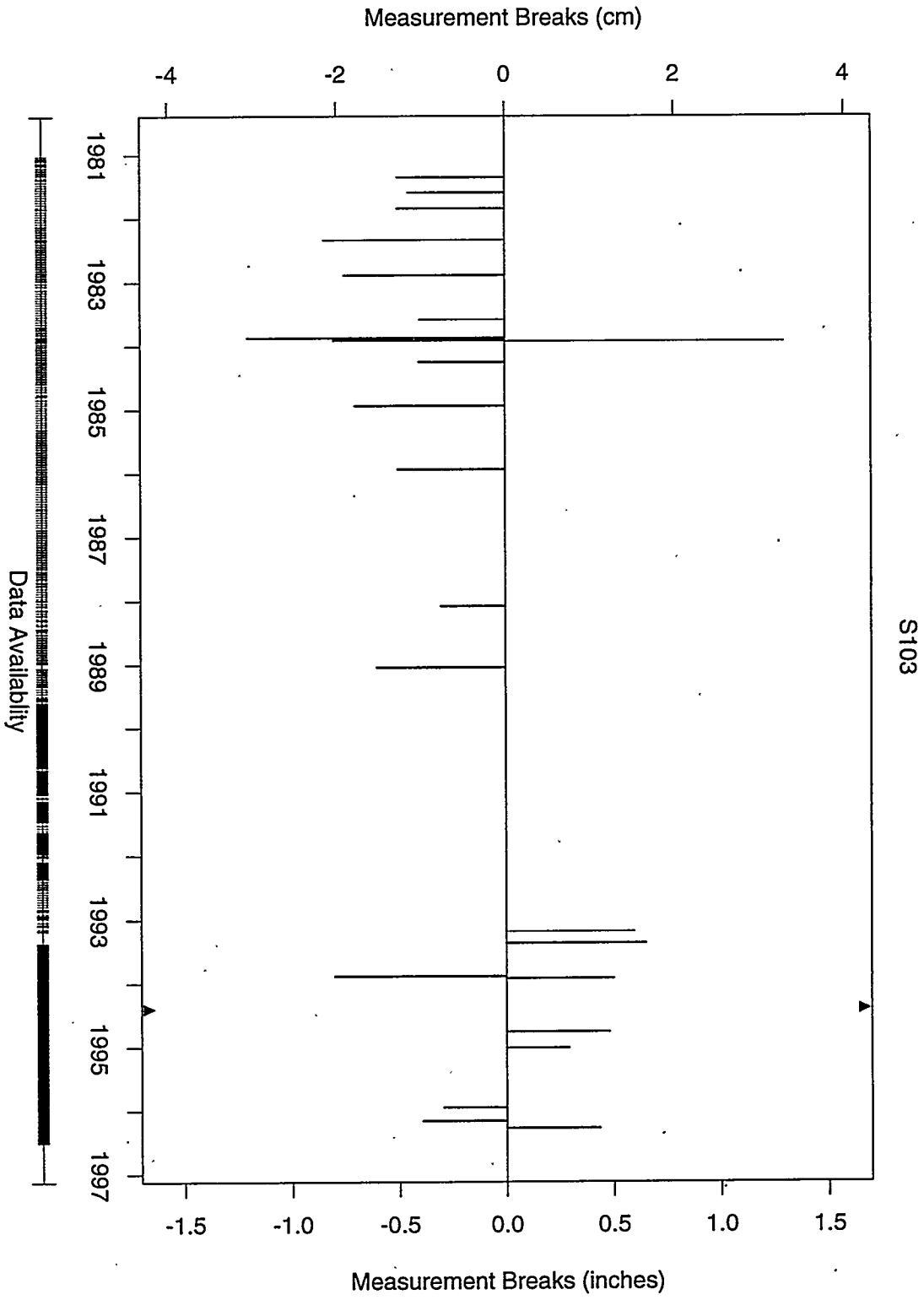

Figure C.17: Tank S-103 detected breaks and break sizes.

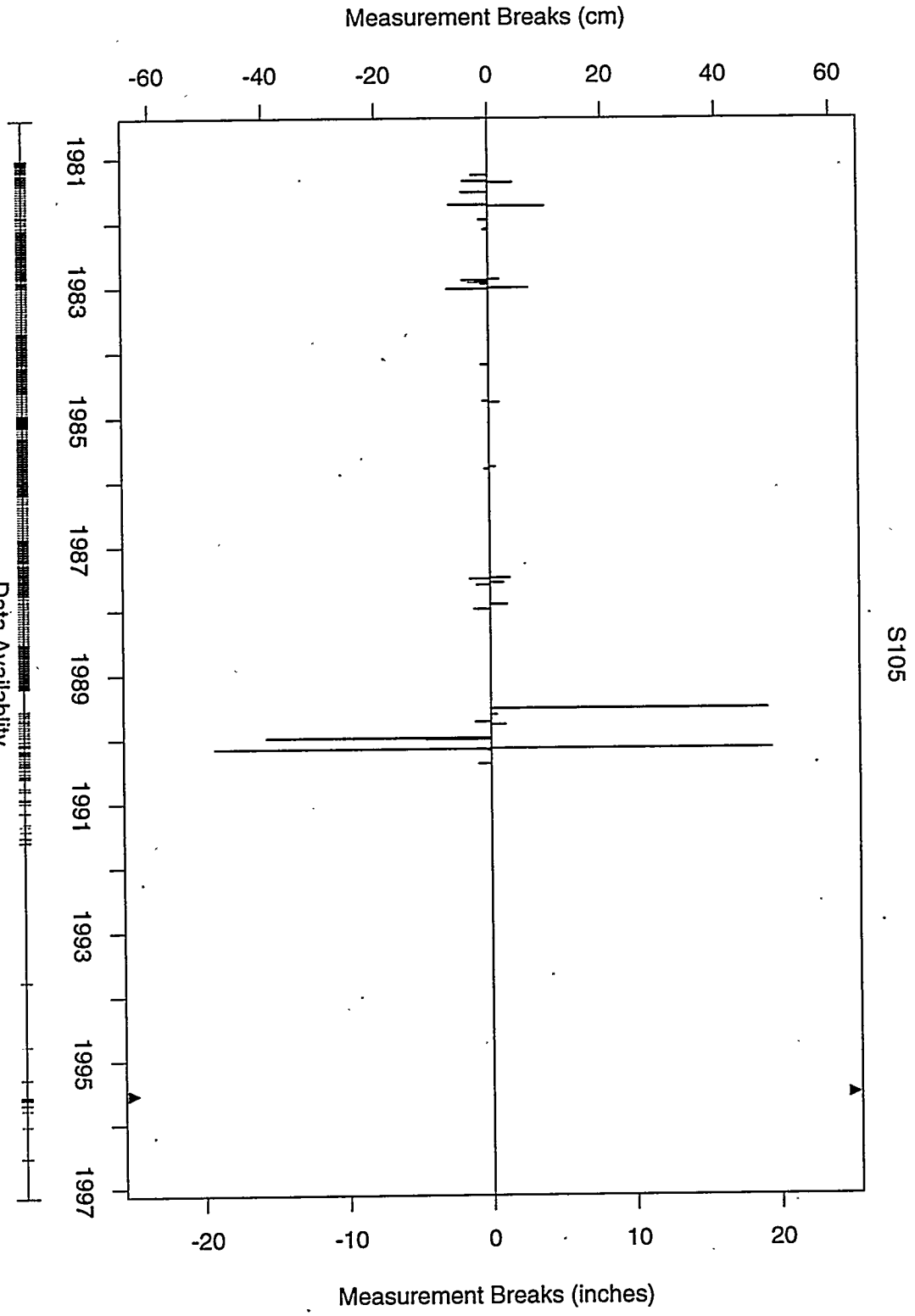

Figure C.18: Tank S-105 detected breaks and break sizes.

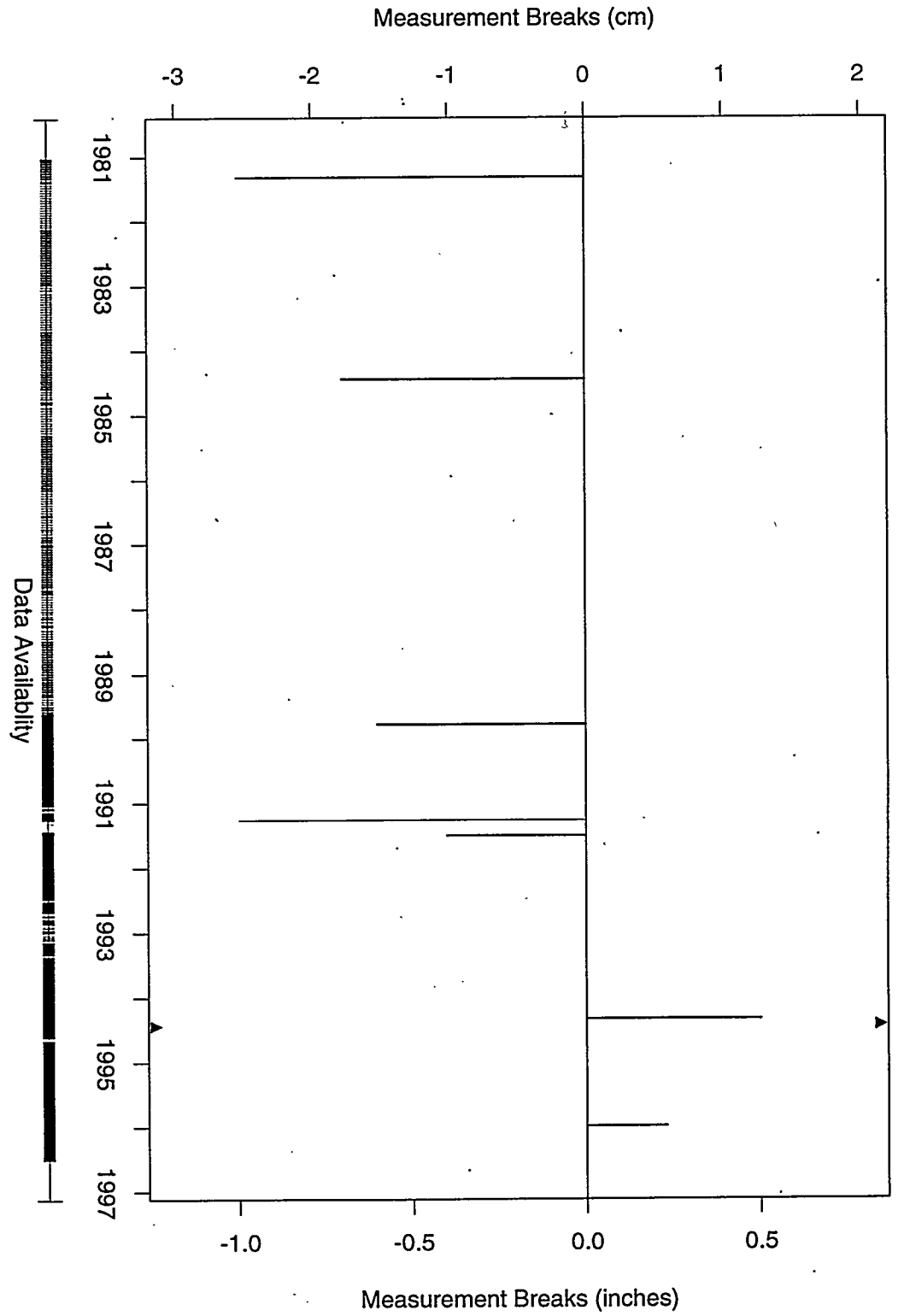

Figure C.19: Tank S-106 detected breaks and break sizes.

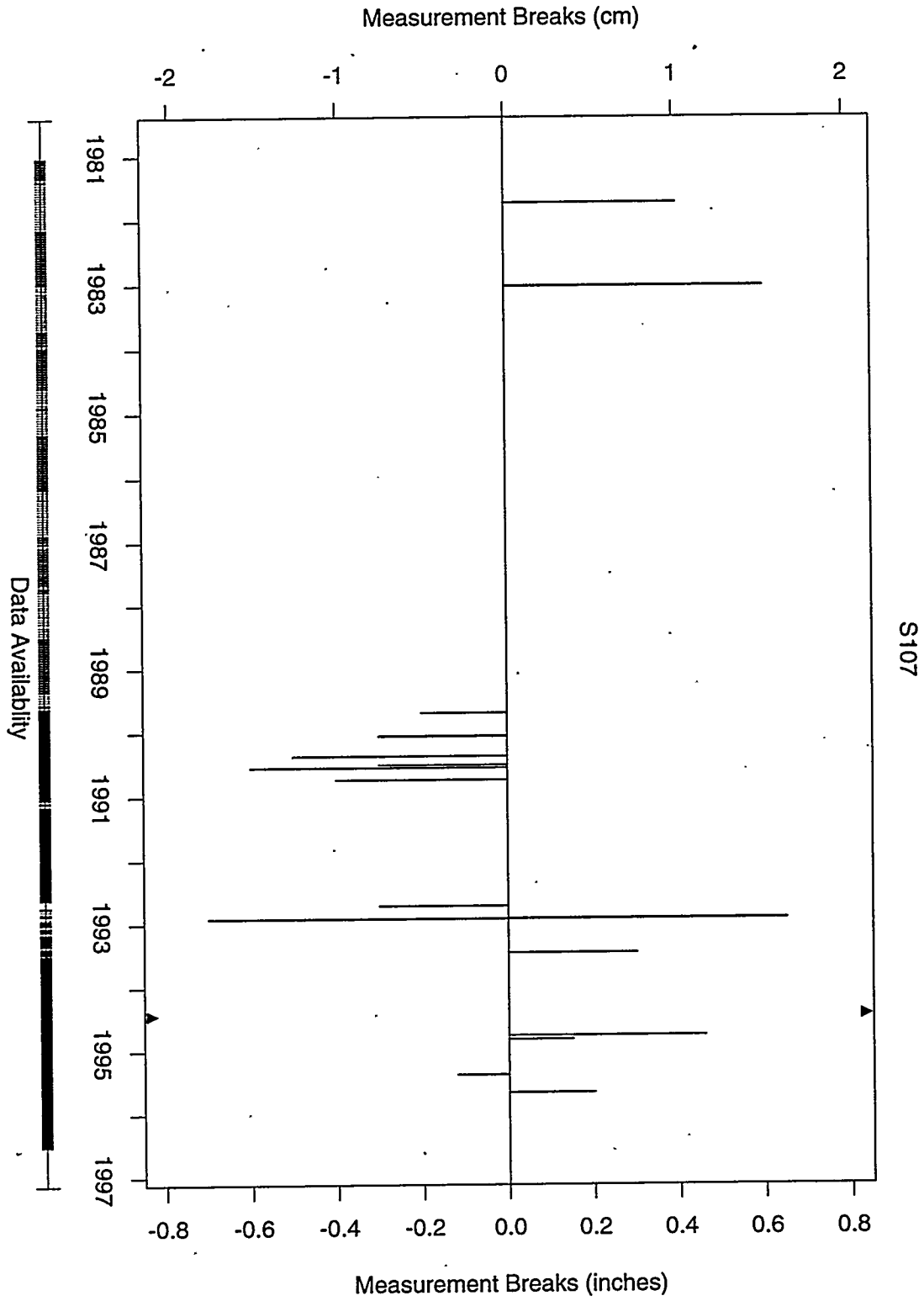

Figure C.20: Tank S-107 detected breaks and break sizes.

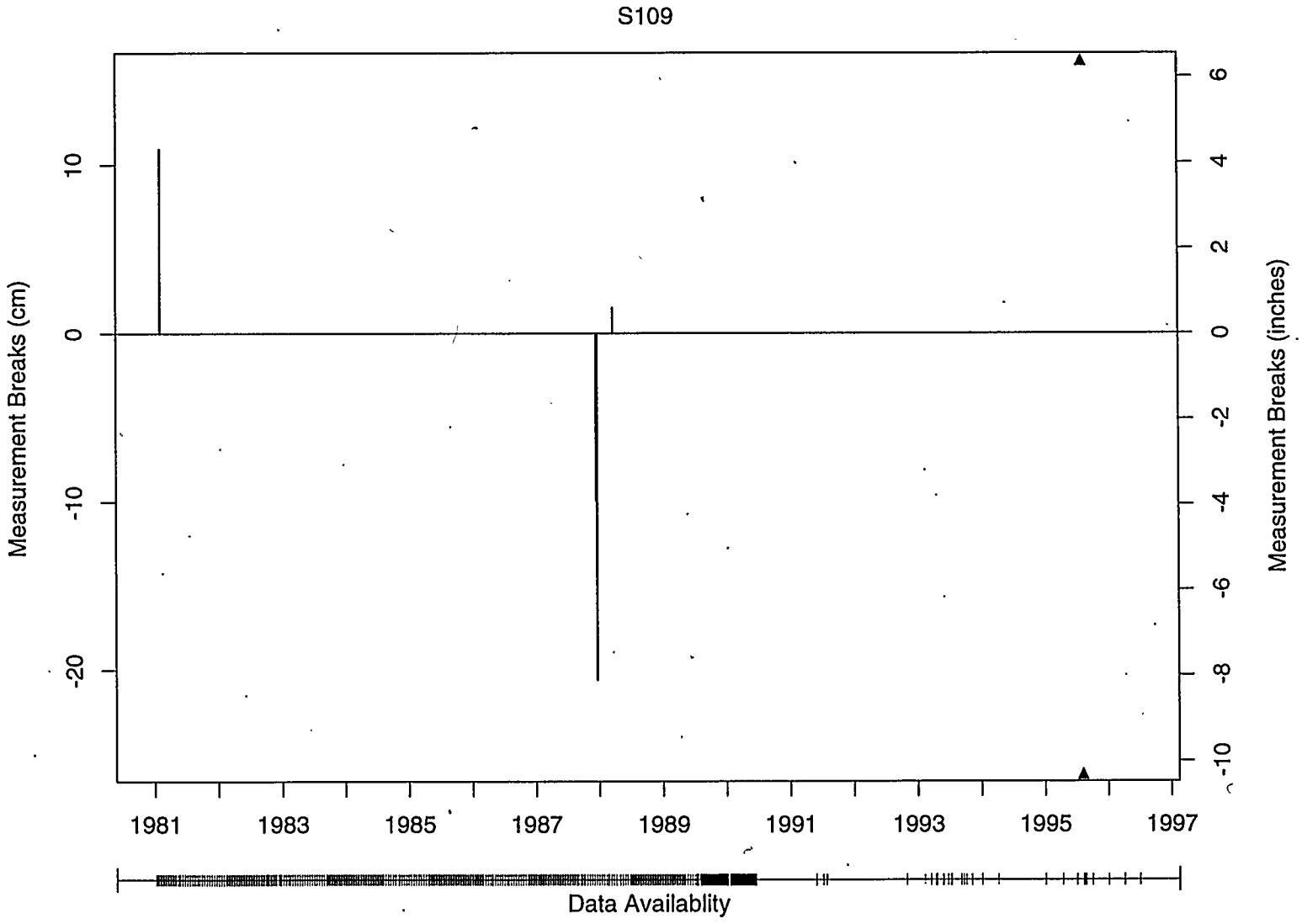

Figure C.21: Tank S-109 detected breaks and break sizes.

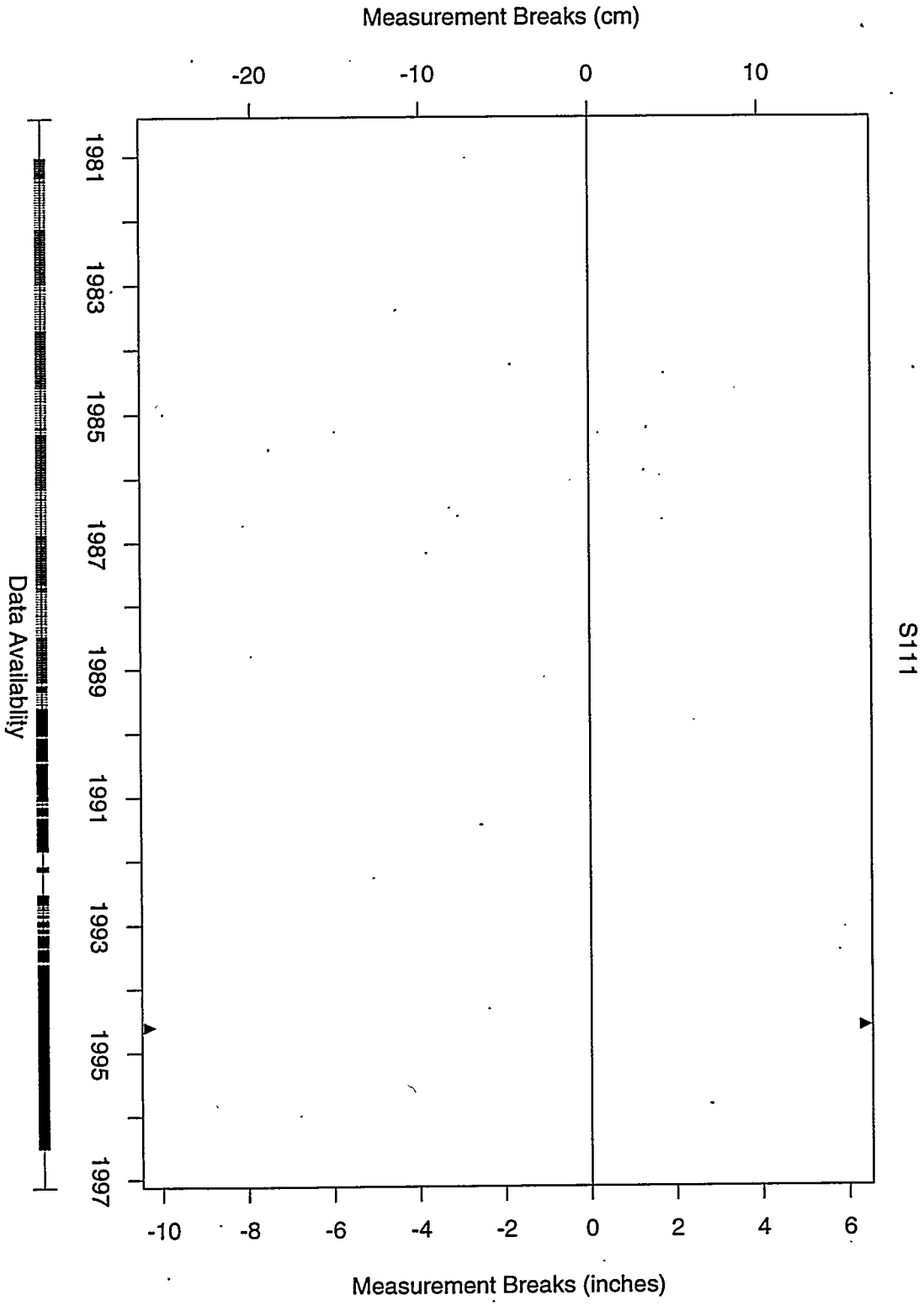

Figure C.22: Tank S-111 detected breaks and break sizes.

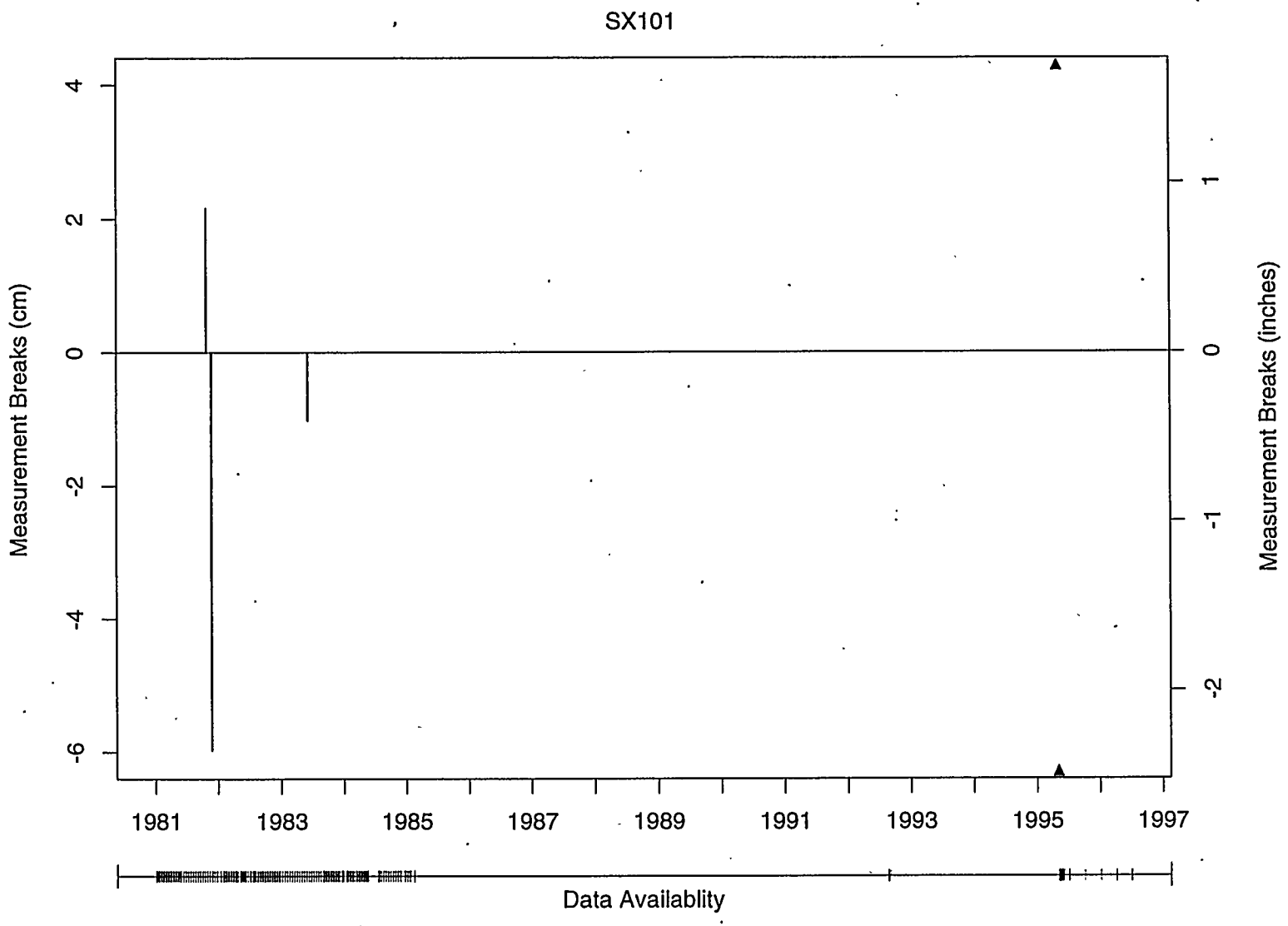

Figure C.23: Tank SX-101 detected breaks and break sizes.

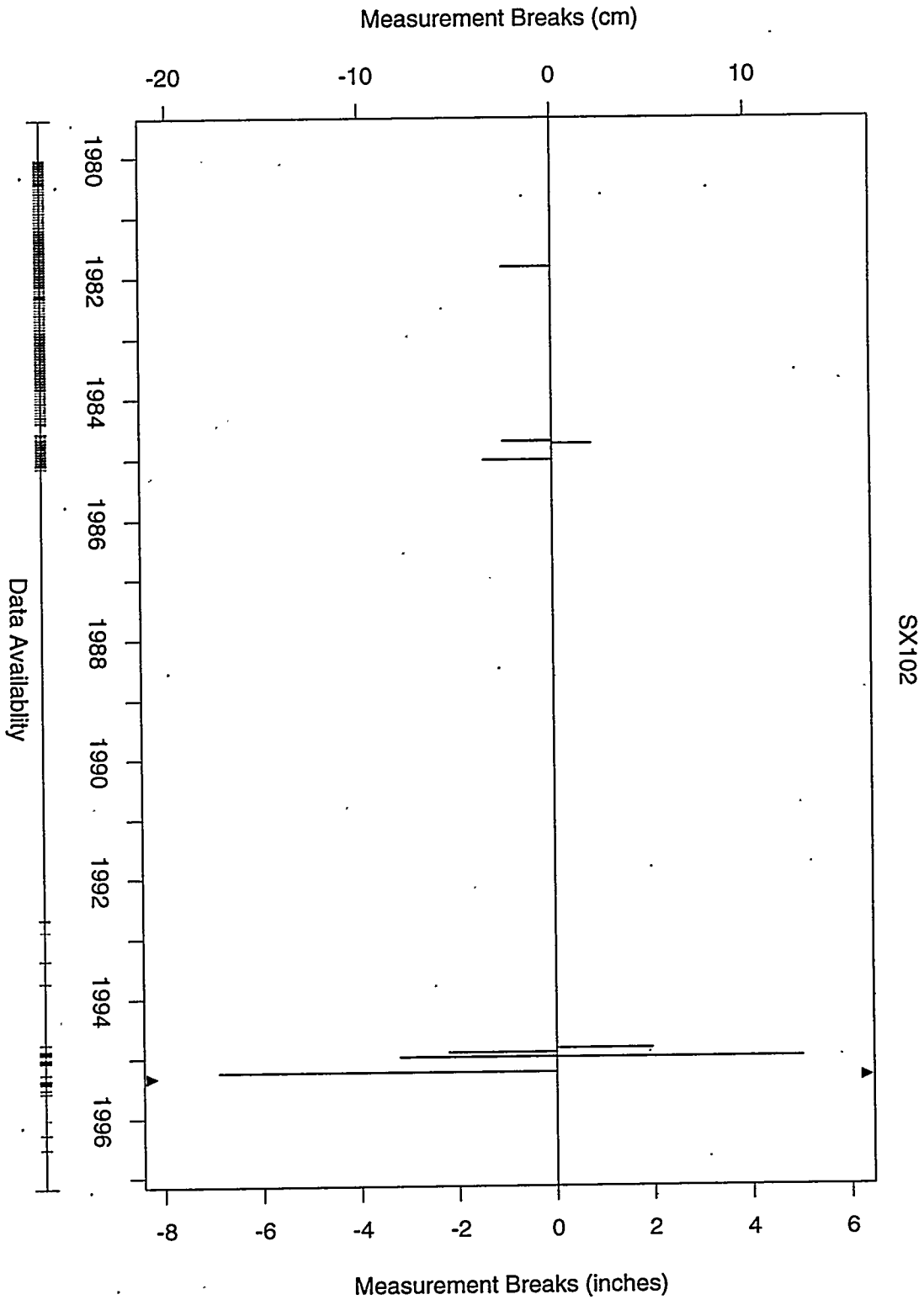

Figure C.24: Tank SX–102 detected breaks and break sizes.

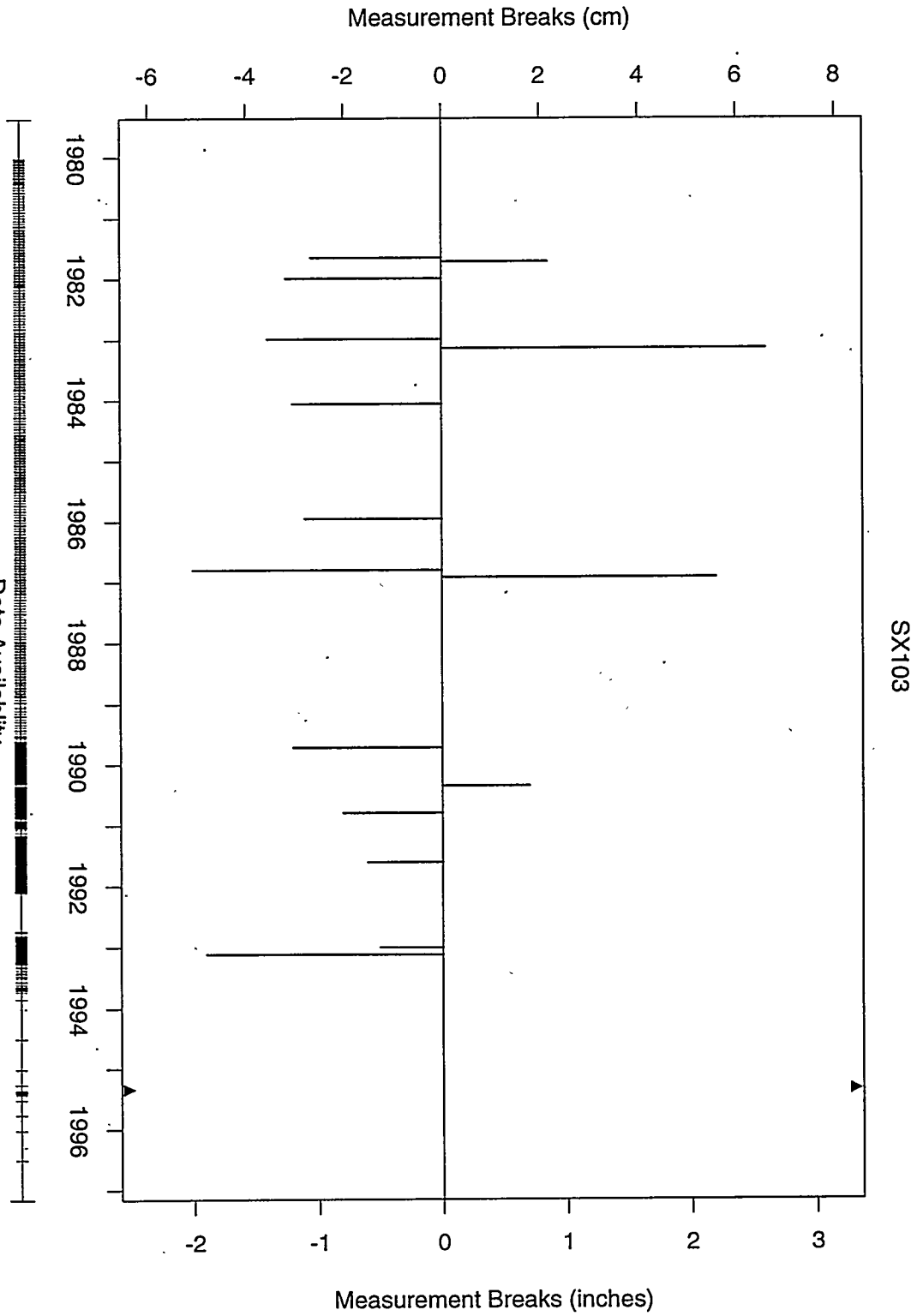

Figure C.25: Tank SX-103 detected breaks and break sizes.

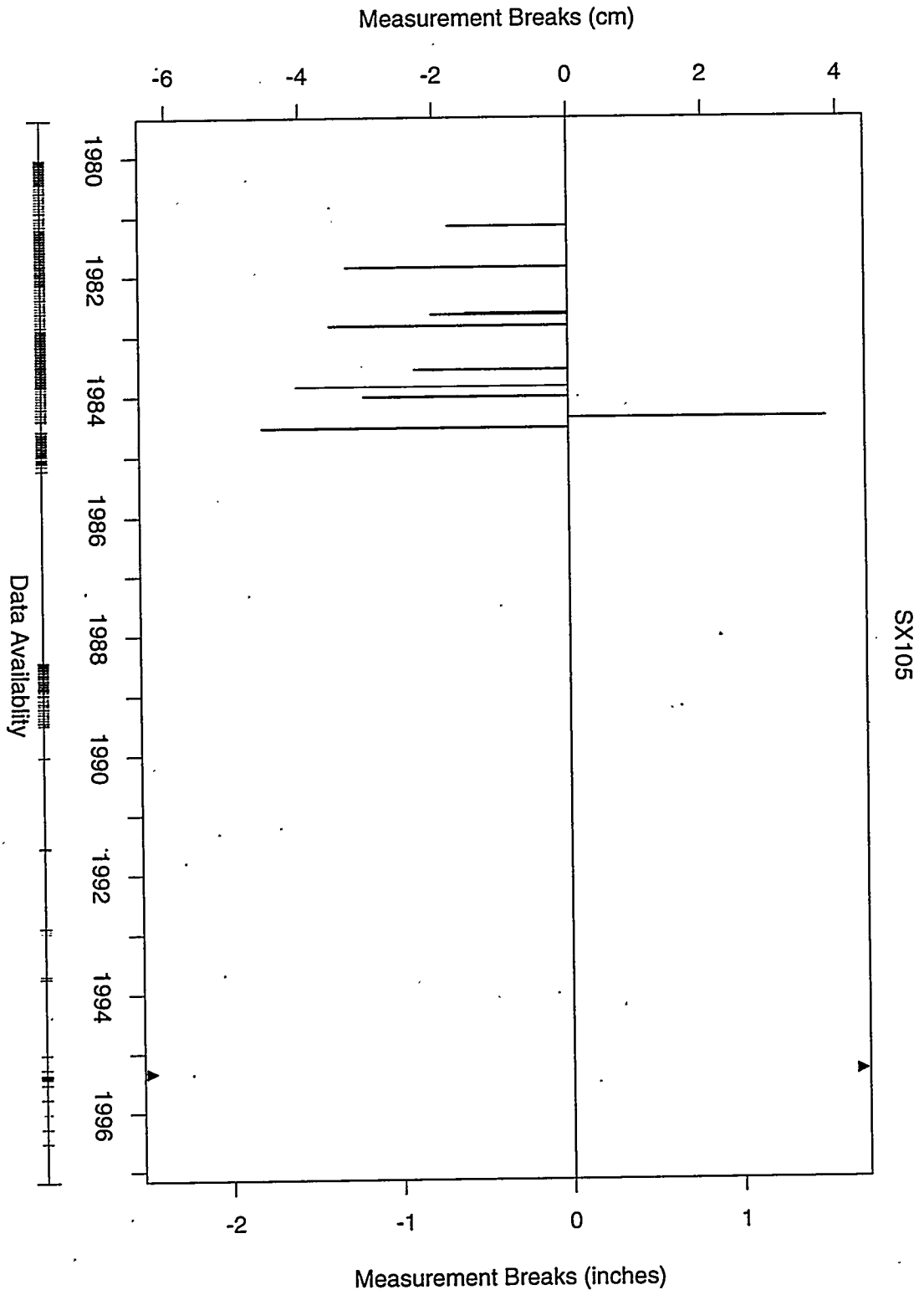

Figure C.26: Tank SX-105 detected breaks and break sizes.

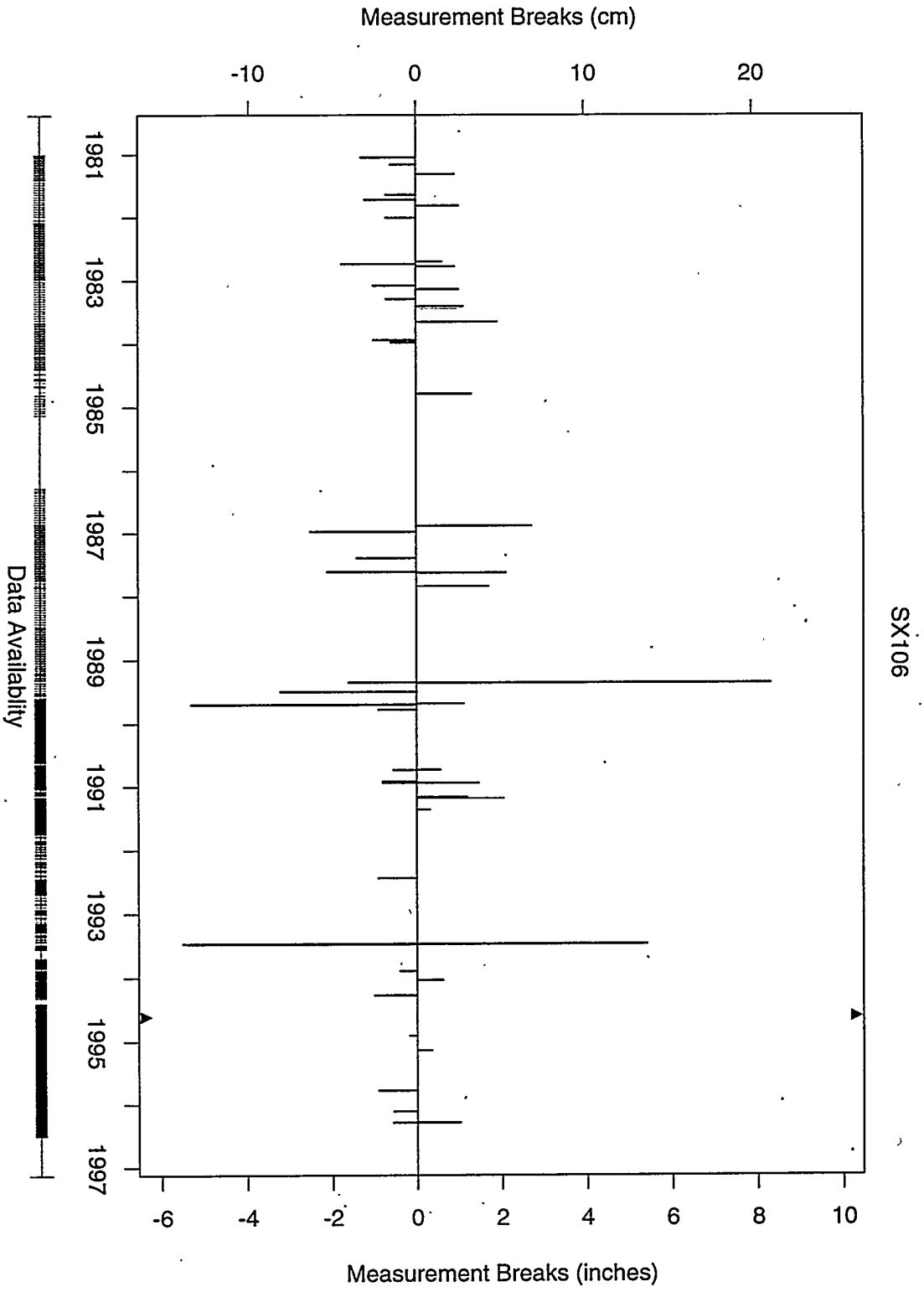

Figure C.27: Tank SX-106 detected breaks and break sizes.

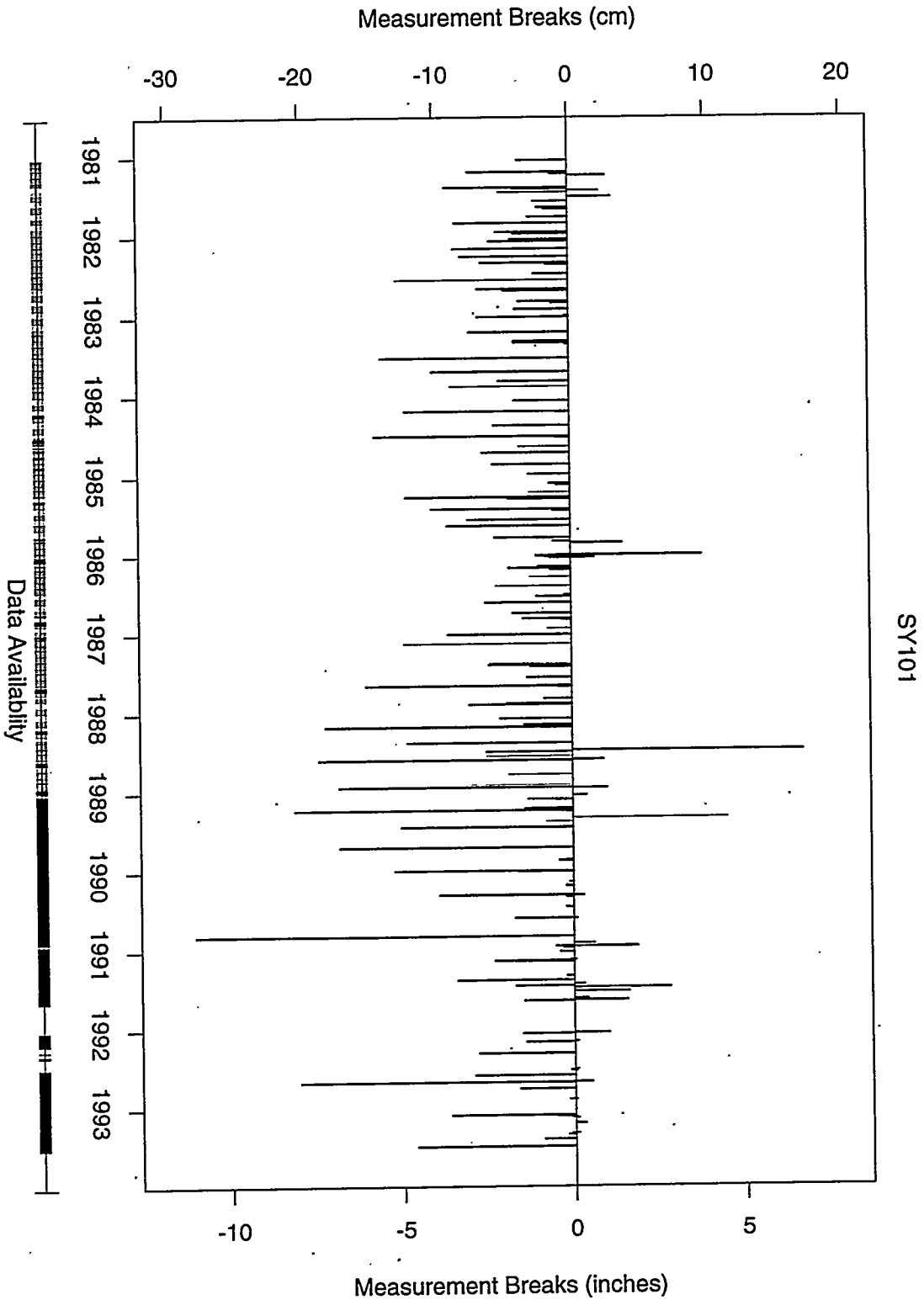

Figure C.28: Tank SY-101 detected breaks and break sizes.

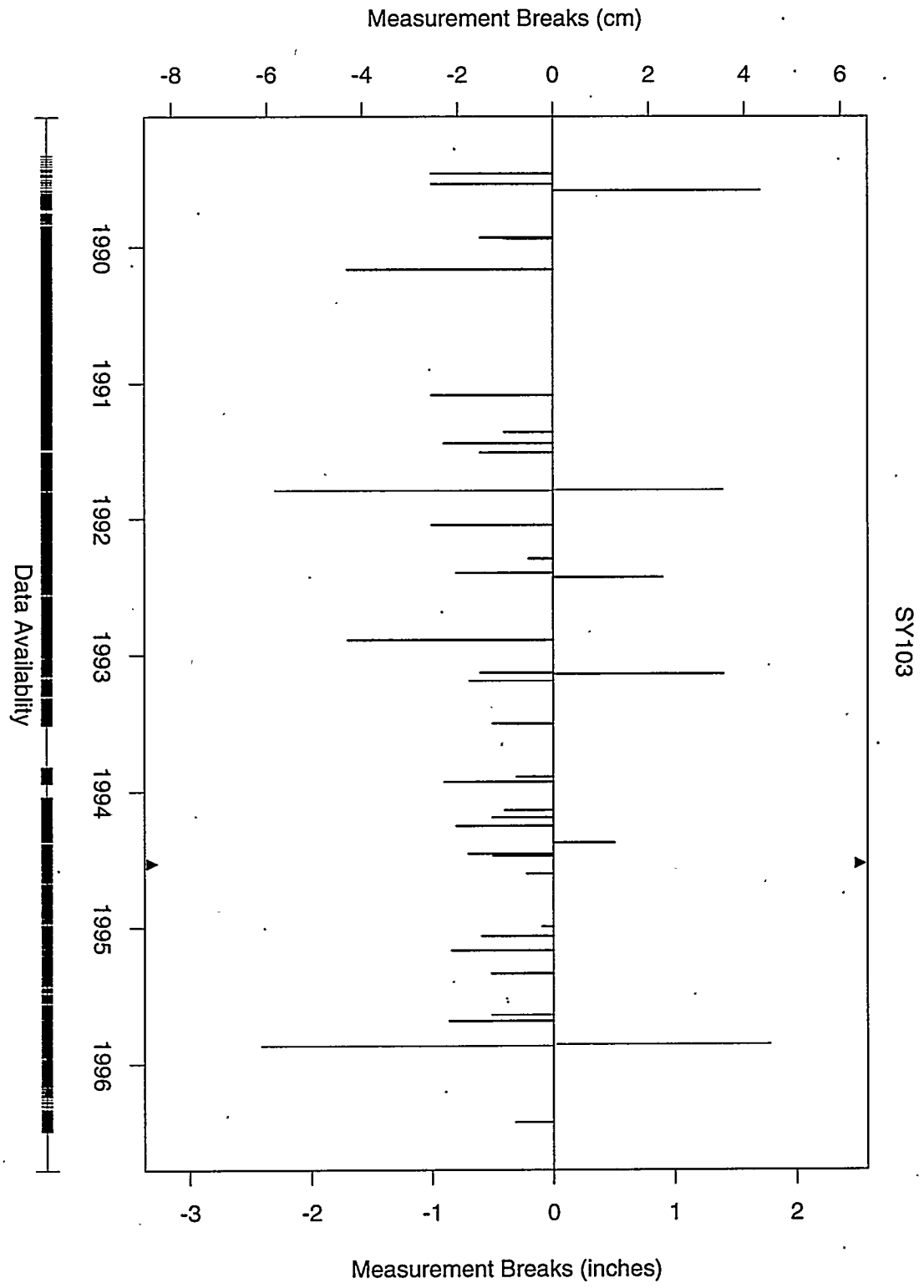

Figure C.29: Tank SY-103 detected breaks and break sizes.

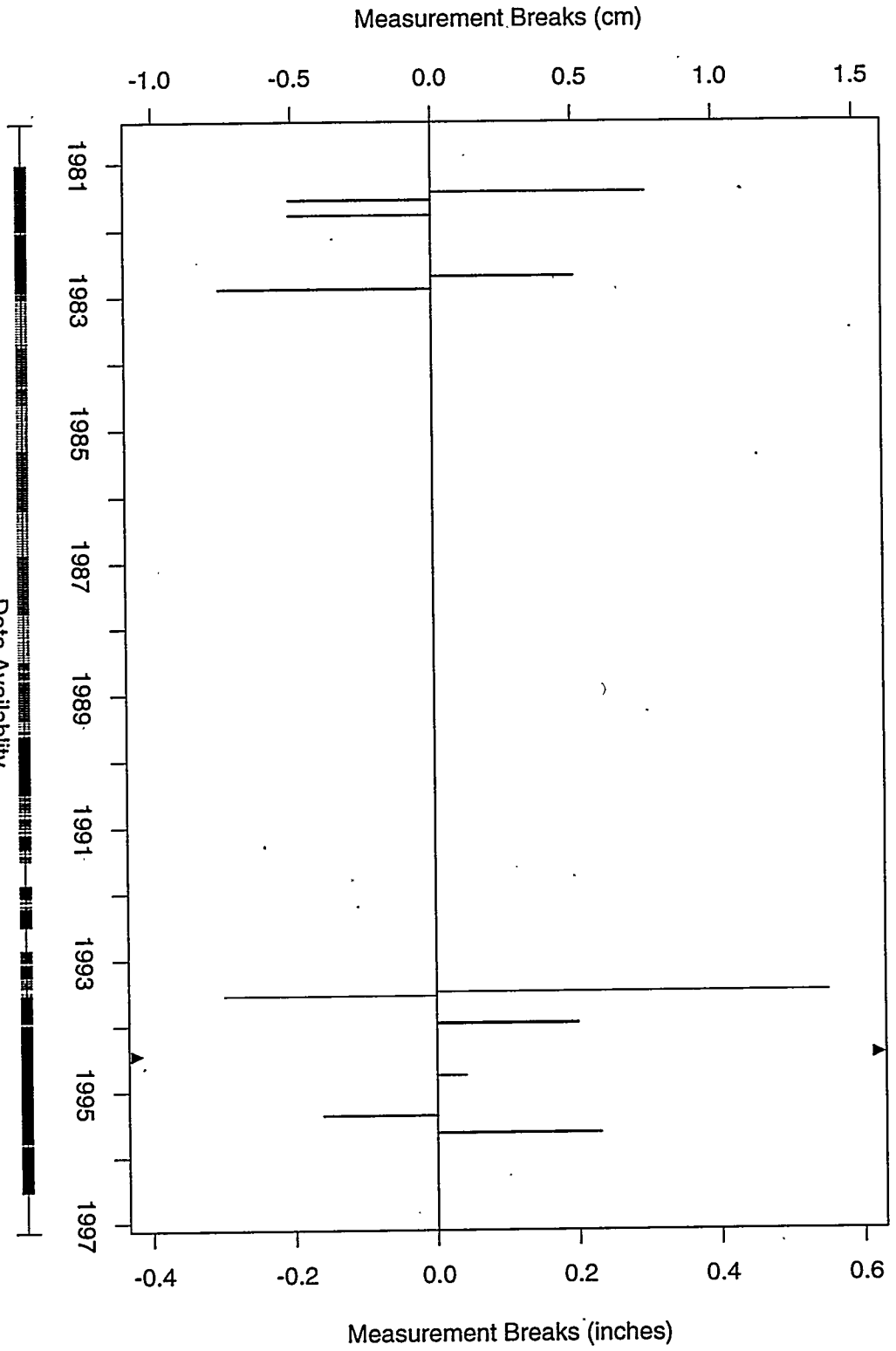

Figure C.30: Tank T-107 detected breaks and break sizes.

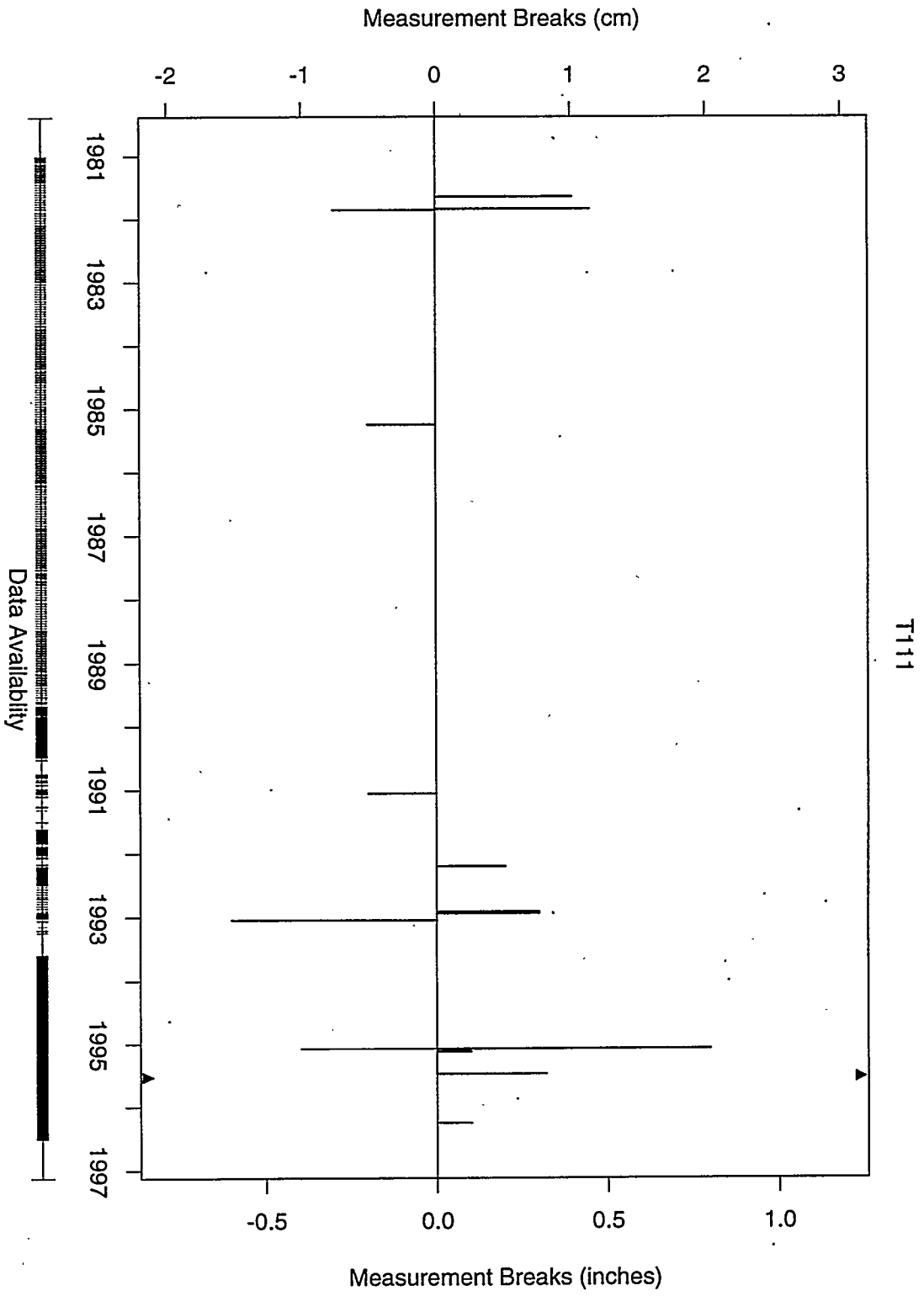

Figure C.31: Tank T-111 detected breaks and break sizes.

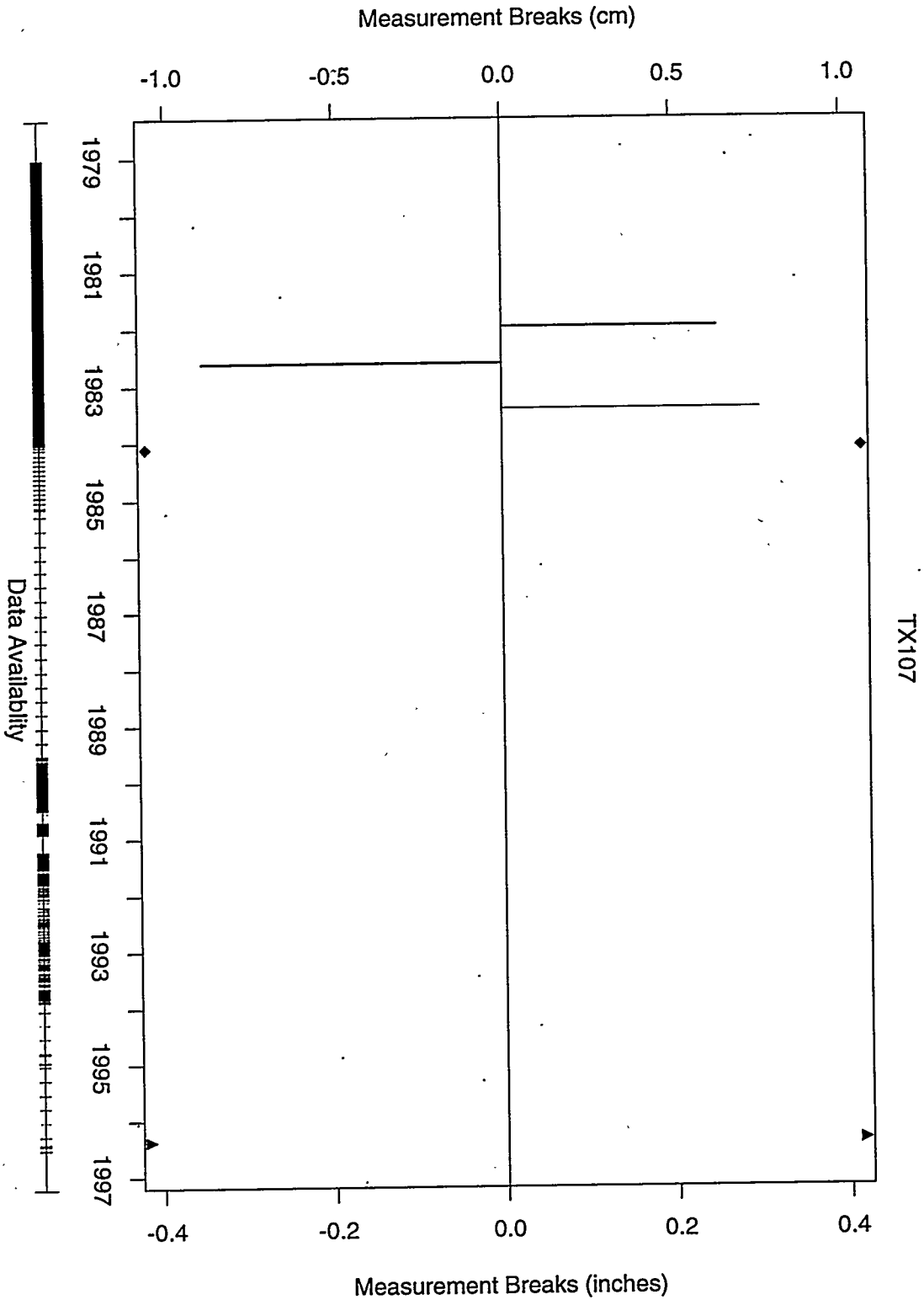

Figure C.32: Tank TX–107 detected breaks and break sizes.

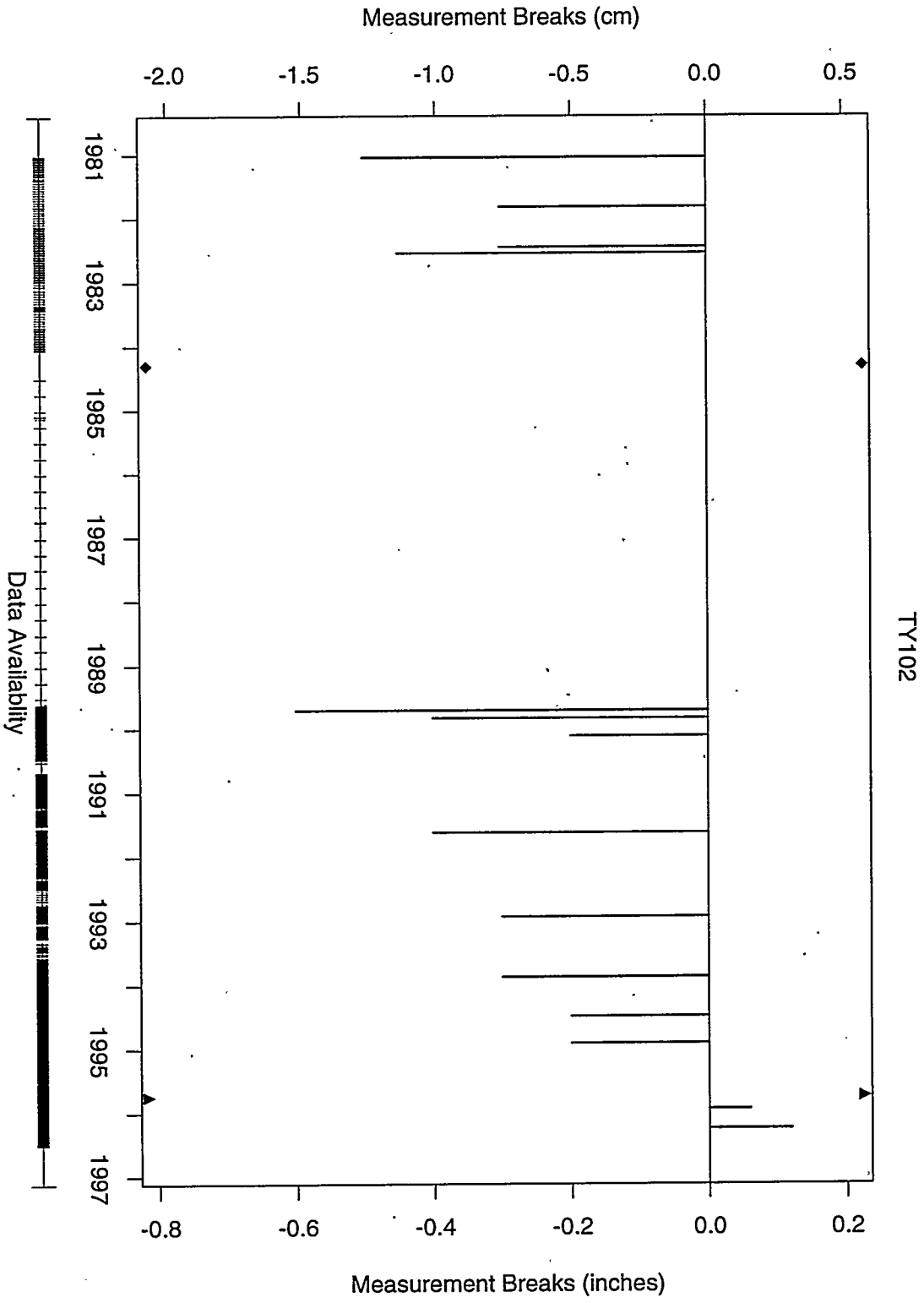

Figure C.33: Tank TY–102 detected breaks and break sizes.

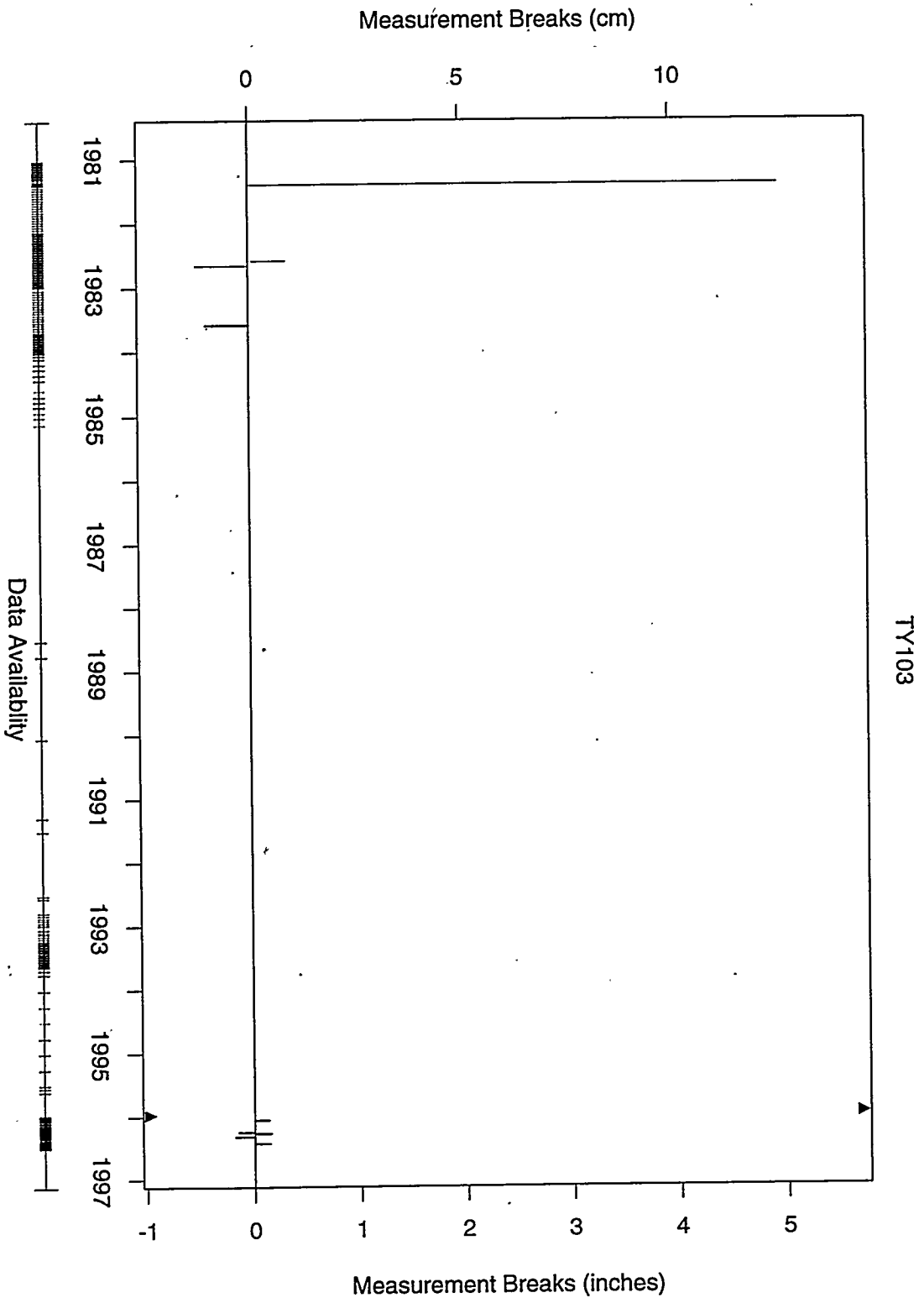

Figure C.34: Tank TY-103 detected breaks and break sizes.

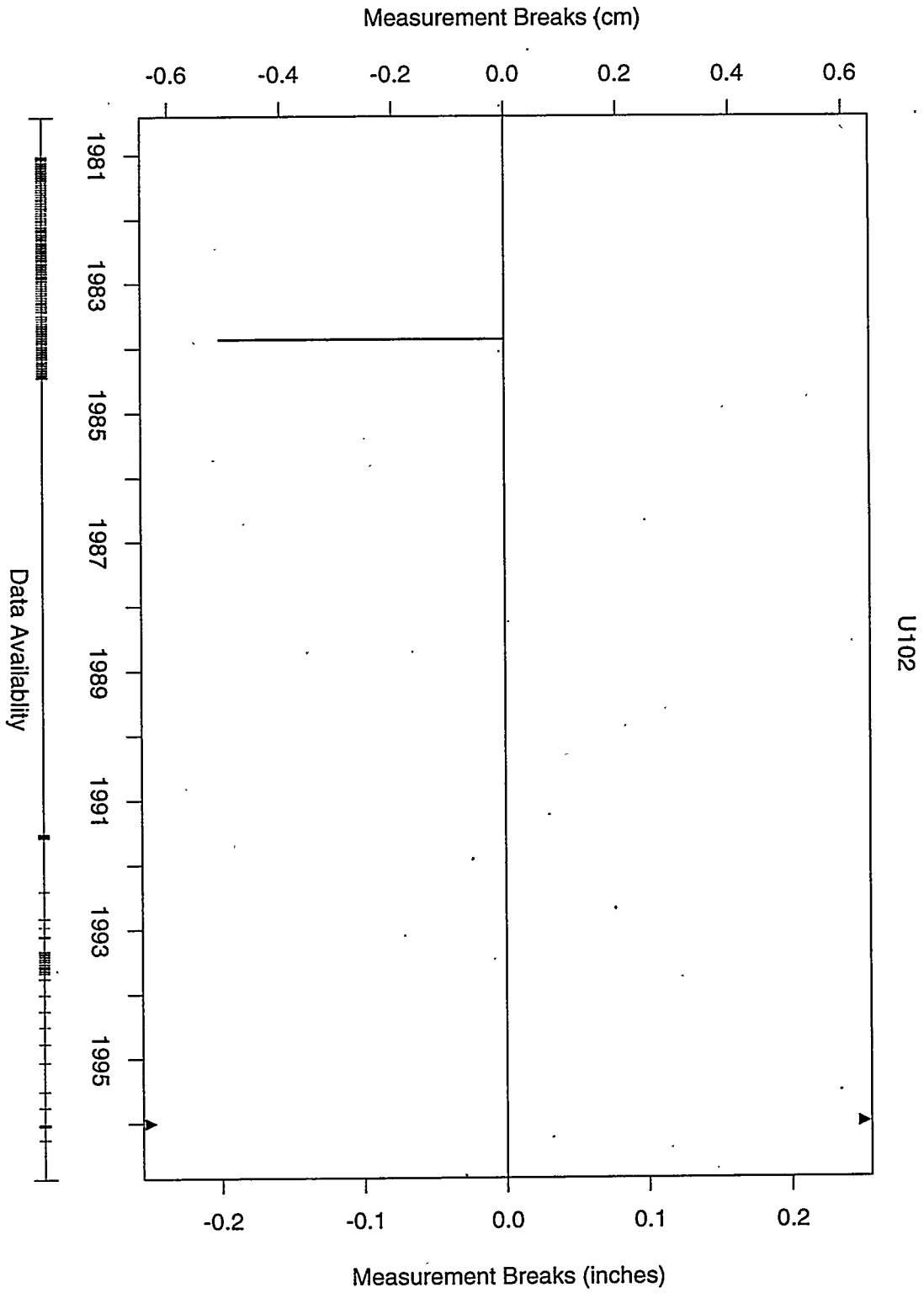

Figure C.35: Tank U-102 detected breaks and break sizes.

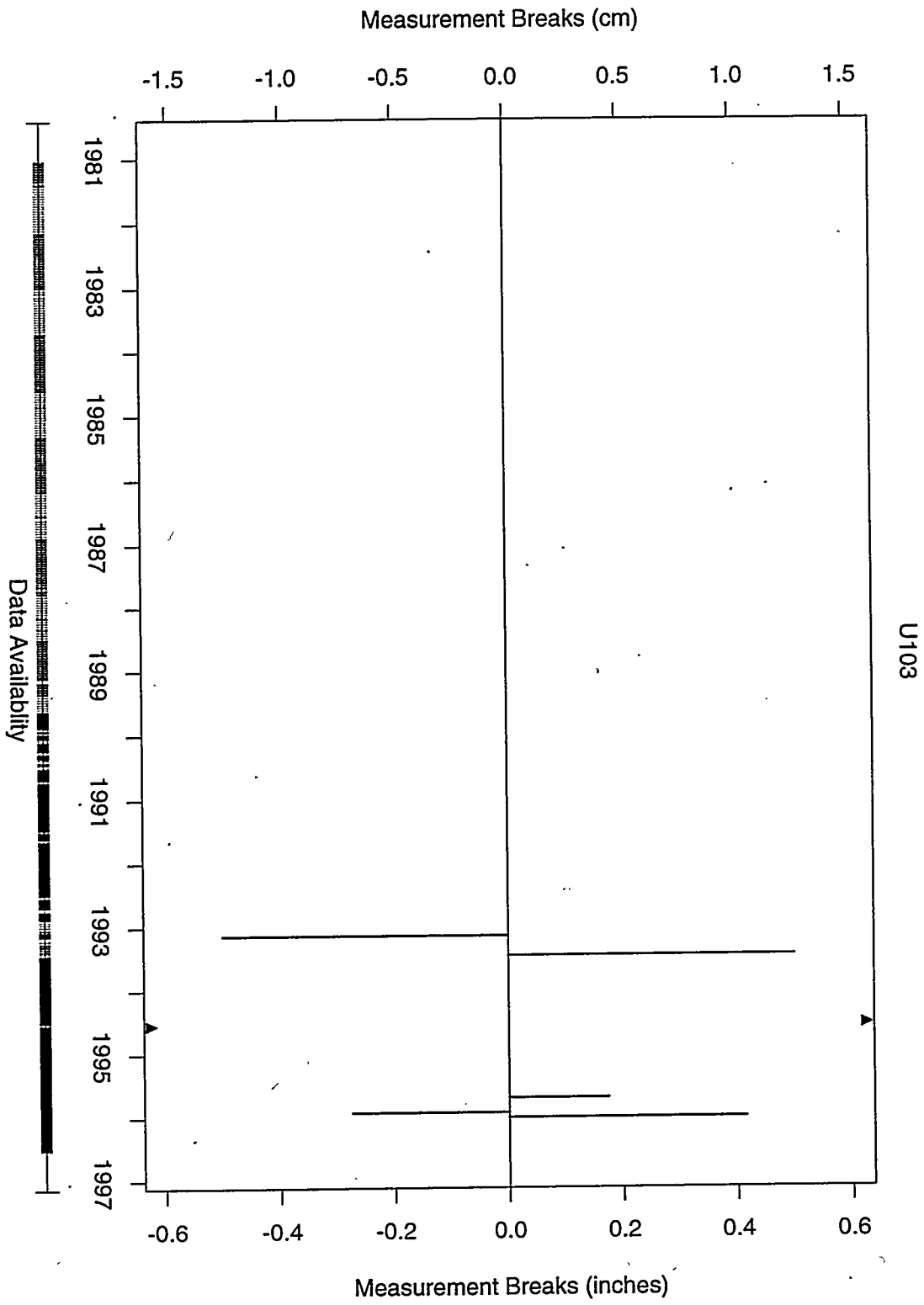

Figure C.36: Tank U-103 detected breaks and break sizes.

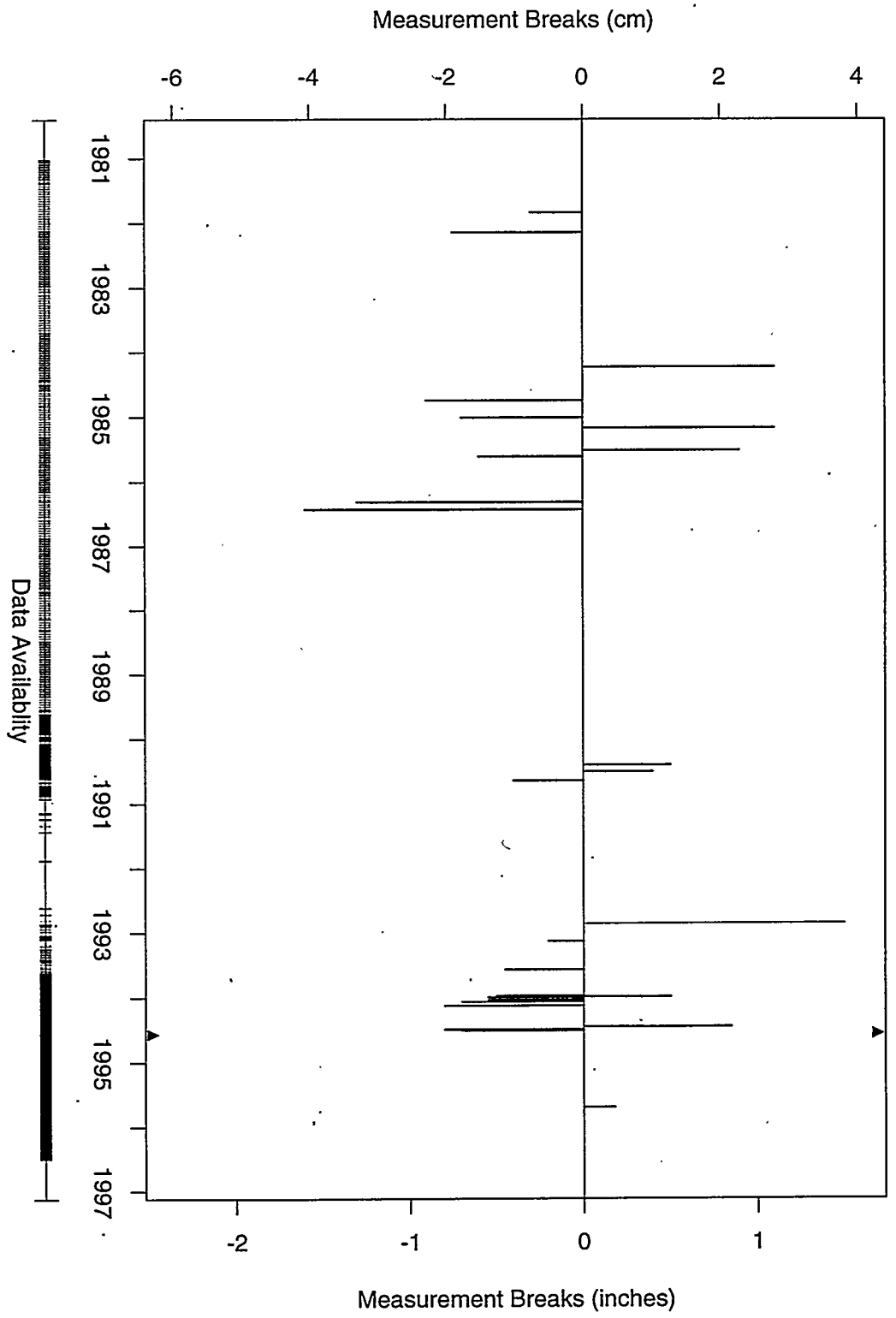

Figure C.37: Tank U-105 detected breaks and break sizes.

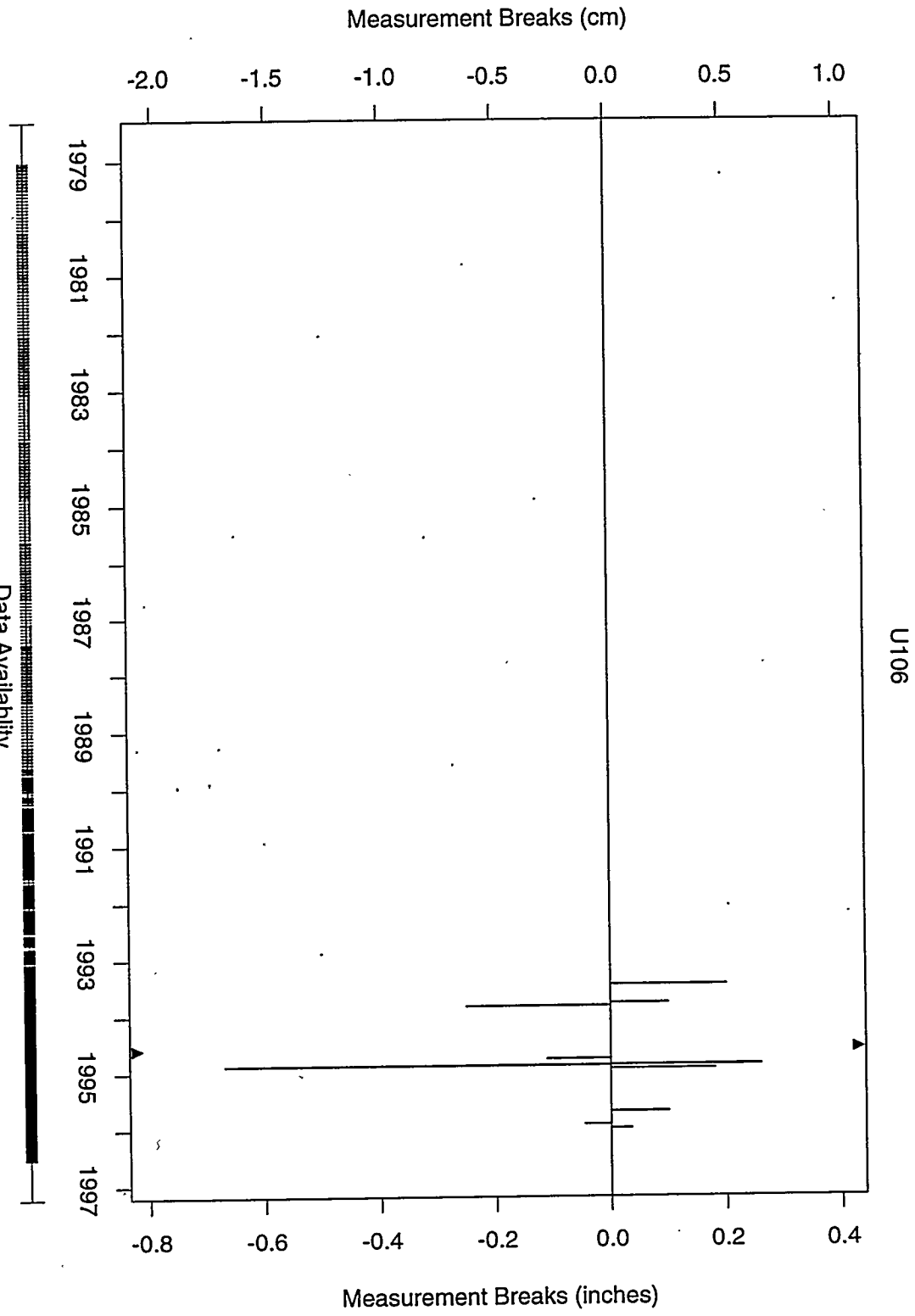

Figure C.38: Tank U-106 detected breaks and break sizes.

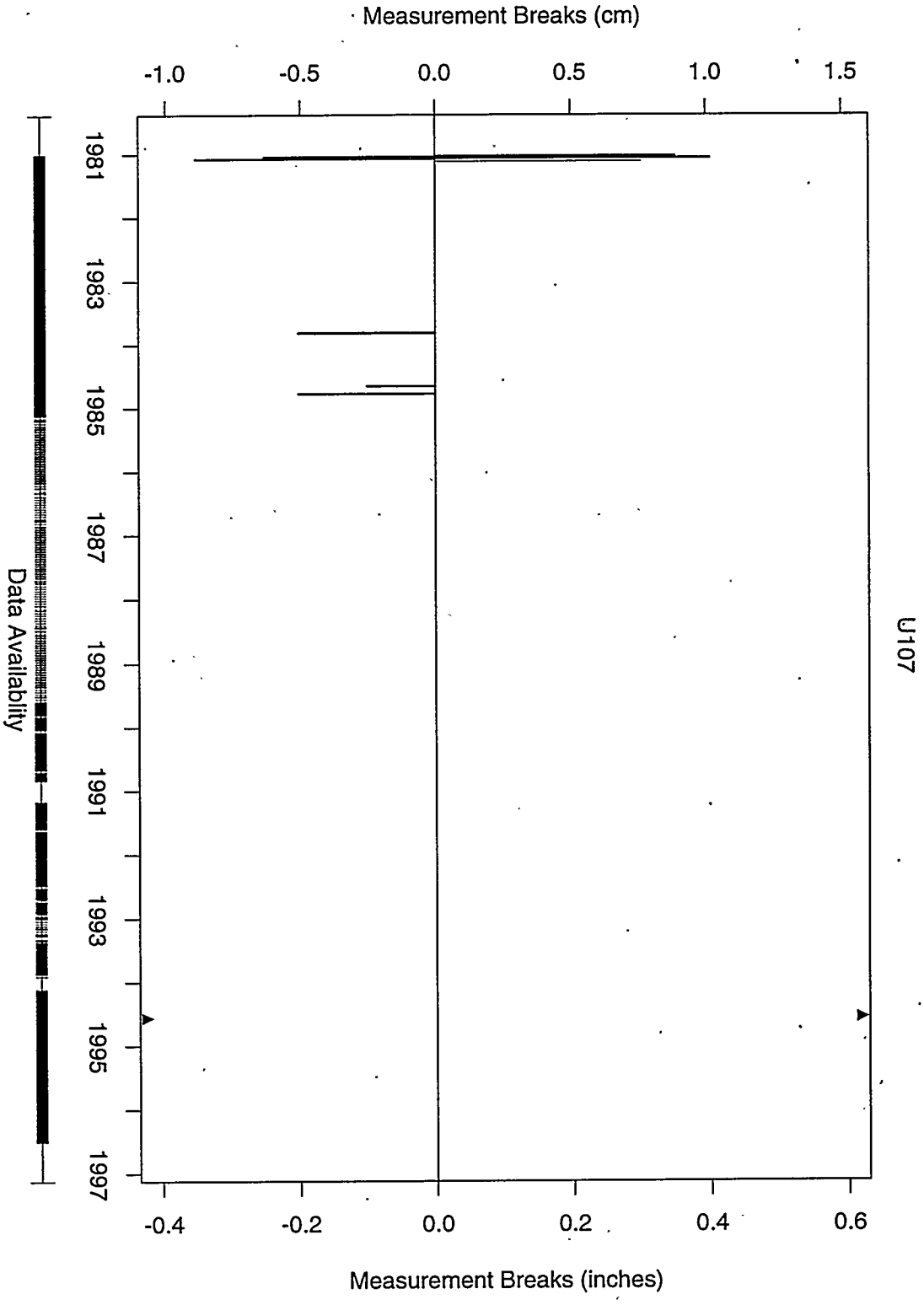

Figure C.39: Tank U-107 detected breaks and break sizes.

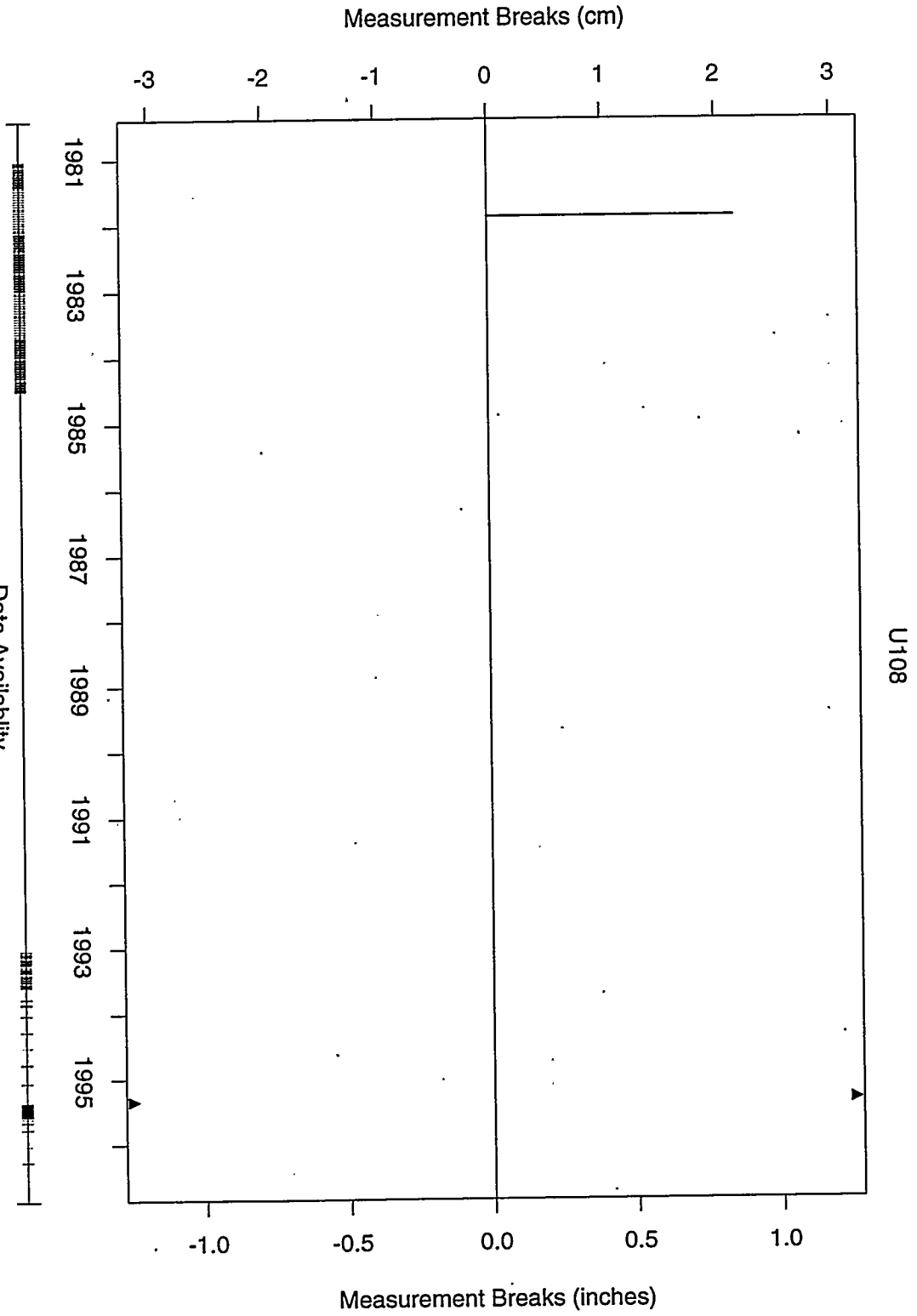

Figure C.40: Tank U-108 detected breaks and break sizes.

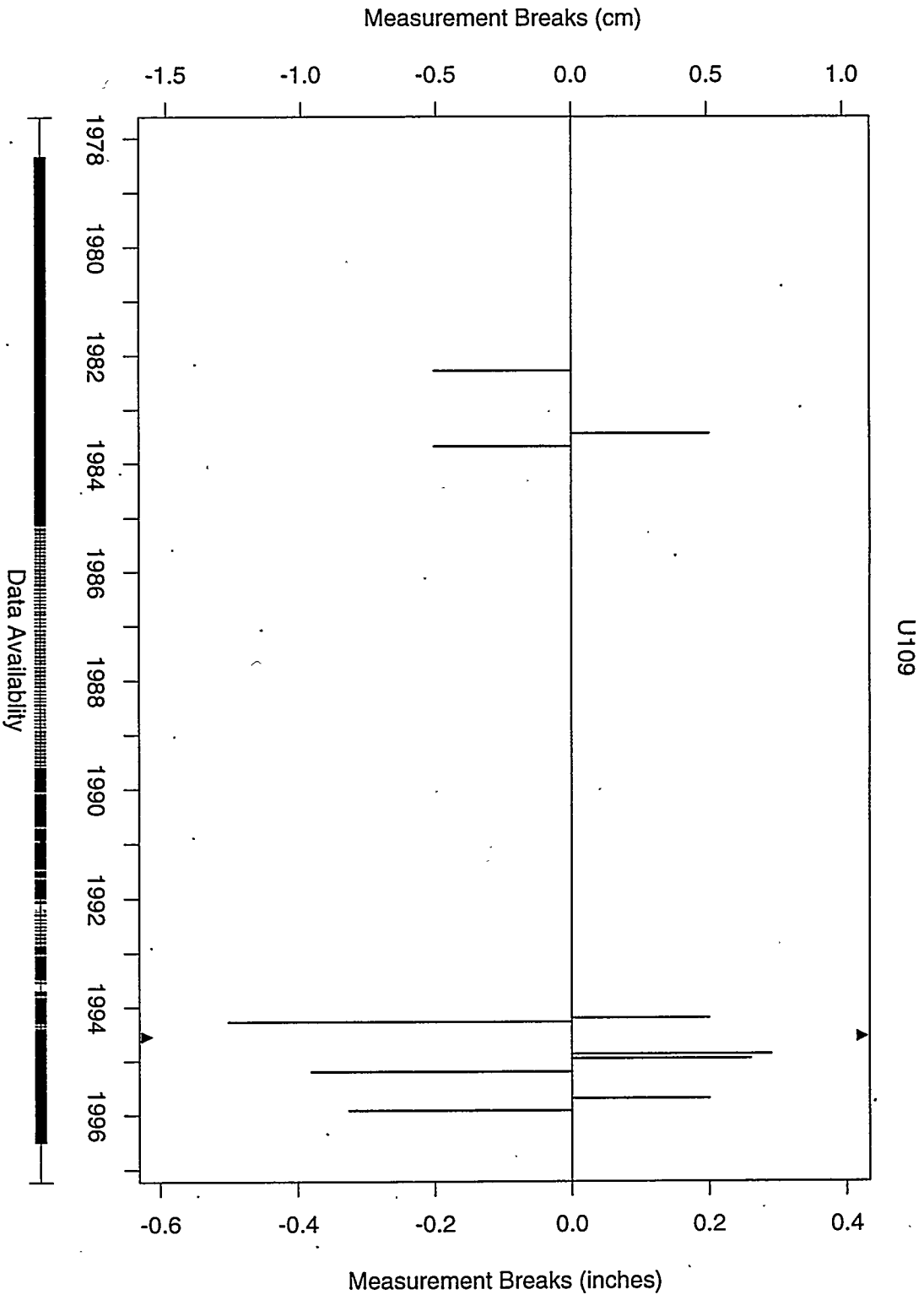

Figure C.41: Tank U-109 detected breaks and break sizes.

Distribution

No. of Copies

OFFSITE

3 Los Alamos National Laboratory
P.O. Box 1663
Los Alamos, NM 87545
Agnew, S.F. J5-86
Kubic, W.L. K5-75
White, J.R. H5-09

1 Sandia National Laboratories
Nuclear Facilities Safety Dept.
P.O. Box 5800
Albuquerque, NM 87185
Powers, D.A. 0744

1 Campbell, D.O.
102 Windham Road
Oak Ridge, TN 37830

1 Hudson, B.C.
202 North Ridge Court
Lindsborg, KA 67456

1 Nuclear Consulting Services, Inc.
P.O. Box 29151
Columbus, OH 43229
Kovach, J.L.

1 Kress, T.S.
102-B Newridge Road
Oak Ridge, TN 37830

1 Larson, T.E.
2711 Walnut Street
Los Alamos, NM 87544

1 Slezak, S.E.
806 Hermosa NE
Albuquerque, NM 87110

No. of Copies

ONSITE

4 **DOE Richland Operations Office**

S.O. Branch S7-54
J.M. Gray S7-54
C.A. Groendyke S7-54
G.W. Rosenwald S7-54

1 **Other**

M.H. Campbell(MACTEC) S7-73

28 **Hanford Contractors**

H. Babad S7-30
M.J. Bailey T4-07
D.A. Barnes R1-80
G.S. Barney T5-12
W.B. Barton R2-11
R.E. Bauer S7-14
J.B. Billetdeaux S7-15
R.J. Cash S7-14
D.B. Engelman L6-37
J.M. Grigsby A3-37
R.C. Hill R1-51
G.D. Johnson (5) S7-14
N.W. Kirch R2-11
C.E. Leach R1-49
J.A. Lechelt R2-11
J.W. Lentsch S7-14
J.E. Meacham S7-14
D.M. Ogden H0-34
T.E. Rainey S7-12
R.E. Raymond S7-12
G.R. Sawtelle A3-37
E.R. Siciliano H0-31
R.J. Van Vleet A3-34
N.E. Wilkins R2-11

J.M. Bates	K7-15
M.E. Brewster	K9-62
J.W. Brothers (5)	K9-20
C.D. Carlson	P7-25
P.A. Gauglitz	P7-41
R.T. Hallen	P8-38
P.G. Heasler	K5-12
V.L. Hunter	K7-97
N.E. Miller	K5-12
B.J. Palmer	K7-15
P.E. Panisko	P7-82
L.R. Pederson	K2-44
B.A. Pulsipher	K5-12
F.M. Ryan	K5-12
C.W. Stewart	K7-15
P.D. Whitney (10)	K5-12
Information Release Office (7)	K1-06